CHEMICAL WEATHERING PROCESSES LEADING TO SOIL DEVELOPMENT IN ARCTIC GLACIAL FOREFIELDS

Joshua John Blacker

Submitted in accordance with the requirements for the degree of

Doctor of Philosophy

January 2018

School of Earth and Environment

UNIVERSITY OF LEEDS

Declaration

The candidate confirms that the work submitted is his own, except where work which has formed part of jointly-authored publications has been included. The contribution of the candidate and the other authors to this work has been explicitly indicated below. The candidate confirms that appropriate credit has been given within the thesis where reference has been made to the work of others.

Work included in Chapter 5 has been published in a scientific peer reviewed journal as part of a paper co-authored: Bradley, James & Arndt, Sandra & Šabacká, Marie & Benning, Liane & Barker, Gary & **Blacker, Joshua** & Yallop, Marian & E. Wright, Katherine & Bellas, Christopher & Telling, Jon & Tranter, Martyn & Anesio, Alexandre. (2016). Microbial dynamics in a High Arctic glacier forefield: A combined field, laboratory, and modelling approach. Biogeosciences. 13. 5677-5696. 10.5194/bg-13-5677-2016.

The candidate performed the experiments, analyses (except: part of the stable carbon isotope and x-ray florescence analyses conducted at the German Research Centre for Geosciences and microbial carbon biomass and soil nitrogen quantification done at the University of Bristol, in collaboration with the NERC grant Arctic Soils, which were carried out by Sylvia Pinkerneil and Andrea Gottsche and James Bradley and Thomas Turpin-Jelfs, respectively), data processing, interpretation and preparation of the manuscript.

Dedication

This work is dedicated to my parents. I cannot put into words how grateful I am for their continual support and encouragement in all aspects of my life and for this, I am extremely fortunate to have them. To my brothers for their quick-witted responses that always manage to cheer me up. Also, to my grandparents for their support and kindness. Finally, to my girlfriend Hannah, who through the final year of my PhD managed to put up with my tedious moaning, awkwardness and provided me with endless cups of tea, bacon butties, pizza, ice cream and a clout around the lugholes when needed.

Food for thought… as former president of the United States of America, Roosevelt D. Franklin once quoted “The Nation that destroys its soils destroys itself.”

Acknowledgements

I am heartily thankful to my primary supervisor Liane G. Benning for her continual support, pragmatic approach, meticulous attention to detail and general guidance from the initial to final stage of my PhD. Without Liane's know-how, I would have struggled to overcome many academic hurdles during my PhD. Liane has proactively encouraged the application and attendance of grants to carry out additional field work and to take part in extracurricular courses. For these experiences, I am very grateful and will treasure these memories.

I extend a warm thank you to my secondary supervisor Simon Bottrell for whose encouragement, guidance and thought-provoking discussions from the start of year two to the final stage enabled me to develop an improved understanding of geochemistry. For his support, I am extremely appreciative.

I offer my regards and gratitude to all of those who supported me, firstly the laboratory technicians at Leeds University, Andy Connelly, Steven Reid, Fiona Keay and Lesley Neve for without their training, help and patience I would have not been able to carry out my laboratory analytical work. Also, the laboratory technicians at the German Research Centre for Geosciences (GFZ), specifically Anja Maria Schleicher and Andrea Gottsche with their help carrying out XRF analyses and Sylvia Pinkerneil for helping with stable carbon isotope and total organic carbon analyses. For fieldwork help, I would like to thank the members of staff at the British Antarctic Survey base in Ny Ayesund and the Tarfalla Research Station, Sweden. Also, to Alex Anesio, Martyn Tranter and James Bradley for their help with carrying out fieldwork at these locales and discussions as part of the NERC consortium project Arctic Soils that involved the University of Leeds and Bristol.

I would also like to thank Eva Avbelj and Rachel Beaumont Cohen Geochemistry Group interns who helped me in general day-to-day lab work and particularly with iron speciation extractions and pH measurements and my colleagues in this group for their open discussions and general comradery, namely but certainly not limited to Yijun (Mark) Xiong, Tim Dixon, Mike Cook, Jenifer Rodley, Tomasz M. Stawsky, Stefanie Lutz, Daniela Meier, Romain Gilbard, David Warburton, Anthony Stockdale, Andy Bray, David Hodkin, Gemma Woodward, Jenny Thompson and Benjamin Mills.

Abstract

Few Arctic forefields have been studied previously for their role in soil formation and in the carbon cycle. Yet, despite their prevailing polar climate, their soils may develop quickly and be extensive. Rock water residence times are prolonged in glacial tills that contain a rock flour component with high surface area and reactive that amasses in the forefields of glaciers as they retreat. Rapid sulfide oxidation and carbonate dissolution could be a potential CO_2 source to the atmosphere, while silicate-weathering and soil organic carbon accumulation a CO_2 sink. The extent of these sink-source reactions, and the soil forming processes that affect these, were tested over a century of Arctic forefield soil formation. In young, subglacial till-based moraine soils, the rapid depletion of accessory sulfide and carbonates minerals in the initial, and up to about 60-years of exposure, reflected widespread sulfide oxidation and carbonate dissolution. Defining young forefield soils as a potential transient CO_2 source to the atmosphere, since potential CO_2 sinks, namely calcium silicate mineral weathering and soil organic carbon accumulation were retarded, and limited to the older moraine soils. The slow onset of biological evolution in Arctic forefields and proton consumption by carbonates, present in the forefield lithologies, are suggested as the principal reasons for the limited silicate weathering and in turn soil formation. The results from this thesis may have new implications for the carbon cycle. Given glacial–interglacial cycles that have waxed and waned throughout Earth history, and carbonate and sulfide minerals are common in most lithologies made up of low to medium grade metamorphic and metasedimentary rocks. However, higher resolution temporal (diurnal to seasonal) and spatial field studies are needed in-order to more confidentially up-scale these findings beyond a glacier catchment scale.

Table of Contents

Table of Figures

Table of Tables

Chapter 1 . Introduction

This chapter gives a general view on the importance of Earth's soils and how they are changing under contemporary climate change. Combined with the literature review (Chapter. 2), it also details the hypotheses, aims, objectives of this thesis.

1.1 Background

Soils are important commodities on Earth as they provide services to the entire ecosystem. They control our water and food security, climate and nutrient supply. Unsurprisingly, soils fall within the global policy remit, and maintaining them is one of the major challenges humanity faces. Unfortunately, the health of Earth's soils is under threat as the population rises and demands on them increase at the same time as environmental changes are causing widespread degradation and losses (Banwart, 2011). Although the causes of this are complex, Earth's 0.8 °C rise temperature since 1880 (pre-industrial) is certainly one to be accounted for when looking at soils sustainability (Hansen et al., 2010). The urgency of understanding climate change in relation to soil is indicated by the exponential growth of publications since 1970's. In addition, soils are mentioned indirectly as one of the pressing issues facing Earth's climate in the latest scientific report on International Climate Change (Chapter on Carbon and other Biogeochemical Cycles; Stocker, 2013).

Under Earth's current climatic conditions, warming is predicted to intensify over the next century and this has implications for precipitation events (Fig 1.1). In some regions, raised temperature-induced lower annual rainfalls increase the need for irrigation and the potential risk of soil salinization (Rengasamy, 2006). Moreover, drought conditions can lead to desertification and dust bowl conditions, e.g. American Great Plains 1930's (Schubert et al., 2004). Raised temperatures increase the variability, frequency and intensity of rainfall and storms which can lead to increased soil erosion (Stocker, 2014). *In-situ* soil warming causes increased biological activity that changes soils carbon stocks and functions. For example, warming can accelerate enzymatic biodegradation through increased soil biological activity, which in turn aids soil fertility. This may in turn further promote the growth of carbon biomass through photosynthetic organisms that further capture atmospheric CO_2. However, this process leading to bettered soil fertility is often at the cost of soil CO_2 emission to the atmosphere. If soil carbon stocks are depleted without being replenished, the shift in equilibria may degrade

the soils' functionality and sustainability (Leheman and Kelber, 2016; Davidson and F, 2006). This summary shows not only that soil environments are intrinsically and extrinsically sensitive to climate, but that the carbon balance, input, and storage can dramatically affect atmospheric CO_2 concentrations that control Earth's temperature. The changes to climate and soils are spatially and temporally variable across Earth's surface, Figure 1.1.

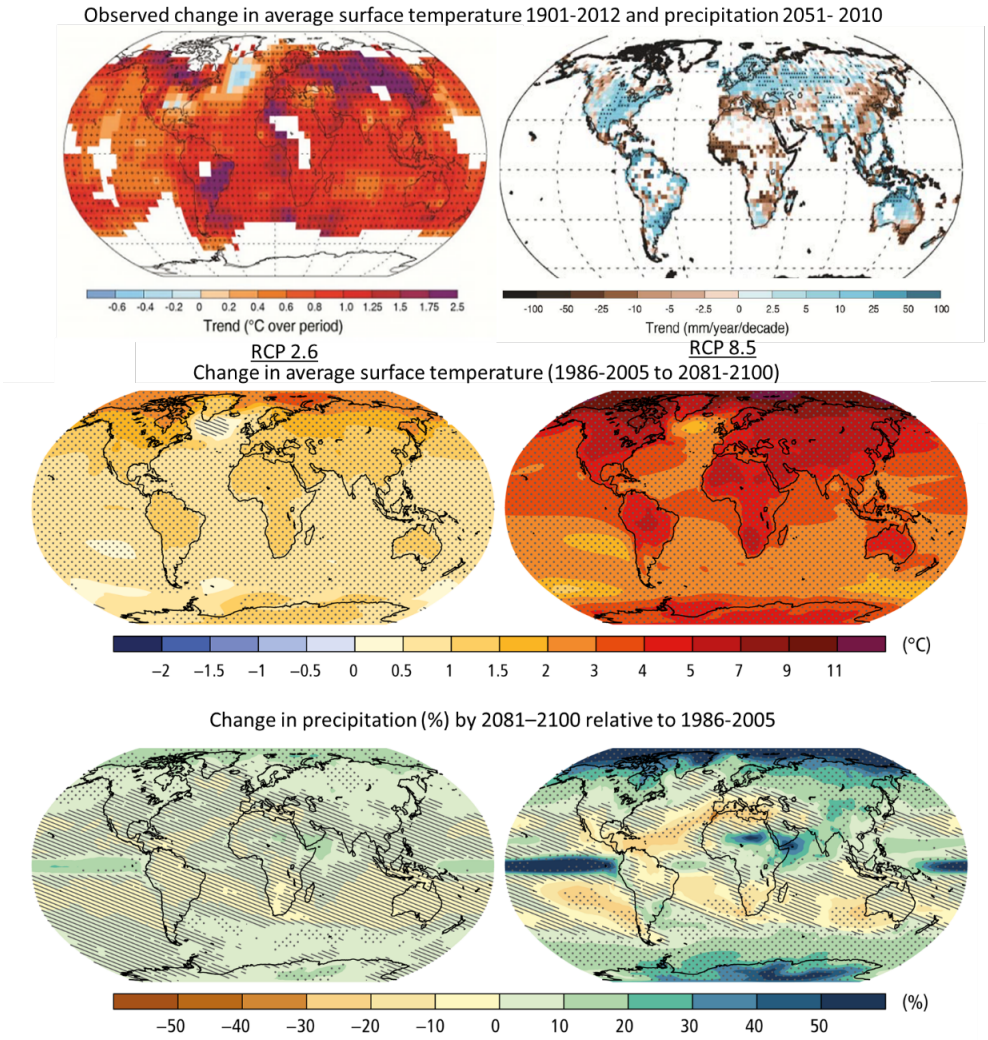

Figure 1.1. Observed and predicted changes in average surface temperatures and precipitation. Note: the regional variability, lack of observations in polar regions and thus uncertainty, in addition to Earth's 'Arctic Amplification' under scenarios RCP 2.6 (low emissions) and RCP 8.5 (high emissions). For each emission scenario breakdown, see Appendix A, Table A1.

As soils are intrinsically linked to the global carbon cycle, they play a major role in the function and wellbeing of planet Earth. Carbon is found in two forms, organic and inorganic, although within the carbon cycle these are readily interconverted. The total terrestrial carbon pool is 3,175 giga tonnes (GT), of which 2,500 GT is stored in the soil. This is the second largest, only

the ocean, with a size of about 38,400 GT of C, mostly in inorganic form, is larger (Houghton, 2007). The soil pool is ~3 times larger than the atmospheric pool (800 GT) (Oelkers & Cole 2008; Lal, 2008). Around 1550 GT carbon is stored as soil organic matter (SOM), whilst living biomass and inorganic carbon represents 950 GT. Inorganic carbon is contained primarily within calcareous rocks, (e.g. limestone and dolomite) and their carbonate minerals (e.g. calcite and dolomite) (Lal, 2008). Soil carbon functions that lead to carbon being transferred to different carbon cycle pools, requires continual monitoring. Firstly, because soils and their health are highly sensitive to climate a small change can result in a rapid and large transfer in carbon from one pool to the other. Secondly, the soil carbon pool exerts a strong control on the global mass of atmospheric C and on the delivery of dissolved carbon (organic or inorganic) to lakes and rivers. These combine to affect the production and storage of greenhouse gases and nutrient potential in a closed loop feedback that results in amplification of temperature change.

The warming of Earth and soils are highly spatially and temporally variable. One region identified as being amongst the most prone to change is the Arctic. This has led to the notion of 'Arctic amplification', as unprecedented climatic changes have, and are being observed here (e.g. Serreze and Francis, 2006). The effects of Arctic amplification on sensitive Arctic ecosystems alone remains a pressing issue that is not well quantified. This effect is further exacerbated because an estimated 50% of the soil carbon stocks on Earth are found in Arctic soils, yet we have very little quantitative knowledge about it (Tarnocai et al., 2009; Hugelius et al., 2014).

In general, soils in high latitude ecosystems have large quantities of C stored in unglaciated and deglaciated regions, laid down before and after the last glacial maximum (Zimov et al. 2006a, b; Harden et al. 1992). Carbon accumulation is considered to have arisen through the sequestration of organic carbon in newly exposed soils during deglaciation of the Laurentide Ice Sheet. Prevailing cold and wet soil conditions during this period inhibited decomposition of dead plant tissue that enters the soil organic matter pool (Kirschbaum, 2000; Zimov et al. 2006a, b; Harden et al. 1992). Whilst Arctic amplification intensity in recent decades could lead to carbon mineralization of these accumulated stocks, studies continue to suggest that Arctic tundra soils have acted as a sink for atmospheric CO_2. These estimates are constantly being re-evaluated as new data emerges. The latest mean estimate from various process-based model simulations highlights a substantial uncertainty in the range of estimates of soil C stored in high-latitude regions (McGuire et al., 2012). In addition, pan-Arctic soils observation, that

constrain model simulations, show significant spatiotemporal shifts in soil C, and whether they are CO_2 are sinks or sources (Corradi et al. 2005; Kwon et al. 2006, Schuur et al. 2009; Lloyd 2001; Soegaard et al. 2000, Groendahl et al. 2007; Aurela et al. 2004, Johansson et al. 2006). A solution to these uncertainties was identified as better spatial and temporal coverage of Arctic soils C monitoring across strategically located terrestrial Arctic ecosystems (McGuire et al., 2009; McGuire et al., 2012).

One re-emerging area of interest over the last two decades is newly forming soils in glacial forefields occurring in response to regional warming and deglaciation (Anderson et al., 2000; Bernasoni et al., 2011; Marvis et al., 2010). Unlike the vast amassed literature on Arctic tundra soils, and how they are responding to climate change, considerably less is known about newly forming soils in glacial forefields. This is surprising, since accumulation of organic carbon in response to glaciation is responsible for the vast amounts of carbon stocks found in the tundra (Kirschbaum, 2000; Zimov et al. 2006a, b; Harden et al. 1992). Perhaps, the obvious reason for this is that newly forming glacial forefields soils are typically mineral rich, and therefore, contain orders of magnitude less organic carbon compared to that stored in tundra permafrost soils (frozen for two consecutive years). Despite this, mounting evidence suggests that young, developing mineral soils in glacial forefields can significantly promote or attenuate carbon storage, through the rapid transfer of not only organic, but also inorganic carbon to and from the atmospheric and hydrological carbon pools (Anderson et al., 2000; Smittenberg et al., 2012).

It seems this is largely a result of the properties and weathering processes that occur in glacially-derived tills from which forefield soils form. Glacial tills weathered in subglacial environments are known to consist of an abundant ‘rock flour’ component with a high specific surface area and reactive sulfide and carbonate minerals (Tranter et al., 1993). The presence of subglacial till in forefields, combined with their long residence time, and the fact they are subjected to flushing with dilute meteoritic and glacial waters is believed to be a factor that enhances chemical weathering rates, and with this soil formation (Marvis et al., 2010). Yet, little attention has been put on distinguishing between subglacial and other till types from which soils form in forefields. This is a problem because each till type has its own physical and chemical properties, thus reactivity and weathering. Furthermore, soil organic carbon within Alpine forefields soils have been shown to accumulate as ecosystem biomass develops (Bernasoni et al., 2011). However, these organic carbon forms are highly sensitive to climate

change, responding rapidly with variations in growth of the biomass or the biodegradation of such newly formed soil carbon (Smittenberg et al., 2012). Similarly, Arctic forefields are also likely to respond to the unprecedented temperature and precipitation changes (Serreze and Francis, 2006). The lack of Arctic forefield studies, and data derived from such proglacial environments, means the role of organic carbon in these settings is largely unknown. This is surprising, since retreat of glacial forefields, from the last maximum, would expose a large proportion (28%) of the terrestrial land mass in the Northern Hemisphere (Gibbs and Kump., 1994). Their retreat would certainly have a major role on the Arctic's, and possibly also global carbon cycle.

1.2. Thesis hypothesis, aims and objectives

The hypothesis, aims and objectives have been developed by considering the gaps in knowledge identified in the Chapter 2 Literature review, and are as follows:

Hypothesis: Young soils forming from subglacial till 'parent material' in forefield's weather through a combination of rapid sulfide oxidation and carbonate dissolution. This delays the onset of silicate-weathering and soil organic carbon accumulation, defining these zones as potential transient CO_2 sources to the atmosphere.

Aim 1: To test this hypothesis, the extent of biogeochemical reactions that occur during the initial stages of soil formation in the deglaciating High- Arctic forefield, Midtre Lovénbreen, Svalbard were identified and assessed. With this information, the potential for such glacial tills to be sources or sinks of atmospheric CO_2 was evaluated.

To meet this aim, the following objectives were defined:

Objective 1. Conduct a detailed forefield evaluation and sampling campaign along transects to create a soil chronosequence from the glacier snout to the furthest Little Ice Age (LIA) moraine. In this way, any trends of gradients in chemical and physical parameters can be plotted and analysed as a function of moraine age, in a statistically relevant manner, taking the inherent spatiotemporal heterogeneity of the soils forming in glacial forefields into consideration.

Objective 2. To compare and contrast chemical and physical properties of two macroscopically identifiable till types (supraglacial and subglacial) and evaluate how each till type affects chemical weathering processes.

Objective 3. To determine, and quantify, forefield weathering modes and their dominance in the forefield using bulk elemental (major, minor and trace) and stable carbon isotope analyses of all samples. Carry out a thorough regression and stoichiometric mass balance analysis to evaluate the strength of empirical relationships, and their statistical significance with respect to weathering and soil formation in the samples.

Objective 4. To combine all the above results, assess the dominant spatiotemporal weathering reactions, and evaluate whether over a century of forefield-forming chemical weathering and soil processes, High Arctic glacial forefields are potential atmospheric CO_2 sinks or sources.

Aim 2: Derive an integrated understanding of soil organic carbon dynamics in different Arctic forefield environments: 1x High-Arctic and 2x sub-Arctic to understand how the Arctic warming trends could be affecting organic carbon dynamics in these temperature sensitive environments.

To achieve this aim, the following objectives were made:

Objective 5. Use a regression model to determine if organic carbon and calculated SOC stocks accumulate as a function of moraine age. Combined with stable carbon isotopes measurements of the signatures of bulk surficial soils develop an isotopic mixing model to constrain isotopic end members along a mixing line.

Objective 6. Formulate a carbon budget to account for major relative shifts in microbial, plant, or kerogen contributions, and combine with other chemical elemental data (i.e. iron and phosphorus speciation) to evaluate any relationship between organic carbon and other weathering parameters in the newly formed soils.

Objective 7. Use data sets from the various forefields, and combined with *in-situ* field and soil property data, as well as existing data (ecological, modelling, biogeochemical, and

metrological and climate) and evaluate, if possible, a cumulative mass of soil organic carbon stocks and rates of dynamic changes over a century of soil development.

Aim 3: Combining all the above, develop insight into the biogeochemical weathering processes during the initial stages of soil development, and assess if they are potential CO_2 sinks or sources to the atmosphere.

1.3. Thesis outline and structure

This introductory chapter is followed by a literature review in which the existing knowledge base is evaluated. This was crucial in identifying research gaps and helped to develop research areas and ideas leading to the hypotheses, aims and objectives described above. In Chapter 3, the study areas are described in detail along with the methods employed: field, analytical and statistical approaches. In two longer Chapters, 4 and 5, the main results of this thesis are outlined. The wide range of data sets generated were analysed and interpreted using appropriate computational methods. This was discussed with, and deemed appropriate, by my thesis supervisors. In Chapter 4 empirical relationships between carbonate vs. silicate weathering were evaluated. The role of sulfide oxidation in driving weathering in subglacial or supraglacial dominated glacial tills in the forefield of Midre Lovénbreen in Svalbard was also assessed. These processes were selected as each can act as an atmospheric sink or source of CO_2 in glacial and non-glacial terrain to help with Aim 3. Chapter 5 focuses on organic carbon dynamics in response to soil formation in newly deglaciating terrains: one High-Arctic, and two Sub-Arctic. Comparing the results from both bulk stable carbon isotopic analyses with a carbon mass balance enabled the determination what carbon sources, pedogenic processes and factors drive organic carbon dynamics. Furthermore, carbon stocks and rates were calculated as a function of moraine age. These results were then compared to other Arctic and non-Arctic forefields to reveal if soil organic stocks are comparable, and whether they have similar accumulation functions over the same order of soil formation. Chapters 6 and 7 contain a combined summary and general conclusions about the work presented. Some knowledge gaps have been identified that could form the basis of future studies.

1.4. References

Anderson, S. P., Drever, J. I., Frost, C. D. & Holden, P. 2000. Chemical weathering in the foreland of a retreating glacier. *Geochimica Et Cosmochimica Acta,* 64**,** 1173-1189.

Aurela, M., Laurila, T. and Tuovinen, J.P., 2004. The timing of snow melt controls the annual CO2 balance in a subarctic fen. *Geophysical research letters*, *31*(16).

Banwart S (2011) Save our soils, Nature, 474, pp.151-152. doi: 10.1038/474151a

Bernasconi, S. M., Bauder, A., Bourdon, B., Brunner, I., Bunemann, E., Christl, I., Derungs, N., Edwards, P., Farinotti, D., Frey, B., Frossard, E., Furrer, G., Gierga, M., Goransson, H., Gulland, K., Hagedorn, F., Hajdas, I., Hindshaw, R., Ivy-Ochs, S., Jansa, J., Jonas, T., Kiczka, M., Kretzschmar, R., Lemarchand, E., Luster, J., Magnusson, J., Mitchell, E. a. D., Venterink, H. O., Plotze, M., Reynolds, B., Smittenberg, R. H., Stahli, M., Tamburini, F., Tipper, E. T., Wacker, L., Welc, M., Wiederhold, J. G., Zeyer, J., Zimmermann, S. & Zumsteg, A. 2011b. Chemical and Biological Gradients along the Damma Glacier Soil Chronosequence, Switzerland. *Vadose Zone Journal,* 10**,** 867-883.

Corradi, C., Kolle, O., Walter, K., Zimov, S.A. and Schulze, E.D., 2005. Carbon dioxide and methane exchange of a north-east Siberian tussock tundra. *Global Change Biology*, *11*(11), pp.1910-1925.

Davidson, E. A. & Janssens, I. A. 2006. Temperature sensitivity of soil carbon decomposition and feedbacks to climate change. *Nature,* 440**,** 165-173.

Gibbs, M.T. and Kump, L.R., 1994. Global chemical erosion during the last glacial maximum and the present: sensitivity to changes in lithology and hydrology.

Paleoceanography, 9(4), pp.529-543.

Groendahl, L., Friborg, T. and Søgaard, H., 2007. Temperature and snow-melt controls on interannual variability in carbon exchange in the high Arctic. *Theoretical and Applied Climatology*, *88*(1), pp.111-125.

Hansen, J., Ruedy, R., Sato, M. and Lo, K., 2010. Global surface temperature change. *Reviews of Geophysics*, *48*(4).

Harden, J.W., Sundquist, E.T., Stallard, R.F. and Mark, R.K., 1992. Dynamics of soil carbon during deglaciation of the Laurentide ice sheet. *Science*, New York Then Washington, *258*, pp.1921-1921.

Houghton, R.A., 2007. Balancing the global carbon budget. *Annual. Rev. Earth Planet. Sci.*, *35*, pp.313-347.

Hugelius, G., Strauss, J., Zubrzycki, S., Harden, J.W., Schuur, E., Ping, C.L., Schirrmeister, L., Grosse, G., Michaelson, G.J., Koven, C.D. and O'Donnell, J.A., 2014. Estimated stocks of circumpolar permafrost carbon with quantified uncertainty ranges and identified data gaps. *Biogeosciences*, *11*(23), pp.6573-6593.

Johansson, T., Malmer, N., Crill, P.M., Friborg, T., Aakerman, J.H., Mastepanov, M. and Christensen, T.R., 2006. Decadal vegetation changes in a northern peatland, greenhouse gas fluxes and net radiative forcing. *Global Change Biology*, *12*(12), pp.2352-2369.

Kirschbaum, M.U., 2000. Will changes in soil organic carbon act as a positive or negative feedback on global warming? *Biogeochemistry*, *48*(1), pp.21-51.

Kwon, F.A., Zhao, M., Running, S.W., Kimball, J.S., Nemani, R.R., Davis, K.J., Bolstad, P.V., Cook, B.D., Desai, A.R., Ricciuto, D.M. and Law, B.E., 2006. Evaluation of remote sensing based terrestrial productivity from MODIS using regional tower eddy flux network observations. *IEEE Transactions on Geoscience and Remote Sensing*, *44*(7), pp.1908-1925.

Lal, R. 2008. Carbon sequestration. *Philosophical Transactions of the Royal Society B: Biological Sciences,* 363**,** 815-830.

Lehmann, J. & Kleber, M. 2015. The contentious nature of soil organic matter. *Nature,* 528**,** 60-68.

Lloyd, C.R., 2001. The measurement and modelling of the carbon dioxide exchange at a high Arctic site in Svalbard. *Global Change Biology*, *7*(4), pp.405-426.

Mavris, C., Egli, M., Plotze, M., Blum, J. D., Mirabella, A., Giaccai, D. & Haeberli, W. 2010. Initial stages of weathering and soil formation in the Morteratsch proglacial area (Upper Engadine, Switzerland). *Geoderma,* 155**,** 359-371.

McGuire, A.D., Christensen, T.R., Hayes, D.J., Heroult, A., Euskirchen, E., Yi, Y., Kimball, J.S., Koven, C., Lafleur, P., Miller, P.A. and Oechel, W., 2012. An assessment of the carbon balance of Arctic tundra: comparisons among observations, process models, and atmospheric inversions. *Biogeosciences Discussions*, *9*, p.4543.

McGuire, A.D., Anderson, L.G., Christensen, T.R., Dallimore, S., Guo, L., Hayes, D.J., Heimann, M., Lorenson, T.D., Macdonald, R.W. and Roulet, N., 2009. Sensitivity of the carbon cycle in the Arctic to climate change. *Ecological Monographs*, *79*(4), pp.523-555.

Oelkers, E.H. and Cole, D.R., 2008. Carbon dioxide sequestration a solution to a global problem. *Elements*, *4*(5), pp.305-310.

Rengasamy, P., 2006. World salinization with emphasis on Australia. *Journal of experimental botany*, *57*(5), pp.1017-1023.

Schubert, S.D., Suarez, M.J., Pegion, P.J., Koster, R.D. and Bacmeister, J.T., 2004. On the cause of the 1930s Dust Bowl. *Science*, *303*(5665), pp.1855-1859.

Schuur, E. A., Vogel, J. G., Crummer, K. G., Lee, H., Sickman, J. O. & Osterkamp, T. 2009. The effect of permafrost thaw on old carbon release and net carbon exchange from tundra. *Nature,* 459**,** 556-559

Serreze, M.C. and Francis, J.A., 2006. The Arctic amplification debate. *Climatic change*, *76*(3-4), pp.241-264.

Smittenberg, R.H., Gierga, M., Göransson, H., Christl, I., Farinotti, D. and Bernasconi, S.M., 2012. Climate-sensitive ecosystem carbon dynamics along the soil chronosequence of the Damma glacier forefield, Switzerland. *Global Change Biology*, *18*(6), pp.1941-1955.

Soegaard, H., Nordstroem, C., Friborg, T., Hansen, B.U., Christensen, T.R. and Bay, C., 2000. Trace gas exchange in a high-Arctic valley: 3. Integrating and scaling CO2 fluxes from canopy to landscape using flux data, footprint modelling, and remote sensing. *Global Biogeochemical Cycles*, *14*(3), pp.725-744.

Stocker, T. ed., 2014. *Climate change 2013: the physical science basis: Working Group I contribution to the Fifth assessment report of the Intergovernmental Panel on Climate Change*. Cambridge University Press.

Tarnocai, C., 2009. The impact of climate change on Canadian peatlands. *Canadian Water Resources Journal*, *34*(4), pp.453-466.

Tranter, M., Brown, G., Raiswell, R., Sharp, M. & Gurnell, A. 1993. A conceptual model of solute acquisition by Alpine glacial meltwaters. *Journal of Glaciology,* 39**,** 573-581.

Zimov, S.A., Davydov, S.P., Zimova, G.M., Davydova, A.I., Schuur, E.A.G., Dutta, K. and Chapin, F.S., 2006. Permafrost carbon: Stock and decomposability of a globally significant carbon pool. *Geophysical Research Letters*, *33*(20).

Zimov, S.A., Schuur, E.A. and Chapin, F.S., 2006. Permafrost and the global carbon budget. *Science*, *312*(5780), pp.1612-1613.

Chapter 2 . Literature Review

The earliest glacial forefield studies are from Crocker et al. in 1955. These link chronological developments of soils and ecosystem growth to carbon dynamics and subsequently climate. Nearly half a century later, in 1992, Harden et al. proposed that soil-ecosystems can develop negative feedbacks, causing atmospheric CO_2 drawdown and carbon storage in response to warming-induced deglaciation (Fig. 2.1). The authors of this paper emphasised that a clear understanding of all processes in these complex systems is seriously hampered by the lack of data. Furthermore, that time-series data and process-based studies would greatly benefit our knowledge. Since then, researchers have reported a number time-series and process studies with a unified view that soil development in a deglaciating environment can act as CO_2 a sink. The studies are based predominantly on findings in Alpine environments. There is a lack of spatial context, with worryingly few studies in Arctic forefields where Earth's average warming trend is most amplified. This is particularly crucial, since up to ~28% of the modern land surface in the Northern Hemisphere may have been subjected to proglacial conditions at some stage during deglaciation following the last glacial maximum. The little data there is suggests that biogeochemical weathering processes during the initial stages of soil development could act either as a potential CO_2 sink or source to the atmosphere and hydrosphere. (Gibbs and Kump, 1994).

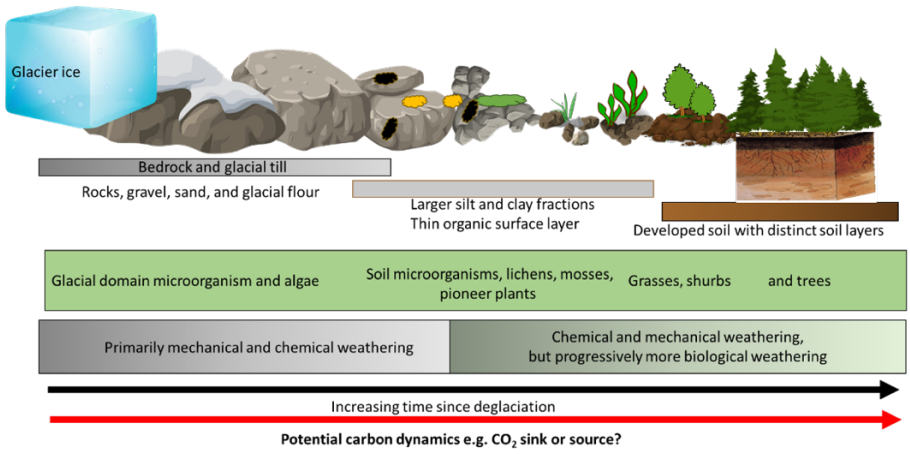

Figure 2.1 The classic model of the general characteristic of soil development along a glacial forefield chronosequence typical of forefields in Alpine environments. Whether this holds true in relation to the carbon cycle in Arctic forefields, is addressed in this review.

2.1. Soil, processes and its formation

Soils are typically composed of solid (50% w/w), liquid (20-30% w/v) and gaseous (20-30% v/v) phases. The solid phase can be further divided into the mineral (45% w/w) and organic

(5% w/w) fractions. The organic fraction is comprised of fresh and partially decomposed plant and animal tissues, and biomass. The mineral fraction is composed of primary and secondary minerals including most silicates, and particularly clay minerals and other oxides (Ellis and Mellor, 1995).

The definition of a soil is being continually updated as new scientific advances are made. For many geochemists and soil scientists this is often a personal definition based on experience, however, one recent definition that has sustained traction is "a soil is the integral and central unit of the critical zone, the thin surface layer that extends from the top of vegetation to the bottom of groundwater circulation and supplies humans with most life-sustaining resources" (Brantley et al., 2007; Anderson et al., 2004). To this end, other ecosystems benefit from a soil ecosystem and vice versa (Amundson, et al., 2007). As a soil contains life, and where there is life there is carbon, a soil is intrinsically linked to the global carbon cycle; modulating biogeochemical weathering reactions that control climate (Melillo et al., 2002). A more systematic perspective defines soils as a system, (Fig. 2.2). Like every system, soils consist of *additions* (inputs) *transformations, transfers* (process/functions) and *losses* (outputs). In other words, soil is a reactive layer that mediates the flow of energy, mass, and biodiversity. These inputs transform the soil system and generate output flows to groundwater, vegetation and the atmosphere, while laterally replenishing surface waters (Banwart et al., 2017). This highlights the complex continuum of actions and interactions in soil, however, for simplicity, hereafter, soil formation processes (also called pedogenesis and soil development) will be discussed as additions, transformations, transfers and losses. The focus is on the former two processes, and, in the context of soil formation, factors in glacial forefields. Soil forming factors are: climate, biota, topography, parent material, time, (Eq. 2.1)(Jenny, 1994), with the more recent addition of anthropogenic soil management practices.

Factors of Soil Formation	$S = f(cl, o, r, p, t, m \ldots)$ **Equation 2.1.**
cl = climate	the chemical breakdown of the p is influenced by heat and cold, ice formation, wind etc.
o = biota (eukaryotes & prokaryotes)	Biota activity- roots bind soil particles, and cleave rocks, whilst animals burrow into the soil and mix the various components including organic matter from decaying organisms, mineral particles and chemicals produced by physical - chemical and biological activity in the soil.
r = topography	- i.e. slope and land form

p = parent material	- i.e. lithological physical and chemical properties
t = time	- the time soil is exposed to weathering, soil forming processes influences soil properties
m = management	(or mis-management) by people - ploughing, fertilising etc.

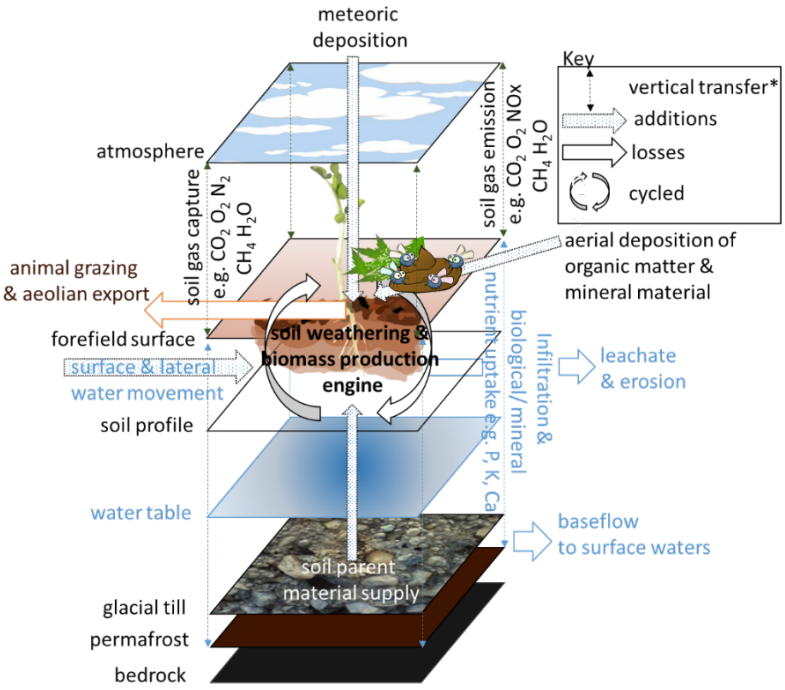

Figure 2.2. A schematic diagram from a layered modelling prospective of a newly forming soil in a glacial forefield and the theoretical *transfers* and their direction through the soil system in the context of the critical zone. Inputs (*additions*) feed the soil weathering and biological production engine (*transformation*) leading to outputs (*losses*) that delivery nutrient to downstream ecosystems or release dissolved or gas phase carbon species to the hydrological and atmospheric system. *Vertical transfers in the water table (blue hashed arrows) control both additions and losses to a soil. This is dependent on the prevailing water table level influenced by the extent of permeability permafrost (if present) and bedrock layers below a soil. While atmospheric vertical transfers (black hashed arrows) can lead to gas emission or capture depending on system equilibria, controlled biogeochemical reactions in the soil engine. Note: size of the arrow is not proportional to quantity. Modified from Banwart et al., 2017.

2.2. Glacier forefields as natural laboratories for understanding soil formation and carbon dynamics

Glacial forefields are ideal natural laboratories and of great importance for understanding time-dependent biogeochemical weathering reactions and soil forming processes. This is because laboratory experiments often struggle to replicate the subtle changes in intrinsic and extrinsic weathering environments for minerals such as silicates that weather slowly over long-time scales (White and Brantley, 2003; Hodson et al., 1998). They are also useful because of the

short-long term response in the SOM pool to environmental changes (Smittenberg et al., 2012). As glaciers retreat the moraines are deposited. These can be dated using satellite imagery and historic aerial photographs (up to approximately a century; Huggett, 1998; Bernasconi et al., 2011), or radiocarbon dating (up to <50,000 years; Hodkinson et al., 2003; Coleman, 2012). A chronosequence links distance to time, and infers a temporal trend of a set of sites at different spatial positions. These are sampled at the same time, and can therefore be used to resolve weathering reaction rates and soil evolution at short (annual, bi-annual, decadal), and long-term (century, thousand), time-scales (Huggett, 1998; Egli et al., 2001) (Fig. 2.3). This approach only provides a snapshot of the intergraded effects on the complex processes that govern soil evolution. So, without extensive sampling at suitable spatial and temporal resolution, rapid changes could be missed, for example seasonality.

Despite the heterogeneities manifested in glacial forefields and some of their tills, biological, chemical and physical patterns and gradients are observed at all scales (Bernasconi et al., 2011). This is due to an additional benefit of the time-space sequence approach that enables independent replicates to be collected in co-aligned transects to increase reliability. This is one of the reasons large multidisciplinary teams have adopted this approach as part of major projects i.e., Swiss Big Link Project as part of the Critical Zone Observatory international initiative (Bernasconi and Big Link Project, 2008; Banwart et al., 2012). This approach is commended, as significant scientific advancements have been achieved from these projects. The Big Link project assessed processes around the forefields in the Damma and Morteratsch glaciers in the Swiss Alps. The study provided an outstanding example of how such approaches could better quantify soil-forming processes in natural settings. The results from these observatories offer a unique, well-constrained and valuable opportunity for parametrisation, modelling and up-scaling. However, problems arise if the results are inappropriately applied to those outside the scope of the specific Alpine soil (see also section 2.1 & 2.5)(Jenny, 1941; Schmidt et al., 2011). This is because erroneous results and cross-correlations might be derived. For instance, it has been suggested by Smittenberg et al., 2012 that soil and ecosystem carbon dynamics in the Damma glacier forefield could be applicable to those in the Arctic. Although in some ways Alpine forefields are analogous to those in the Artic due to their high altitude, fundamental differences in climate, biology and other soil forming factors (e.g. those proposed by Jenny, 1941) are apparent (Table. 2.1). Furthermore, in-depth empirical studies from Arctic glacial forefield perspectives are required to better understand their soil formation and carbon dynamics.

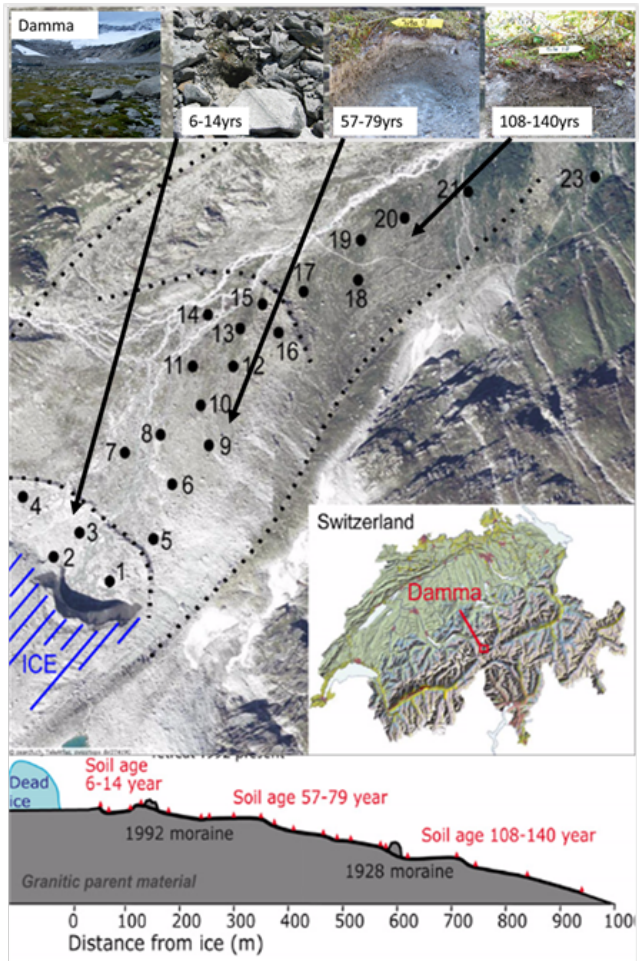

Figure 2.3. Example of an atypical glacial forefield natural laboratory used for in-depth soil development studies, in this example shown is the most well-studied forefield of the Damma Glacier, Swiss Alps. Modified from Bernasconi et al., 2008.

Table 2.1 Characteristics that affect soil forming factors from an array of globally notable glacial forefield observatories

Locale	Deglaciation Period	Latitude & Altitude	Lithology	Glacial till and bedrock characteristics	Till Types	Prevailing Climate	Forefield Topography	Biome and Vegetation
Forefield name	*(years)*	*(°) (m asl)*	*(Major rock group, rock types)*		*(Supra, En, Sub)*			
High-Arctic								
[1]Werenskiold	0 to 80	77, N 25–75	[a]*Metasedimentary* chlorite-mica-schist marble quartzite conglomerates dolomite phyllites amphibolites	[a]'Considered to be polymineral and relatively homogenous'	[c]Supra, En, Sub	[a]*Polar* Mean annual precipitation 1979–2006 was about 430 mm, relatively high when compared toother records from Spitsbergen. The mean annual air temperature was−4.4 °C (2012) Mean annual air temperature has increased +0.095 °C a^{-1} over the last three decades.	[a,b] Undulating moraine complex: fluted moraine, changing towards the west into a flat moraine	[a]*Polar desert* Growth season: late June to mid-August Vegitation: Lichens (12 hens (12 yrs) Saxifraga S. oppositifolia (30 -80 yrs) S. caespitosa (30 - 80 yrs) P. arctica & Cerastium alpinum (80yrs)
European Alps								
[2]Morteratsch Swiss-Alps	0 to 128	48, N 1900-2117	[d]*Granitoid* metagranites greeenschist facies	[d]The soil parent material can be considered as relatively homogeneous	[e]Supra, En, Sub	[d]*Alpine* Post 1850 there has been a similar prevailing climate ±1-1.5 °C mean annual air temperature 5 °C and approx. 1000–1300 mm mean annual precipitation	[d]Undulating moraine complex with a mean slope of <10%	[d]*Alpine/alpine tundra* Growth season: late June to mid-October Vascular plants *Epilobium fleischeri* and *Linaria alpina* (7yrs); *Oxyrietum digynae* (12yrs) green alder grows continuously and is the dominate species at 100yrs, larch and pine forest establish at 77 yrs

[3]Damma, Swiss-Alps	0 to 136	46, N 1900-2100	[f,g]*Granitoid* metagranites greeenschist facies	[g]Bedrock reflects the mineralogical composition and along the chronosequence this is relatively constant	[j]Supra, En, Sub	[h]*Alpine* 2007 to October 2009, the mean annual air temperature was 2.2°C and mean annual precipitation was 2300 mm yr^{-1}	[g]Moraine complex with braided stream system that merges downstream urther away from the forefield in a relatively flat area	[h,i]*Alpine/alpine tundra* Growth season: late June to mid-October mosses, lichens, forbs, and grasses and vascular plants: species: *Agrostis gigantea Roth, Rumex scutatusL., Cerastium unifl orum Th om. ex Reichb., and Oxyria digyna (L.)* grostis gigantea, Salix spp (6-13yrs); Deschampsia cespitosa (L.) Roem. & Schult., and Athyrium alpestre (Hoppe) Milde (57-79yrs). Vegetation cover is full and is characterized by woody plants such as Rhododendron ferrugineum L. and Salix spp.
Lys NW Italian Alps	0-150	45°, N 1990-2480	[k]*Serpentine of theantigoritic type and* ~10% gneiss	[k]Bedrock that is homogeneous	[m]Supra, En, Sub	[k]*Alpine* the mean precipitation is 1200 mm yr^{-1} The mean annual air temperature is between -1 and +2°C	[k]Forest floor and present-day glacier front the slope is steep and eroded, after 200m it levels out, slope mean 13.5%	[k]*Alpine/alpine tundra* Growth season: late June to mid-October Larch forest with R. ferrugineum and grazed grassland for detailed species list, see D'Amico et al., 2014
Verra Grande NW Italian Alps	0-150	45°, N 2070-2320	[l]*Serpentine antigoritic type*	[l]Does not state although as monolith assumed to be homogeneous	No info available although as the glacier has a temperate thermal regime it likely has Supra,En, Sub	[l]*Alpine* the mean precipitation is 730 mm yr^{-1} The mean annual air temperature is between 0 and +2°C	[l]The western site was lateral morainic crests and the eastern ones (E sites), in the flat intramorainic area, remnants of frontal/recessional moraines (C sites), No info other on forefield topography	[l]*Alpine/alpine tundra* Growth season: late June to mid-October Salix ssp, Dryas octopetala L., basophilous grasses and serpentine endemic and Ni- hyperaccumulator species Outer slope are dominated by European larch (Larix decidua Mill.), with sparse stone pine (Pinus cembra L.), 192 Norway spruce (Picea abies Karst.) and birch (Betula pendula Roth) specimens

USA, Alaska								
Mendenhall	0-200	58, N, 1,893	[n]*Primarily granitoid* with subunits of amphibolites and and tonalite	[n]Leaching of the moraines may have begun before they were free of glacial ice mostly uniform till 80% grantic rock along the sequence	[n,p]Supra, En, Sub	[n,o]*Polar* The mean annual precipitation is ca. 250 cm and mean annual air temperature <8°C although like much lower as recorded near sea level in Juneau	[n]Undulating moraine complex	[n]*Tundra/montane forest* Growth season: n/a dwarf fireweed, followed successively by willow and alder trees and then spruce, which dominate the oldest moraine lupines (Lupinus sp.)
China, Tibetan plateau								
[4]Hailuogou		29, N 2982 to 2855	[q]*Metasedimentary* chlorite schists, quartzite, smaller amount of phyllite	[q]'mixed'	[s]Supra, En, Sub	[q]*TibetanPla-teau Frigid Zone and the Warm-humid Subtropic Monsoon Zone* The mean annual temperature and mean annual precipitation is 4.2 °Cand 1947 mm, respectively	[q]All sampling pits were under canopies of the dominant plants of each stage, not on steep slopes or near small streams within the chronosequence	[q,r] Bare rock (0yrs) Astragalus adsurgens Pall., Hippophae rhamnoides L.(12yrs) Hippophae rhamnoides L., Populus purdomii Rehder (30yrs) Populus purdomii Rehder (half-mature) (40yrs) Abies fabri (Mast.) Craib (half-mature) (52yrs) Abies fabri (Mast.), Craib Picea brachytyla (Franch.) E.Pritz.(80yrs) Picea brachytyla (Franch.) E.Pritz., Abies fabri (Mast.) Craib (120yrs)

Citations: [a]Kabala & Zapart, 2009; [b]Kabala & Zapart, 2012; [c]Sen & Jun, 1995; [d]Mavris et al., 2010; [e]Cook & Swift, 2012; [f]Bernasconi, 2008; [g]Bernasconi et al., 2011; [h]Smittenberg et al., 2012; [i]Banwart et al., 2011; [j]Hindshaw et al., 2011; [k]D' Amico et al., 2014; [l]D' Amico et al., 2014; [m]Badino et al., 2001; [n]Alexander & Burt, 1996; [o]Burt & Alexander, 1996; [p]Gimbert et al., 2016; [q]Zhou et al., 2016; [r]Xun & Shangfa, 1995; [s]Geng-nian et al., 2009

2.3. Glacial forefield rock heterogeneities and how they affect soil formation

Pioneering non-glacial forefield soil development studies have provided evidence that the parent material determines the original supply of nutrient elements that are released by weathering. This in turn influences the balance between inorganic and organic nutrient loss and retention (Torn et al., 1997; Jenny, 1994). Considering this, understanding the properties of the parent material is integral to the initial stages of soil development. Yet, to date, studies on multi-lithological parent materials are lacking. In some studies, mono-lithological glacial catchment areas were targeted instead, as these contain more chemically and physically homogenous parent materials (Alexander & Burt, 1996; Bernasconi, 2008; Mavris et al., 2010; D' Amico et al., 2014). The use of more homogenous parent material is advantageous, because it provides a consistent baseline (Jenny, 1994). Other studies conducted on multi-lithological parent material (e.g. Kabala & Zapart, 2009; Zhou et al., 2016) have tried to overcome the heterogeneity issues by sampling 'mixed' parent rocks. However, their use causes doubt over how representative the material is. Moreover, these studies assume that the glacial soils are relatively homogenous because of glacial mixing' (e.g. Kabala & Zapart, 2012; Zhou et al., 2016), but there is little evidence for this. For example, Burt and Alexander, 1995 state that "leaching of the moraines may have begun before they were free of glacial ice", but is not backed up with evidence. No consideration was given to variations in glacial till types derived from supraglacial, englacial and subglacial domains that give rise to considerable variance in their physical and chemical properties.

Studies of the differential rates of soil formation in forefield sequences have been shown to be dependent on the lithological properties of the parent material (e.g., D'Amico et al., 2014). In this study, comparison of the forefield till parent materials' lithologies, showed formation rates, in monolithic serpentine, granitoid and serpentine with 10% gneiss, characterized by higher initial rates than those with gneiss and granitoid, Fig. 2.4 (Egli et al., 2012; Egli et al., 2014; D'Amico et al., 2014). The best fit was a decay function for the gneiss/granitoid lithologies, while serpentine lithology showed a slower initial onset rate characterized by a humped function. Retarded soil formation rates from serpentine were a consequence of declined soil fertility, caused by the paucity of macronutrients (N, P, K). Abundant toxic heavy metals (Ni, Cr, Co) in the parent material, and weathering resulted in low Ca:Mg ratios, poor soil structure and nutrient retention.

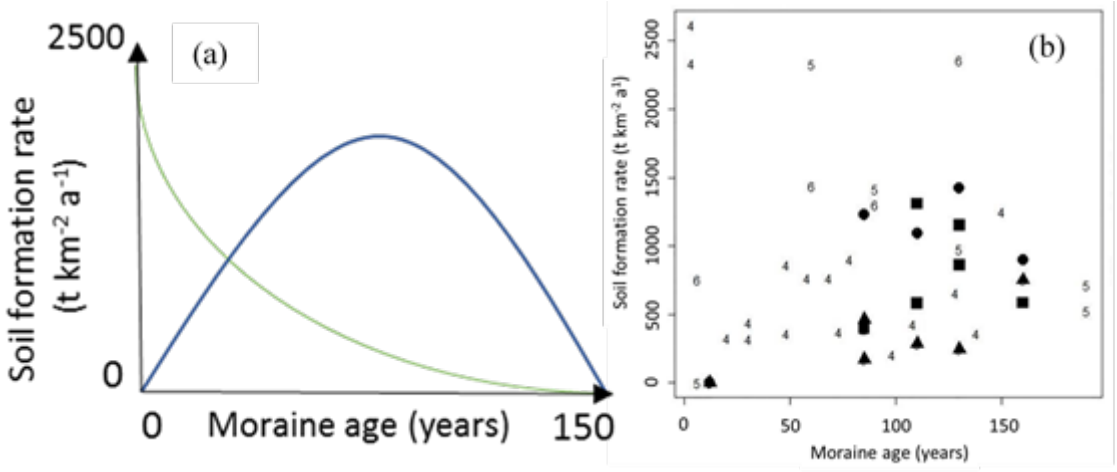

Figure 2.4. Soil formation rates from D'Amico et al., 2014 (a) from their collated empirical data (b) in the Morteratsch forefield (plot points no. 4 from Egli et al. 2012 and Egli et al. 2014, Swiss Alps and Lys forefields from D'Amico et al., 2013 and Verra Grande, north-western Italian Alps (the eastern, western and central moraine systems are represented by respectively full circles, triangles and squares) D'Amico et al., 2014

Glacial sedimentological studies have shown that in many complex geological catchments glacial tills are inhomogeneous due to their lithological provenances and transits through the glacial domain (Benn and Evans, 2014). Debris transported by glaciers is derived either from erosion of the subglacial bed, or supraglacially from the valley sides. Since many of the forefields studied previously consist of subglacial and supraglacial till types this is potentially an important factor that has been overlooked, (Table. 2.1). The glacial till type affects the forefields' soils parent material composition and development. Supraglacial till is a product of rock wall fracturing and landslides above the glacier onto its surface, and comprises a dominantly coarse fraction with angular boulders, and a bimodal grain size distribution. As a result,, englacial or supraglacial transport is passive so little comminution occurs, meaning finer and potentially more reactive particle sizes are less abundant. Supraglacial till also undergoes little homogenisation prior to its deposition in the forefield. In contrast to this, the subglacial till debris eroded from bedrock is initially transported in a basal traction zone beneath a glacier. In this zone, particles frequently meet the glacier bed and are comminuted into fine glacial flour by the large ice-till-bedrock forces that are generated here (Boulton, 1978). Glaciofluvial processes in the subglacial domain causes substantial mechanical mixing and abrasion of the glacial till. This can increase its lithological homogeneity prior to its deposition in the forefield, while predisposing brittle (e.g. platy minerals like mica) and/or low hardness minerals and their surfaces to chemical weathering (Föllmi et al., 2009). Where the

till is turned to fine glacial flour, it promotes rapid dissolution of microparticles (Petrovic et al., 1976). Their high reactivity is a result of their high surface area and newly exposed surfaces (Tranter, 1982), with geochemically reactive phases, such as carbonates and sulfides (Tranter et al., 1993; Raiswell and Thomas, 1984; Anderson et al., 1997). In addition to this, there is a lack of inorganic (e.g. iron oxyhydroxides and clays) and/or organic coatings on heterogeneous mineral surfaces (Tranter, 1982). Finally, there is often a high proportion of silt-sized particles in subglacial glacially derived moraine. Importantly, the factors that can affect the reactivity of subglacial till are strongly dependent on the structure of the drainage system. Glacial till, present in a forefield coming from a subglacial system with predominately distributed and delayed melt-water flow, may be depleted in a comminuted and chemically reactive till-size fraction. For instance, under slow flow conditions a prolonged residence time prevails, so, reactive phases are left inhibited (Tranter et al., 1994). Conversely, a subglacial drainage system with channelized and high velocity melt-water flow can rapidly remove freshly eroded till and deposit it in a forefield. It is evident from the differences in subglacial and supraglacial tills that their characteristics need to be evaluated, as they are parent materials which may affect soil development in forefields.

2.4. Mineral material and organic carbon additions and pools

Forefield soils consist of two main materials, minerals and organic matter. These can be added *in-situ* within the soils itself (autochthonous), or externally (allochthonous). In a glacial forefield a multitude of mineral material and organic matter soil additions have been identified that contribute to changing the carbon pools (Fig. 2.5). For a detailed review of organic carbon and other nutrients in forefields, Bradley et al., 2014 should be consulted. The soil addition pathways that primarily concern those that impact the carbon cycle, are discussed briefly below.

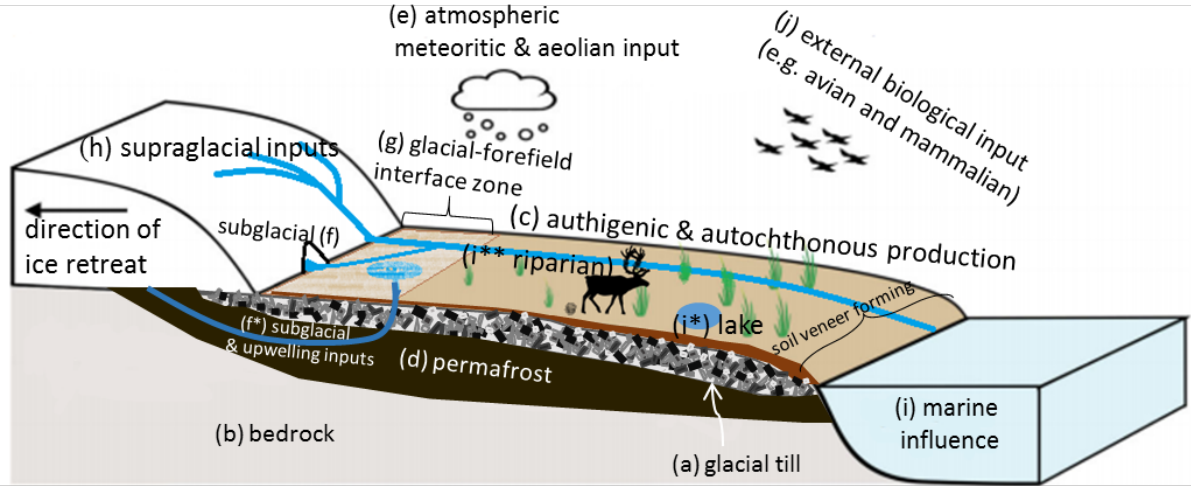

Figure 2.5. Schematic diagram of a glacial forefield and their key characterises and inputs to the soil veneer that, in general, forms with increased soil age away from the retreating glacier. Modified from Bradley et al., 2014.

The mineralogical composition of the parent material is dependent upon the type of lithological units present in a glacier catchment. Common rock-forming minerals in forefield parent materials, that are important in the carbon cycle, are primarily Ca-Mg silicates. Namely, olivine, diopside, wollastonite and various feldspars (albite Na endmember and Ca endmember anorthite). The carbonate minerals calcite and dolomite, or minerals like sulfides e.g., pyrite enhance weathering reaction kinetics through geo-bio-catalytic reactions (Anderson et al., 2000). Authigenic (c), or allochthonous addition of sheet-silicates, (e.g., phyllosilicates; that consists of the mica group, serpentine and clay minerals) play a crucial role in forming soil structure. This is by aiding soil particle aggregation that can stabilize carbon (discussed in section, 2.5.1) (Six et al., 2002; McBride, 1989). Organic carbon is also found in glacial till parent materials, as evidenced through isotopic and organic-carbon based speciation. These analyses also revealed that organic carbon is primarily present as either diagenetic kerogen (aromatic hydrocarbon compounds) and/or other carbon-based polymeric compounds, from paleo sols and relic soils frozen, as permafrost (Bardgett et al., 2007; White et al., 2007; Bernasconi et al., 2011).

Allochthonous atmospheric, and aeolian additions to forefields, are an emerging area of interest. Their quantity is unconstrained, and could be important in soil forming processes (Bradley et al., 2014; Bradley et al., 2016b). For example, over the Damma glacier in the Swiss Alps, proximal to the forefield, 0.4 to 1.2 g of C per m^2 per year was deposited, and could therefore be a considerable input to the carbon stocks in the forefield soils (Brankatschk et al.,

2011). Although unquantified, the annual melt of snow cover in a forefield has been observed to supply black carbon, N and other pollutants (Larose et al., 2013). Modelling indicates that in older soils (>40-years) increased deposition of organic carbon helps sustain higher rates of bacterial and vegetation production. Heterotrophic respiration is predicted to lead to a decrease in the net ecosystem CO_2 efflux from Arctic forefield soils, and is another factor that sustains a stable soil organic carbon pool there (Bradley et al., 2016b). The models relies, in part, on data from non-Arctic forefields, and as little data from Arctic forefield exists, the stability of the soil organic carbon pool in glacial remains largely unknown.

Autochthonous production (c) in a soil-forming forefield is strongly dependent upon the rate of soil ecosystem evolution, and in turn the other ecosystems it supports. Soil fauna and flora communities assemble as a function of soil age (Hodkinson et al., 2001; Hodkinson et al., 2003; Conen et al., 2007). However, in Alpine forefields this can be non-linear, occurring as spatially distributed micro-niche soil fauna and flora communities (Burga, 1999). Organic carbon inputs include carbon-based plant parts, algae, fungi, lichen and their litter, invertebrates, microbes and their necromass. In Alpine forefield ecosystems, plants are the dominant autochthonous addition to the soil, while microbial biomass is lower. The relative proportion of the remaining biomass is unexplored (Conen et al., 2007; Bernasconi et al., 2011). In Arctic forefields, limited knowledge exists on autochthonous production additions. It has been found that autotrophic microbes occur at a higher relative abundance in younger soil age, while heterotrophic and autotrophic microbes are abundant at older soil ages (Hodkinson et al., 2001; Hodkinson et al., 2003; Bradley et al., 2016b). There is poor knowledge of the relative proportion of carbon-based biomass microbial, vegetation and ancient carbon. A simple mass balance of the results used to constrain the model, suggests that ~99.9% of the TOC is unaccounted for (Table 2.2).

Table.2.2 Microbial biomass in the forefield of Midtre Lovénbreen (brackets show 1 standard deviation). Table obtained from Bradley et al., 2016

Soil age (years)	Autotrophic microbial biomass (µg C g⁻1)	Heterotrophic microbial biomass (µg C g ⁻1)	Total organic carbon (µg C g ⁻1)
0	0.171 (0.042)	0.059 (0.034)	792.984 (127.206)

Furthermore, vegetation biomass is overlooked and not currently incorporated into the latest High-Arctic microbial and biogeochemical dynamics in glacier forefield ecosystem models (Bradley et al., 2016). Fundamental to this is the lack of in-field empirical data. Quantification of microbial and vegetation contributions in carbon soil additions, would better inform short

and long-term soil organic dynamics; despite the possible rapid temporal and spatial fluctuation (Bradley et al., 2016a; Bradley et al., 2017).

Other external soil additions are delivered by episodic flood/discharge events (Wadham et al., 2001). Aqueous solutions form from upwellings in the sub- and supra-glacial domains (Irvine-Fynn and Hodson, 2010), or glacial meltwater mixing and ground saturation at the glacial-forefield interface zone. Solution addition also occurs in the vadose zone around channels that ingress the forefield. These channels transport both glacial and forefield solutes laterally through till deposits into the forefield (Cooper et al., 2002). Glacial tills also receive additions from geogenic and biogenic weathering-derived particulate and leachate, not limited to sulfides and sulfates, inorganic and organic phosphorus, diagenetic nitrogen and organic matter, base cations (Ca, Mg, K and Na) and silica. For a more detailed review of glacially derived nutrients to proximal environments consult Hodson et al., 2005; Bradley et al., 2014; Anesio et al., 2017. From the supraglacial environment, the forefield receives particulates and leachate that consists of organic and inorganic nutrients. As ice melt is usually quite dilute (ionic strengths < 40 umol/l), their concentration in meltwater runoff tends to be low (Hodgkins et al., 1997). The interaction of unsaturated supraglacial meltwater with crushed subglacial till, could lead to enhanced reaction rates and soil formation at the glacial-forefield interface.

Marine, limnological, and riparian influences supply sources of organic matter and nutrients through aerosols and lateral groundwater to soil-forming tills (Wadham et al., 2001b; Cooper et al., 2002 Barrett et al., 2007). Furthermore, secondary efflorescent salts (e.g. gypsum) are added or removed to the soil as they precipitate or dissolve thought the melt season (Cooper et al., 2002). It is the prevailing metrological conditions that regulate the supply of these nutrients to a forefield, through changes in the groundwater level and thermal regime of the soil/permafrost controls (Cooper et al., 2002; Cooper et al., 2010). The tills proximity to the ocean, and waterbodies such as kettle ponds and proglacial channels, affects the salts, organic matter and nutrient delivery to a forefield. Tills nearest to these nutrient stores generally receive higher delivery, yet have a lower residence time, as aerosol and precipitation inputs result in nutrient leaching (Anderson et al., 2000; Cooper et al., 2010).

External biological inputs e.g. avian and mammalian, guano and droppings both act as a carbon inputs as well as a soil fertiliser. Nutrient inputs such as these, provide biologically assimilable P, N and (Hodkinson et al., 2003; Mindl et al., 2007). Where nesting bird colonies are near

glacial forefields, neighbouring soils are often highly fertile (Simas et al., 2007; Robinson et al., 1995). In open and exposed Arctic forefields, predation from Arctic foxes means guano benefits to a soil are limited, as fewer birds nest and feed there (Larson, 1960). Dung inputs from macro fauna may also enhance soil fertility. However, areas grazed by reindeer are generally nutrient poor, such as High Arctic forefields, as their dung mostly contains resistant, lignin-based carbon (Ritchie et al., 1998).

2.5. The carbon cycle in newly deglaciating terrain

The biogeochemical carbon cycle is where carbon, inorganic or organic, is exchanged among the biosphere, pedosphere, geosphere (lithosphere), hydrosphere, and atmosphere of Earth. In glacial forefields these spheres converge readily, meaning that carbon species can interchange frequently. The hydrosphere and atmosphere meet the geosphere and interact as glaciers melt and rock-water interactions take place. While the connection of these spheres facilitates the development and mutual stimulation of pedosphere and biosphere. Collectively this series of interactions between spheres regulates the carbon transfer in glacial forefields.

For simplicity, and since substantially more literature exists on organic carbon dynamics in forefields, compared to inorganic carbon, these types of carbon are addressed separately.

2.5.1. Organic carbon dynamics

As almost half of life's dry mass on earth, and also half of the organic matter accumulating in soil, is composed of carbon, the carbon cycle has a central role in biochemical processes in almost all ecosystems (Chapin et al., 2006; Chapin et al., 2009). Glacial forefields' ecosystems are no exception, and although a multitude of components in the carbon cycle have been identified, this is largely unexplored. Forefield carbon cycling is known to proceed over short-term, annual, and long-term timescales by a series of biogeochemical reactions. A breakdown of all forefield carbon cycle chemical reactions not explicitly mentioned in this chapter are given in Appendix. A. Table. 2. The longevity of organic carbon residence time in a soil is strongly temperature dependent. This is predominantly due to biota that has a q^{10} temperature coefficient of respiration. Biota, necromass and biochemical reactions such as photosynthesis adds carbon to a soil. Soil biota also breakdown carbon by oxidation as part of their metabolic

functions. Therefore in forefields both temperature and biota can have a rapid effect on carbon transfers between the atmosphere, biosphere, pedosphere and hydrosphere in warming induced glaciating forefields (Smittenberg et al., 2012; Kirschbaum, 2000).

In a developing forefield ecosystem, in response to soil formation, organic carbon cycling can proceed with autotrophic organisms (i.e. plants) that produce their own organic compounds (e.g. polysaccharide compounds), using CO_2 from air through photosynthesis. Heterotrophs, like bacteria and fungi that feed on autotrophs, can transfer carbon to the biosphere and facilitate its stabilization in the pedosphere as soil organic matter. The biota's intimate association with soil minerals, means SOM of a soil helps retain its nutrients and act as a carbon sink, ~50-58% (Torn et al., 1997; Périé, C and Ouimet, R. 2008). Soil organic matter consists of a continuum of organic fragments, and is continuously processed by the decomposer community from large plant and animal residues towards smaller molecular size (Lehmann and Kleber, 2015). Biodegradation causes CO_2 to be released back to the atmosphere through respiration Eq. 2.2, 2.3, 2.4 and thus, completing the cycle.

$6CO_2 + 6H_2O + \text{Light Energy (Sun)} \rightarrow C_6H_{12}O_6 + 6O_2$ – photosynthesis Equation 2.2.

$C_6H_{12}O_6 + 6O_2 \rightarrow 6CO_2 + 6H_2O$ – respiration (oxic) Equation 2.3.

$2H^+ + SO_4^{2-} + 2CH_2O \rightarrow 2CO_2 + H_2S + 2H_2O$ – biodegradation of C in anoxic soils Eq. 2.4.

Evidence of ecological and pedogenic evolution in response to deglaciation has shown total organic carbon to accumulate rapidly in newly deglaciated terrain, over just a century or two. Interestingly, TOC seems to accumulate irrespective of forefield locale, suggesting similar processes could contribute to its accumulation. The rate of initial TOC accumulation, temporal variability in its concentration, and the asymptotic value, seems to be strongly dependent upon regional factors (Fig. 2.6). This suggests that soil forming factors control these (Eq. 2.1). To critically evaluate the differences in TOC, the controls of soil formation in newly deglaciating terrain were assessed.

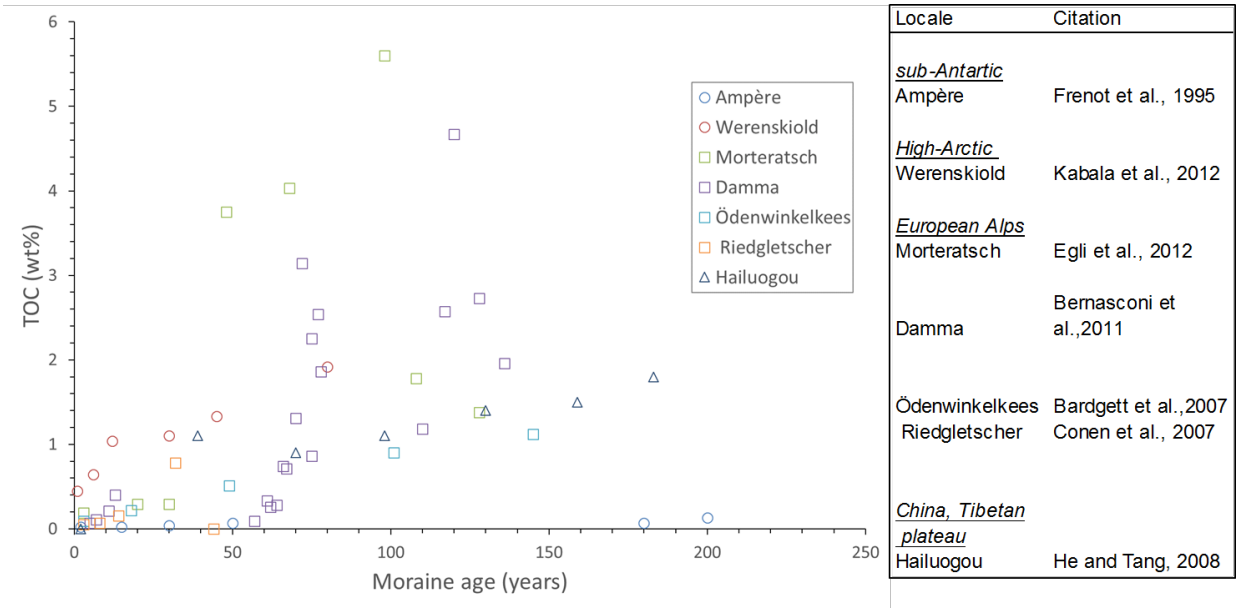

Figure 2.6. Total organic carbon concentrations from different glacial forefields at different locale. Note: forefields in polar region have lower TOC concentrations and rates of accumulation, while forefields in the European Alps have higher TOC and rates, but considerable temporal variation. Note: Each source of data is tabulated to the left of the figure.

In soil, TOC is present primarily as SOM, therefore its turnover and controls are subsequently discussed. The mean residence time of SOM in soils is ~50-years, but decadal variance occurs dependent on the type of organic carbon present (e.g. Schmidt et al., 2011; Fig. 2.7.a). Although the effects of carbon substrate on TOC dynamics has not been directly observed, its effects on SOM dynamics over a century or two of deglaciation are apparent. Forefield soil development studies have observed a chronological shift in the carbon species that make up SOM. There is a shift with increasing soil age, from aromatic carbon, formed as part of 'ancient' paleosols, to primarily 'modern' microbial-derived, aliphatic carbohydrates and proteinaceous species (Bardgett et al., 2007; Dümig et al., 2011). Mounting evidence from soil development studies in forefields indicate that it is ecosystem evolution of fauna and flora that drives this shift in SOM carbon species. This is an interesting characteristic that common to different forefield environments, for example, and European Alpine forefield (Damma) (White et al., 2007; Dümig et al., 2011; Dümig et al., 2012). It can be inferred that the chronological shift in carbon species, during ecosystem evolution and soil development, is less dependent on local factors and more dependent on the rates of chemical change. Additional validation of such a chronological shift in carbon type within SOM has been shown using radio-carbon based aging. These results showed that at soil ages of <50-years, ancient carbon was the dominant source of soil-respired CO_2. In older soils, >150-years, 90 % of the soil-respired CO_2 from modern

carbon biotic inputs, while ancient carbon concentrations remained unchanged (Guelland et al., 2013a; Guelland et al., 2013b).

In ecosystem evolution, carbon species shift and soil development is mutually interlinked. The notion suggested by Schmidt et al., 2011 is that soil organic matter is more of an ecosystem property. This de-emphasises the role of molecular structure as a control on SOM. They suggest that molecular structure alone does not control SOM stability, rather, that environmental and biological controls predominate (Schmidt et al., 2011). If this were the case, both finite stores of lithogenic, ancient aromatic carbon and modern aliphatic carbon could be expected to be respired over a century or two soil chronosequence. As discussed in the previous paragraph, this is not the case, and there is a distinct switch from aromatic to aliphatic carbon, despite the aromatic store remaining in the soil. The molecular structure of SOM seems to play a controlling role on C stability, which is more fitting of the effects of 'negative priming' (Kuzyakov et al., 2000). Negative priming is defined as soil organic matter mineralisation retardation due to any treatment such as the addition of a new substrate. It may occur due to the divergence of microbes, or their enzymes, to utilise the more easily available substrate. Or, to the inhibition of microbial activity because of a change in the soil environment. Another plausible form of negative priming in forefields are modern carbon inputs by organo-mineral stabilization, physical disconnection and freeze/thaw processes (Fig 2.7.b). These are often discussed as SOM preservation mechanisms: the added substrate contains an absorptive component or porous material, in an environment prone to thermal-mechanical processes. Sorption and a soils porosity, are in principle strongly dependent upon the molecular properties of SOM and its residence time; highlighting its importance as an SOM control (McBride, 1989; Lehmann and Kleber, 2015). Sorption and desorption processes are linked to soil particle aggregation. Particle disintegration is also strongly influenced by soil mineralogy, and its interaction with SOM (discussed in detail below). The molecular properties of SOM have a significant role in controlling its stability in soil. Moreover, SOM controls soil functionality and is important in determining the quantity, and stability, of organic carbon stored in soil (Torn et al., 1997).

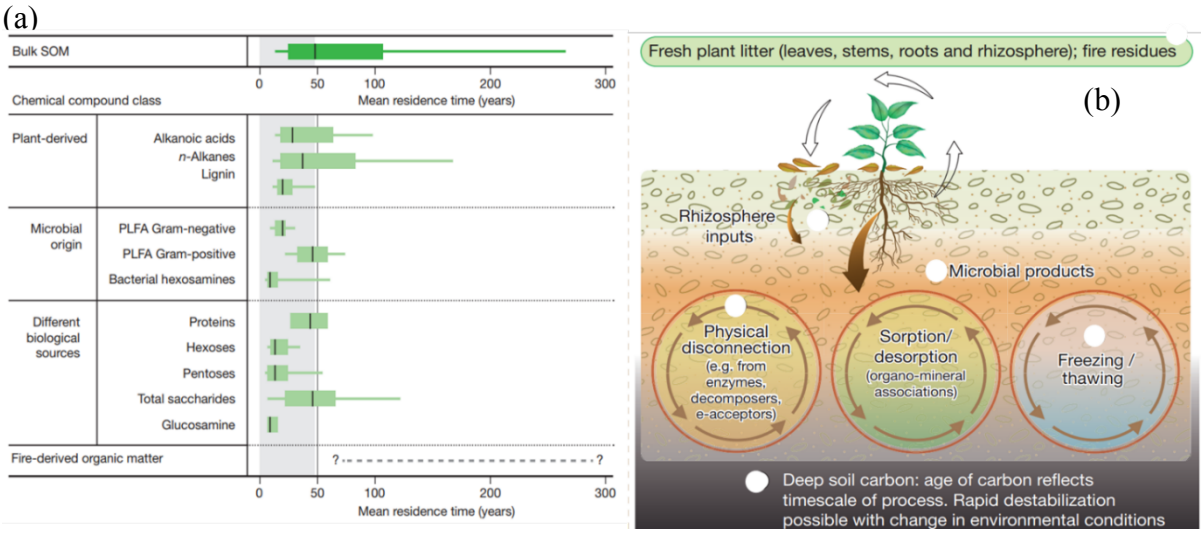

Figure 2.7. (a) Mean residence time for organic carbon compounds in soils that is plant-derived, microbial origin, and other biological sources. **(b)** soil organic matter protection mechanisms, modified from Schmidt et al., 2011.

Clay minerals and poorly crystalline mineral phases, e.g. ferrihydrite, can significantly affect a soils carbon storage (Oades, 1988). When SOM interacts with mineral surfaces to form organo-mineral associations it is affected by pH, the base saturation of the soil. The strength and longevity of organo-mineral associations depends upon the minerals' surface charge, the types of functional groups in the organic matter, the presence of proteins and surface reactivity inhibitors. Organo-mineral associations often occur as occluded zonal layers away from the mineral surface (Kelber, 2007). A few common mechanisms for organo-mineral complexations are presented in Fig. 2.8, for a detailed account organo-mineral interaction see, McBride, 1989.

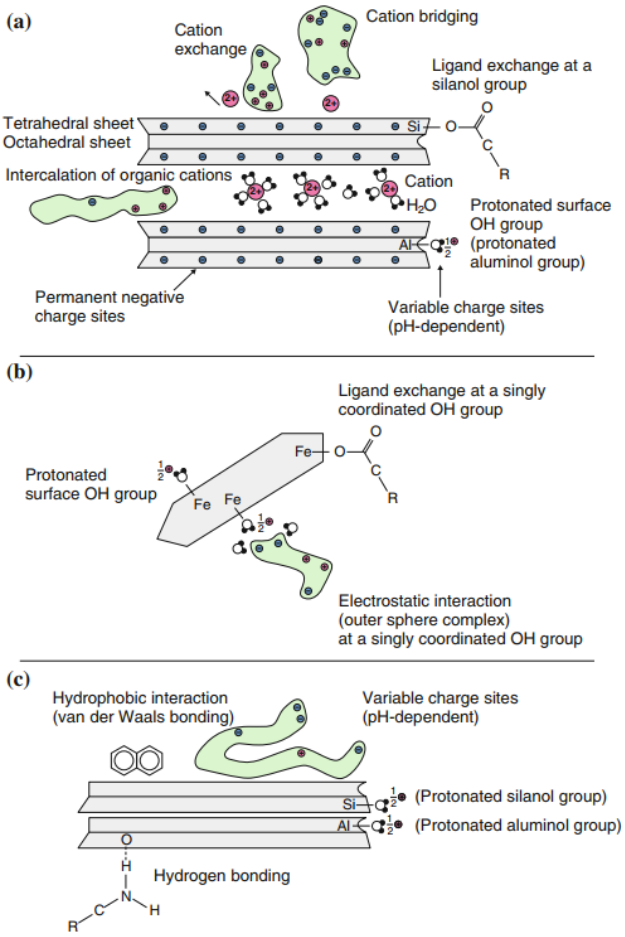

Figure 2.8. Binding mechanisms of clay-humus coupling in the soil. (a) On phyllosilicates with permanent charge, (b) on hydroxide surfaces with variable charge, (c) on minerals with neutral surfaces. Modified from Blume et al., 2015.

Soil formation studies in forefield have helped in paving the way to understanding organo-mineral interactions in natural systems. They have revealed the interactions of mineral weathering and organic carbon accumulation, linked to soil stability and ecosystem growth (Dumid et al., 2012). This leads to the understanding that young soils have 3–4 orders of magnitude higher rates of development than old soils ($10^5$to 10^6yr) (Egli et al., 2014). For example, in the Damma forefield, results have shown that organo–mineral associations form stepwise over ~100 year of deglaciation; proteinaceous compounds and carbohydrates accumulated in the proglacial area by microbial-plant synthesis (75 and 120-year-old clay fractions). This was preceded by the production of organic acids through vegetation expansion that lowered soil pH and increased parent material weathering. This in turn released aluminum and iron from the parent material as poorly crystalline phases, such as ferrihydrite. The organic carbon which accumulated, was, over time, adsorbed onto these mineral surfaces, and this in turn had an inhibitory effect on their crystallization to increase their stabilization. Finally, soil

aging further enhanced OM sorption, as protonation made the surface hydroxyl groups more ion exchangeable (Dümig et al., 2011; Dümig et al., 2012). Concurrent with these observations, Kabala and Zapart, 2012 found that in the foreland of Werenskiold in the High-Arctic, biota assemblage was slow compared to the Damma forefield due to the prevailing polar climate. Since chemical weathering evolution was slow, there was a negligible decline in the pH, thus pedogenic Fe formation of poorly crystalline mineral phases, and in turn organic carbon accumulation was limited. These contrasting results, highlight the dependency of chemical weathering rates on climatic and soil biota states in developing forefield soils.

Other than poorly crystalline iron and aluminum, minerals that facilitate organic carbon storage, and have high specific surfaces areas, are clay minerals. Particular examples are expandable phyllosilicates i.e. smectites like vermiculite with charged mineral surfaces, (Bergaya, 2006). In forefield settings, organic carbon stabilization by clay minerals is shown to be less wide-spread than poorly crystalline iron and aluminum minerals (Dumid et al., 2012). This is a product of differential rates of silicate weathering, leading to either minimal clay mineral production (e.g. the Damma; Bernasconi et al., 2011), or a low abundance of 2:1 smectites from biotite weathering (e.g. the Morteratsch Mavris et al., 2010). Alternatively, an intensive weathering regime gives early formation of 1:1 kaolinite from plagioclase (Mavris et al., 2011). Kaolinite can have a lower adsorption of organic carbon due to its low, and often uncharged mineral surface, although some hydrophobic organic compounds may also associate with its surface (Kleber et al., 2007). The difference in the Damma and Morteratsch forefields' silicate weathering regimes are discussed in more detail in Section 2.5.2.

From the evidence presented, glacial forefields have been paramount in providing a contemporary view on soil carbon dynamics. Traditionally, it was believed that organic matter stabilization was achieved by 'humifaction', condensation reactions that led to the organic matter having a 'recalcitrant' molecular property. However, lack of evidence for 'humic substances' (Schmidt et al., 2011) has led to a new paradigm, the soil continuum model (SCM) (Lerhman and Kebler., 2015). The model proceeds as follows: organic carbon stabilization is regulated through aggregate formation-destruction and mineral weathering that facilitates the sorption-desorption of assimilable <600 Da, and non-assimilable >600 Da, which arises due to a series biogeochemical degradation reactions. These reactions are largely controlled by temperature and precipitation, Fig. 2.9. As glacial forefields are ideal natural laboratories

(discussed in Section.2.2) new advancements in soil and its carbon dynamics within the carbon cycle will be continued to be made.

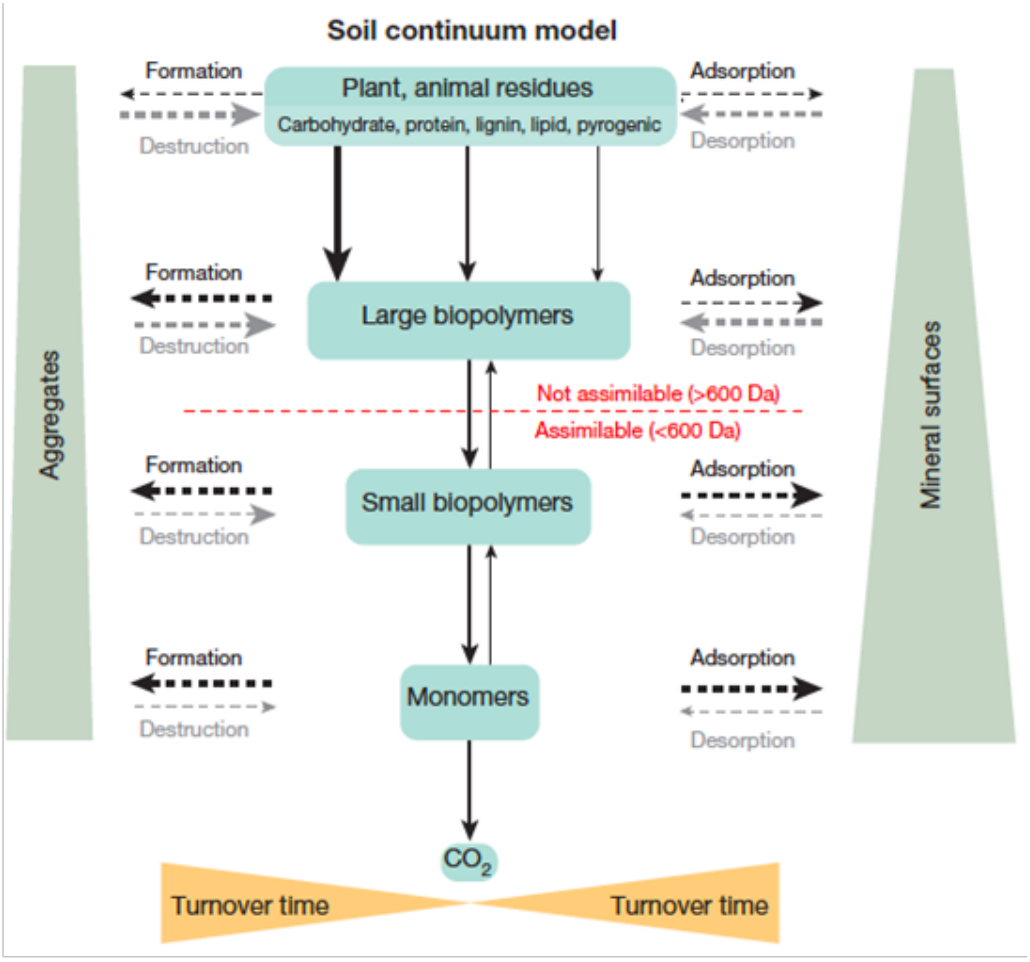

Figure 2.9. The soil continuum model (SCM), a new paradigm of soil organic matter regulation in a soil, obtained from Lerhman and Kebler., 2015.

2.5.2. Mineral weathering of inorganic carbon from silicates and carbonates

In comparison to the biological carbon cycle, mineral weathering in the geosphere is considered part of the long-term geological carbon cycle, though both are intrinsically linked (Berner et al., 2003; Berner and Berner, 2012). Biological mediated weathering involves the capture or release of CO_2 and this can improve a soil's structure to support the growth of biota. The role of biological weathering as a catalyst in weathering is highlighted in the following silicate, sulfide and carbonate mineral weathering sections.

2.5.2.1 Silicate weathering

Ebelmen, in 1845, originally proposed weathering of Ca/Mg silicate minerals that draws down atmospheric CO_2 and locks it in the lithosphere as marine carbonates (Urey, 1952). This reaction is responsible for lowering global temperature on geological timescales (Berner, 1994), (see Appendix. A. Table. 2). Silicate weathering occurs over geological timescales, however the rate limiting step is affected by environmental and chemical factors. Limitations to silicate weathering generally include two different processes: transport limitation and kinetic limitation. To transport-limited weathering regimes, the supply of water, acids and (organic) ligands relative to the supply of silicate minerals is large (West et al., 2005). Whereas, where kinetic limitation (Eq. 2.5) is the main control on chemical weathering, silicate weathering ω depends on the kinetic rate of mineral dissolution W, the supply of material (e.g., by erosion) *e*, and the time *t* available for reaction (West et al., 2005).

$\omega = W.e.t$ Equation 2.5.

Glacial forefields offer a unique terrestrial setting for accelerated silicate weathering. At the glacial-forefield interface, and to some extent in moraine complexes, they are transport-limited environments. Consequently, the kinetic limitation is low because:

a) Large areas of glacial till within a moraine remain *in-situ*, unless it is hydrological or thermally re-worked.

b) Intense physical weathering precedes chemical weathering to produce finely comminuted, highly reactive 'rock flour' which can be a significant proportion of subglacial forefield tills, discussed in Section 2.3, (White and Brantley, 1995; Boulton, 1973).

c) The young soil has mineral surfaces that are enriched with charged, unreacted metals (e.g. oxidised or hydrolysed), or are inhibited by mineral precipitation or adsorption of compounds (e.g. organic matter, ferrihydrite and phosphate); although, this depends on the parent material i.e. glacial till, pre-forefield history, discussed in section 2.3.

d) As weathering proceeds, biota assembles in the forefield soil and their evolution may enhance weathering. It has been shown in other soil forming environments that biological weathering can enhance rates by a factor of 2 or 3 as the pH is lowered by plant root respiration (Drever, 1994). The acidity can drive silicate dissolution, hydrolysis, and also promote organic ligand complexes with metal ions to increase their mobilization (Drever, 1994).

e) Glacial meltwater chemistries may contain an abundance of protons (acidity) that arise from the rapid oxidation of sulfides e.g. pyrite (if present in glacier catchment lithology). Protons have a high affinity for anionic silicate surfaces, or can replace metal ions at reactive sites within glacial rock flour.

f) Rock-water residence times are prolonged and enhance silicate hydrolysis. Furthermore, soil waters are episodically recharged and flushed by water inputs during the melt season and this can lower the ion concentration of soil solutions to promote silicate weathering (Anderson et al., 2000).

g) Climatic changes in Arctic glacial forefields have led to increased soil temperatures, and lengthened melt and growing season. In these polar deserts improvements in soil moisture have made favourable growing conditions to enhance biological weathering. In turn, better soil water retention improves its quality and leads to accelerated biogeochemical weathering rates (Borin et al., 2010; Kabala and Zapart, 2012; Smittenberg et al., 2012).

These environmental states could alleviate the kinetic limitation on silicate weathering compared to non-forefield soil-forming environments. For an in-depth review of silicate weathering rates in soils see White & Brantley et al., 1995.

There is no agreement about the rate of silicate weathering reactions in glacial forelands. Soil evolution and weathering models are generally best described by a humped or exponential function. Forefields with a humped function show that soil production and weathering is maximised at a certain soil depth or time and thereafter decreases (Mavris et al., 2010) (Fig. 2.4). Exponential decay functions in forefield soils are more common than humped functions and display a decrease in weathering rate with increased soil age (Egli et al., 2014). Interestingly, two forefields in the Swiss Alps, Morteratsch and Damma, evidenced either a humped or exponential decay function. This is despite both having over a century deglaciation and similar environmental conditions that control silicate weathering e.g. lithology (see, Table. 2.1). In these forefields, elemental and mineralogical analyses showed that the Morteratsch had significant weathering of biotite, hornblende, plagioclase formed smectite (with a low charge), vermiculite (with a high charge), and kaolinite. In the latter mineral, this occurred after only a decade (Marvis et al., 2010 and 2011). Conversely, in the Damma forefield, only a small extent of silicate to kaolinite clay mineral transformations was observed at >150 years. This was shown by the chemical weathering index of alteration and its incipient values CIA= 55-65 (fresh=50 weathered =100 i.e. kaolinite) (Bernasconi et al., 2011; Dumid et al., 2011). These results correspond with the low specific surface areas of the clay fraction, 7-22 $m^2 g^{-1}$ compared

to 35-100 m^2 g^{-1}, from various non-forefield soils that are significantly more advanced (Dumid et al., 2012). By comparison of measured forefield attributes, a significant difference in precipitation of 1300m compared to 2300m is apparent, (Table 2.1). As highlighted in a forefield in the New Zealand Alps, rainfall precipitation gradients cause a rapid, non-linear change in the total exchangeable cations, and increase in the movement and redistribution of metals, i.e. chemical weathering (Dixon et al., 2016). Even within the same region, silicate weathering rates in forefields are strongly dependent upon localised controls. In Arctic forefields' soils after <150 years of development there is a lack of vegetation that results from a prevailing polar climate. It was concluded silicate weathering is not enhanced (Kabala and Zapart, 2009). Unlike Alpine forefields, where Ca/Mg silicate weathering contributes to the sink of atmospheric CO_2, the retardation of Ca/Mg silicate weathering in Arctic forefields, as a CO_2 sink, is thought to be minimal. Continual proglacial meltwater measurements of base cation flux showed <10% silicate weathering products from proglacial melt streams (Anderson et al. 2000; Wadham et al., 2001). Meltwater chemistries are ideal for obtaining high-resolution chemical time-series data, measuring short-term changes as 'a continuum of snapshots' over the melt season. Good examples of such studies are from Sharp et al., 1995; Hodson et al., 2000; Wadham et al., 2001a; Wadham et al., 2007; Hindshaw et al., 2014. The method is limited by relying on sample collection at prescribed times, and thus may miss longer-term spacio-temporal variations. Furthermore, these approaches are valid only if it provides a truly representative environmental state of the chemical quality of water at the sampling site. As pointed out by Anderson: water flow in a forefield, through heterogeneous glacial till, is strongly dependent upon the prevailing hydrometeorological conditions, meaning a weathering signal maybe missed (Anderson et al., 2000). To compensate for this, corrections are made before upscaling, however, uncertainties in spacio-temporal variations may be large (Allan et al., 2006). Bulk measurements of forefield till would provide a complementary data set which validates the short-term, to reveal longer-term weathering trends.

2.5.2.1.1 Weathering indices, and sample mass gains and losses, for determining the extent of silicate weathering in newly forming glacial soils.

Chemical weathering indices are commonly used to quantify the rates of mineral erosion. Ideally, a chemical weathering index should permit the comparison of different localities, on different parent materials, and on weathering samples of different ages. Their application

encompasses a wide range of natural materials, such as soils. Indices are versatile, and if appropriately applied, effective, in accounting for complex material types and their weathering environments. Testament to this, is their application in quantifying weathering intensities in incipiently weathered heterogeneous glacial tills, homogenous volcanic, and intensely weathered lateritic soil types (Nesbitt and Young, 1989; Fedo et al., 1995; Chadwick et al., 1990; Egli et al., 2000; Brantley et al., 2008).

A chemical weathering index is based on a mass balance, and relies on selecting typically alkali and alkaline earth metals, that remain either immobile, and are enriched, or become mobile and are depleted, as weathering intensifies (Price and Verbel., 2003). Weathering indices are conventionally calculated using the proportions of major element oxides. Weathering indices normalize a mobile elemental oxide to an immobile one, to assess the relative change. Stoichiometric changes during weathering are reflected in the index value. However, this assumption is not always warranted. An elements mobility during chemical weathering generally depends on its ionic charge and ionic radius size (Å), together termed ionic potential (IP). The ionic potential is related to the elements bond strength with oxygen, Fig. 2.10 (Buggle et al., 2011; Parker, 1970). In low temperature environments, the changes in redox, pH and ion co-ordination environment can result in major differences in an elements mobility and weathering, for example: redox state Fe^{2+} to Fe^{3+}; ionic radius K^{+} 1.37 to 1.64 Å. Therefore, a good understanding of a samples environmental conditions is needed to select an appropriate index to fully utilise a weathering intensity.

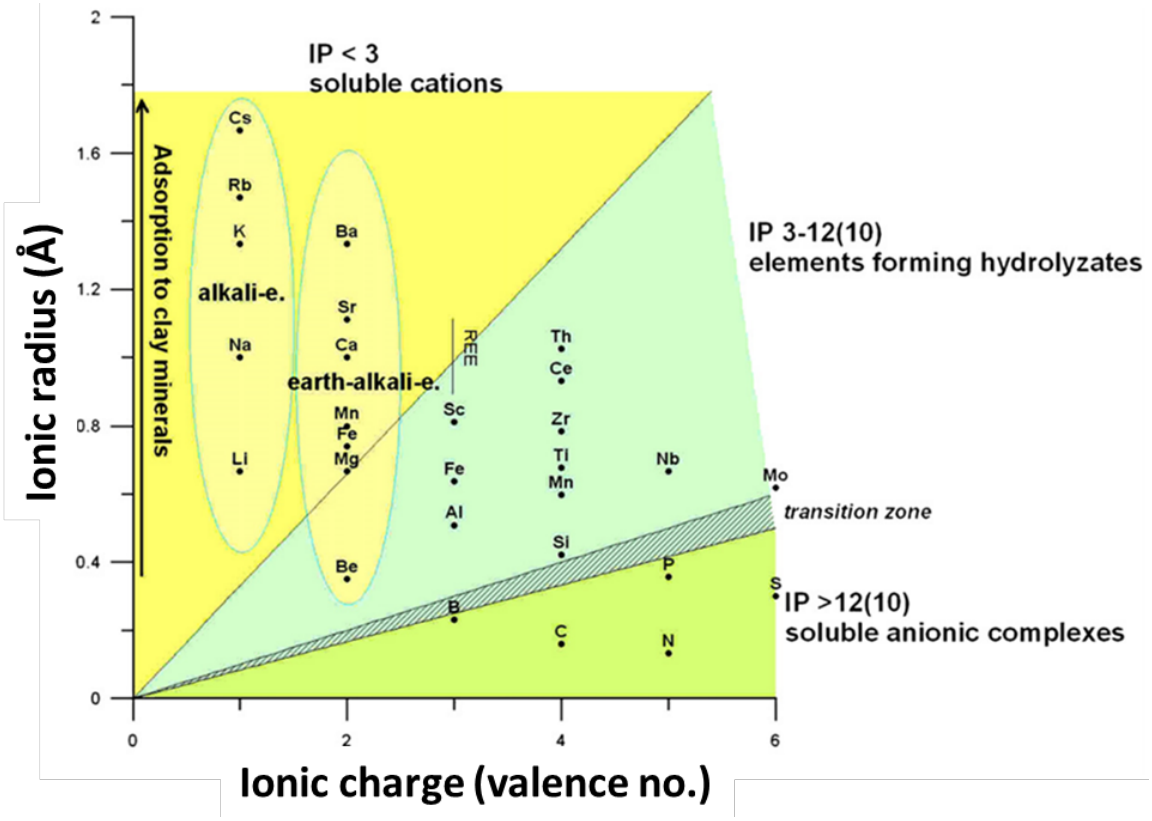

Figure 2.10. Classification of the elements according to the ionic potential (IP). Values for the ionic potential and ionic radius are taken from Mason and Moore (1985). Cations having - an IP below 3 are generally soluble in water, whereas cations with an IP between 3 and 10 (according to Mason and Moore, 1985) or 12, respectively (Goldschmidt, 1937; Kabata-Pendias and Pendias, 2001), form insoluble, immobile hydrolysates under near-neutral conditions. Elements having a higher IP tend to form soluble anionic complexes. The adsorption to clay minerals tends to increase with the radius of the cation (Nesbitt et al., 1980; Smykatz-Kloss, 2003) Obtained from Buggle et al., 2011.

The molecular proportion of each oxide is calculated easily from the weight percent of the oxide. Weathering index application is used commonly to determine either a soil depth profile or its age. Bulk density often serves as an independent measure to validate physical and chemical weathering strain processes in a soil volume (Price and Verbel., 2003). Although bulk densities are useful, quantification using weathering indices can be obtained without this data. This makes chemical weathering indices ideal for heterogeneous materials, where bulk densities can be difficult to obtain. For example, in glacial till that is often an unsorted, unstratified mixture of clay, silt, sand, gravel, and boulders with dissimilar distributions over short distances (Crocker et al., 1955). In addition, chemical weathering indices can be applied to materials that do not weather iso-volumetrically (e.g. saprolitic soils), and have been affected by mechanical processes e.g., biologically or thermally-induced turbation in soils.

Based on a review of the literature, the utility of weathering indices in cold region environments, where weathering maybe incipient and parent material heterogeneity may be an issue, have been classified by the need to meet several criteria.

Criteria 1. The application of a chemical weathering index to weathered materials should involve chemical elements common in glacial till-forming soils. This is desirable for wide applicability and maximum comparability with other studies in potentially different environments.

Criteria 2. Weathering indices should be applied appropriately, by considering the weathering environment intensity and the chemical and physical properties of the parent material and soil fractions. Weathering indices based exclusively on the more immobile elemental oxides may not be applicable to assessing profiles or intervals representing early weathering stages. This is because they are likely to not have been depleted, unless subjected to an intensive weathering regime (Eswaran et al., 1973). Intense physical or chemical weathering, at a localised scale within profiles, or at intervals, could result in movement of elements, generally considered immobile. For instance, commonly used immobile elemental oxides, aluminium (Al_2O_3) and titanium (TiO_2), may become mobile at a low soil pH <4.5 (Gardner et al 1978; Gardner 1980; Keller, 1978). Furthermore, metal complexation with organic ligands, such as oxalic and citric acid that are common in soil, can cause immobile elements to become soluble. This is unlikely to have a pronounced effect in forefield soils, where biochemical weathering is thought to be minimal. Nevertheless, this is important in more developed soils, where biota is abundant and the concentration of organic ligands is low 10^{-5} to 10^{-6} M (Jones, 1998; Ullman and Welch, 2002). Trialing a weathering index, which incorporates elements with a range of mobility in the weathering environment, can often help refine it and the immobile and mobile variables (Harnois, 1988).

Criteria 3. Linked to Criteria 2, the utility of a weathering index on glacial till-forming soils is to exhibit chemically appropriate trends with increased weathering. For example, the index can vary as a monotonic function with soil profile, depth or age, and should change greatly with increasing weathering. Using regression analysis, the slope and shape of the line infer the stoichiometry of the chemical weathering reactions. The direction of the index indicates the pathway from parent material to weathering products. Determination of weathering trends is especially important in profiles developed on metasedimentary parent rocks. Metasedimentary rocks are commonly

layered at scales much smaller than the overall dimensions of the weathering profile. As such, a weathering signal can be masked by background heterogeneity.

Criteria 4. A weathering index used on forefield-forming soils should be applicable to a wide range of rock sizes and types, as both these attributes are characteristic of glacial till soils. The validity of the index should be assessed for specific catchment rock types, and validated through standard rock type testing. It should yield values for the unweathered parent material that are distinct from those of the weathered soil fraction, regardless of rock type (Fedo et al., 1995). Metamorphosed sediment, and sedimentary rocks exhibit ‘‘weathered’’ chemical signatures. This is from their pre-metamorphic history, metamorphism and ‘chemical maturation’ that occurs during the general sedimentary cycle, and specifically glacial transport. Low weathering indices can result from metasomatism, for example of K in connection with the conversion of illite to K-feldspar. The illitisation of kaolinite is the most commonly cited cause (Nesbitt and Young, 1989; Fedo et al., 1995). Also, differential erosion and grain-size sorting can result in pseudo-weathering changes, observed in indices. This can arise due to preferential physical sorting, removal or incorporation of older or younger, strongly weathered or parent material in glacial deposits that form soils (Nesbitt and Young, 1997). Alternatively, from selective analysis of soil grain size fractions, it has been shown that their size concentrates aluminous clays in the fines, deriving highly weathered index values. Conversely, feldspars are found in larger, sand sized particles, giving less weathered values. Similarly, sorting of source rock within a glacial till deposit, shows a modal abundance that is not due to *in-situ* chemical weathering. The modal abundance of a sediment’s mineralogy can be used as an alternative method to validate chemical mineral weathering and indices. It is determined using either a point-counting method (Bayly, 1960), quantitative X-ray diffraction, or a calculated algebraic method (Nesbitt and Young, 1996). The latter method relies on knowing qualitatively the sample’s mineral composition, and the bulk chemical composition. Mineral modal abundance is derived from the total oxide content, equated with the sum of the oxide in each mineral. For example, the modal abundance in SiO_2 (bulk) of a sample containing quartz (Qz; SiO_2), albite (Ab; $NaAlSi_3O_8$), illite (Il; $K_{0.7}Al_{2.7}Si_{3.3}O_{10}[OH]_2$), and kaolinite (Ka, $Al_2Si_2O_5[OH]_4$) is shown in Eq. 2.6

$$1Qz + 3Ab + 3.3Il + 2Ka = SiO_2\ (bulk) \qquad \text{Equation. 2.6}$$

The algebraic method is difficult to apply to complex mixtures of rocks and their minerals, that have unknown solid solutions between mineral endmembers.

As discussed in Section 2.3 different modes of glacial transport can significantly alter the glacial till parent material by the physical and chemical properties. This occurs from their post glacial lithological origin to their subsequent deposition in a forefield. A useful weathering index should allow users to distinguish between a ‘‘chemically mature’’ metasedimentary parent material post-metamorphically altered and post forefield deposition weathered, from that of the “chemically immature” parent material and catchment source rock lithological units.

Criteria 5. Ideally, a chemical weathering index should not assume that any element used is immobile. This is often assumed, and difficult to apply in practice. Any element may be mobile in a weathering environment. As a default, those elements that are least mobile should be used and knowledge of a sample’s weathering environment used. The concentration of immobile elements can be determined and compared to the values of the unweathered parent material, the glacial till and to the catchment source rocks that make up a glacial till. This is done using the formula in Eq.4.2.

The Ruxton Ratio (R), and Silica–Titania Index (STI), are common weathering indices used in regions of high weathering intensity such as humid, tropical regions. These indices are also used with uniformed acid to intermediate silicate rocks, often high grade, with constant sesquioxide content during weathering. This is because, they produce secondary weathering products which have mole ratios of SiO_2/Al_2O_3 of 2:1. As soils in glacial forefields typically have incipient levels of silicate mineral weathering, these indices are unlikely to be appropriate. Silicate weathering measured in the discharge waters draining from two Arctic forefields, found <10% of the solute was accounted for by the weathering of these minerals (Anderson et al., 2000; Wadham et al., 2001).

Weathering indexes that are fitting, are the Chemical Index of Alteration (CIA), the Plagioclase Index of Alteration (PIA) and the Weathering Index of Parker (WIP). This is because these indices are interpreted as a measure of a wide range of weathering. They all use highly mobile elements; sodium, potassium, magnesium and calcium to assess the conversion of primary minerals (feldspars which dominate the upper crust, plagioclase and orthoclase) to clays such as kaolinite. The CIA and PIA indices use Al_2O_3 as an immobile element. This is beneficial, as this elemental oxide is ubiquitous in silicate minerals, and therefore probably present as a uniform concentration in a glacial till’s volume. The assumption is that it remains inert and immobile in a soil volume with a well-mixed drain size distribution. Minerals containing other

commonly used immobile elemental oxides, TiO_2 and ZrO_2, are often more susceptible to zonal gravitation sorting by density (Hubert, 1962). Unlike the CIA and PIA, the WIP index allows for aluminium mobility. It considers the individual mobility of sodium, potassium, magnesium and calcium, based on their bond strengths with oxygen (Parker, 1970). Use of this wide range mobile alkali and alkaline earth metals makes the WIP best to use in the study of weathered regoliths. A limitation is that the index is based on easily weathered, mobile elements, so should not be used in intensive weathering environments.

Table 2.3 Common chemical weathering indices used on (1) heterogeneous, incipiently and (2) homogenous, intensive weathered materials.

Chemical Weathering Index	Formula	Optimum (*fresh* to weathered values)	Ideal weathering trend (increase in weathering)	Reference
[1]CIA	$(100)[(Al_2O_3/ (Al_2O_3 + CaO^* + Na_2O + K_2O)]$	*50* to 100	Positive	Nesbitt and Young (1982)
[1]PIA	$(100)[(Al_2O_3/(Al_2O_3 + CaO^* + Na_2O - K_2O)]$	*50* to 100	Positive	Fedo et al., (1995)
[1]WIP	$(100)[(2Na_2O/0.35)+(MgO/0.9) + (2K_2O/0.25)+(CaO^*/0.7)]$	*>100* to 0	Negative	Parker (1970)
[2]R	SiO_2/Al_2O_3	*> 10* to 0	Negative	Ruxton (1968)
[2]STI	$(100)\ [(SiO_2/TiO_2)/((SiO_2/ TiO_2) + (SiO_2/ Al_2O_3) + (Al_2O_3/ TiO_2))]$	*>90* to 0	Negative	De Jayawardena and Izawa (1994)

Another, similar approach is the elemental mass gains and losses method. This compares the ratio of soil fraction and parent material of mobile and immobile oxide concentrations in a bulk material (White et al., 2001; White et al., 1997). These fractions can be defined from the elemental oxide concentration, with soil fraction grain size <2mm, compared with the soil forming parent material. The mass gain and losses method requires to test the immobility of the elemental oxide. ε_v (V; mol/kg) is the ratio of an immobile element *i*, in the un-weathered

parent material *uw*, relative to the weathered soil, *w*.

$$\varepsilon_v = \frac{[V_{i,uw}]}{[V_{i,w}]} - 1 \qquad \text{Equation 2.7}$$

Values clustered around zero ($\varepsilon_v = 0$) indicate limited mobility in the soil fraction relative to the parent material. Negative values of ε_v are indicative that an element is not immobile in the soil fraction relative to the parent material, whereas a positive value of ε_v means an additional external factor affected the value.

Quantitative losses and gains of elements during weathering are described in terms of mass transfer, T_e, of a chemical weathered element V in the <2mm grain-size fraction. The ratio of the total weathered material V_w * $V_{i,\mathrm{w}}$ to the immobile unweathered material $\mathrm{V}_{i,uw}$ gives the corrected term CV_w (mol/kg), Eq. 2.8. The difference between the corrected, CV_w, and un-weathered element V_{uw} gives the mass transfer of an element during chemical weathering, Eq. 2.9.

$$[CV_w] = \frac{[V_w][V_{i,w}]}{[V_{i,uw}]} \qquad \text{Equation 2.8}$$

$$\mathrm{T}_{e\,=[CV_w]-[V_{uw}]} \qquad \text{Equation 2.9}$$

When T_e is negative, elemental concentrations have been depleted during chemical weathering, a positive number means an increase in elemental concentration and when $T_e = 0$ elements remain refractory during chemical weathering with respect to the parent material.

2.5.2.2 Carbonate and sulfide weathering

Besides silicates, the other inorganic mineral important in the carbon cycle is carbonate, in minerals such as calcite, dolomite and limestone. This reservoir is considered unimportant to the global carbon cycle over $>10^6$ y, because it provides a balanced source and sink of atmospheric CO_2. This occurs as carbonate minerals precipitate and dissolve from carbonic acid (Berner et al., 1983; Liu et al., 2011). Carbonate mineral reactions may impact upon the carbon cycle at short interglacial-glacial timescales (10^2 to10^5 y), because of the alternation between exposed glacial sediments, warmer temperature, and greater run-off during interglacial compared with glacial times (Anderson et al., 1997). Carbonate minerals' rapid dissolution kinetics increases dissolved inorganic carbon (DIC) concentrations, and may represent a net atmospheric CO_2 sink. Primary productivity consumes DIC, resulting in burial of organic carbon in fluvial systems in carbonate terrains (Berner et al., 1983; Liu et al., 2011).

Alternatively, carbonate minerals are dissolved by sulfuric acid to generate CO_2. This process would represent an atmospheric source of this greenhouse gas, with no rapid balancing of the atmospheric sink, as the sulfate residence time in the oceans $>10^7$ y, (Martin; Claypool et al., 1980; Calmels et al., 2007).

At young ages, in newly deglaciated terrain (the glacial forefield interface), carbonate weathering could be enhanced. Near-freezing point glacial meltwaters may exert a four-fold increase on the rate of calcite dissolution between 0-50°C (Garrels and Christ, 1965). In addition, the solubility of CO_2 is higher at low temperature (Weiss, 1974) producing a higher concentration of H_2CO_3, particularly when under saturated with respect to $CaCO_3$. This is important when the soil and its parent material are flushed with low ionic strength (<40 mmol l^{-1}) supraglacial meltwater (Tranter and Wadham, 2014). For the genesis of non-crustal carbonates, pedogenic calcite may be an important factor to consider. In fine grained gravelly soils these are common, particularly in semi-arid environments where dissolved carbonates re-precipitate on the surfaces of finer grain sizes (Treadwell-Steitz and McFadden, 2000). This process occurs either by plant respiration of CO_2, or calcite dissolution and re-precipitation when Ca^{2+} and HCO_3^- ions concentrate in the soil solution. Water percolating through the sediment degasses and this shifts the equilibrium to the right, consuming carbonic acid, (Eq. 2.10). To compensate for this, the equilibrium moves to the left and $CaCO_3$ can re-precipitate, Eq. 2.11 (McFadden et al., 1998; Retallack, 2005). Soil calcite can persist independently of gypsum as it less soluble. Consequently its occurrence is more widespread in semi-arid soils, like those present in pan-Arctic forefields (Visconti et al., 2010).

$$H_2CO_3 \rightleftarrows H_2O + CO_2 \qquad \text{Equation 2.10}$$

$$H_2CO_3 + CaCO_3 \rightarrow Ca^{2+} + 2HCO_3^- \qquad \text{Equation 2.11}$$

Despite the ubiquity of carbonate dissolution, mounting evidence is showing that sulfide oxidation producing sulfuric acid is coupled to carbonate dissolution. This is often referred to a sulfide oxidation carbonate dissolution (SOCD), and this coupled reaction often dominates at young ages in deglaciating forelands. This is observed even if trace carbonates and sulfides, such as pyrite, are present in the parent material (Anderson et al., 2000; Wadham et al., 2007). The dominance of SOCD has been evidenced from the anion stoichiometry i.e. HCO_3^- and SO_4^{2-} that is inferred from sulfide and carbonate mineral weathering. These anions dominate the meltwater flux in proglacial streams that drain the forefield, due to the rapid dissolution

kinetics, and the properties of their tills (discussed in Section 2.3). Other evidence arises from PCO_2 measurements in young areas of the glacial forefield, where proglacial streams drain forefield tills, where heterotrophic biota are negligible. These young soil waters were shown to be a source of CO_2 (Fig. 2.11). The PCO_2 signature over one melt season was higher than that of atmospheric levels ($PCO_2 = 10^{-3.5}$ atm.) (Wadham et al., 2007). Validation of this coupled reaction, through bulk analysis of the mineral residuals in glacial tills, could result in glacial-ground-water mixing of anions derived from either sulfide oxidation, carbonate dissolution or both. This, combined with the fact that sulfide and carbonate weathering often are governed by surface controlled reactions (as opposed to transport diffusion), often leads to non-stoichiometric release of their weathering products that could lead to erroneous inferences (McKibben and Barnes, 1986; Morse and Arvidson et al., 2002; Sjöberg, 1976).

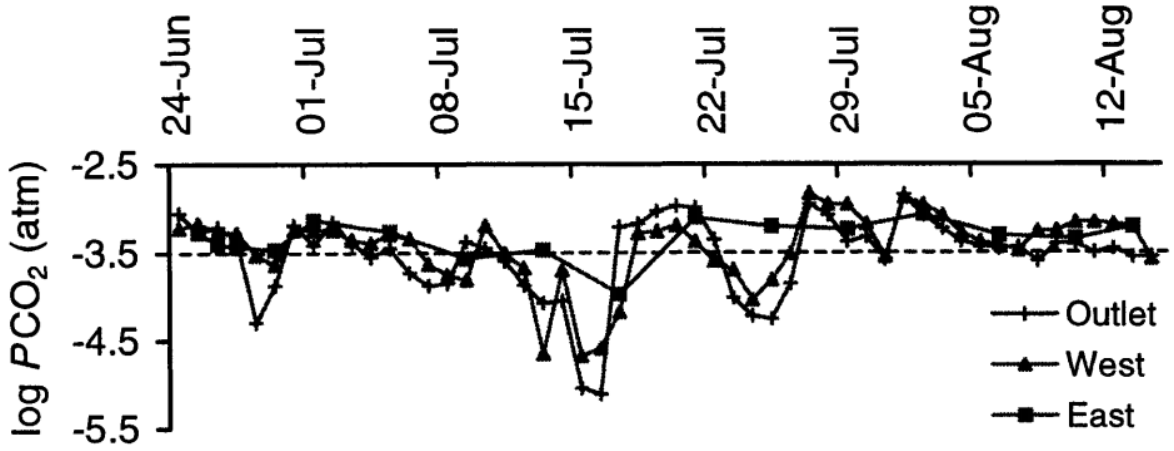

Figure.2.11 Temporal variations in the concentration of PCO_2 of the bulk meltwaters sampled at East, West and Outlet gauging stations over one melt season in 1999 from Finsterwalderbreen, Svalbard (atmospheric PCO_2 is delineated with a dashed line). Note: the considerable period of PCO_2 above atmospheric levels that was thought to be driven by SOCD, suggesting the forefield is a source of CO_2 to the atmosphere. Obtained from Wadham et al., 2001.

1.6. References

Alexander, E. & Burt, R. 1996. Soil development on moraines of Mendenhall Glacier, southeast Alaska. 1. The moraines and soil morphology. *Geoderma,* 72**,** 1-17.

Allan, J.D. and Castillo, M.M., 2007. Stream ecology: structure and function of running waters. Springer Science & Business Media.

Amundson, R., Richter, D.D., Humphreys, G.S., Jobbágy, E.G. and Gaillardet, J., 2007. Coupling between biota and earth materials in the critical zone. *Elements*, *3*(5), pp.327-332.

Anderson, S.P., Blum, J., Brantley, S.L., Chadwick, O., Chorover, J., Derry, L.A., Drever, J.I., Hering, J.G., Kirchner, J.W., Kump, L.R. and Richter, D., 2004. Proposed initiative would study Earth's weathering engine. Eos, Transactions American Geophysical Union, 85(28), pp.265-269

Anderson, S. P., Drever, J. I., Frost, C. D. & Holden, P. 2000. Chemical weathering in the foreland of a retreating glacier. *Geochimica Et Cosmochimica Acta,* 64**,** 1173-1189.

Anderson, S.P., Drever, J.I. and Humphrey, N.F., 1997. Chemical weathering in glacial environments. Geology, 25(5), pp.399-402.

Anesio, A.M., Lutz, S., Nathan, A., Chrismas, M. and Benning, L.G., 2017. The microbiome of glaciers and ice sheets. npj Biofilms and Microbiomes, 3, p.1.

Banwart, S., Bernasconi, S. M., Bloem, J., Blum, W., Brandao, M., Brantley, S., Chabaux, F., Duffy, C., Kram, P., Lair, G., Lundin, L., Nikolaidis, N., Novak, M., Panagos, P., Ragnarsdottir, K. V., Reynolds, B., Rousseva, S., De Ruiter, P., Van Gaans, P., Van Riemsdijk, W., White, T. & Zhang, B. 2011. Soil Processes and Functions in Critical Zone Observatories: Hypotheses and Experimental Design. *Vadose Zone Journal,* 10**,** 974-987.

Banwart, S., Menon, M., Bernasconi, S. M., Bloem, J., Blum, W. E. H., De Souza, D. M., Davidsdotir, B., Duffy, C., Lair, G. J., Kram, P., Lamacova, A., Lundin, L., Nikolaidis, N. P., Novak, M., Panagos, P., Ragnarsdottir, K. V., Reynolds, B., Robinson, D., Rousseva, S., De Ruiter, P., Van Gaans, P., Weng, L., White, T. & Zhang, B. 2012. Soil processes and functions across an international network of Critical Zone Observatories: Introduction to experimental methods and initial results. *Comptes Rendus Geoscience,* 344**,** 758-772.

Banwart, S. A., Bernasconi, S. M., Blum, W. E. H., De Souza, D. M., Chabaux, F., Duffy, C., Kercheva, M., Krám, P., Lair, G. J., Lundin, L., Menon, M., Nikolaidis, N. P., Novak, M., Panagos, P., Ragnarsdottir, K. V., Robinson, D. A., Rousseva, S., De Ruiter, P., Van Gaans, P., Weng, L., White, T. & Zhang, B. 2017. Chapter One - Soil Functions in Earth's Critical Zone: Key Results and Conclusions. *In:* STEVEN, A. B. & DONALD, L. S. (eds.) *Advances in Agronomy.* Academic Press.

Bardgett, R. D., Richter, A., Bol, R., Garnett, M. H., Bäumler, R., Xu, X., Lopez-Capel, E., Manning, D. a. C., Hobbs, P. J., Hartley, I. R. & Wanek, W. 2007. Heterotrophic microbial communities use ancient carbon following glacial retreat. *Biology Letters,* 3**,** 487-490.

Barrett, J.E., Virginia, R.A., Lyons, W.B., McKnight, D.M., Priscu, J.C., Doran, P.T., Fountain, A.G., Wall, D.H. and Moorhead, D.L., 2007. Biogeochemical stoichiometry of Antarctic dry valley ecosystems. Journal of Geophysical Research: Biogeosciences, 112(G1).

Bayly, M B (1960) Modal analysis by point-counter-the choice of sample area. J Geol Soc Ausl, 16, l19-129

Benn, D. & Evans, D. J. 2014. *Glaciers and glaciation*, Routledge.

Bergaya, F. and Lagaly, G., 2006. General introduction: clays, clay minerals, and clay science. Developments in clay science, 1, pp.1-18.

Bernasconi, S. M., Bauder, A., Bourdon, B., Brunner, I., Bünemann, E., Christl, I., Derungs, N., Edwards, P., Farinotti, D., Frey, B., Frossard, E., Furrer, G., Gierga, M., Göransson, H., Gülland, K., Hagedorn, F., Hajdas, I., Hindshaw, R., Ivy-Ochs, S., Jansa, J., Jonas, T., Kiczka, M., Kretzschmar, R., Lemarchand, E., Luster, J., Magnusson, J., Mitchell, E. a. D., Venterink, H. O., Plötze, M., Reynolds, B., Smittenberg, R. H., Stähli, M., Tamburini, F., Tipper, E. T., Wacker, L., Welc, M., Wiederhold, J. G., Zeyer, J., Zimmermann, S. & Zumsteg, A. 2011. Chemical and

biological gradients along the damma glacier soil chronosequence, Switzerland. *Vadose Zone Journal,* 10**,** 867-883.

Bernasconi, S. M. & Biglink Project, M. 2008. Weathering, soil formation and initial ecosystem evolution on a glacier forefield: a case study from the Damma Glacier, Switzerland. *Mineralogical Magazine,* 72**,** 19-22.

Berner, E., Berner, R. & Moulton, K. 2003. Plants and mineral weathering: present and past. *Treatise on geochemistry,* 5**,** 169-188.

Berner, E. K. & Berner, R. A. 2012. *Global environment: water, air, and geochemical cycles*, Princeton University Press.

Berner, R. A. 1994. GEOCARB II: A revised model of atmospheric CO [sub 2] over phanerozoic time. *American Journal of Science;(United States),* 294.

Berner, R. A., Lasaga, A. C. & Garrels, R. M. 1983. The carbonate-silicate geochemical cycle and its effect on atmospheric carbon dioxide over the past 100 million years. *American Journal of Science,* 283**,** 641-683.

Blume, H.P., Brümmer, G.W., Fleige, H., Horn, R., Kandeler, E., Kögel-Knabner, I., Kretzschmar, R., Stahr, K. and Wilke, B.M., 2015. Scheffer/Schachtschabel soil science. Springer.

Borin, S., Ventura, S., Tambone, F., Mapelli, F., Schubotz, F., Brusetti, L., Scaglia, B., D'acqui, L. P., Solheim, B., Turicchia, S., Marasco, R., Hinrichs, K. U., Baldi, F., Adani, F. & Daffonchio, D. 2010. Rock weathering creates oases of life in a High Arctic desert. *Environmental Microbiology,* 12**,** 293-303.

Boulton, G. S. 1978. Boulder shapes and grain-size distributions of debris as indicators of transport paths through a glacier and till genesis. *Sedimentology,* 25**,** 773-799.

Bradley, J., Anesio, A. & Arndt, S. 2017. Microbial and biogeochemical dynamics in glacier forefields are sensitive to century-scale climate and anthropogenic change. *Frontiers in Earth Science,* 5.

Bradley, J., Singarayer, J. & Anesio, A. 2014. Microbial community dynamics in the forefield of glaciers. *Proc R Soc B Biol Sci,* 281**,** 20140882.

Bradley, J. A., Anesio, A. M. & Arndt, S. 2016a. Bridging the divide: a model-data approach to Polar and Alpine microbiology. *FEMS Microbiology Ecology,* 92**,** fiw015-fiw015.

Bradley, J. A., Arndt, S., Šabacká, M., Benning, L. G., Barker, G. L., Blacker, J. J., Yallop, M. L., Wright, K. E., Bellas, C. M., Telling, J., Tranter, M. & Anesio, A. M. 2016b. Microbial dynamics in a High Arctic glacier forefield: a combined field, laboratory, and modelling approach. *Biogeosciences,* 13**,** 5677-5696.

Brankatschk, R., Töwe, S., Kleineidam, K., Schloter, M. and Zeyer, J., 2011. Abundances and potential activities of nitrogen cycling microbial communities along a chronosequence of a glacier forefield. The ISME journal, 5(6), p.1025.

Brantley, S.L., 2008. Kinetics of mineral dissolution. In Kinetics of water-rock interaction (pp. 151-210). Springer New York.

Brantley, S. L., Goldhaber, M. B. & Ragnarsdottir, K. V. 2007. Crossing disciplines and scales to understand the critical zone. *Elements,* 3**,** 307-314.

Buggle, B., Glaser, B., Hambach, U., Gerasimenko, N. and Marković, S., 2011. An evaluation of geochemical weathering indices in loess–paleosol studies. Quaternary International, 240(1), pp.12-21.

Burga, C. A. 1999. Vegetation development on the glacier forefield Morteratsch (Switzerland). *Applied Vegetation Science,* 2**,** 17-24.

Calmels, D., Gaillardet, J., Brenot, A. & France-Lanord, C. 2007. Sustained sulfide oxidation by physical erosion processes in the Mackenzie River basin: Climatic perspectives. *Geology,* 35**,** 1003-1006.

Chadwick, O.A., Brimhall, G.H. and Hendricks, D.M., 1990. From a black to a gray box—a mass balance interpretation of pedogenesis. Geomorphology, 3(3), pp.369-390.

Chapin Iii, F., Stuart., Mcfarland, J., David Mcguire, A., Euskirchen, E. S., Ruess, R. W. & Kielland, K. 2009. The changing global carbon cycle: linking plant–soil carbon dynamics to global consequences. *Journal of Ecology,* 97**,** 840-850.

Chapin, F.S., Woodwell, G.M., Randerson, J.T., Rastetter, E.B., Lovett, G.M., Baldocchi, D.D., Clark, D.A., Harmon, M.E., Schimel, D.S., Valentini, R. and Wirth, C., 2006. Reconciling carbon-cycle concepts, terminology, and methods. Ecosystems, 9(7), pp.1041-1050

Claypool, G. E., Holser, W. T., Kaplan, I. R., Sakai, H. & Zak, I. 1980. The age curves of sulfur and oxygen isotopes in marine sulfate and their mutual interpretation. *Chemical Geology,* 28**,** 199-260.

Coleman, D. C. 2012. *Carbon isotope techniques*, Academic Press.

Conen, F., Yakutin, M. V., Zumbrunn, T. & Leifeld, J. 2007. Organic carbon and microbial biomass in two soil development chronosequences following glacial retreat. *European Journal of Soil Science,* 58**,** 758-762.

Cooper, R., Hodgkins, R., Wadham, J. and Tranter, M., 2011. The hydrology of the proglacial zone of a High-Arctic glacier (Finsterwalderbreen, Svalbard): sub-surface water fluxes and complete water budget. Journal of Hydrology, 406(1), pp.88-96.

Cooper, R. J., Wadham, J. L., Tranter, M., Hodgkins, R. & Peters, N. E. 2002. Groundwater hydrochemistry in the active layer of the proglacial zone, Finsterwalderbreen, Svalbard. *Journal of Hydrology,* 269**,** 208-223.

Crocker, R.L. and Major, J., 1955. Soil development in relation to vegetation and surface age at Glacier Bay, Alaska. The Journal of Ecology, pp.427-448.

D'amico, M. E., Freppaz, M., Filippa, G. & Zanini, E. 2014. Vegetation influence on soil formation rate in a proglacial chronosequence (Lys Glacier, NW Italian Alps). *Catena,* 113**,** 122-137.

D'amico, M. E., Freppaz, M., Leonelli, G., Bonifacio, E. & Zanini, E. 2014. Early stages of soil development on serpentinite: the proglacial area of the Verra Grande Glacier, Western Italian Alps. *Journal of Soils and Sediments,* 15**,** 1292-1310.

Dixon, J. L., Chadwick, O. A. & Vitousek, P. M. 2016. Climate-driven thresholds for chemical weathering in postglacial soils of New Zealand. *Journal of Geophysical Research: Earth Surface,* 121**,** 1619-1634.

Drever, J. I. 1994. The effect of land plants on weathering rates of silicate minerals. *Geochimica et Cosmochimica Acta,* 58**,** 2325-2332.

Duemig, A., Smittenberg, R. & Koegel-Knabner, I. 2011. Concurrent evolution of organic and mineral components during initial soil development after retreat of the Damma glacier, Switzerland. *Geoderma,* 163**,** 83-94.

Dümig, A., Häusler, W., Steffens, M. & Kögel-Knabner, I. 2012. Clay fractions from a soil chronosequence after glacier retreat reveal the initial evolution of organo-mineral associations. *Geochimica et Cosmochimica Acta,* 85**,** 1-18.

Dümig, A., Smittenberg, R. & Kögel-Knabner, I. 2011. Concurrent evolution of organic and mineral components during initial soil development after retreat of the Damma glacier, Switzerland. *Geoderma,* 163**,** 83-94.

Ebelmen, J.J., 1845. Sur les produits de la décomposition des espèces minérales de la famille des silicates. In Annales des Mines (Vol. 7, No. 3, p. 66).

Egli, M., Dahms, D. & Norton, K. 2014. Soil formation rates on silicate parent material in alpine environments: Different approaches–different results? Geoderma, 213, 320-333.

Egli, M., Filip, D., Mavris, C., Fischer, B., Götze, J., Raimondi, S. & Seibert, J. 2012. Rapid transformation of inorganic to organic and plant-available phosphorous in soils of a glacier forefield. *Geoderma,* 189–190**,** 215-226.

Egli, M. and Fitze, P., 2000. Formulation of pedologic mass balance based on immobile elements: a revision. Soil Science, 165(5), pp.437-443.

Egli, M., Fitze, P. & Mirabella, A. 2001. Weathering and evolution of soils formed on granitic, glacial deposits: results from chronosequences of Swiss alpine environments. *CATENA,* 45**,** 19-47.

Ellis, S. and Mellor, A., 1995. Soils and environment. Taylor & Francis US.

Fedo, C. M., Nesbitt, H. W. & Young, G. M. 1995. Unraveling the effects of potassium metasomatism in sedimentary rocks and paleosols, with implications for paleoweathering conditions and provenance. Geology, 23, 921-924

Föllmi, K. B., Hosein, R., Arn, K. & Steinmann, P. 2009. Weathering and the mobility of phosphorus in the catchments and forefields of the Rhône and Oberaar glaciers, central Switzerland: Implications for the global phosphorus cycle on glacial–interglacial timescales. *Geochimica et Cosmochimica Acta,* 73**,** 2252-2282.

Frenot, Y., Vanvlietlanoe, B. & Gloaguen, J. C. 1995. Particle Translocation and Initial Soil Development on a Glacier Foreland, Kerguelen Islands, Sub-Antarctic. *Arctic and Alpine Research,* 27**,** 107-115.

Gardner, L.R., 1980. Mobilization of Al and Ti during weathering—isovolumetric geochemical evidence. Chemical Geology, 30(1-2), pp.151-165.

Gardner, L.R., Kheoruenromne, I. and Chen, H.S., 1978. Isovolumetric geochemical investigation of a buried granite saprolite near Columbia, SC, USA. Geochimica et Cosmochimica Acta, 42(4), pp.417-424

Garrels, R. M. & Christ, C. L. 1965. Solutions, minerals, and equilibria..

Gibbs, M. T. & Kump, L. R. 1994. Global chemical erosion during the Last Glacial Maximum and the present: Sensitivity to changes in lithology and hydrology. *Paleoceanography,* 9**,** 529-543.

Guelland, K., Esperschuetz, J., Bornhauser, D., Bernasconi, S. M., Kretzschmar, R. & Hagedorn, F. 2013a. Mineralisation and leaching of C from C-13 labelled plant litter along an initial soil chronosequence of a glacier forefield. *Soil Biology & Biochemistry,* 57**,** 237-247.

Guelland, K., Hagedorn, F., Smittenberg, R. H., Goransson, H., Bernasconi, S. M., Hajdas, I. & Kretzschmar, R. 2013b. Evolution of carbon fluxes during initial soil formation along the forefield of Damma glacier, Switzerland. *Biogeochemistry,* 113**,** 545-561.

Harden, J.W., Sundquist, E.T., Stallard, R.F. and Mark, R.K., 1992. Dynamics of soil carbon during deglaciation of the Laurentide ice sheet. Science-New York, Washington, 258, pp.1921-1921.

He, L. & Tang, Y. 2008. Soil development along primary succession sequences on moraines of Hailuogou Glacier, Gongga Mountain, Sichuan, China. *Catena,* 72**,** 259-269.

Hindshaw, R. S., Rickli, J., Leuthold, J., Wadham, J. & Bourdon, B. 2014. Identifying weathering sources and processes in an outlet glacier of the Greenland Ice Sheet using Ca and Sr isotope ratios. *Geochimica et Cosmochimica Acta,* 145**,** 50-71.

Hindshaw, R. S., Tipper, E. T., Reynolds, B. C., Lemarchand, E., Wiederhold, J. G., Magnusson, J., Bernasconi, S. M., Kretzschmar, R. & Bourdon, B. 2011. Hydrological control of stream water chemistry in a glacial catchment (Damma Glacier, Switzerland). *Chemical Geology,* 285**,** 215-230.

Hodkinson, I. D., Coulson, S. J., Harrison, J. & Webb, N. R. 2001. What a wonderful web they weave: spiders, nutrient capture and early ecosystem development in the high Arctic – some counter-intuitive ideas on community assembly. *Oikos,* 95**,** 349-352.

Hodkinson, I. D., Coulson, S. J. & Webb, N. R. 2003. Community assembly along proglacial chronosequences in the high Arctic: vegetation and soil development in north-west Svalbard. *Journal of Ecology,* 91**,** 651-663.

Hodson, A., Mumford, P., Kohler, J. & Wynn, P. M. 2005. The High Arctic glacial ecosystem: new insights from nutrient budgets. *Biogeochemistry,* 72**,** 233-256.

Hodson, A., Tranter, M. & Vatne, G. 2000. Contemporary rates of chemical denudation and atmospheric CO2 sequestration in glacier basins: an Arctic perspective. *Earth Surface Processes and Landforms,* 25**,** 1447-1471.

Hodson, M.E., Langan, S.J., Kennedy, F.M. and Bain, D.C., 1998. Variation in soil surface area in a chronosequence of soils from Glen Feshie, Scotland and its implications for mineral weathering rate calculations. Geoderma, 85(1), pp.1-18.

Hodgkins, R., 1997. Glacier hydrology in Svalbard, Norwegian high arctic. Quaternary Science Reviews, 16(9), pp.957-973.

Hubert, J.F., 1962. A zircon-tourmaline-rutile maturity index and the interdependence of the composition of heavy mineral assemblages with the gross composition and texture of sandstones. Journal of Sedimentary Research, 32(3).

Huggett, R. J. 1998. Soil chronosequences, soil development, and soil evolution: a critical review. *CATENA,* 32**,** 155-172.

Irvine-Fynn, T. D. L. & Hodson, A. J. 2010. Biogeochemistry and dissolved oxygen dynamics at a subglacial upwelling, Midtre Lovenbreen, Svalbard. *Annals of Glaciology,* 51**,** 41-46.

Jenny, H. 1941. Factors of Soil Formation. *Soil Science,* 52**,** 415.

Jenny, H., 1994. Factors of soil formation: a system of quantitative pedology. Courier Corporation.

Kabala, C. and Zapart, J., 2009. Recent, relic and buried soils in the forefield of Werenskiold Glacier, SW Spitsbergen. Pol. Polar Res, 30(2), pp.161-178.

Kabala, C. & Zapart, J. 2012. Initial soil development and carbon accumulation on moraines of the rapidly retreating Werenskiold Glacier, SW Spitsbergen, Svalbard archipelago. *Geoderma,* 175–176**,** 9-20.

Kleber, M., Sollins, P. and Sutton, R., 2007. A conceptual model of organo-mineral interactions in soils: self-assembly of organic molecular fragments into zonal structures on mineral surfaces. Biogeochemistry, 85(1), pp.9-24.

Kirschbaum, M. U. F. 2000. Will changes in soil organic carbon act as a positive or negative feedback on global warming? *Biogeochemistry,* 48**,** 21-51.

Kuzyakov, Y., Friedel, J.K. and Stahr, K., 2000. Review of mechanisms and quantification of priming effects. Soil Biology and Biochemistry, 32(11), pp.1485-1498.

Larose, C., Dommergue, A. & Vogel, T. M. 2013. The dynamic arctic snow pack: an unexplored environment for microbial diversity and activity. *Biology,* 2**,** 317-330.

Larson, S., 1960. On the influence of the arctic fox Alopex lagopus on the distribution of arctic birds. Oikos, 11(2), pp.276-305.

Lehmann, J. & Kleber, M. 2015. The contentious nature of soil organic matter. *Nature,* 528**,** 60-68.

Liu, Z., Dreybrodt, W. & Liu, H. 2011. Atmospheric CO2 sink: Silicate weathering or carbonate weathering? *Applied Geochemistry,* 26, Supplement**,** S292-S294.

Martin, J. B. Carbonate minerals in the global carbon cycle. *Chemical Geology*.

Mavris, C., Egli, M., Plotze, M., Blum, J. D., Mirabella, A., Giaccai, D. & Haeberli, W. 2010. Initial stages of weathering and soil formation in the Morteratsch proglacial area (Upper Engadine, Switzerland). *Geoderma,* 155**,** 359-371.

Mavris, C., Plotze, M., Mirabella, A., Giaccai, D., Valboa, G. & Egli, M. 2011. Clay mineral evolution along a soil chronosequence in an Alpine proglacial area. *Geoderma,* 165**,** 106-117.

McBride, M.B., 1989. Reactions controlling heavy metal solubility in soils. In Advances in soil science (pp. 1-56). Springer New York.

Mcfadden, L. D., Mcdonald, E. V., Wells, S. G., Anderson, K., Quade, J. & Forman, S. L. 1998. The vesicular layer and carbonate collars of desert soils and pavements: formation, age and relation to climate change. *Geomorphology,* 24**,** 101-145.

Mckibben, M. A. & Barnes, H. L. 1986. Oxidation of pyrite in low temperature acidic solutions: Rate laws and surface textures. Geochimica et Cosmochimica Acta, 50, 1509-1520.

Melillo, J.M., Steudler, P.A., Aber, J.D., Newkirk, K., Lux, H., Bowles, F.P., Catricala, C., Magill, A., Ahrens, T. and Morrisseau, S., 2002. Soil warming and carbon-cycle feedbacks to the climate system. Science, 298(5601), pp.2173-2176.

Mindl, B., Anesio, A. M., Meirer, K., Hodson, A. J., Laybourn-Parry, J., Sommaruga, R. & Sattler, B. 2007. Factors influencing bacterial dynamics along a transect from supraglacial runoff to proglacial lakes of a high Arctic glacieri. Fems Microbiology Ecology, 59, 307-317.

Morse, J.W. and Arvidson, R.S., 2002. The dissolution kinetics of major sedimentary carbonate minerals. Earth-Science Reviews, 58(1), pp.51-84

Nesbitt, H. and Young, G.M., 1982. Early Proterozoic climates and plate motions inferred from major element chemistry of lutites. Nature, 299(5885), pp.715-717.

Nesbitt, H.W. and Young, G.M., 1996. Petrogenesis of sediments in the absence of chemical weathering: effects of abrasion and sorting on bulk composition and mineralogy. Sedimentology, 43(2), pp.341-358.

Nesbitt, H.W., Young, G.M., McLennan, S.M. and Keays, R.R., 1996. Effects of chemical weathering and sorting on the petrogenesis of siliciclastic sediments, with implications for provenance studies. The Journal of Geology, 104(5), pp.525-542.

Nowak, A. & Hodson, A. 2015. On the biogeochemical response of a glacierized High Arctic watershed to climate change: revealing patterns, processes and heterogeneity among micro-catchments. *Hydrological Processes,* 29**,** 1588-1603.

Parker, A., 1970. An index of weathering for silicate rocks. Geological Magazine, 107(6), pp.501-504.

Perie, C. and Ouimet, R., 2008. Organic carbon, organic matter and bulk density relationships in boreal forest soils. Canadian Journal of Soil Science, 88(3), pp.315-325.

Petrović, R., Berner, R.A. and Goldhaber, M.B., 1976. Rate control in dissolution of alkali feldspars—I. Study of residual feldspar grains by X-ray photoelectron spectroscopy. Geochimica et Cosmochimica Acta, 40(5), pp.537-548.

Price, J. R. & Velbel, M. A. 2003. Chemical weathering indices applied to weathering profiles developed on heterogeneous felsic metamorphic parent rocks. Chemical Geology, 202, 397-416.

Raiswell, R. and Thomas, A.G., 1984. Solute acquisition in glacial melt waters. I. Fjallsjökull (south-east Iceland): Bulk melt waters with closed-system characteristics. Journal of Glaciology, 30(104), pp.35-43.

Retallack, G. J. 2005. Pedogenic carbonate proxies for amount and seasonality of precipitation in paleosols. *Geology,* 33**,** 333-336.

Ritchie, M. E., Tilman, D. & Knops, J. M. 1998. Herbivore effects on plant and nitrogen dynamics in oak savanna. *Ecology,* 79**,** 165-177.

Robinson, C., Wookey, P., Parsons, A., Potter, J., Callaghan, T., Lee, J., Press, M. & Welker, J. 1995. Responses of plant litter decomposition and nitrogen mineralisation to

simulated environmental change in a high arctic polar semi-desert and a subarctic dwarf shrub heath. *Oikos*, 503-512.

Schmidt, M. W., Torn, M. S., Abiven, S., Dittmar, T., Guggenberger, G., Janssens, I. A., Kleber, M., Kögel-Knabner, I., Lehmann, J. & Manning, D. A. 2011. Persistence of soil organic matter as an ecosystem property. *Nature,* 478**,** 49-56.

Sharp, M., Tranter, M., Brown, G. H. & Skidmore, M. 1995. Rates of chemical denudation and CO2 drawdown in a glacier-covered alpine catchment. *Geology,* 23**,** 61-64.

Simas, F.N., Schaefer, C.E.G., Melo, V.F., Albuquerque-Filho, M.R., Michel, R.F., Pereira, V.V., Gomes, M.R. and da Costa, L.M., 2007. Ornithogenic cryosols from Maritime Antarctica: Phosphatization as a soil forming process. Geoderma, 138(3), pp.191-203.

Six, J., Conant, R., Paul, E. A. & Paustian, K. 2002. Stabilization mechanisms of soil organic matter: implications for C-saturation of soils. *Plant and soil,* 241**,** 155-176.

Smittenberg, R. H., Gierga, M., Göransson, H., Christl, I., Farinotti, D. & Bernasconi, S. M. 2012. Climate-sensitive ecosystem carbon dynamics along the soil chronosequence of the Damma glacier forefield, Switzerland. *Global Change Biology,* 18**,** 1941-1955.

Sjöberg, E.L., 1976. A fundamental equation for calcite dissolution kinetics. Geochimica et Cosmochimica Acta, 40(4), pp.441-447.

Torn, M. S., Trumbore, S. E., Chadwick, O. A., Vitousek, P. M. & Hendricks, D. M. 1997. Mineral control of soil organic carbon storage and turnover. *Nature,* 389**,** 170-173.

Tranter, M., 1982. Controls on the chemical composition of alpine glacial meltwaters (Doctoral dissertation, University of East Anglia).

Tranter, M., Davies, T.D., Wigington, P.J. and Eshleman, K.N., 1994. Episodic acidification of freshwater systems in Canada—physical and geochemical processes. *Water, Air, and Soil Pollution*, *72*(1-4), pp.19-39.

Tranter, M., Brown, G., Raiswell, R., Sharp, M. & Gurnell, A. 1993. A conceptual model of solute acquisition by Alpine glacial meltwaters. *Journal of Glaciology,* 39**,** 573-581.

Tranter, M. & Wadham, J. L. 2014. 7.5 - Geochemical Weathering in Glacial and Proglacial Environments. *In:* TUREKIAN, H. D. H. K. (ed.) *Treatise on Geochemistry (Second Edition).* Oxford: Elsevier.

Treadwell-Steitz, C. & Mcfadden, L. D. 2000. Influence of parent material and grain size on carbonate coatings in gravelly soils, Palo Duro Wash, New Mexico. *Geoderma,* 94**,** 1-22.

Visconti, F., De Paz, J. M. & Rubio, J. L. 2010. Calcite and gypsum solubility products in water-saturated salt-affected soil samples at 25°C and at least up to 14 dS m−1. *European Journal of Soil Science,* 61**,** 255-270.

Urey, H.C., 1952. On the early chemical history of the earth and the origin of life. Proceedings of the National Academy of Sciences, 38(4), pp.351-363.

Wadham, J., Cooper, R., Tranter, M. & Hodgkins, R. 2001a. Enhancement of glacial solute fluxes in the proglacial zone of a polythermal glacier. Journal of Glaciology, 47, 378-386.

Wadham, J. L., Cooper, R. J., Tranter, M. & Bottrell, S. 2007. Evidence for widespread anoxia in the proglacial zone of an Arctic glacier. *Chemical Geology,* 243**,** 1-15.

Wadham, J. L., Cooper, R. J., Tranter, M. & Hodgkins, R. 2001b. Enhancement of glacial solute fluxes in the proglacial zone of a polythermal glacier. *Journal of Glaciology,* 47**,** 378-386.

Weiss, R. F. 1974. Carbon dioxide in water and seawater: the solubility of a non-ideal gas. *Marine chemistry,* 2**,** 203-215.

West, A. J., Galy, A. & Bickle, M. 2005. Tectonic and climatic controls on silicate weathering. *Earth and Planetary Science Letters,* 235**,** 211-228.

White, A. F. & Brantley, S. L. 1995. Chemical weathering rates of silicate minerals: an overview. *Chemical Weathering Rates of Silicate Minerals,* 31**,** 1-22.

White, A. F. & Brantley, S. L. 2003. The effect of time on the weathering of silicate minerals: why do weathering rates differ in the laboratory and field? *Chemical Geology,* 202**,** 479-506.

White, D. M., Hodkinson, I. D., Seelen, S. J. & Coulson, S. J. 2007. Characterization of soil carbon from a Svalbard glacier-retreat chronosequence using pyrolysis–GC/MS analysis. *Journal of Analytical and Applied Pyrolysis,* 78**,** 70-75.

Zhou, J., Bing, H., Wu, Y., Yang, Z., Wang, J., Sun, H., Luo, J. & Liang, J. 2016. Rapid weathering processes of a 120-year-old chronosequence in the Hailuogou Glacier foreland, Mt. Gongga, SW China. *Geoderma,* 267**,** 78-91.

Chapter 3. Study Areas and Methods

3.1. Study areas

The full details of the three glacial forefield areas studied are described in the results chapters 4 & 5. In this chapter an overview of each of the studied sites is presented.

Midtre Lovénbreen and its glacial forefield are situated in a north-facing catchment on Brøggerhalvøya, Northwest Svalbard (78°50′ N., 12° E.). The forefield consists of a hummocky moraine complex, interspersed with epithermal incising proglacial streams, an icing and kettle lakes, Fig. 3.1. The forefield is somewhat flat, with an average gradient decrease of 6.6% over 2km, across an elevation change of 123-0 m.a.s.l. The annual air temperature and precipitation recorded at NY-Alesund from 1961-1990 (approximately 5km East of Midtre Lovénbreen) during the summer and snow-free months are -5.8 °C and 20mm (Svendsen et al., 2002). Midtre Lovénbreen is a polythermal glacier with a subglacial drainage system (Irvine-Fynn and Hodson, 2010a). Glacier mass balance studies have documented its decline since 1967 (Hagen and Liestøl, 1990; Hagen et al., 2003). The ~2 km^2 forefield contains a succession of moraines deposited at an average retreat rate of ~14 m/ year since the last Holocene ice maximum in 1890-1905 (Glasser and Hambrey, 2001; Hambrey et al., 2005).

The dominant lithological rock units in the glacier catchment are metasediments that are primarily felsic with some carbonate rocks and coal seams interdispersed. This complex lithological mixture, created a glacial till within the forefield that is highly heterogeneous in nature. Two macroscopically identifiable glacial till types are observable in the forefield, subglacial till and supraglacial till; these each have their own chemical and physical characteristics.

A chronosequence with respect to primary plant succession begins with lichens, mosses and bryophytes, and progresses towards isolated vascular plants (i.e. *Saxifraga*) at >60 y (Hodkinson et al., 2003). The soils and glacial till are affected by cryoturbation processes that result, in part, from an annual active thaw layer of discontinuous permafrost (Hodkinson et al., 2001; Hodkinson et al., 2002; Hodkinson et al., 2003; White et al., 2007). Where soil has developed, these are classified as cryo-Leptosols and Regosols, reflecting the fact there were no horizons, and they were immature and stony in nature owing to their parent material (gneiss) glacier till (FAO, 2006; Hodkinson et al., 2003).

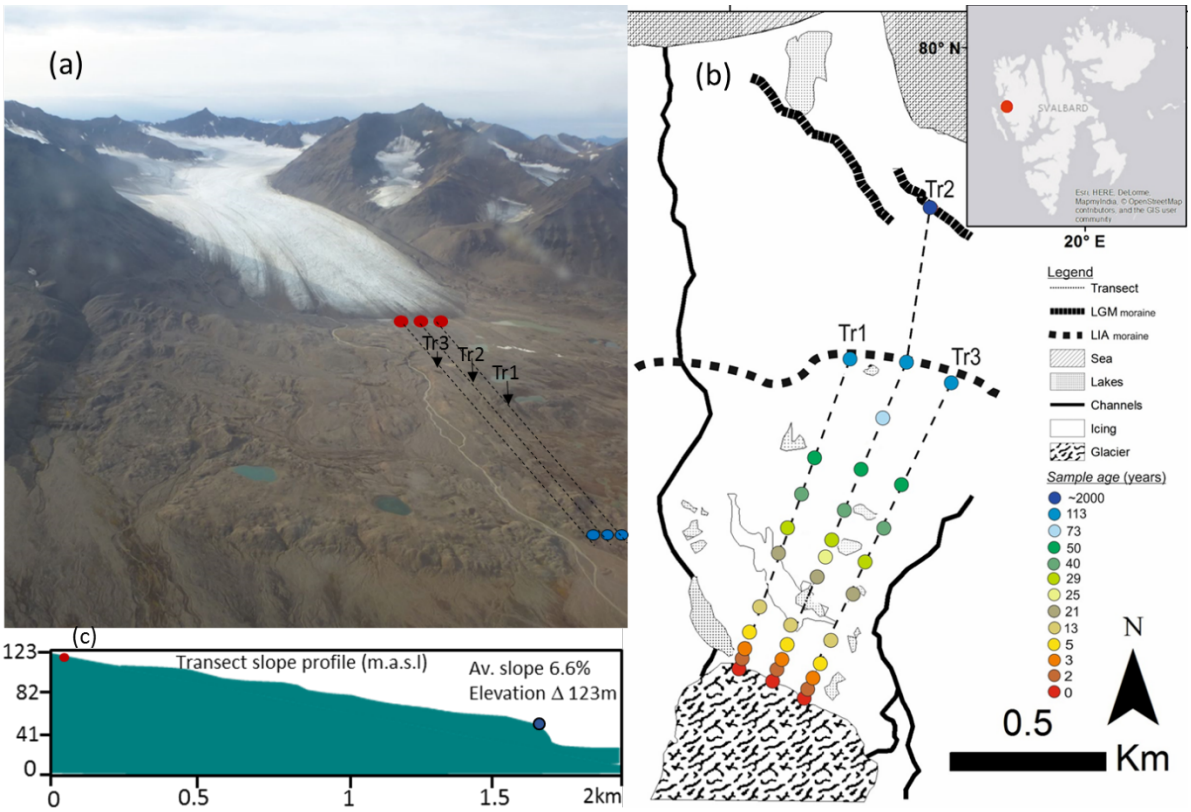

Figure 3.1. (a) Aerial photograph of Midtre Lovénbreen and its forefield and **(b)** schematic map of the forefield and its key landscape features showing the sampled sites and their ages along three transects, one with primarily subglacial till (Tr1) and two with supraglacial till. Plot **(c)** shows the average slope and elevation change as a function of distance.

Storglaciären (67°54'N, 18°34'E) and **Rabot's glacier** (67°55′N, 18°30′E) in sub-Arctic Sweden are classified as small valley glaciers of about 3 km^2 in (planar) area. Storglaciären is located on the east side of the Kebnekaise massif (Fig.3.2), while Rabot's glacier is on the west side (Fig. 3.3). Their forefields are 0.5 km^2 and 1 km^2, respectively, with an elevation decrease of roughly 115 m and 80 m from their glacier snouts to the terminal moraine (aged 1910). These topographic, elevation changes result in the Storglaciären forefield having a steep slope relief (Avg. slope 27%), whilst Rabot's glacier was more gently sloped (Avg. slope 12%). In both forefields, several braided river systems have incised into the inner moraines and given a pronounced terminal moraine (Karlén, 1973; Jahn, 1991).

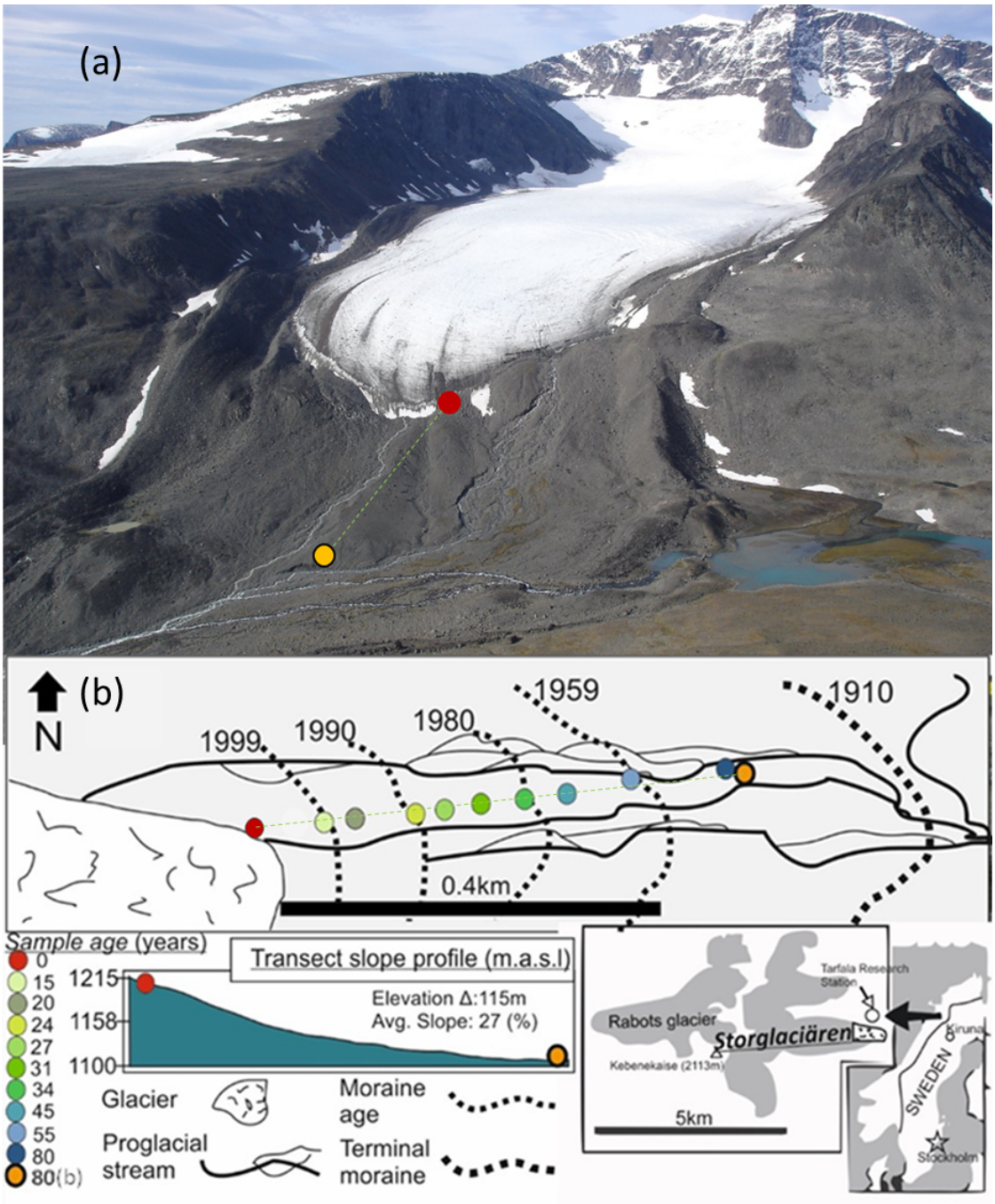

Figure 3.2. (a) Aerial photograph of Storglaciären and its forefield, Sweden and **(b)** schematic map of the forefield and its key landscape features showing the sampled sites and their ages along the transect delineated as a green hashed line.

The mean annual air temperature (1965–2014) at the Tarfala Research Station (TRS) (1130 m a.s.l and 0.5km away from Storglaciären) is −3.5 ± 0.9C°. While the average summer temperature (1946–2014) is 5.9 ± 1.2C° with maximum temperatures up to 20–25C°, and the mean winter temperature (1965–2014) is −6.6 ± 1.1◦C with minimum temperatures of −25°C (Grudd et al., 1996; updated with unpublished data from the TRS). The mean annual

precipitation measured at the TRS has been estimated as 1997-450 mm, of which 400–600 mm falls between June and August (Dahlke et al., 2012).

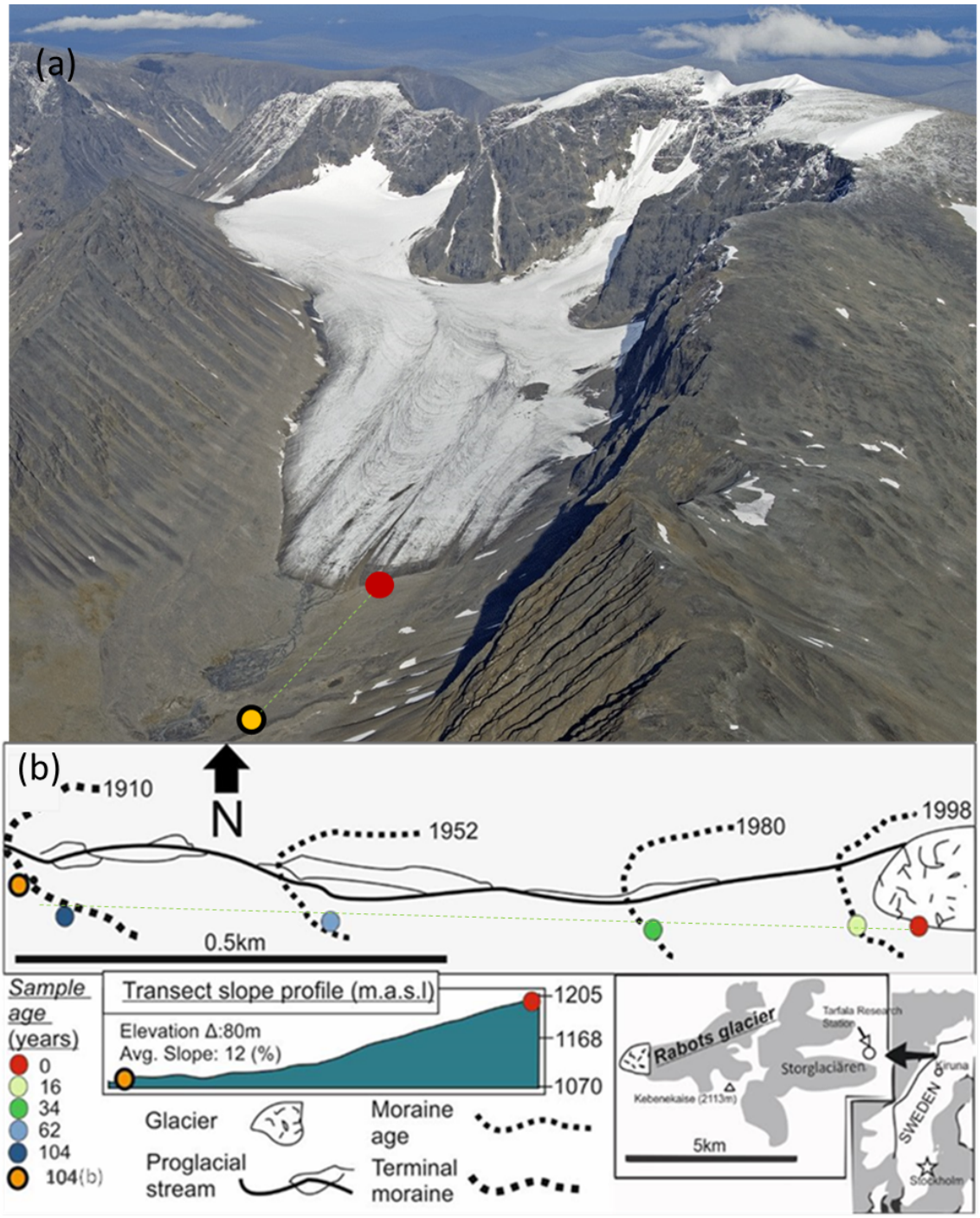

Figure 3.3. (a) Aerial photograph of Rabot's glacier and its forefield, Sweden and **(b)** schematic map of the forefield and its key landscape features showing the sampled sites and their ages along the transect delineated as a green hashed line.

The Kebnekaise massif that Storglaciären and Rabot's forefields are situated on, is a part of the late Precambrian Seve belt of the Scandinavian Caledonides (Andréasson and Gee, 1989). The

lithological units that both forefield catchment consist of, are high grade metamorphic felsic and mafic rocks. The glacial tills present in each forefield naturally reflect these in their heterogeneity (Andréasson and Gee, 1989). The predominant type of glacial till is subglacial, although supraglacial tills that propagate outward from the glaciers surface are interspersed as a superficially deposit on top of this.

In Storglaciären and Rabot's, vegetation succession is evidenced as a function of moraine age (Stork, 1963). It consists of pockets of micro-niche communities, however, in general at the glacial termi, lichen are present, and with time the community shifts to vascular plants (e.g. *Saxifraga*) and moss carpets. The soils in the forefields characteristically have no horizons and typically include a high stone content deriving from their glacier till genesis. Consequently, they are classified as Leptosols and Regosols (FAO, 2006). These soils are affected by cryoturbation processes (Jahn, 1991) that in part result from an annual active layer thaw depth of discontinuous permafrost to a mean depth of 1.5 to 1.6m (Bolin Centre for Climate Research, 2013).

3.2. Methods

The full details of sample preparation and handling, the sampling strategy and the *in-situ* field measurements are described in the results chapters 4 & 5. In this section, basic sample preparation, terminology and common Earth science analytical techniques used in this thesis are outlined.

3.2.1. Basic properties and sample preparation

Samples from the various glacial forefields were collected in 2013 and 2015 following strict protocols (see Chapter 4). Upon return to the lab, the samples were oven-dried for 48 h at 40 °C. The dried samples from 2013 were sieved to < 7 mm, while the samples collected in 2015 were sieved to three size fractions (>7mm, 7mm to 2mm and <2mm). Hereinafter, the <2mm size fractions from 2013 and 2015 will be referred to as "*soil samples*", while the >7mm and 7mm to 2mm size fractions will be referred to as "*parent material*", while the unweathered rocks, representative of the local lithologies, are termed "*source rocks*". Aliquots of all dried soil, parent and source rock samples, were crushed using an agate disk-crushing mill and sieved to <63µm prior to any further analyses. In the samples from Midtre Lovénbreen, five selected

samples spanning the chronosequences were used for separation of the clay mineral fraction using gravity dispersion. The method is as follows: a dried, finely ground powdered bulk sample was placed into a labelled 1 L separating tube, filled with water to the 600 mm line, then 1 mL of sodium hexametaphosphate dispersant was added, and it was shaken for 10 min. and left to settle for approximately 16 h. The time was calculated using the Atterberg computer program to the time or height of fall. Dispersed samples were filtered using Millipore Isopore 0.4 μm filter papers.

3.2.2. Soil pH

The pH of a solution is defined as $-\log_{10}$ of the activity of hydronium ion concentration (H^+ or, more precisely, H_3O^+ aq). This definition of pH was introduced in 1909 by the Danish biochemist, Sorensen. It is expressed mathematically in Equation 3.1 as:

$$pH = -\log[H^+] \qquad \text{Equation. 3.1}$$

where: $[H^+]$ is hydrogen ion concentration in mol/L

The pH value is an expression of the ratio of $[H^+]$ to $[OH^-]$ (hydroxide ion concentration). Hence, if the $[H^+]$ is greater than $[OH^-]$, the solution is acidic. Conversely, if the $[OH^-]$ is greater than the $[H^+]$, the solution is basic. the pH values are affected by temperature due to changes in dissociation constants of the ions in the solution being measured. Therefore, the temperature a measurement was taken should always be stated, and the pH electrode should be held near the reference temperature probe.

In soils, pH is a fundamental variable that controls biogeochemical reactions such as the dissolution and precipitation of minerals, or the soils mineral cation exchange capacity or the adsorption / desorption of organic compounds or metals onto mineral surfaces. The optimum range for most soils is at a pH of 5.5 to 7.5 although many plant species are adapted to metabolise outside this range. Ultra-acidic soils (pH<3.5) and very strongly alkaline soils (pH>9) are rarer.

In the soil samples analysed for pH measurements were taken both *in-situ* using litmus pH indicator paper, and on return from the field in a laboratory. Field pH was measured using a

1:2 ratio of soil: deionized water after vigorous shaking for 30 seconds. After inserting the litmus paper into a soil slurry, it was removed, left to dry for 30 seconds and the semi-quantitative result was noted. Upon return to Leeds, pH analyses were done using deionized water (Millipore, Milli-Q) in a 1:2.5 soil: water ratio. This mix was left to react for 30 min. on a shaker, then left to settle for 60 min. before taking a reading of the pH in the supernatant using a glass electrode (VWR, #622-1759) and a pH meter (Hanna 210) calibrated just prior to use using NIST standard buffer solutions at 18 and 19 °C.

3.2.3. Ultraviolet and visible (UV-Vis) absorption spectroscopy and atomic absorption spectrometry

This technique was used to measure the change in light (because of adsorption) after passing through a solution. It works at the ultraviolet and rainbow portion of the electromagnetic spectrum (e.g., λ = 180-900 nm). The Beer-Lambert law (Eq. 3.2) shows the fundamental relationship used to evaluate changes in light absorbance (Perkampus et al., 1992).

$$A = log_{10}\frac{I_0}{I} = \varepsilon lc \qquad \text{Equ.3.2}$$

Where

A = absorbance

I_0 = intensity of incident beam ($W.cm^{-2}$) and a given wavelength (λ; nm)

I = intensity of beam after transmission

Ɛ = molar adsorption coefficient

l = length of the solution the light passes through (cm)

C = concentration of solution ($mol.dm^{-3}$)

This principle was used to determine concentrations of phosphate and iron in samples following sequential extractions (see details in section 3.2.8 & 3.2.10). Phosphate was measured colourimetrically on a spectrophotometer at a wavelength of λ = 880 nm, following the phosphomolybdate blue method of Koroleff (1976). Although iron could also have been measured colourimetrically using the ferozzine method, due to the low concentrations, analyses were done using atomic absorption spectroscopy (AAS) at a wavelength of λ = 248.3 nm using a flame atomizer. Both the spectrophotometer and AAS were calibrated using prepared iron and phosphorus standard solutions.

3.2.4. X-ray diffraction spectroscopy

X-ray diffraction (XRD) is a non-destructive technique used to identify and quantify the mineralogical phases present in a sample. The oscillating electric field interacts with the charged particles of an atom causing these to oscillate at the same frequency. Crystalline anisotropic materials, e.g. quartz, are characterized by periodicity and symmetry in their atomic distribution, and these scatter the X-rays in specific directions. If mineral soil samples also contain fractions of amorphous and isotropic, or nano-crystalline materials (i.e., amorphous iron oxides, silica or even volcanic glasses), these do not scatter well, consequently the X-rays are distributed in all directions, resulting in a distorted and broad X-ray pattern and low intensities.

Recording the intensity of the diffracted rays (in counts) as a function of twice the incident angle of the beam to the samples (θ; degrees) results in an XRD pattern. X-Ray diffraction patterns and intensities are linked through Bragg's Law (Eq. 3.3), as diffracted rays reveal the lattice spacing (d; nm) in a crystalline sample and the detector processes and counts the diffracted rays, Fig. 3.4.

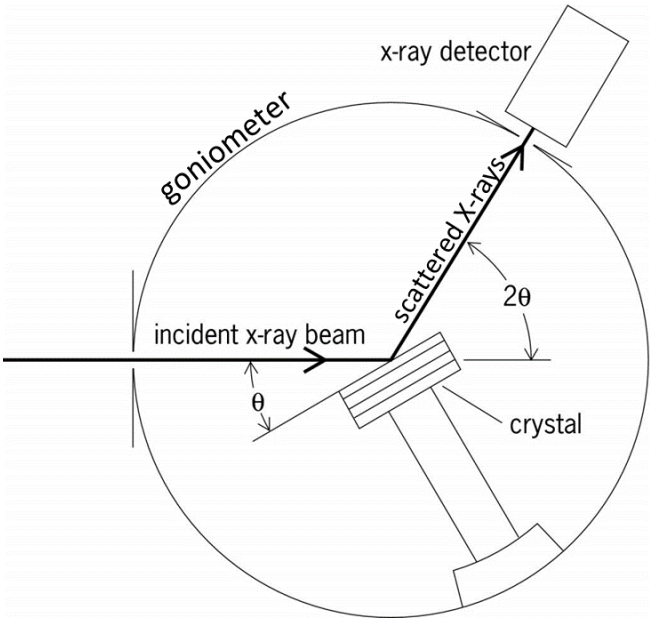

Figure 3.4. The main components of modern X-ray powder diffractometer shown together with the goniometer. Obtained from Borie, 1965.

$$n\lambda = 2d \sin(\theta) \qquad \text{Equation 3.3}$$

During this research, mineral powders were analysed using a Bruker D8 diffractometer that was run using a CuK-1 source and using the following parameters: 2θ range 0-90°; resolution 0.105°/step; counting time 1s / step. The resulting XRD patterns were analysed qualitatively with the EVA software (version 4) and quantitatively with TOPAS (version 4).

Quantitative XRD analysis using the computer software (TOPAS) was limited by inaccurate decoupling of similar phases with a high degree of reflection overlap, particularly minor phases in the bulk mineral assemble. For example as shown in Kahle et al., (2002) simple mixtures of calcium carbonate and dolomite phases resulted in uncertainties of roughly ±3%. Using this technique it was unsurprising that no mineralogical trends in carbonates or clay minerals were observed, as they made up on average <3% of the bulk material. To overcome this, the total inorganic carbon analyses were used in tandem with stable isotopes $\delta^{13}C_{TIC}$ to determine the content of carbonates, and to evaluate calcite and dolomite equivalents in the samples. Furthermore, the selected clay minerals were analysed by XRD to better characterise the type of clay minerals present, and their modal abundance as a function of moraine age.

3.2.5. X-ray florescence spectroscopy

X-ray fluorescence (XRF) is a technique that can typically analyse elemental concentrations of major, minor and trace elements e.g. ranging high wt.% to parts per million (ppm). Samples are measured as solids, either as pressed pellets (non-destructive, less accurate), or glass bead fluxes (destructive, more accurate).

The principle of XRF uses the fact that individual atoms, when excited by an external energy source, emit X-ray photons of a characteristic energy or wavelength. From first principles at an atomic level, a stable atom is made of a nucleus and electrons orbiting it. The electrons are arranged in energy levels or shells (K, L, M, N) and different energy levels can hold different numbers of electrons at a certain orbit. Therefore, when a high energy primary X-ray of kilo electron volts (keV), or wavelength in nanometres (nm), collides with a stable atom, an electron is ejected by ionization from a low energy level and a vacancy is created, making the atom unstable. To compensate for the instability, an electron from a higher energy level falls into this vacancy and excess energy emitted in the form of a secondary X-ray. There are a limited number of ways in which this can happen, as shown in, Figure 3.5. The main transitions are given names: an L→K transition is traditionally called K_{α}, an M→K transition

is called K_β, while an M→L transition is called L_α (not shown).

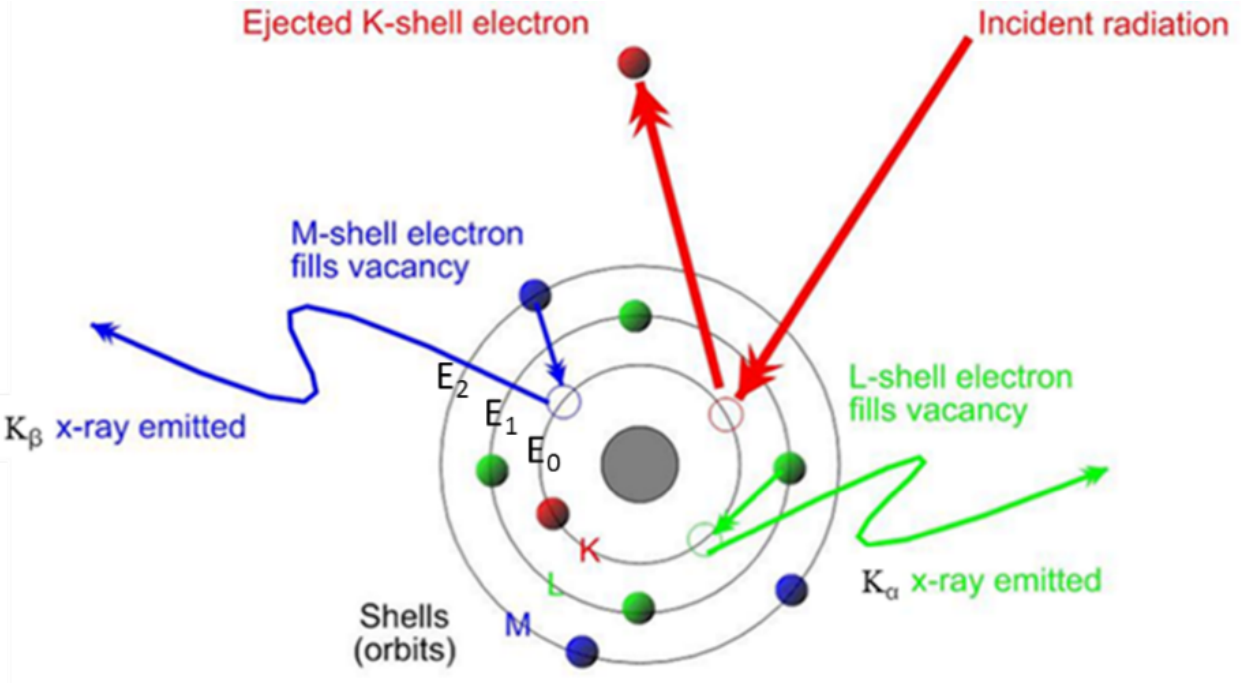

Figure 3.5. X-ray fluorescence of an atom: electron excitation and relaxation in different shells K, L, M and an example of their transition pathways ΔE=E1-E0= Kα and ΔE=E2-E0= Kβ. Obtained from Cesareo, 2010.

The amount of energy lost is equivalent to the difference in energy between the two electron shells, which is determined by the distance between them. The distance between the two orbital shells is unique to each element. The energy lost collected by a detector, processed and transformed to generate a spectrum trace consisting x-ray intensity peaks *vs.* their energy, Fig. 3.6. The X-ray emitted from the sample is and converted to a graphical format using energy-dispersive analysis or e.g. unique atomic structure has a unique set of peaks on its electromagnetic emission spectrum that can be characterised. The peak energy identifies the element and its peak area (or intensity) gives an indication of its amount in the sample.

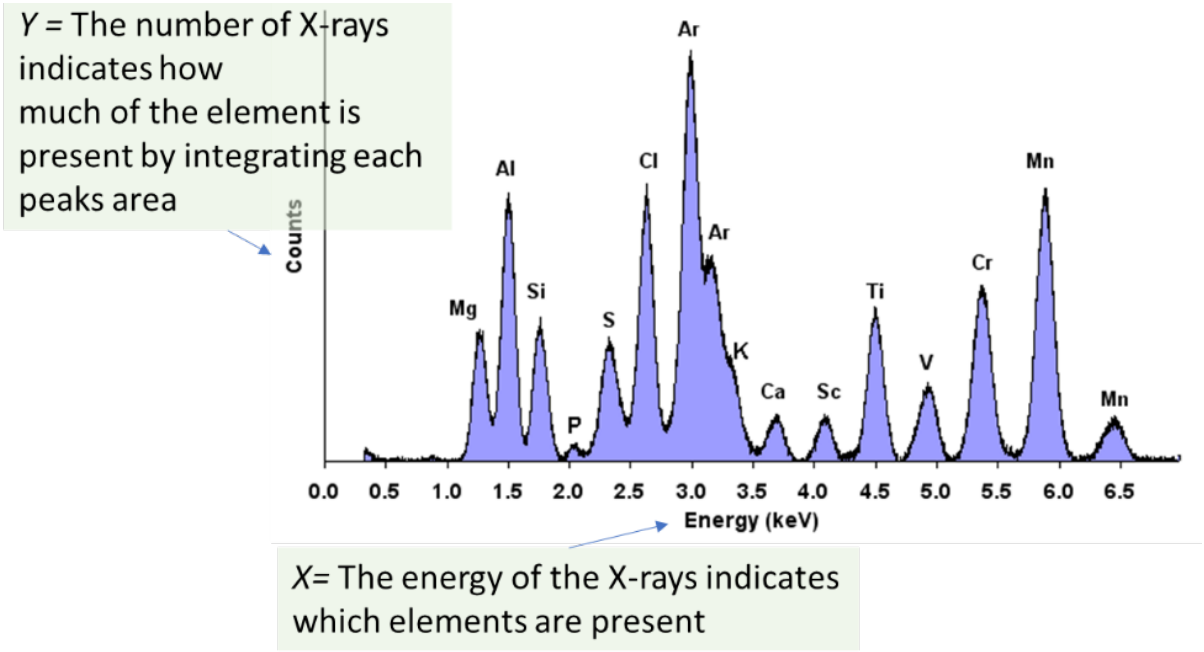

Figure 3.6. Example of an X-ray fluorescence spectrum trace. Modified from Cesareo, 2010.

To prepare a fused glass bead for XRF analyses, all soil samples, parent material and source rocks were crushed using a jaw crusher, and ground in an agate disk mill to a fine powder roughly 1-63µm. Fused glass beads have an advantage over powder pellet preparation because it creates a homogenous sample for analysis alleviating common matrix effects and is of higher accuracy for some elements. Matrix effects include particle size mis-matching of samples in relation to certified reference materials, as natural samples are often heterogeneous (Van Grieken, 2001). Fused glass bead preparation began by weighing 2.5 g ±0.00001 of ground, oven-dried powders that were heated to 105 °C for 24 h to drive-off any remaining adsorbed water (and determine the % H_2O) into platinum crucibles. Subsamples of the dried powders were mixed at a 1:6 ratio sample to lithium metaborate flux. In addition, ~1g NH_4NO_2 was added as an oxidising agent to remove organics and sulfides, which deteriorate platinum crucibles and cause erroneous XRF results. Fused bead was cast by gradually dissolving individual samples in the lithium metaborate flux on a furnace stage that ranged 450 to 1100 °C over a 30 min. melting period in platinum crucibles to create a homogenous, flat surfaced fused glass bead. Sample volatiles were accounted for by measuring the loss on ignition (LOI) that was calculated gravimetrically, weighing the sample before and after the fusion process. Where sample LOI's were unobtainable separate CO_2 and H_2O measurements were made using a C H elemental analyser. For major elements the data is reported as oxides in *wt%*, while minor and trace elements are reported as elements in *ppm*.

3.2.6. Total sulfur and carbon (TC, TOC and TIC) elemental and isotopic analyses

Total carbon (TC) and total sulfur (TS) analyses in the powdered samples were weighed out to 5 decimal places. Masses of sample were weighed to between 200-300mg. Analyses done to determine the carbon and sulphur content were done using a LECO SC-144DR Dual Range Sulfur and Carbon Analyser (*model*: vario EL). Soil samples were placed into the tube furnace kept at a constant 1350 °C with a pure oxygen atmosphere and combusted releasing CO_2 and SO_2. These gases then flowed through two anhydrone tubes to remove water and a separate halogen trap before going through a IR detection cell to measure the concentration of CO_2 and SO_2. The instrument converts these measurements into weight percentage values considering the original starting sample mass and calibration using certified standards.

Total organic carbon was determined as the difference between the initial TC and a second analyses of total carbon performed after acid treating the initial samples with 10% HCl at room temperature for 24 h to dissolve all inorganic carbonates (Schumacher, 2002). The results were compared gravimetrically with CO_2 lost through effervescence, Eq. 3.4.

$$TOC = TC - TIC \qquad \text{Equation 3.4}$$

3.2.7. Stable isotope $\delta^{13}C_{org}$

Carbon has two natural and abundant stable isotopes, ^{13}C and ^{12}C that are useful tracers and proxies in the study of soil in the carbon cycle. Carbon stable isotopes ^{13}C and ^{12}C are measured using isotope-ratio mass spectrometry (Fig. 3.7). In principle, the instrument operates by ionizing a gaseous sample of a fine powdered and homogenized sample of soil or rock. The sample is then accelerated over a potential in the kilo-volt range, and the stream of ions are then separated according to their mass-to-charge ratio (m/z). Beams with heavier ions bend at a larger radius than beams with lighter ions. The current of each ion beam is then measured using a detector.

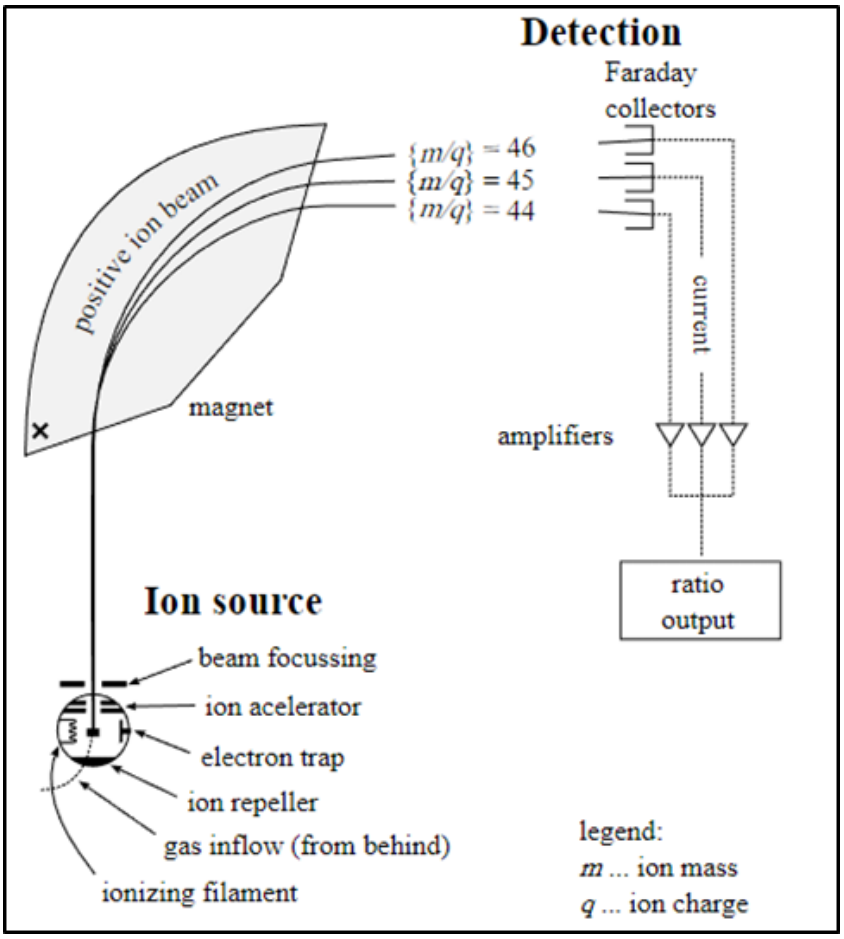

Figure 3.7. A schematic diagram of isotope-ratio mass spectrometry used to measure stable carbon isotopes concentrations in natural samples like soils and rocks.
The variation in 13C and 12C is a result of isotopic fraction during physical, chemical and biological processes. Natural materials of range from 0-110‰. Obtained from Faure and Mensing, 2005.

The quantity of ^{13}C and ^{12}C measured is expressed as an absolute quantity, the relative difference between the isotope ratio of the and standard gases, as follows

$$\partial^{13}\mathrm{C}\ (‰) = \left(\frac{R_{sample} - R_{standard}}{R_{standard}} - 1\right) 1000 \qquad \text{Equation. 3.5}$$

The sample and that of the standard, and R is the mass of 45/44 ratio of the same or gas standard.

All samples measured were expressed by the international convention, $\delta^{13}C$ relative to the $^{13}C/^{12}C$ of the Pee Dee Belemite (PDB) standard in delta (δ) per mille (‰). This standard was

a limestone fossil of *Belemnitella Americana* from the Cretaceous Pee Dee formation in South Carolina. As the basis of the PDB scale, it has been a $\delta^{13}C$ of 0‰.

The $\delta^{13}C_{TIC}$ for soil samples was prepared by producing CO_2 by reacting carbonate minerals at 50 °C with phosphoric acid following procedures like those described by McCrea (1950). Data were corrected per Craig, 1957. For $\delta^{13}C_{TOC}$ measurements, samples were combusted in sealed tubes with CuO at 900 °C for 2 h to convert all organic matter to CO_2. This CO_2 was then purified on a vacuum line, and splits of the purified gas were taken for $\delta^{13}C_{org}$ analyses using a mass spectrometer (DELTAplusXL ThermoFisher).

3.2.8. Iron extractions

The sequential extraction procedure of Poulton and Canfield (2005) is designed to quantitatively define seven operationally derived iron pools in a range of terrestrial and marine sediments, see Table. 3.1.

Table 3.1. The sequential extraction for Fe-bearing phases in sediments like soils and glacial tills

Terminology	Extraction step (*target phases*)	Reaction (*calculation*)
(1) Fe_{ox1}	Easily reducible oxides, *poorly crystalline ferrihydrite*	Reduction of Fe^{3+} using ascorbic acid treatment
(2) Fe_{ox2}	Reducible oxides *goethite, hematite and akaganèite*	Reduction of Fe^{3+} by dithionite and subsequent chelation by citrate
(3) Fe_{mag}	Magnetite *magnetite*	Chelation by ammonium oxalate
(4) Fe_{PRS}	Poorly reactive sheet silicate *Fe sheet silicate:* nontronite, chlorite, glauconite, biotite	Protonation of the silicate lattice so it dissociates the Fe using boiling hydrochloric acid
(5) Fe_{py}	Fe pyrite *pyrite*	Oxidisation of Fe^{2+} in iron sulfides e.g. pyrite using chromous chloride distillation
(7)Fe_U	Total Fe *unreactive silicate Fe; pyroxene and* amphiboles	*The difference between total Fe and the sum of each of the extraction phases, is the unreactive iron (Fe_u)*

All operationally defined iron species were quantified using extractions according to Poulton and Canfield, 2005, unless otherwise stated. Exactions were performed under oxic conditions in constantly agitated 15ml centrifuge tubes (Polyethylene: Sarstedt: Ref. 60.732.001) except for the boiling HCL that used preformed in glass test tubes. The samples were subjected to a series of sequential extractions that progressive remove more stable forms (stronger bound) iron species as follows: 1) ascorbic acid treatment that targets poorly crystalline ferrihydrite (Raiswell et al., 2010) and 2) a sodium dithionite solution ($50g^{-}l^{-1}$) buffered to pH 4.8 with a 0.35 M acetic acid/0.2 M sodium citrate was used to extract 'reducible' crystalline iron oxides (goethite, hematite and akaganeite). Together extractions 1&2 are termed the highly reactive Fe fraction (Fe_{HR}). An ammonium oxalate (3) 0.2 M solution (pH 3.2) was used to extract magnetite. However, as the dithionite extraction was performed before the oxalate extraction (as suggested by Poulton and Canfield, 2005) magnetite Fe may slightly underestimate (by around 5%). A concentrated boiling hydrochloric acid (HCL) extraction (step 4) using a 12N HCL (5 ml volume) for 1 min was applied to quantify Fe remaining from certain sheet-silicate minerals (nontronite, chlorite, glauconite, biotite). Extractions 3 & 4 are termed the poorly reactive Fe fractions (Fe_{PR}). The total Fe (Fe_{total}) was measured using X-ray florescence spectroscopy as explained above (step 5). The difference between total Fe and the sum of each of the extraction phases, is the unreactive iron (Fe_u), plus pyrite Fe. This fraction consists of residual silicate iron, specifically from pyroxenes and amphiboles, which are essentially unreactive towards dissolved sulfide (Poulton and Canfield, 2005). Each of the extract solutions were measured for their Fe concentration using atomic absorbance spectroscopy (see Section 3.2.3).

3.2.9. Pyrite extraction

Pyrite and acid volatile sulfides were determined via the chromous chloride distillation technique (Canfield et al. 1986). The sulfur extracted is precipitated as AgS_2 using $Ag(NO_3)_2$, and the concentration of FeS_2 is calculated from the gravimetric difference between the starting mass of the sample and the end product and the conversion of AgS_2 to FeS_2 using their molar ratios.

3.2.10. Phosphorous extraction

The SEDEX sequential extraction method of Ruttenberg (1992) was developed for the quantification of 5 sedimentary phosphorus reservoirs, and has been shown to be a robust extraction method for a variety of sedimentary settings including soils. The main aim of the method is to chemically separate authigenic P phases from detrital apatite of igneous or metamorphic origin (FAP), and hence this dictates the sequence of the extractions, and the conditions required. The method combines extractions previously used in selective leaching schemes for metals and P, which have then been modified to enhance the recovery of the desired P-bearing phases all of which are present in soils. The sequential extractions and its target phases are as follows in Table 3.2. Following each extraction (apart from step 2), solutions were analysed for phosphorus colourimetrically on a spectrophotometer, following the phosphomolybdate blue method of Koroleff (1976), see Section 3.2 for more details on this analytical method.

Table 3.2. The SEDEX sequential extraction for P-bearing phases in sediments like soils and glacial tills

Terminology	Target phase extracted	Reaction
(1)	Exchangeable or loosely sorbed P	Formation of $MgPO_4^-$ complex and/or mass action displacement by Cl^-
(2)	Easily reducible or reactive ferric Fe-bound P	Reduction of Fe^{3+} by dithionite and subsequent chelation by citrate
(3)	CFAP + biogenic hydroxaptite + $CaCO_3$ bound P	Acid dissolution at moderately low pH and/or chelation of Ca^{2+} by acetate
(4)	FAP	Acid dissolution
(5)	Organic P	Dry oxidation at $550^{\circ C}$ 1M HCL extraction of ashed residue

3.2.11. Statistical analysis

All data analyses were conducted with SPSS (IMB®) or the Microsoft Excel® computer software. To examine the relationships between moraine age (independent variable) and dependent variables such as chemical concentrations both simple and multiple regression analyses were conducted. Simple regression was used to identify the patterns (e.g. linear or nonlinear) of the relationship with each dependent variable. Data normality was checked using

a Shapiro-Wilk test and Z scores and histograms to select appropriate parametric or non-parametric statistical tests. For the statistical comparison of means, using their sum of squares, a test for homogeneity of variances is required and for this Levene's test was applied. If the variance level from this test was >0.05 a one-way ANOVA test was used to test independent data sets for their statistical significance (significance level 0.05) on one dependent variable and two or more (independent variables) groups. Furthermore, data with unequal variances (Levene's test <0.05) were tested for their significance using Welch's ANOVA test (Manly, 2008).

3.3. References

Anderson, S. P., Drever, J. I., Frost, C. D. & Holden, P. 2000. Chemical weathering in the foreland of a retreating glacier. *Geochimica et Cosmochimica Acta,* 64**,** 1173-1189.

Anesio, A. M., Hodson, A. J., Fritz, A., Psenner, R. & Sattler, B. 2009. High microbial activity on glaciers: importance to the global carbon cycle. *Glob Chang Biol,* 15**,** 955-960.

Anesio, A. M., Sattler, B., Foreman, C., Telling, J., Hodson, A. & Tranter, M. 2010. Carbon fluxes through bacterial communities on glacier surfaces. *Ann Glaciol,* 51**,** 32-40.

Ansari, A. H. 2016. Stable isotopic evidence for anaerobic maintained sulphate discharge in a polythermal glacier. *Polar Science,* 10**,** 24-35.

Borie, B., 1965. X-Ray Diffraction in Crystals, Imperfect Crystals, and Amorphous Bodies. *Journal of the American Chemical Society*, *87*(1), pp.140-141.

Borin, S., Ventura, S., Tambone, F., Mapelli, F., Schubotz, F., Brusetti, L., Scaglia, B., D'acqui, L. P., Solheim, B., Turicchia, S., Marasco, R., Hinrichs, K. U., Baldi, F., Adani, F. & Daffonchio, D. 2010. Rock weathering creates oases of life in a High Arctic desert. *Environmental Microbiology,* 12**,** 293-303.

Canfield, D.E., Raiswell, R., Westrich, J.T., Reaves, C.M. and Berner, R.A., 1986. The use of chromium reduction in the analysis of reduced inorganic sulfur in sediments and shales. *Chemical geology*, *54*(1-2), pp.149-155.

Carter, M. R., Angers, D. A., Gregorich, E. G. & Bolinder, M. A. Characterizing organic matter retention for surface soils in eastern Canada using density and particle size fractions. Can. J. Soil Sci. 83, 11–23 (2003).

Cesareo, R., 2010. *X-Ray Fluorescence Spectrometry*. Wiley-VCH Verlag GmbH & Co. KGaA.

Cooper, R. J., Wadham, J. L., Tranter, M., Hodgkins, R. & Peters, N. E. 2002. Groundwater hydrochemistry in the active layer of the proglacial zone, Finsterwalderbreen, Svalbard. *Journal of Hydrology,* 269**,** 208-223.

Craig, H., 1957. Isotopic standards for carbon and oxygen and correction factors for mass-spectrometric analysis of carbon dioxide. *Geochimica et cosmochimica acta*, *12*(1-2), pp.133-149.

Farquhar, G.D., Ehleringer, J.R. and Hubick, K.T., 1989. Carbon isotope discrimination and photosynthesis. *Annual review of plant biology*, *40*(1), pp.503-537.

Faure, G. and Mensing, T.M., 2005. *Isotopes: principles and applications*. John Wiley & Sons Inc.

Glasser, N. F. & Hambrey, M. J. 2001. Styles of sedimentation beneath Svalbard valley glaciers under changing dynamic and thermal regimes. *Journal of the Geological Society,* 158**,** 697-707.

Hagen, J. O. & Liestøl, O. 1990. Long-term glacier mass-balance investigations in Svalbard. *Annals of Glaciology,* 14**,** 102-106.

Hagen, J. O., Melvold, K., Pinglot, F. & Dowdeswell, J. A. 2003. On the net mass balance of the glaciers and ice caps in Svalbard, Norwegian Arctic. *Arctic, Antarctic, and Alpine Research,* 35**,** 264-270.

Hambrey, M. J., Murray, T., Glasser, N. F., Hubbard, A., Hubbard, B., Stuart, G., Hansen, S. & Kohler, J. 2005. Structure and changing dynamics of a polythermal valley glacier on a centennial timescale: Midre Lovenbreen, Svalbard. *Journal of Geophysical Research-Earth Surface,* 110.

Hjelle, A. 1993. Geology of Svalbard. *Norsk Polarinstitutt Handbook,* 7.

Hodkinson, I. D., Coulson, S. J., Harrison, J. & Webb, N. R. 2001. What a wonderful web they weave: spiders, nutrient capture and early ecosystem development in the high Arctic – some counter-intuitive ideas on community assembly. *Oikos,* 95**,** 349-352.

Hodkinson, I. D., Coulson, S. J. & Webb, N. R. 2003. Community assembly along proglacial chronosequences in the high Arctic: vegetation and soil development in north-west Svalbard. *Journal of Ecology,* 91**,** 651-663.

Hodkinson, I. D., Webb, N. R. & Coulson, S. J. 2002. Primary community assembly on land – the missing stages: why are the heterotrophic organisms always there first? *Journal of Ecology,* 90**,** 569-577.

Hodson, A., Anesio, A. & Tranter, M. 2008. Glacial ecosystems. *Ecol Stud,* 78**,** 41-67.

Hodson, A., Mumford, P., Kohler, J. & Wynn, P. M. 2005a. The High Arctic glacial ecosystem: new insights from nutrient budgets. *Biogeochemistry,* 72**,** 233-256.

Hodson, A., Murnford, P. & Lister, D. 2004. Suspended sediment and phosphorus in proglacial rivers: bioavailability and potential impacts upon the P status of ice-marginal receiving waters. *Hydrological Processes,* 18**,** 2409-2422.

Hodson, A., Tranter, M. & Vatne, G. 2000. Contemporary rates of chemical denudation and atmospheric CO2 sequestration in glacier basins: an Arctic perspective. *Earth Surface Processes and Landforms,* 25**,** 1447-1471.

Hodson, A. J., Mumford, P. N., Kohler, J. & Wynn, P. M. 2005b. The High Arctic glacial ecosystem: new insights from nutrient budgets. *Biogeochemistry,* 72**,** 233-256.

Irvine-Fynn, T. & Hodson, A. 2010a. Biogeochemistry and dissolved oxygen dynamics at a subglacial upwelling, Midtre Lovénbreen, Svalbard. *Annals of Glaciology,* 51**,** 41-46.

Irvine-Fynn, T. D. L., Barrand, N. E., Porter, P. R., Hodson, A. J. & Murray, T. 2011. Recent High-Arctic glacial sediment redistribution: A process perspective using airborne lidar. *Geomorphology,* 125**,** 27-39.

Irvine-Fynn, T. D. L. & Hodson, A. J. 2010b. Biogeochemistry and dissolved oxygen dynamics at a subglacial upwelling, Midtre Lovenbreen, Svalbard. *Annals of Glaciology,* 51**,** 41-46.

Irvine-Fynn, T. D. L., Moorman, B. J., Sjogren, D. B., Walter, F. S. A., Willis, I. C., Hodson, A. J., Williams, J. L. M. & Mumford, P. N. 2005. Cryological processes implied in Arctic proglacial stream sediment dynamics using principal components analysis and regression. *Cryospheric Systems: Glaciers and Permafrost,* 242**,** 83-98.

Kahle, M., Kleber, M. and Jahn, R., 2002. Review of XRD-based quantitative analyses of clay minerals in soils: the suitability of mineral intensity factors. *Geoderma*, *109*(3-4), pp.191-205.

Koroleff, F., 1976. Determination of total phosphorus. *Methods of Seawater. Verlag Chemie, Weinheim*, *168172*.

Manly, B.F., 2008. *Statistics for environmental science and management*. Crc Press.

Mapelli, F., Marasco, R., Rizzi, A., Baldi, F., Ventura, S., Daffonchio, D. & Borin, S. 2010. Bacterial Communities Involved in Soil Formation and Plant Establishment Triggered by Pyrite Bioweathering on Arctic Moraines. *Microbial Ecology,* 61**,** 438-447.

McCrea, J.M., 1950. On the isotopic chemistry of carbonates and a paleotemperature scale. *The Journal of Chemical Physics*, *18*(6), pp.849-857.

Midgley, N. G., Glasser, N. F. & Hambrey, M. J. 2007. Sedimentology, structural characteristics and morphology of a Neoglacial high-Arctic moraine-mound complex: Midre Lovenbreen, Svalbard. *Glacial Sedimentary Processes and Products,* 39**,** 11-22.

Oades, J. M. The retention of organic matter in soils. Biogeochem. 5, 35–70 (1988).

Ohta, T. & Arai, H. 2007. Statistical empirical index of chemical weathering in igneous rocks: A new tool for evaluating the degree of weathering. *Chemical Geology,* 240**,** 280-297.

Patino, L. C., Velbel, M. A., Price, J. R. & Wade, J. A. 2003. Trace element mobility during spheroidal weathering of basalts and andesites in Hawaii and Guatemala. *Chemical Geology,* 202**,** 343-364.

Perkampus, H.H., 1992. *UV-VIS atlas of organic compounds*. VCH.

Poulton, S. W. & Canfield, D. E. 2005. Development of a sequential extraction procedure for iron: Implications for iron partitioning in continentally derived particulates. *Chemical Geology,* 214**,** 209-221.

Raiswell, R., Vu, H. P., Brinza, L. & Benning, L. G. 2010. The determination of labile Fe in ferrihydrite by ascorbic acid extraction: Methodology, dissolution kinetics and loss of solubility with age and de-watering. *Chemical Geology,* 278**,** 70-79.

Reimann, C., Matschullat, J., Birke, M. & Salminen, R. 2010. Antimony in the environment: Lessons from geochemical mapping. *Applied Geochemistry,* 25**,** 175-198.

Ruttenberg, K.C., 1992. Development of a sequential extraction method for different forms of phosphorus in marine sediments. *Limnology and oceanography*, *37*(7), pp.1460-1482.

Schumacher, B.A., 2002. Methods for the determination of total organic carbon (TOC) in soils and sediments.

Taylor, A. & Blum, J. D. 1995. Relation between Soil Age and Silicate Weathering Rates Determined from the Chemical Evolution of a Glacial Chronosequence. *Geology,* 23**,** 979-982.

Van Grieken, R. and Markowicz, A. eds., 2001. Handbook of X-ray Spectrometry. CRC Press.

Wadham, J., Cooper, R., Tranter, M. & Hodgkins, R. 2001. Enhancement of glacial solute fluxes in the proglacial zone of a polythermal glacier. *Journal of Glaciology,* 47**,** 378-386.

Wadham, J. L., Cooper, R. J., Tranter, M. & Bottrell, S. 2007. Evidence for widespread anoxia in the proglacial zone of an Arctic glacier. *Chemical Geology,* 243**,** 1-15.

White, D. M., Hodkinson, I. D., Seelen, S. J. & Coulson, S. J. 2007. Characterization of soil carbon from a Svalbard glacier-retreat chronosequence using pyrolysis–GC/MS analysis. *Journal of Analytical and Applied Pyrolysis,* 78**,** 70-75.

Wynn, P. M., Hodson, A. & Heaton, T. 2006. Chemical and isotopic switching within the subglacial environment of a High Arctic glacier. *Biogeochemistry,* 78**,** 173-193.

Wynn, P. M., Hodson, A. J., Heaton, T. H. E. & Chenery, S. R. 2007. Nitrate production beneath a High Arctic Glacier, Svalbard. *Chemical Geology,* 244**,** 88-102.

Yang, X.M., Drury, C.F., Reynolds, W.D. and Yang, J.Y., 2016. How do changes in bulk soil organic carbon content affect carbon concentrations in individual soil particle fractions?. Scientific reports, 6, p.27173.

Chapter 4. Results: Sulfide Oxidation, Carbonate Dissoultion and Silicate Weathering in A High-Arctic Forefield

Abstract

Melting glaciers and ice-sheets scour out landscapes creating expansive forelands where tills are deposited. Depending on the glacier catchment lithological units and its sediment-transport regime, geochemical highly reactive mixtures of carbonates, sulfides and silicates may be present in a forefield weathering arena. In such arenas weathered sulfide mineral producing acid can be attenuated through neutralization of this acid by the dissolution of carbonate and silicate minerals. Such reactions could be important in newly deglaciating, soil forming-landscapes as they can either act as potential sinks or sources of CO_2. To this end, this chapter aimed to evaluate the extent of the linkages between sulfide, carbonate and silicate weathering processes and if and how they can regulate CO_2 budgets during the initial stages of soil formation in the High-Arctic progalcial area of Midtre Lovénbreen in Svalbard, Norway. Tills within this forefield, consisted subglacial tills interspersed by superficial drapes of supraglacial till. These till types are known to be subjected to different glacial transit and weathering regimes prior to forefield deposition. Consequently, the properties of each till type were compared for their geochemical reactivity. Both till types are made up of a sedimentary and metasedimentary rock-mixture from predominately mica schists and phyllites that contained traces of carbonate and sulfides. Till types were sampled along three century-long chronosequence at annual-decadal time intervals and at two depths as well as in two years (2013 and 2015). Elemental and mineralogical composition of sampled soils and of unweathered rocks were analysed and are discussed in most cases as a function of moraine age. Comparing empirical relationships highlights the importance of having a a prior knowledge of a tills history and transit through the glacial domain. Subglacial derived till evidenced clear biogeochemical gradients, while these trends were weaker or absent in the more heterogenous supraglacial till samples. In terms of chemical weathering regime, with increased moraine age the soils rapidly became depleted in sulfides and inorganic carbonates. Stoichiometric mass balance calculations showed that both trends were driven by sulfide oxidation coupled to carbonate dissolution (SOCD). These trends were further validated by similar chronological trends in soil pHs and iron oxide concentrations, as well as the reliative abundance of sulfide oxidation mediating microbes. Preferential acid neutralisation by carbonates accounted for the slow onset of silicate weathering in the early ages of the chronosequence. This was also mirrored by a low abundance of forefield flora and fauna that only began to establish at ages ~ >60-years. Consequently, over a century of deglaciation, silicate weathering is somewhat limited and SOCD dominates the weathering processes. Thus, this could be a potential short-term transient CO_2 source to the atmosphere. This has implications for contemporary climate change in addition to deglaciation scenarios, where only primitive life existed and sulfides and carbonates are present in a glaciers catchment lithology.

4.1. Introduction

An increase in regional temperatures over prolonged periods in glaciated areas causes deglaciation, increasing water availability and facilitating weathering in the pro- glacial till. This ultimately leads to the development of soils, and a forefield ecosystem (Bernasconi et al., 2011). Silicates and carbonate weathered during the initial stages of soil formation deliver key nutrients, induce pH changes and aid the development of soil structure and texture and thus increase a soils fertility so it can help support life (Ellis and Mellor, 1995). Moreover, forefield weathering controls the capture and release of CO_2, a potent greenhouse gas (Anderson et al., 2000). Nevertheless, few studies have been conducted in high-Arctic glacier forefields, particularly with the goal to assess their CO_2 sink or source potential. Contemporary 'Arctic warming' is leading to the continual expansion of proglacial forefields (Serreze and Barry, 2011). Since the last glacial maximum, ~ 20k years ago, ~28% of the Northern Hemisphere's glacier and ice-sheets have retreated and new land has been exposed (Gibbs and Kump, 1994).

Forefields are dynamic environments due to the often extensive glacio-fluvial reworking. However, large parts of glacier forefields are also transport-limited, primarily the complex moraine areas. Here, rock:water residences times can be prolonged, with infrequent flushing by meteoric inputs or by meltwaters from *in-situ* melting snow and ice or active layer thaw. This contrasts with the glacier to forefield interface where, over the course of a melt season surface or subsurface glacier melt-water drains into the emergent forefield. The surface glacial melt-water input is quite a dilute, low ionic strength fluid (<40 mmol; (Tranter and Wadham, 2014), while the subglacial melt-waters can be more often nutrient-rich (Wadham et al., 2001; Irvine-Fynn and Hodson, 2010b). At the receding glacier snout, new bedrock is sometimes exposed, yet often overlain with a complex amalgamation of cm to meters-thick glacial till consisting of heterogeneous mixtures of ground-up bedrocks from within the catchment area of the glacier (Boulton, 1978; Glasser and Hambrey, 2001). It is well-known in the glaciological literature, that glacial till and its transit through the subglacial, supraglacial or englaical domain results in highly heterogeneous chemical and physical characteristics. However, the differences that such processing would cause in the glacial forefield have so far not been studied, although these differences are potential important for soil formation in glacial forefields. Subglacial till has a ground-up fraction that is a mixture of finely comminuted 'glacial flour', which is characterised by a large and chemical reactive surface area binding the

mm – cm ‘soil’ fractions (Tranter et al., 1993; Brown, 2002). On the other hand, supraglacial till is typically well-lithified, angular and less mechanically weathered (Boulton, 1978) Consequnelty, it is likley that it has different chemical weathering dynamics to subglacal till (for a full review of glacial till types see, Chapter 2, Section 2.3). In this study all till types and ground-up bedrock mixture exposed in the forefield are termed the ‘parent material’ (from which soils form) and their composition exert a major control on weathering and soil formation rates (Bluth and Kump, 1994). This is contrasted to “source rocks”, which reflect the totally unweathered bedrocks lithological units in the catchment area and the ‘soil’ fractions, which is all material smaller than 7 mm. This differentiation will be followed through the whole thesis.

In the High-Arctic forefield studied in this work, the source rocks consist primarily of felsic rocks and thus are predominantly made up of silicates minerals, but these are occasionally interspersed with sedimentary carbonate layers (see section 2.1.). In silicate dominated weathering environments, it is possible that even trace amounts of carbonate and sulfide minerals present can dominate the weathering reactions. Linked to this, also chemical changes in meltwater fluxes of aqueous carbon, cation (primarily Ca_2^+) (e.g. Blum et al., 1998; Jacobson and Blum, 2000) and / or sulfur speciation (e.g. Anderson et al., 2000; Wadham et al., 2001 & 2007; Hindshaw et al., 2016). Previous studies suggested that proglacial activity favours carbonate weathering if present, despite their relative scarcity compared to silicates, which weathering is delayed to longer time periods (Tranter, 2003).

The balance between carbonate *vs.* silicate weathering reactions in part controls global C cycle dynamics. Silicate weathering such as the weathering of Ca/Mg-feldspars (e.g., anorthite or olivine) ultimately leads to one mole of atmospheric CO_2 being captured in carbonates, exerting a negative feedback on a warming climate (Berner et al., 1983). On the contrary and unlike silicate weathering, carbonate weathering has been conventional perceived as being either a short-term sink of CO_2 on glacial-interglacial timescales (Anderson et al., 1997; Martin, 2016), or being carbon natural over geological time scales (Kump et al., 2000). Interestingly, sulfides oxidation (such as, pyrite) can enhance carbonate and silicate weathering rates through the production of sulfuric acid. Although it is only carbonate weathering by sulfuric acid that is a CO_2 source on timescales of the sulfur cycle 10^7. Only recently has this reaction gained attention from the biogeochemical community as being an important and potential CO_2 source in non-glacial and glacial forefield s (e.g. Anderson et al., 2000; Wadham et al., 2001; Wadham et al., 2007; Lerman et al., 2007; Torres et al., 2014; Hindshaw et al., 2016). For all general

chemical reactions that act as potential CO_2 sinks or sources, See Appendix A. Table. 2 and Chapter 2. Section. 2.5.1.

Arctic glaciers in Svalbard have progressively retreated since the end of the Holocene ice maximum. Fortuitously, this presents a unique opportunity as natural laboratories are created that are advantageous for studying time-resolved processes along choronosequences. As glaciers retreat, a succession of moraines are deposited that can be dated (Huggett, 1998). A space for time, chronological approach enables a detailed temporal and spatial-resolved, evolutionary understanding of the abiotic-biotic processes that govern or control the weathering of carbonates, sulfides and silicates. Concomitantly with the physical or chemical weathering, high-Arctic glacial forefields are also likely sites of the slow development of microbial ecosystem (Bradley et al., 2017) and later plant colonization (Hodkinson et al., 2003). Such a geo-bio interaction, provides therefore, an ideal modern day analog system for elucidating soil-forming reactions during their initial stages.

Silicate weathering intensity in transport-limited environments is principally driven by mineral dissolution kinetics that is strongly dependent on temperature (West et al., 2005). A small deviation in temperature such as the regional warming in Svalbard over the last century (Bradley et al., 2017; Førland et al., 2011) could lead to changes in silicate weathering in forefield settings as they further exacerbate physical and chemical weathering (Tranter and Wadham, 2014). In climate-sensitive forefield ecosystems in European Alpine forefields (Smittenberg et al., 2012), in some cases, document a significant transformation of plagioclase to kaolinite over a decade of deglaciation (Mavris et al., 2010; Mavris et al., 2011). However, other studies could not confirm this and their data lacked evidence for significant silicate weathering prior to about 100 years of exposure (Bernasconi et al., 2011). In high-Arctic forefields, so far only two studies reported that silicate weathering was limited or only occurred after ~ 100 years (Anderson et al., 2000; Wadham et al., 2007). Their findings were, however, solely based on two melt-seasons worth of melt-water chemistry measurements and no evidence of what happens in the new soils was available. In contrast, the studies in European Alpine forefields (Marvis et al., 2010, 2011 and Bernasconi et al 2011a) measured silicate weathering both through melt-water chemical changes, but also through analyses of the weathered rocks and proglacial soils. Both approaches (aqueous only or aqueous / solid analyses) have advantages and limitations. Chemical changes measured in soil and rocks represent the long-term average of an integrated effects of weathering from the point of

sampling (West et al., 2005). In contrast, continually measured melt-waters chemistries capture a continuum of short-term changes in seasonality. A comparison with other weathering arenas in more temperate or alpine settings is needed to evaluate the long-term effects of that have occurred in deglaciating and emerging Arctic forefields. In this study, for the first time a rather comprehensive suite of complementary chemical, physical and biological analyses to assess the changes in the solid materials (soils, glacial till) an approach that has so far not been attempted. The aim is to derive evidence for reactions that dominate the weathering arena, in subglacial and supraglacial till, and evaluate if combined –geo-bio weathering in High-Arctic pro-glacial settings are a potential source and sink of CO_2. In this chapter, primarily carbonate and silicate weathering is addressed and in Chapter 5, organic carbon and other nutrient dynamics.

It is hypothesised that in a transport-limited forefield consisting primarily of glacial till derived soils that are characterized by silicate rocks containing only minor sulfide and carbonate components, sulfide oxidation will nevertheless drive carbonate dissolution, and only at a later stage will silicate weathering set in. To test this hypothesis, three chronosequences will be analysed in a High-Arctic glacial forefield in Svalbard.

4.2. Methods

4.2.1. Study area

Midtre Lovénbreen and its glacial forefield are situated in a north-facing catchment on Brøggerhalvøya, Northwest Svalbard (78°50′ N., 12° E.) (Fig. 4.1). The mean annual air temperature and precipitation recorded at NY-Alesund from 1961-1990 (approximately 5km East of Midtre Lovénbreen) during the summer and snow free months are -5.8 °C and 20mm, respectively (Svendsen et al., 2002). Midtre Lovénbreen is a polythermal glacier with a subglacial drainage system (Irvine-Fynn and Hodson, 2010a). Glacier mass balance studies have documented its decline since 1967 (Hagen and Liestøl, 1990; Hagen et al., 2003). The ~2 km^2 forefield contains a succession of moraines deposited at an average retreat rate of ~14 m/ year since the last Holocene ice maximum in 1890-1905 (Glasser and Hambrey, 2001; Hambrey et al., 2005). The forefield consists of a clear vegetation chronosequence (Fig.4.2) and where soil has developed it is immature stony in nature and this reflects its parent material

glacier till genesis. The soils also have no horizons and subsequently they are classified as Leptosols and Regosols (FAO, 2006). Soils and glacial till are however effected by cryoturbation processes that in part result from an annual active layer thaw depth of discontinuous permafrost (Hodkinson et al., 2001; Hodkinson et al., 2002; Hodkinson et al., 2003; White et al., 2007).

Unlike most high-Arctic forefields, this location has been well studied in terms of its glaciological, periglacial, and glacigenic geomorphological depositional processes (Glasser and Hambrey, 2001; Irvine-Fynn et al., 2005; Midgley et al., 2007; Irvine-Fynn et al., 2011) as well as of its glacial and proglacial nutrient cycling (Hodson et al., 2004; Hodson et al., 2005; Wynn et al., 2006; Wynn et al., 2007; Hodson et al., 2008; Anesio et al., 2009; Irvine-Fynn and Hodson, 2010b; Anesio et al., 2010; Mapelli et al., 2010; Borin et al., 2010; Ansari, 2016). Furthermore, several studies have addressed the colonization of the glacial forefield areas by vegetation and invertebrates (Hodkinson et al., 2001; Hodkinson et al., 2002; Hodkinson et al., 2003; White et al., 2007).

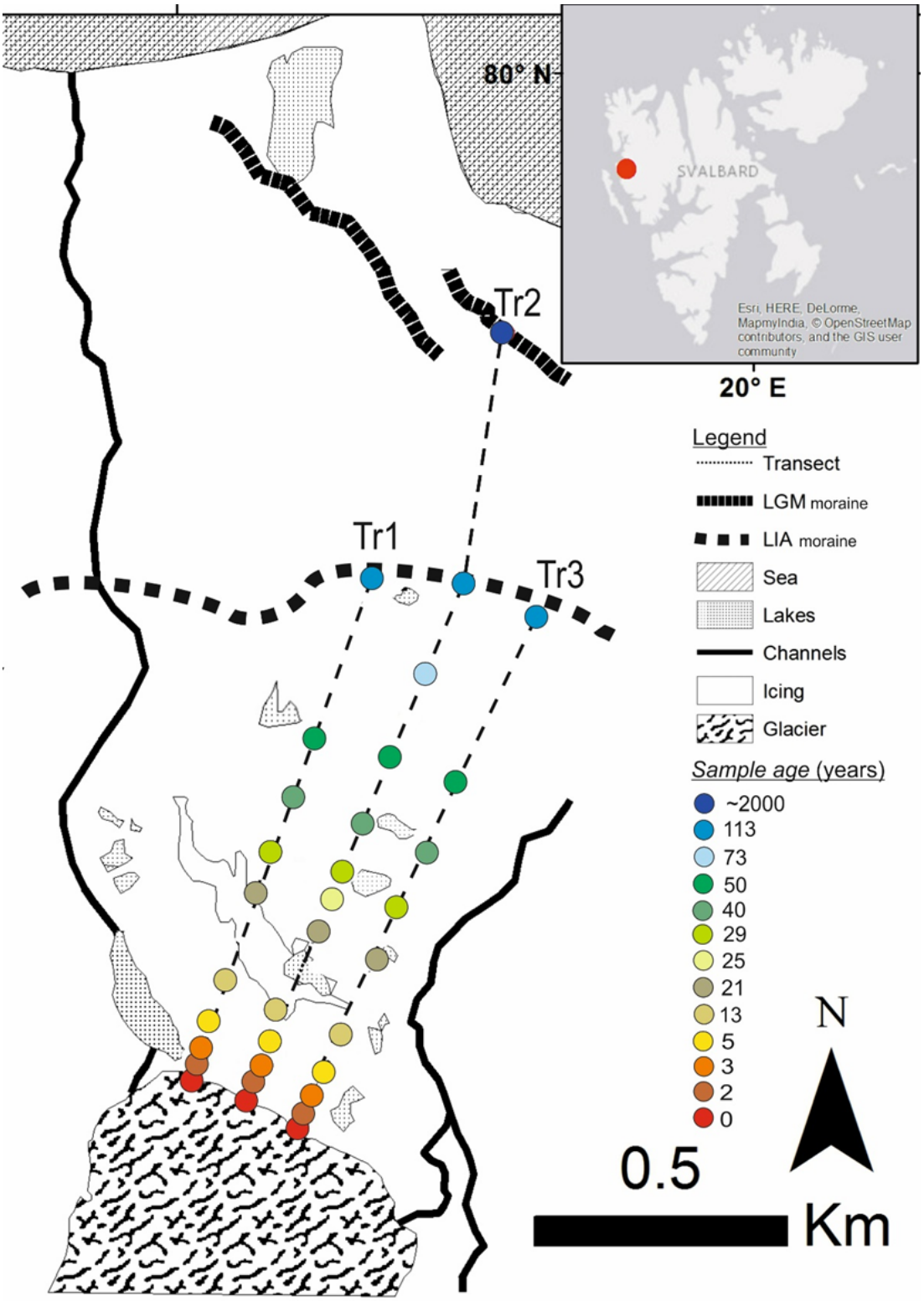

Figure 4.1. Schematic map of the Midtre Lovénbreen and its forefield including some of the main landscape features and the sites sampled along transects Tr1, Tr2, and Tr3. Also shown are two of the major moraines deposited at the end of the little ice age (LIA), which in Svalbard is late and this moraine was dated to be from ~1920 and an older moraine dated as > ~2000 years old (Hodkinson et al., 2003); this outermost moraine is sometimes interpreted as representing the remnants of a final ice retreat following the late end of the last glacial maximum (LGM) in Svalbard ~ 9-12 K years (Mangerud et al., 1992).

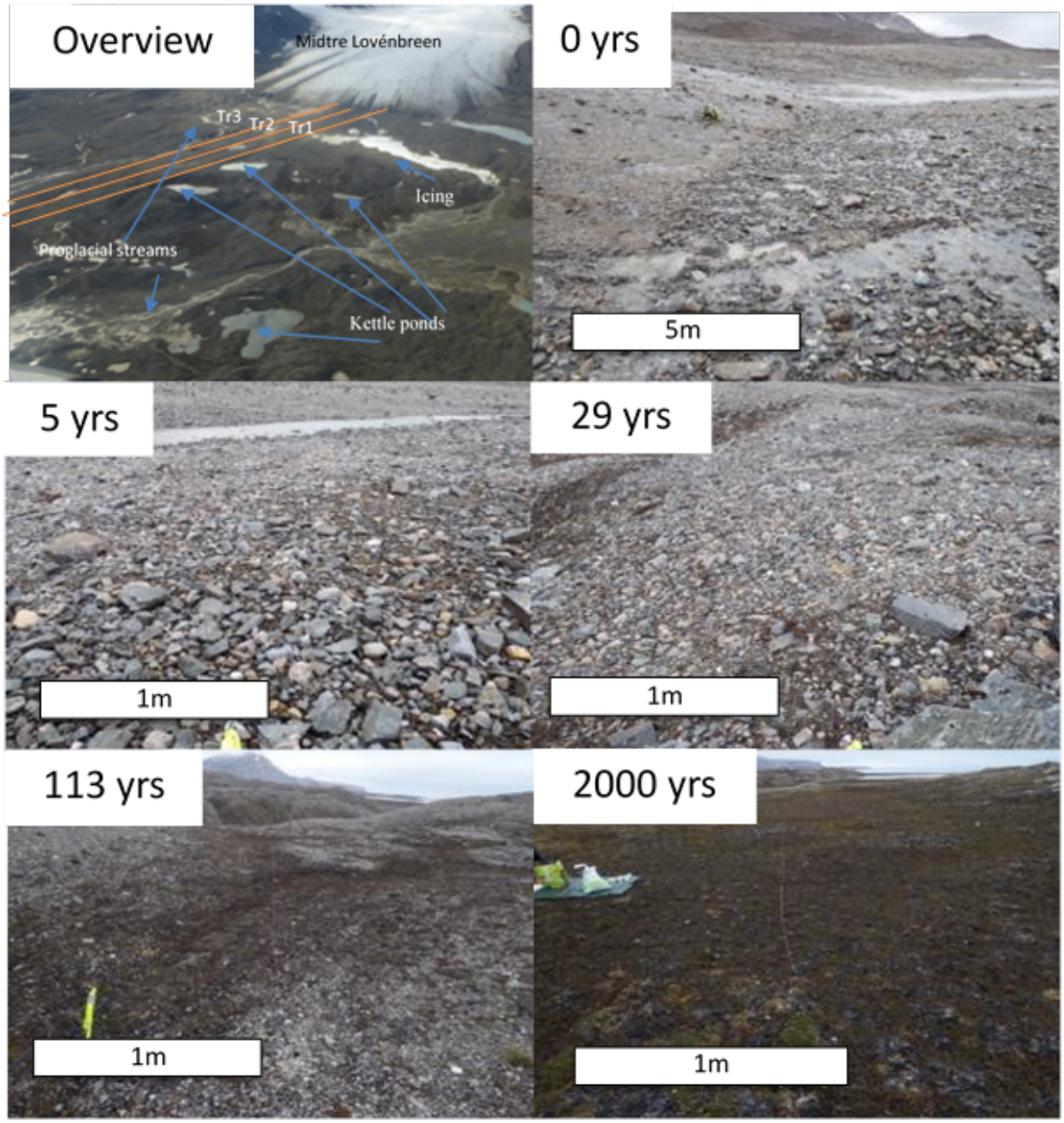

Figure 4.2. Photograph mosaic of the sampled and dated moraine sites from Midtre Lovénbreen, Svalbard. The overview photo included, an aerial photograph (facing north), shows the forefields, key landscape features and the transects sampled that are delineated and labelled. Note: not all ages sampled were photographed those taken represented clear observational changes in the forefield with increased age. The site ages present in this figure show at zero-years (the glacier snout) the ground was fully saturated with glacial melt-water runoff. Here only lichens were observed. Similar characteristics persisted until the >50-year-old moraine where isolated vegetation patches consisting of mosses and cyanobacterial matts (photo not available) were observed. These became expansive vegetation carpets at the 113-year-old moraine where mosses, sphagnum, grass forbs and vascular plants of the Saxi genus were well-established. At site 2000-years (a reference site) vegetation coverage was 100% and comprised of a diverse range of mosses, sphagnum, grasses and vascular plant of the Saxi genus. A thick OM layer >15cm was observed.

The dominant lithological rock units in the glacier catchment are metasediments. The headwall is composed primarily of metamorphic mica schists and quartz-carbonate-conglomerates of the Proterozoic Kongsvegan Group (Harland et al., 1997). The lower section of the glacier erodes a mixture of phyllites, quartzites and psammites of the Nielsenfjellet formation (Norwegian Polar Institute: www.svalbardkartet.npolar.no, 2013). Finally, Permian chert outcrops and dolostone of the Gipsdalen Group (Glasser and Hambery, 2001), conglomerates (Borin et al., 2010) and sandstone rocks (Hodson et al., 2005; Irvine-Fynn and Hodson, 2010) have also been noted in the proglacial area. This complex lithological mixture evidences the heterogeneous nature of the rocks to be found in the Midtre Lovénbreen forefield.

4.2.2. Types of glacial till in Midtre Lovénbreen forefield

Midtre Lovénbreen's forefield is comprised of two macroscopically identifiable glacial till types. The most visually prominent type is supraglacial (with a minor component of englaical) and this is expressed as dark till strips composed of angular clastic material that propagate from the glacier surface and continue across the forefield. Between these strips, the second type of till, with characteristic prominent white till strips is composed of a mixture of gravel that spans all sizes from clay, silt sand to pebble and boulder gravel; these originated from wet-based and fluvial subglacial conditions, and are in part mixed with englaical till (Glasser and Hambrey, 2001). The supraglacial-subglacial dark-white alternating banding is clearly seen in, Figure 4.3.

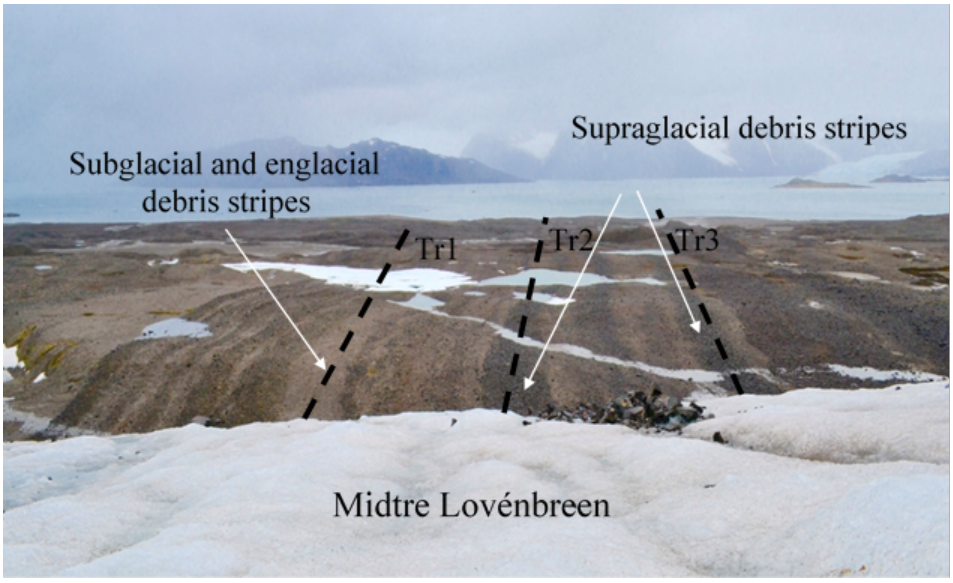

Figure 4.3. Photograph facing north towards Kongsfjorden showing two types of till stripes in the Midtre Lovénbreen forefield; dark stripes represent remnants of supraglacial till, while lighter stripes represent subglacial till. Transects Tr1, Tr2 and Tr3 are delineated by black dotted lines. Photograph copyright: Alexandre Anesio

4.2.3. Sampling procedure and in-field geochemical measurements

The glacial forefield and its supraglacial and subglacial till areas were sampled during July, 2013 along three ~ 1.5 to 2 km long mostly linear traverses (Tr1, Tr2 and Tr3) previously delineated using GPS points (Table. 4.1). The selected sampling points were set to avoid obvious hydrological features and areas subject to major surface re-distribution by thermal, aeolian and fluvial processes post glacial retreat (e.g., (Irvine-Fynn et al., 2011). One set of samples was collected from an ephemeral proglacial washout plain (estimated to be ~ 73-year-old; see below).

Table 4.1. Midtre Lovénbreen glacial forefield chronology: moraine ages along the three traverses (Tr1, Tr2, Tr3) were derived from either Hodkinson., et al 2013 (through C_{14} (RC) dating and aerial photography, H); or from satellite imagery (S) from Landsat 4, 5 and 7 Quickbird and those on from the Norwegian Polar Institute: www.svalbardkartet.npolar. Unknown ages were estimated by pro-rata distance between two known ages (P) assuming a linear rate of retreat (Hambery et al., 2005). * not sampled.

Moraine Age (years)	Dating Approach #	Tr1 #	Tr2 #	Tr3 #
0	S, G	12°3'4.504 E 78°53'48.134 N	12°3'20.233 E 78°53'46.85 N	12°3'38.759 E 78°53'44.903 N
2	S, G	12°3'5.902 E 78°53'48.942 N	12°3'24.428 E 78°53'47.73 N	12°3'40.507 E 78°53'45.778 N
3	S, L	12°3'6.951 E 78°53'49.615 N	12°3'24.777 E 78°53'48.471 N	12°3'42.255 E 78°53'46.519 N
5	S, G	12°3'9.048 E 78°53'50.894 N	12°3'26.875 E 78°53'49.009 N	12°3'44.003 E 78°53'46.99 N
13	P	12°3'16.388 E 78°53'55.327 N	12°3'30.021 E 78°53'49.952 N	12°3'52.741 E 78°53'50.288 N
21	P	12°3'26.525 E 78°53'59.845 N	12°3'34.215 E 78°53'52.442 N	12°3'45.325 E 78°53'55.807 N
25	P	*	12°3'48.896 E 78°53'59.172 N	*
29	H	12°3'31.419 E 78°54'2.268 N	12°3'3.461 E 78°53'57.826 N	12°4'11.966 E 78°53'58.903 N
40	H	12°3'39.109 E 78°54'6.709 N	12°3'52.392 E 78°54'06.653 N	12°4'22.453 E 78°54'2.403 N
50	H	12°3'46.449 E 78°54'11.149 N	12°4'9.869 E 78°54'9.4 N	12°4'33.638 E 78°54'7.516 N
73	H	*	12°4'21.404 E 78°54'14.446 N	*
113	H	12°4'2.528 E 78°54'19.558 N	12°4'32.29 E 78°54'18.953 N	12°4'57.058 E 78°54'17.201 N
2000	H, RC	*	12°4'45.523 E 78°54'34.89 N	*

At each site, three points were sampled at two depths (0-15 and 15-30cm) along a 10-meter line perpendicular to the traverses. Sampling was done by evacuating the material selected at a point surface and digging a soil pit down to 30 cm using a cleaned shovel. Once this was done, sterile instruments were firstly introduced to the surrounding soil then used to collect samples. To quantify the effect of time of chemical weathering, a chronosequence approach was employed. The ages 0 years (glacier's snout position in 2013) 2, 3, 5, 13, 21, 25, 29, 40, 50, 73, 113 and ~2000 years (as a reference sample; Table 1) were determined along each of the three transects based on a combination of satellite imagery for the most recent ages, and aerial photograph for the older ages (source: Norwegian Polar Institute, 2016). All of the ages derived were validated using dated moraine ages (Hodkinson et al., 2003). All ages for sampling points positioned in-between dated moraine ages, were estimated from a linear retreat rate (Hambrey et al 2005). In total n = 196 samples were collected from the proglacial zone of Midtre Lovénbreen.

An additional set of 15 bulk glacial till soils were collected in July, 2015 from the GPS coordinates from sites on Tr1 and Tr2 from the top 15 cm layer. However, in 2015 samples only from ages 0, 3*, 5, 13, 29, 40, 50 and 113 (*collected only on Tr1) were collected. Individual source rocks (n = 10), representing the various lithologies in the glacier catchment, were collected; care was taken to select individual, un-weathered as possible, rocks.

4.2.4. Analytical methods

4.2.4.1. Basic properties and sample preparation

Samples collected in 2013 and 2015 were oven-dried for 48 h at 40 °C. The dried samples from 2013 were sieved to <7 mm, while the samples collected in 2015 were sieved to three size fractions (>7 mm, 7 mm to 2 mm and <2 mm). Hereafter the <2 mm size fractions from 2013 and 2015 will be referred to as "*soil samples*", while the >7 mm and 7 mm to 2 mm size fractions will be referred to as "*parent material*", while the single unweathered rocks representative of the local lithology are termed "*source rocks*". Aliquots of all dried soil, parent and source rock samples were crushed using an agate disk-crushing mill and sieved to <63 µm prior to any further analyses. On five selected samples, from young and old moraine ages, the clay mineral fraction was separated using gravity dispersion. The dried bulk sample was gently broken up and placed into a labelled 1 L separating tube. The tube was filled with water to the 600 mm line, then 1 ml of dispersant was added (sodium hexametaphosphate solution) and it

was shaken for 10 min. and left to settle for approximately 16 h. This time was calculated using the Atterberg computer program to the time or height of fall. Dispersed samples were filtered using Millipore Isopore 0.4µm filter papers.

Soil pH was measured both *in situ* using litmus pH indicator paper, and on return from the field in a laboratory. Field pH was measured using a 1:2 ratio of soil: deionized water after vigorous shaking for 30 s at about 12 °C. After inserting the litmus paper into a soil slurry, it was removed, left to dry for 30 s and the semi-quantitative result was noted. Upon return to Leeds, pH analyses were done using deionized water (Millipore, Milli-Q) in a 1:2.5 soil: water ratio. This mix was left to react for 30 min. on a shaker and then left to settle for 60 min. before taking a reading of the pH in supernatant using a glass electrode (VWR, #622-1759) and a pH meter (Hanna 210) calibrated just prior to use using NIST standard buffer solutions at 19 °C.

4.2.4.2. X-ray diffraction (XRD)

Aliquots of the <63µm sized bulk <7mm and clay mineral fraction powders were analysed for their mineralogical composition using X-ray diffraction (XRD) (Bruker D8) using a step size of 0.03° 2θ and a counting time of 2 s/step over a range of 2–90° 2θ. Constituent mineral phases were identified with reference to the TOPAS Bruker Structure database and the Crystallography Open Database using the software DIFFRAC.EVA v.3.0 and TOPAS v.4.2 for multiphase Rietveld refinement (Rietveld, 1969; Bish and Howard, 1988). Only mineral phases >3% in abundance were assumed to be quantifiable, due to the complex and heterogeneous nature of pro-glacial samples.

4.2.4.3. X-ray florescence spectroscopy (XRF)

Major (Si, Al, Fe, Mg, Mn, Ca, Na, K, Ti, P) as well as minor and trace elemental concentrations (Ba, Co, Cr, Cu, Ga, Ni, Pb, Rb, S, Sr, V, Y, Zn and Zr) in all <63 µm sized powdered samples were analysed using X-ray florescence (XRF) spectroscopy (PANalytical; Axios) on fused glass pellets that were prepared using a 1:6 ratio of sample: fluxona plus 0.7 g of ammonium nitrate. Samples were melted in platinum crucibles by heating them on a five-stage, melting stage. The temperature ranged from 450 to 1100 °C and it was reached over a 30 min. melting period. After the final heating stage, the molten rocks were cast into a platinum

form that was left to cool before being analyzed. For major elements, the data is reported as oxides in *wt%*, while minor and trace elements are reported as elements in ppm. The standard reference material Granit GM (Abbey, 1980; Dulski, 2001) was used and analytical accuarcies of were ± <0.06 (*wt* %) 95.0% confidence limit obtained for most element oxides and ± <8.83 (ppm) 95.0% confidence limit for the minor and trace elements see, Appendix B. Table. 14 & 15.

4.2.4.4. Sulfur and carbon analyses

Total sulfur (TS) and total carbon (TC) were analysed using an elemental analyser (*LECO SC-144DR*) by combusting the samples at 1350°C for 180-seconds. The limits of detection (Hindshaw et al.) were 0.014 wt% for TS and 0.059 wt% for TC while the limits of quantification (LOQ) were 0.04 wt% for TS and 0.154 wt% for TC. The standard reference material, (LECO, soil, part no. 502-062; 0.029 ± 0.004 sulfur (wt%) and 2.02 ± 0.06 carbon (wt%). Repeat analyses gave an analytical accuracy of 0.029 ± 0.001 (wt%) for sulfur and 1.98 ± 0.02 (wt%) for carbon. Total Inorganic Carbon (TIC) was determined as the difference between the initial TC and a second analyses of total carbon performed after acid treating the initial samples with 10% HCl at room temperature for 24 h to dissolve all inorganic carbonates (Schumacher, 2002). Once effervescing of CO_2 gas due to the dissolving carbonates had stopped, samples were centrifuged, the acid washed off and dried at 40 °C to avoid loss of volatile organic carbon (Caughey et al 1995) and re-analyzed.

Isotopic compositions of the inorganic carbonate carbon in the TIC fraction of selected samples (δ^{13}C-TIC) were measured by reacting an aliquot of the initial powdered bulk samples (0-15 cm depth; transect (Tr1) with phosphoric acid at 50 °C to produce carbon dioxide (McCrea, 1950). Data were corrected following the method of Craig (1957) and are reported as delta (δ) per mille (‰) relative to VPDB. Accuracy and reproducibility (sn_1) for δ^{13}C was assessed by replicate analysis of standrads (NBS-18, NBS-19) and an internal standard calcite BCSB. Values obtained for NBS-18 relative to NBS-19 were identical to those reported by Gonfiantini et al. (1995) within the limits of analytical uncertainty. Reproducibility for isotopes were better than 0.1%.

Pyrite and acid volatile sulfides were determined via the chromous chloride extraction scheme (Canfield et al.. 1986) (see Appendix. B. Table. 3).

4.2.4.5. Statistical tests

All statistical analyses of data were conducted with SPSS (IMB®) and Microsoft Excel® computer software. To examine the relationships between independent variables (e.g. moraine age) and dependent variables (e.g. chemical concentration) regression analyses were conducted. Regression was used to identify the pattern (e.g. linear or nonlinear) of the relationship with each dependent variable. Correlation coefficients (Pearson's r value) and significance (p values) denote the strength and significance of correlations. Parametric or non-parametric statistical tests were conducted prior to data normality checks using a Shapiro-Wilk test and Z scores and histograms to select appropriate tests for the statistical comparison of means. Between the two years sampled (using their sum of squares) an independent t-test was used. Prior to using this, Levene's test of homogeneity of variances was used to determine the variance between the variables. If a significance level was >0.05, then equal variance between the variables was assumed.

4.2.4.6. Calculations to quantitative evaluate chemical weathering: Chemical Weathering Indices and mass gains and losses

Chemical weathering indices (Table. 4.2) were used to quantify elemental variations in all samples. Mineralogical changes were inferred by stoichiometric changes in mobile elements (Ca^{2+}, Na^{+} and K^{+}) vs. immobile elements (Al^{3+} from primary and secondary minerals i.e. feldspars and clay minerals). The chemical index of alteration was used as it was derived for metasedimentary rocks and tested on glacial tills (Nesbitt and Young, 1982). Consequently, this was deemed the most appropriate weathering indices for our complex glacial forefield samples. The plagioclase index of alteration (PIA) (Fedo et al., 1995) was also used to quantify any specific trends in chemical weathering of plagioclase, being highly abundant in metasediments. While the WIP index (i.e. Parker, 1970) was used as it has been previously shown to also be an effective indicator of weathering trends in heterogeneous metasediments (Price and Verbel, 2003). Another approach commonly used to quantify weathering is elemental mass gains and losses (White et al., 2001; White et al., 1997) whereby again molecular proportions are reported as ratios of mobile vs. immobile oxide concentrations, but incorporate soil fraction vs. parent material fractions (see below). These approaches are advantageous for materials, which do not weather isovolumetrically or that have been affected by mechanical processes (e.g., turbation in soils) (Price and Vebel., 2003) that tills are subjected to in glacier forefields. Although bulk densities are often used in tandem with

immobile elemental oxides acting as an independent standard against which each index is compared, they are not necessary as volumetric changes are accounted for instead by assuming immobile elemental oxides behave as so (discussed below). Moreover, determination of bulk densities in heterogeneous materials such as glacier tills is difficult since it is often unsorted, unstratified mixtures of clay, silt, sand, gravel, and boulders with dissimilar distributions over short distances (Crocker et al., 1955).

Table 4.2. Chemical weathering indices

Chemical Weathering Index	Formula	Optimum (weathered/ fresh value)	Ideal weathering trend (increase in weathering)	Reference
CIA	$(100)[(Al_2O_3/ (Al_2O_3 + CaO^* + Na_2O + K_2O)]$	100/50	Positive	Nesbitt and Young (1982)
PIA	$(100)[(Al_2O_3/(Al_2O_3 + CaO^* + Na_2O - K_2O)]$	100/50	Positive	Fedo et al., (1995)
WIP	$(100)[(2Na_2O/0.35)+(MgO/0.9) + (2K_2O/0.25)+(CaO^*/0.7)]$	0/>100	Negative	Parker (1970)

$(CaO^*_{silicate} = CaO_{total} - (CaO_{carbonates} + CaO_{apatite})$ Equation 4.1

It is worth noting that when testing the use of various weathering indices to silicate-based materials, to achieve an accurate and precise chemical weathering intensity quantification, several assumptions must be addressed or made.

1) The term CaO represents calcium in silicates only. To this end, all XRF analyses were corrected for Ca contributions from carbonates and apatite (see Equ 4.1. and for full explanation of how this was done see in Appendix B. Table. 18).
2) Chemical weathering indices applied to heterogeneous sediment can derive erroneous results due to an uneven distribution of elements and different modal abundances of minerals in its volume. Glacial till is synonymous with heterogeneous mixtures of physically and chemically altered rocks. Nevertheless, subglacial glacial till deposited in forefields that undergoes glaciofluvial transit may be well-mixed and thus more homogenous than other types of glacial tills (Boulton, 1978). In addition, it is assumed

the weathered fraction is derived from the parent material fraction, which may not be valid for heterogeneous glacier till deposits. Differences observed in immobile elemental oxides behaviours in soils can help evaluate the extent of allochthonous contributions to a soil (see below).

3) The immobile elements selected must remain chemically inert and conservative in the soil volume during weathering. This assumption is unwarranted for samples with a pH below 4.5 (Gardner, 1980) and in a redox active environment, or where biological organic ligands are exuded at even low concentrations, as they can facilitate the release of di- and tri-valent metals (i.e. Al^{3+}) from both octahedral and tetrahedral layers (in sheet-silicates e.g. biotite) (Bray et al., 2015). In the forefield of Midtre Lovénbreen, soil pH is unlikely to reach values <4.5 due presence of carbonates in the catchment lithology, surface tills were observed to porous and aerated (for all measured pH values see Fig 1 in Appendix B) and soil fauna and flora is spars up to 60-years-old (Hodkinson et al., 2003) although could have an effect. Immobile elemental oxides' (Al_2O_3, TiO_2, and ZrO_2) behaviours were tested for whether to infer chemical weathering in the glacial tills in Midtre Lovénbreen, using Eq. 4.2. Those that behaived as inert and conservative as a function of age (i.e. Al_2O_3 which was only slightly mobile, for results: see Appendix. B. Fig.5), were selected for weathering indices and mass gain and loss calculations. Changes in immobile element concentrations are usually described by the elemental concentration ratios (V; mol/kg) of an immobile element, i, in the un-weathered parent material uw, relative to the weathered soil w.

$$\varepsilon_v = \frac{[V_{i,uw}]}{[V_{i,w}]} - 1 \qquad \text{Equation 4.2}$$

Values clustered around zero ($\varepsilon_v = 0$) indicate limited mobility in the soil fraction relative to the parent material. Negative values of ε_v are indicative that an element is not immobile in the soil fraction relative to the parent material, whereas a positive value of ε_v means an additional external factor affected the value.

4) In all of the weathering indices in Table 2, erroneous results can be derived due to the potential influence of K-metasomatic in metasedimentary rocks (Fedo et al., 1995). This is particularly true for CIA values ,as this is particularly relevant to metasediments, yet CIA values within the incipient weathering range (50 to 60) are assumed to not be affected by K-metasomatism.

Quantitative losses and gains of elements due to chemical weathering are described in terms of their compositions in the smaller grain-size fractions relative to the un-weathered larger parent material fractions. Mass transfer due to weathering, T_e, of a chemical weathered element, V, in the <2mm grain-size fraction, V_w, are corrected for CV_w, by ratioing an immobile element in the un-weathered parent material, $V_{i\,uw}$, against the corresponding immobile element concentration (mol/kg), $V_{i,w}$, in the weathered material Eq. 4.3. The difference between the corrected and un-weathered element, V_{uw}, gives the mass transfer of an element during chemical weathering, Equ. 4.4.

$$[CV_w] = \frac{[V_w][V_{i,uw}]}{[V_{i,w}]} \qquad \text{Equation 4.3}$$

$$T_{e=[CV_w]-[V_{uw}]} \qquad \text{Equation 4.4}$$

When T_e is negative, elemental concentrations have been depleted during chemical weathering, a positive number means an increase in elemental concentration and when $T_e = 0$ elements remain refractory during chemical weathering with respect to the parent material.

4.3. Results

4.3.1. Variations in physical-chemical properties

The grain size fractionated samples collected along Tr1 exhibit an increase in the proportion of the smallest fraction <2 mm with age, and decrease in the proportion of the largest fraction, >7 mm within the bulk mixtures, while the median size fraction (2-7 mm) remains roughly constant (Fig 4.4 top plot). The ratio between the smallest (in blue) and largest (in green) size fractions increased markedly with increasing age. In contrast, in the samples from Tr2, a bimodal distribution is evident for all moraine ages (Fig. 4.4, bottom plot), with nominally, slightly increased proportion of larger fraction and decreased in the smallest fraction with age.

The pH in all samples was close to near neutral (6.5-8.3; arithmetic mean 7.5; Appendix. B. Table 1.). When plotting the pH against moraine age an inverse correlation is visible, although

this was only slight and insignificant in Tr2 size fractionated samples (Appendix. B Fig. 1.b). It is however, noteworthy that the pH of the samples of younger ages showed a bigger scatter in values, compared to the older samples that showed less variability. In general, concurrent trends were evident in the grain sized fractioned samples, however, large grain-sized fractions from Tr2 were less dependent on moraine age.

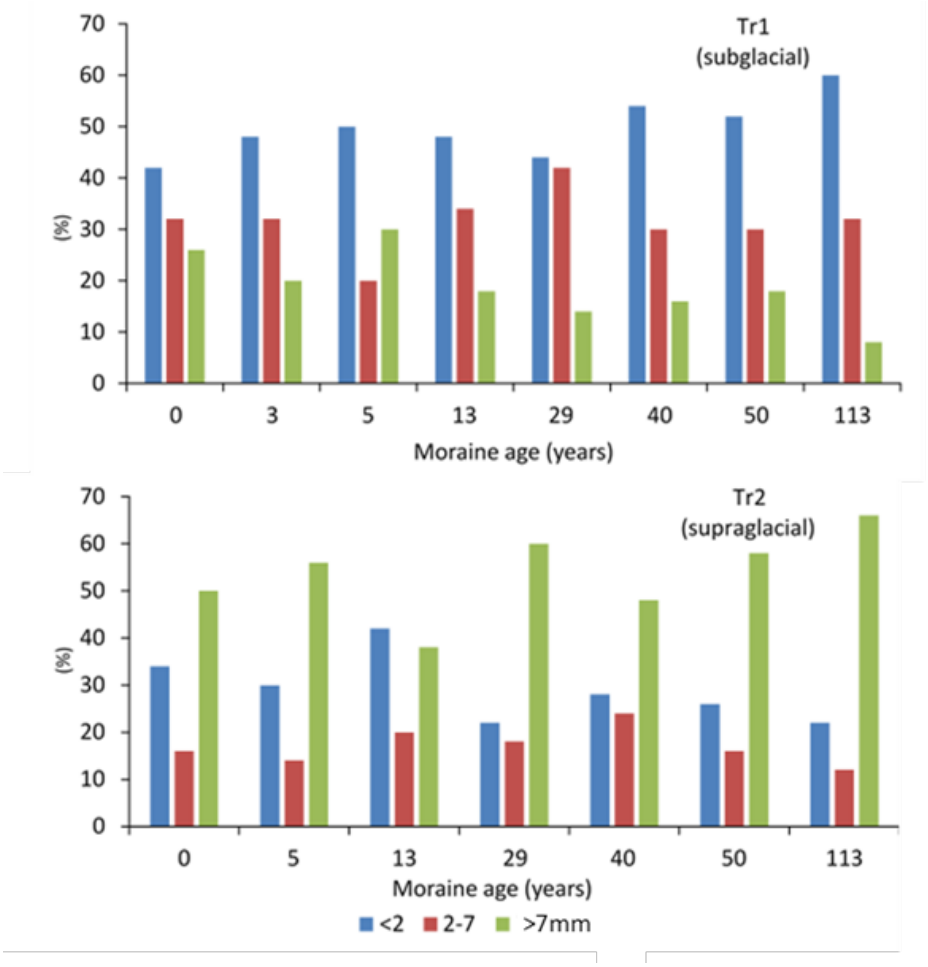

Figure 4.4. Grain size distributions (% of total bulk) for each of the grain size fractions <2mm 2-7mm and >7mm sampled along Tr1 and Tr2 in 2015.

4.3.2. Carbon and Sulfur Variations

Total inorganic carbon (TIC) and total sulfur (TS) (expressed as sulfide) from each size fractionated sample and the source rocks are shown in Fig. 4.5, 4.6 & 4.7. In all samples, TS was assumed to be associated with sulfide minerals (i.e. pyrite; for justification see Appendix.B Table. 3 & Section 4.1). TIC contents in the sandstones, psammites, schist and phyllite (except for psammite 1) varied between negligible and concentrations <1 wt%, while psammite 1 and the conglomerate, which contained a possible carbonate matrix, as well as the dolomite had

higher TIC values (from 2.83 to 10.69 wt %). Source rock TS was lowest in dolomites <0.005 wt% and highest in the conglomerate 0.1 wt%.

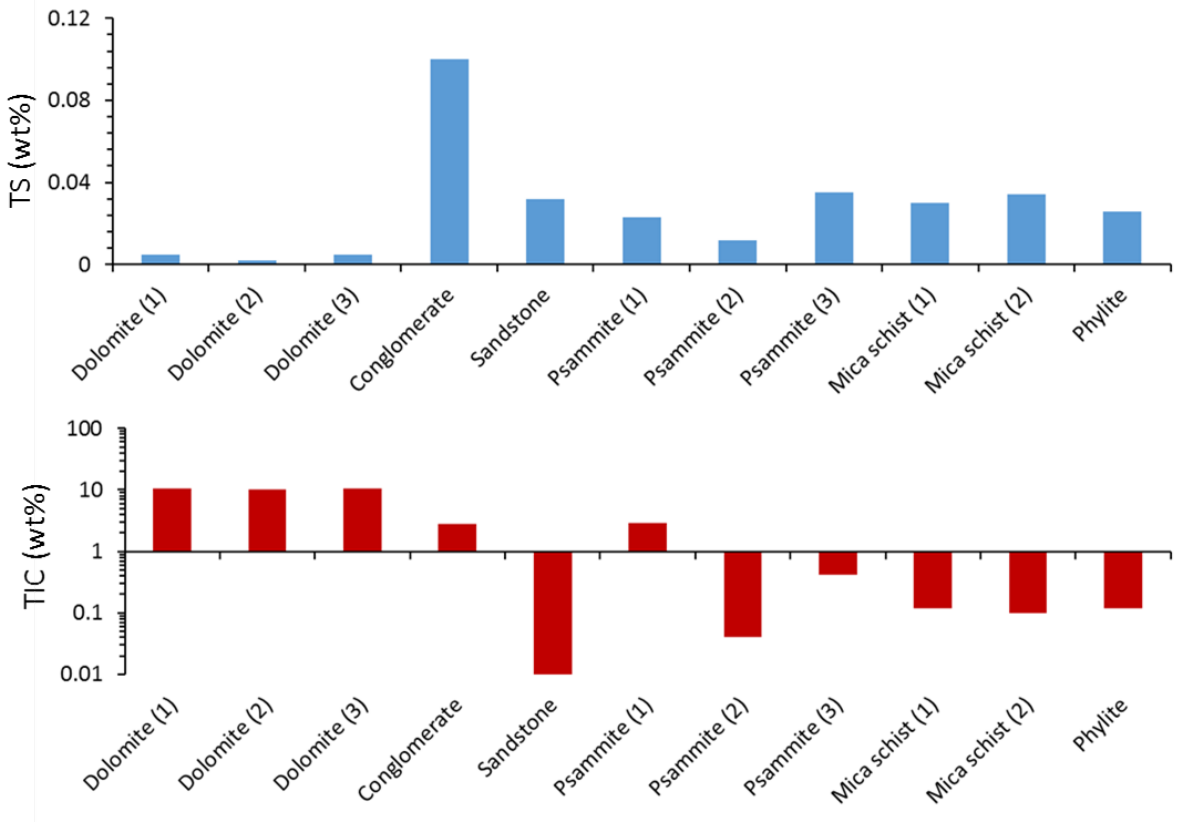

Figure 4.5. Source rock TS and TIC concentrations. Note: TIC is on a log scale.

Overall, regression analyses revealed in all size fractions and depths in the subglacial till (Tr1), a negative correlation in both TIC and TS. In most cases these correlations were moderate to strong (r = 0.38-9.1) and in all cases, significant (<0.01). As such, this indicates a TIC and TS depletion as a function of moraine age, (Fig. 4.6 & 4.7; for correlation coefficients see Appendix B. Table 5 & 6). Conversely, in the supraglacial till bands in Tr2 and Tr3 in most cases, with the exemption of 2-7 and >7 mm size fractions, TS is negatively correlated with age while TIC is uncorrelated. Bulk surface (0-15cm) and subsurface (15-30cm) samples, in general, show no significant difference (p = >0.05) in TS and TIC except TIC in the subglacial till band (Appendix B. Table 8). Interestingly, although similar trends are present between the two years sampled, 2013 and 2015, there is a significant difference between TIS and TIC (Appendix B. Fig. 2. & Table.B.9), which could suggest there is some inter-annual-seasonality in their measured concentrations.

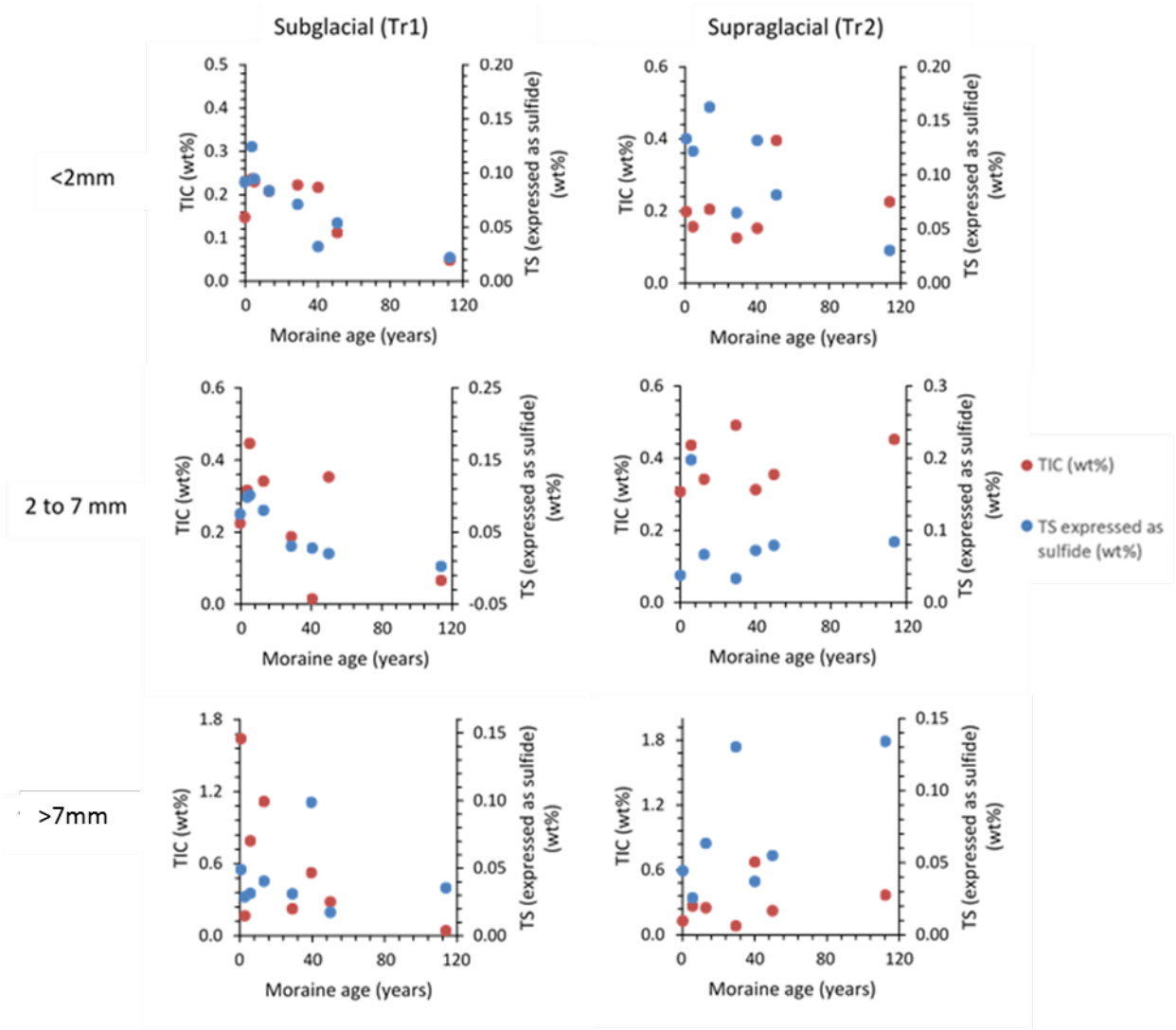

Figure 4.6. Total sulfur (TS, expressed as wt % sulfide, blue) and total inorganic carbon (TIC, wt %; red) as a function of moraine age for the subglacial (Tr1) and supraglacial till (Tr2) sampled in, 2015. Note for regression analyses and pearson's r correlation coefficients see, Appendix B. Table. 6.

Along Tr1 the subglacial till is associated with more TIC and TS variability in the larger grain size fractions. Whereas in the supraglacial debris on Tr2 and Tr3 the TIC and TS variability is independent of grain size fraction and the significant variability likely reflects the heterogeneous nature of these pro-glacial till deposits. Although, in all transects variances were observed primarily at younger age where glacier meltwater runoff caused sediment mixing, and a marked difference was seen at 73 year-old (15-30cm depth in Tr2, TIC = 1.12 *wt*%; Fig. 4.7) moraine located in an ephemeral pro-glacial washout plain. Therefore, this sample was likely an isolated carbonate nugget derived from further up the glacial catchment.

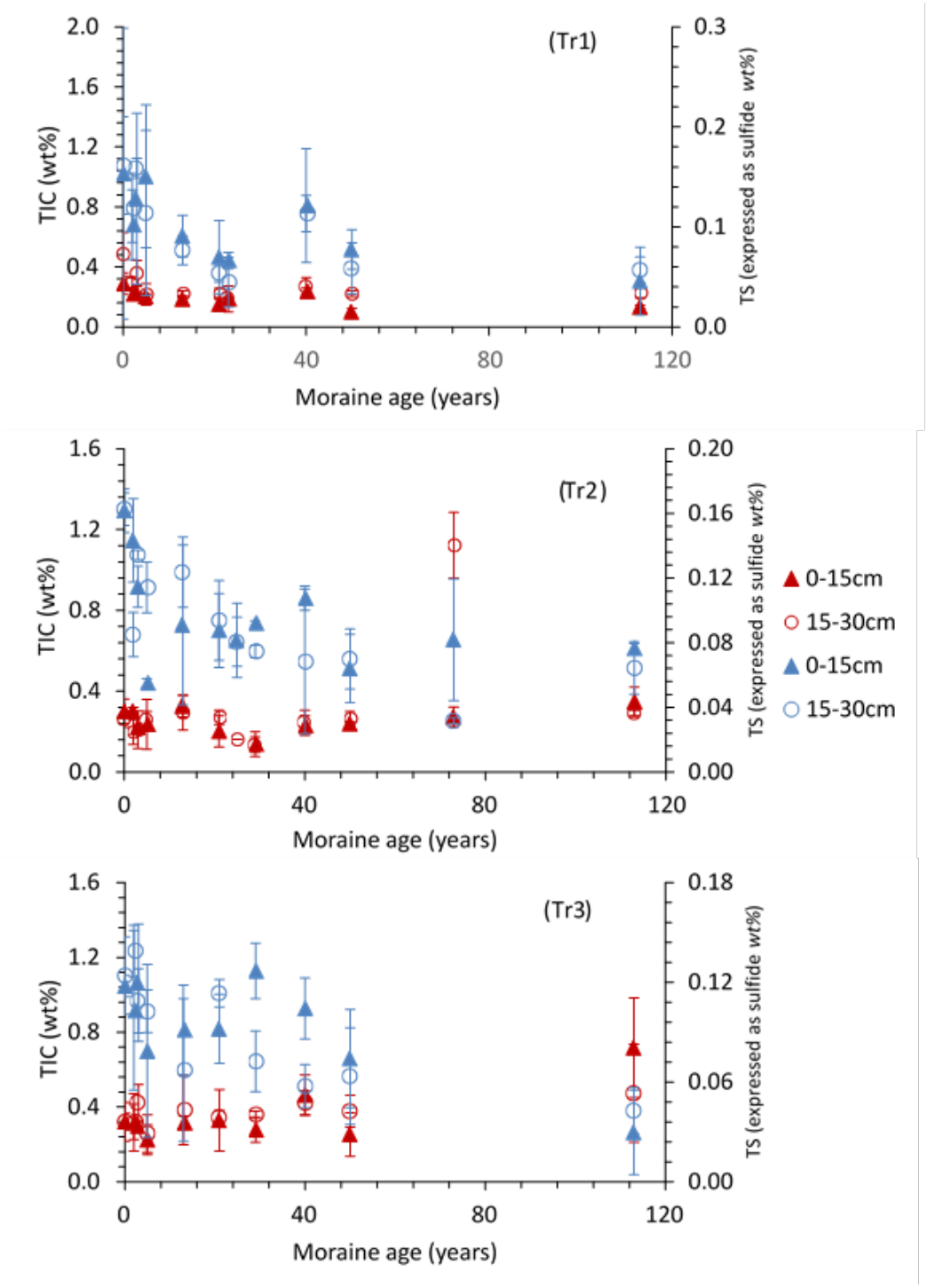

Figure 4.7. Total sulfur (TS; blue) (expressed as sulfide) and total inorganic carbon (TIC; red) and for Tr1, Tr2, and Tr3 as a function of moraine age for the depths 0-15cm and 15-30cm sampled in 2013. Each symbol is $\bar{x}$ of n=3 samples taken at each moraine age along a 10-meter travers and bars repersent 1σ sd. Note for regression analyses and pearson's r correlation coefficients see, Appendix B. Table. 5.

The stable inorganic carbon isotopes (δ^{13}C-TIC) concentrations of bulk soil samples from Tr1 (sub glacial till) at 0-15 cm depth showed little site-specific variation as a function of moraine age with a mean $\bar{x}$ -1.40 ‰ apart from two outliers at -0.2 and 1.7 ‰ at 21 and 29 years-old

(Fig. 4.8.a and tabulated in Appendix. B, Table 1. The δ^{13}C-TIC isotopic signatures of the source rocks the each of the lithologies in the catchment of Midtre Lovénbreen representing Tr1 ranged from -10.6 to +4.4 ‰ with an arithmetic mean of -1.18 ‰ (Fig. 4.8.b). These values are typical of TIC derived from marine carbonates (Anderson and Arthur, 1983; Galimov, 1985). The δ^{13}C-TIC isotopic signatures of the bulk soil samples comprise of mixed source rock TIC within the glacier till parent material and soil samples. Soil sample TIC is predominantly associated with the mica schist -1.40 ‰ source rock. While the other source rocks: psammite 1, 2 & 3, sandstone, conglomerate, dolomite and phyilite are minor components in the bulk soil sample composition. The bulk-soil sample outlier (+1.7 ‰) present at the 25-year-old moraine age likely consists of a higher proportion of dolomite (+2.7 to 4.4 ‰).

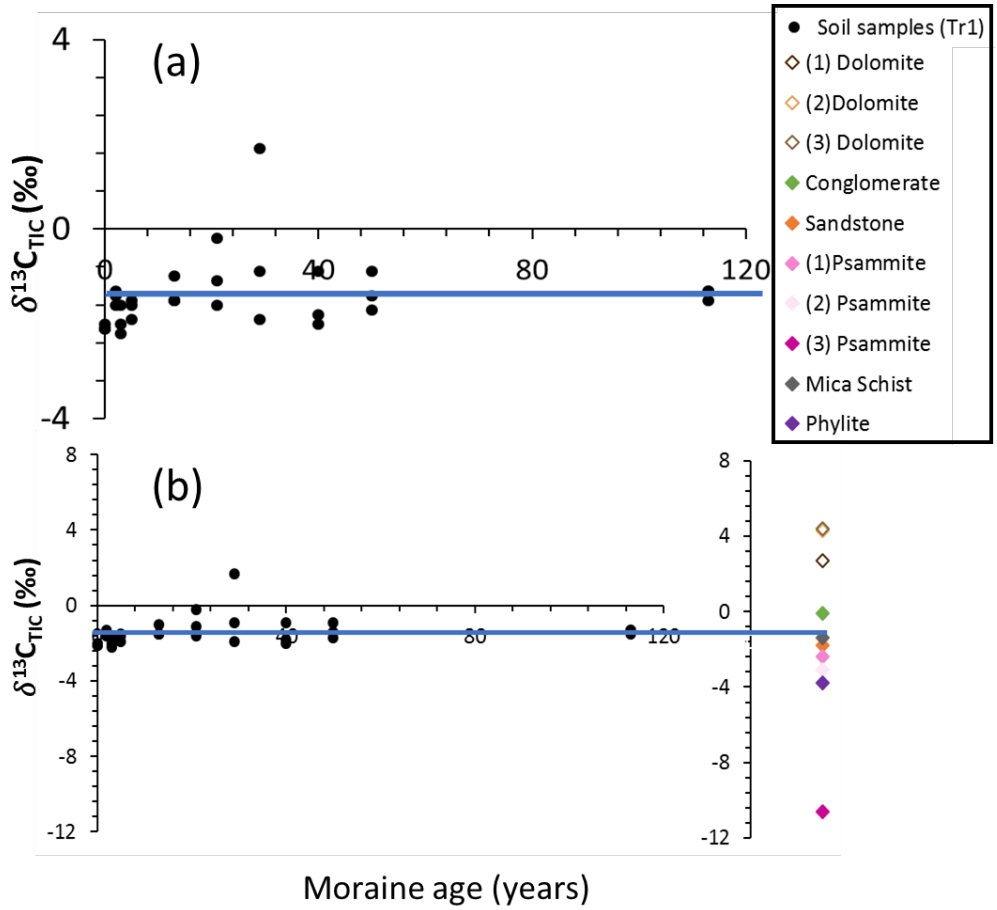

Figure 4.8. $\delta^{13}C_{TIC}$ data (‰) relative to VPDB, for the subglacial till from Tr1 **(a)** and compared with the values of the source rocks **(b)** of each of the rock types found in the glacier catchment. The blue line delineates the soil sample mean -1.40 ‰ that is associated with the mica schist source rock $\delta^{13}C_{TIC}$ composition

4.3.3.1. Weathering indices as a function of age

The CIA, PIA and WIP silicate rock weathering indices show that each of the silicate mineral-bearing source rocks that are representative constituents of the bulk glacial catchment lithology

are defined as weathered when they have values >50 (for CIA, PIA), and <100 (for WIP) (Appendix B. Table. 16). In all weathering indices, the data show that the metamorphosed source rocks were the least altered, except psammite (1). This is particularly evident for the mica schists that comprise the largest proportion of the bulk glacier till. The results from the PIA index again show that foliated metamorphosed rocks are the least altered (i.e. mica schist and phyllite), and contain the most Na_2O and CaO associated with plagioclase. If weathered, these source rocks have a high potential for atmospheric CO_2 drawdown. Non-foliated quartz-rich metasedimentary and sedimentary source rocks (i.e., psammites and sandstones and conglomerate) are the most altered. This is because they are enriched in aluminium yet depleted in easily mobilised elemental oxides.. The presence of these changed source rocks in the bulk tills could lead to them being misinterpreted as weathered in the indices used, hence the need for cautious analysis.

The soil and parent material fractions in the subglacial (Tr1) and supraglacial till (Tr2 and 3) differ between: the 'freshest' un-weathered values of (CIA and PIA = 50), to moderately weathered values of CIA (76), to extremely weathered in the PIA (100) (Fig. 4.9). Despite this, none of the weathering indices show a trend with a clear progression of the feldspar's conversion to clay minerals with moraine age. Instead, marked alterations are moraine age-specific, with higher degrees of chemical alteration corresponding to lower grade metasediments e.g. sandstone, psammite, conglomerate, phyllite. Samples with lower degrees of alteration are similar to higher grade metamorphic rocks i.e. mica schist (Fig. 4.12). To this end, outliers and variability could be due to the high abundance of a particular source rock type within the bulk glacier till samples (<7 mm; Fig 4.9. b & c). Interestingly, although the bulk till samples showed no evidence of pedogenic weathering, the grain size, soil samples and parent materials from the CIA and PIA indices in Tr1, could be due to weathering (Fig 4.9. a.). These soil indices show that in most cases K_2O remains immobile, and the <2 mm size fraction are depleted in mobile elements, whilst enriched in Al_2O_3, compared to its coarser parent material It is evident from comparing the ratios of PIA and CIA that the weathering is predominantly driven by variations in $CaO + Na_2O$ in the silicates.

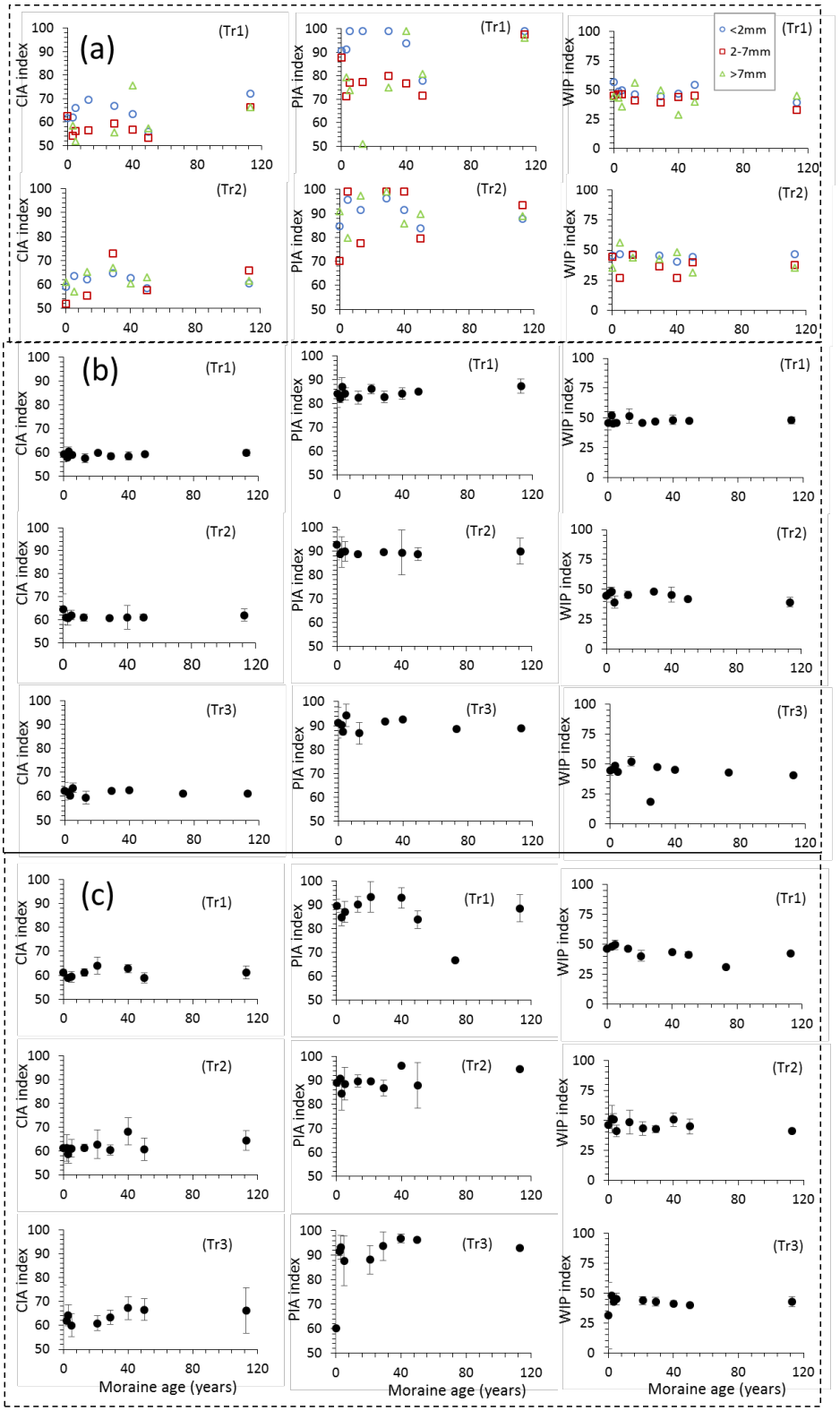

Figure 4.9. CIA, PIA and WIP indices as a function of moraine age for size fractionated samples (a) and >7mm fraction from Tr1 (subglacial till) and Tr2 & Tr3 (supraglacial till) at a depth of 0-15cm (a & b) and 15-30cm (c). Note: the different grain size fractions are shown as blue circles <2mm, red squares 2 to 7mm, green triangles >7mm and black circles <7mm. Symbols denote $\bar{x}$ of n=3 samples from each moraine age along a10-meter travers; bars represent 1σ sd. Note: not all samples aged have a sd because $\bar{x}$ is < n=3 Appendix B. Table. 12.

4.3.3.2. Mass gains and losses in the soil relative to the parent material grain size fractions as a function of moraine age

Elemental variation and distributions as a function of soil fraction relative to the parent material fraction are defined in terms of T_e and plotted vs. moraine age (Fig. 4.10 and 4.11). Of the immobile elements used in mass gain and loss calculations Al_2O_3 behaved as the most refractory as a function of age (Appendix B. Fig. 5). Minimal alteration of the sesquioxides are expected at the pH conditions prevalent in these carbonate buffered developing soils (pH ~ 7) (Appendix B. Fig. 1). Mass gains and losses (T_e) for each element showed no correlation with moraine age, however, elemental variations between the till types and grain size fractions do still occur. For example, SiO_2 and Na_2O are consistently and strongly depleted in the sub- and supraglacial till, and have a non-trending scatter. Similarly, the CaO* is scattered and non-trending, although is both depleted and enriched. The K_2O remained slightly enriched and/or negligibly changed with moraine age.

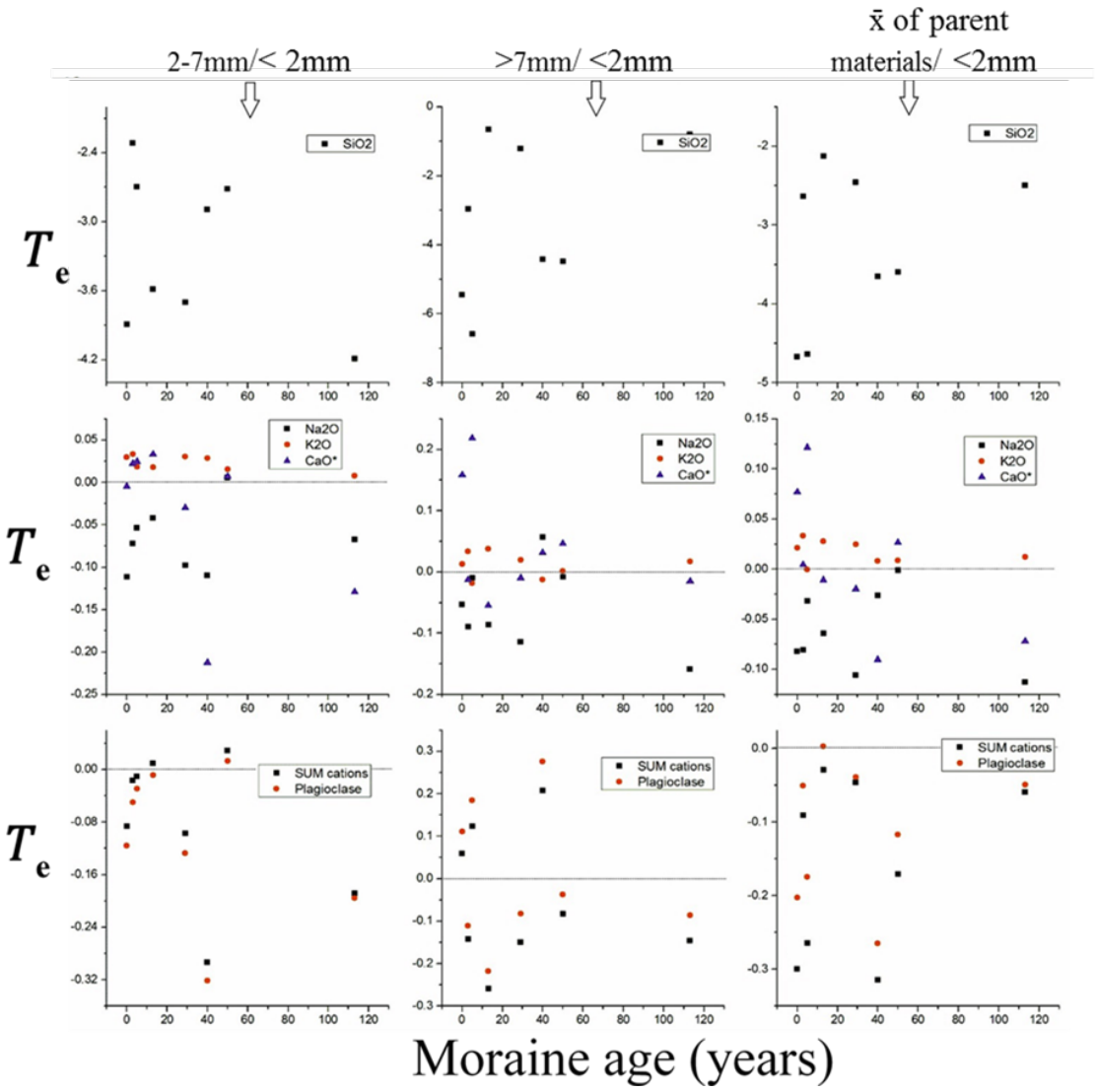

Figure 4.10. Subglacial debris (Tr1) elemental gains and losses plotted vs. moraine age. Displayed are the two parent material fractions 2 to7 and >7mm and average of these fractions all relative to the soil fraction <2mm, Eqn 3&4. Note: CaO* = carbonate corrected CaO; SUM cations = (Na_2O + K_2O + CaO*) and plagioclase = (Na_2O + CaO*)

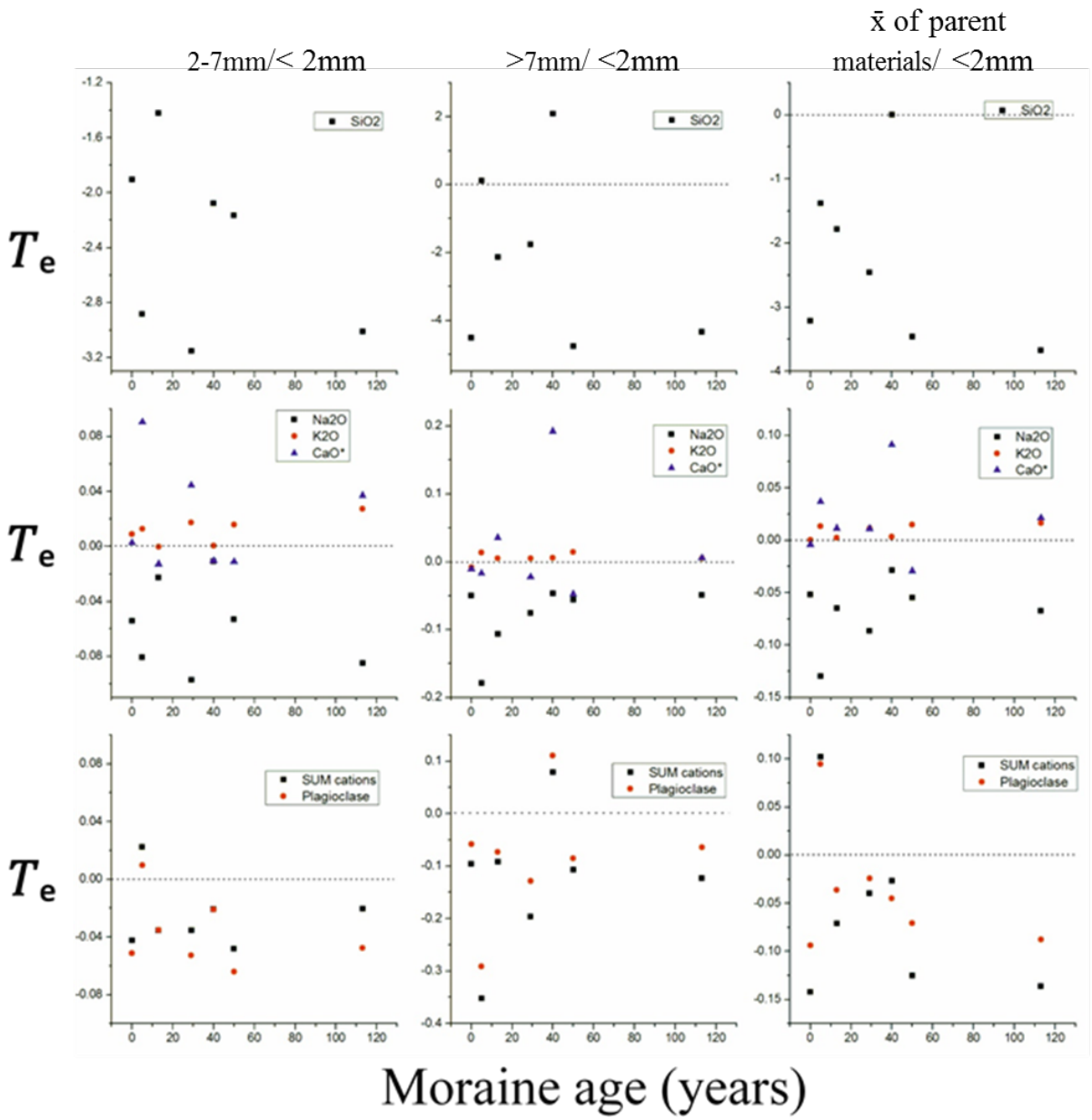

Figure 4.11. Supraglacial debris (Tr2) elemental gains and losses plotted vs. moraine age. Displayed are the two parent material fractions 2 to7 and 7mm to 2cm and average of these fractions all relative to the soil fraction <2mm, Eqn 3&4. Note: CaO* = carbonate corrected CaO; SUM cations = (Na2O + K2O + CaO*) and plagioclase = (Na2O + CaO*)

The CIA index was plotted as a ternary (Fig. 4.12), and shows elemental oxides in the weathered glacier till samples are complex. This arises because elemental oxide proportions vary in relation to their abundance in each mineral phase, the mineral modal abundance in each source rock, and their sorting and distribution of grain sizes. The CIA index values associated with each source rock indicate that mica schists are 'fresh' and relatively unweathered (a CIA of ≤50 in metasediments = unaltered), the sandstone, psammites, conglomerate, phyillite derive weathered values (CIA >50-60 as mentioned above means altered). This is unsurprising as they are sedimentary and lower grade metamorphic rocks, with easily depleted mobile cations, but enriched in immobile Al.

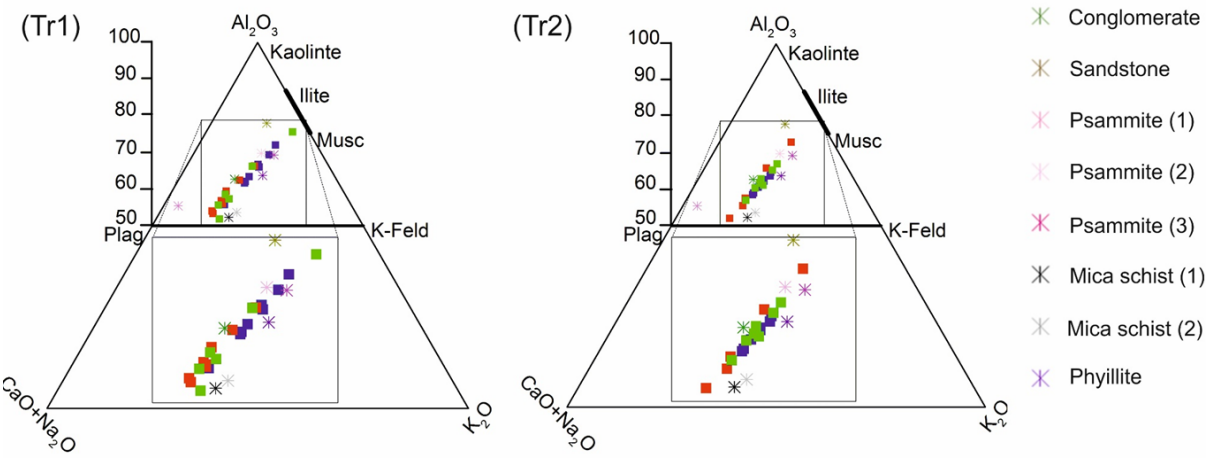

Figure 4.12. Chemical index of alteration (CIA) plotted as molar proportions in a ternary plot using CaO* from silicates only for the subglacial (Tr1) and supraglacial (Tr2) samples. The insets show the distribution of the grain size fractions as squares: blue <2 mm, 2 to 7 mm red and green >7 mm. Colored stars represent each of the silicate bearing source rocks, see legend.

Chemical alteration of the freshest parent material fractions (>7 mm and 2 to 7 mm) represents the begining of chemical weathering (CIA= 50-60). Values considered fresh in the parent material fractions are present in the subglacial and supraglacial till, ranging from 51-60, although they occur primarily in the subglacial samples. These fresh values reflect the chemical composition of the relatively un-weathered endmember, source rock, the mica schist = 52 and 53. Slightly more altered values of 60-70 are associated with the majority of samples in the soil fractions (<2 mm) in the subglacial till, and all grain size fractions in the supraglacial till. Samples within the lower to mid-range of these values have chemical compositions similar to the conglomerate and phyillite source rocks, while those in the higher range reflect psammite (2) and (3). Moderately altered values are observed for K_2O and Al_2O_3 enriched and Na_2O +

CaO that are depleted 70-80, in samples from the <2 mm and >7 mm fraction in the subglacial till, and one sample in the 2-7 mm fraction from the supraglacial till. These samples show a chemical composition associated with the sandstone. All of the grain size fractions follow a chemical weathering trend in which Na_2O and CaO* are depleted, whilst K_2O and Al_2O_3 are enriched. If this were pedogenic weathering, it would suggest plagioclase feldspars are depleted, while muscovite remains unweathered and slightly enriched. If illite was formed from muscovite the K content would be depleted, as they have lower layer charge, with 4–6 mass % lower than that of mica. This weathering trend is most distinguishable in the subglacial till (Tr1) where the soil fraction is more altered than the parent material fractions. Although, plagioclase weathering is inferred from the CIA index, elemental concentrations present in the silicate source rocks do encompass the range of concentrations in observed in all the grain size fraction. Only one anomalous exception is present in Tr1 with a CIA value of 76.

The ratios of major elemental oxide constituents of silicate minerals (Ca, Mg, Na, K, Al and Si) (Fig. 4.13) are based on their association with minerals identified from XRD analyses in the source rocks and glacial till can be compared, (Table. 4.3). Aluminium and silicon are the major constituents of silicates with SiO_2 dominating through the presence of quartz in sandstones and psammites. To assess the behaviour of silicates, Al_2O_3 was plotted as a ratio of each of the silicate cations (Ca, Mg, Na and K). This reveals that the elemental concentrations in the subglacial till are grain size fractionated, and clustered into the parent material and soil, whereas this trend is weaker in the supraglacial till. The source rocks (mica schist and phyllite as the main constituent of the surrounding rocks), with their high proportion of Al associated with K, Na and Ca feldspars, are concentrated in the soil fractions. On the contrary, source rocks containing more of the SiO_2 dominated minerals are more concentrated in the parent material fractions.

The Ca distribution in the soil and parent material fraction till types are derived from multiple provenances, as indicated by the weak correlation between CaO and Al_2O_3. Calcite within the rock matrices, dolomite and calcium-silicate (in the psammites and minor phases in the sandstones) are the dominant Ca sources (Table. 4.3). The mica schist, phyllites and conglomerate contain Ca associated with plagioclase, and thus have positive Ca values. The chemical signatures (CaO/Al_2O_3 ratio) of the mica schist and phyllite rocks reflect primarily those found in the soil fraction. While the parent material fraction consists of a greater mix of the remaining Ca-associated source rocks.

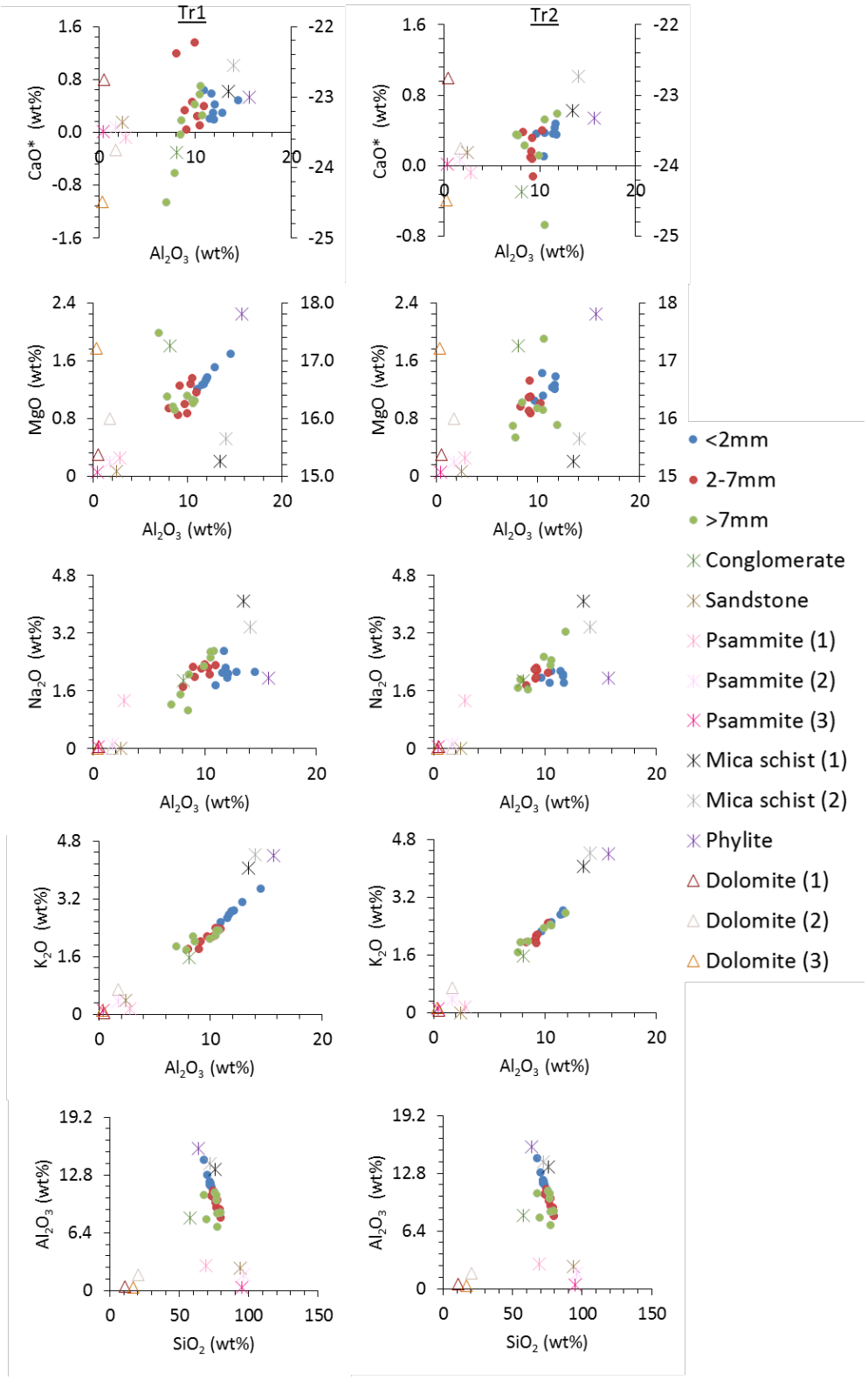

Figure 4.13. Effect of grain size sorting on elemental oxides in the weathered soil fraction <2mm (blue) and the two parent material fractions 2 to 7mm (red), and >7mm (green) collected in 2015 from the Tr1 and Tr2. The catchment area source rocks are plotted to illustrate their mixing ratio in relation to each of the grain sizes (see Legend). Secondary axis's in the CaO/Al2O3 and MgO/Al2O3 plots are for the dolomite source rocks and illustrate the effect of the carbonate correction due their non-stochiometric Ca/Mg chemical composition.

The 40 and 113 year outliers in the 2-7 mm and >7 mm parent material fractions, likely represent a 'nugget' effect that is typical for such the heterogeneous materials; it is likely that those samples contained an anomalous high proportion of anorthite. These outliers, as well as the source rocks, with negligible (pssamites and sandstone) and negative concentrations (dolomite), contain a limited amount of plagioclase, or are likely to have been overcorrected (Eq. 4.1). This can result from 'nuggets' of dolomite within the sampled material.

A weak correlation is observed between MgO and Al_2O_3 in the two types of till. This indicates multiple sources of MgO in the grain sizes from different source rocks; aluminium rich and poor source. Those Mg-bearing rocks that are rich in MgO are dolomite, ~16 (*wt* %). Conversely, those with lower Mg concentrations are phyllite = 2.2 (*wt* %), conglomerate = 1.8 (*wt* %) and mica schist ~3.5 (*wt* %), however, they contribute a large proportion of aluminium silicate Mg to the two till types as they are closest to the till mixing line. These three source rocks contain Mg associated with the mineral chlorite (clinochlore endmember: $(Mg_5Al)(AlSi_3)O_{10}(OH)_8$). The remaining source rocks contain negligible concentrations of Mg (see Table. 4.3).

4.3.4. Mineralogical modal abundance and distributions

The mineralogical compositions of the source rocks are used as endmembers to confirm, not just the rock type, but also, the mineral provenance in the glacier till samples (Table. 4.3.) Quartz, not surprisingly dominates the mineral assemblage in the source rocks with >30 % abundance in all rocks, except dolomite. The dolomites contain 80 to 86 % dolomite and 14 to 20 % calcite. Calcite is also present in higher proportions in the conglomerate and psammite (1) (35 and 30 %, respectively). Foliated, metamorphosed rocks like the phyllite and mica schists, contain abundant plagioclase, 24 to 39%, with an albic endmember composition (An 0-30; Ca*: Na ratio 0.13 ± 0.24 (1*σ)). Plagioclase is also present as a mineral in smaller proportions in the conglomerate (17 %), psammites (12-8 %) and sandstone (<5 %).

Hydrated phyllosilicates (muscovite and chlorite) are present in the phyllite and mica schists, reflecting their pre-metamorphic history and low grade of metamorphism. This also accounts for the chlorite within the conglomerate. The sandstone and conglomerate contain hematite, which likely reflects the pre-Devonian basement rocks in NW Svalbard (Dallmann et al., 1990). Although, the secondary weathering mineral kaolinite was observed in the bulk till, it's

abundance was below or at the limit of quantification <3 %. Separation of the clay-sized fraction in selected samples revealed kaolinite in all samples tested at <20 %, see Appendix. B Table 22. Care must be taken in this interprtation because it is possible that lithogenic and not pedogenic processes may have led to kaolinite being present. Kaolinite can be a common accessory mineral in sedimentary rocks, such as the conglomerate and sandstone, yet in many cases not in high abundance.

Table 4.3. Evaluation of the mineral compositions in the source rocks from the main lithological units in Midtre Lovénbreen's glacier catchment based on the XRD analyses

	Source Rock Types (%)										
	Dolomite (1)	Dolomite (2)	Dolomite (3)	Sandstone	Conglomerate	Psammite (1)	Psammite (2)	Psammite (3)	Phyllite	Mica schist	(2) Mica schist
Mineral (type) (Group)											
Quartz (framework silicate) (*silica mineral*)	0	0	0	86	40	52	96	92	30	48	47
Albite – Anorthite (plagioclase) (*feldspar group*)	0	0	0	5	17	12	4	8	24	36	39
Orthoclase (potassium feldspar) (*feldspar group*)	0	0	0	0	4	6	0	0	0	0	0
Dolomite (Non-silicate) (*carbonate*)	80	86	82	0	0	0	0	0	0	0	0
Calcite (Non-silicate) (*carbonate*)	20	14	18	0	35	30	0	0	0	0	0
Muscovite (layered silicate) (*mica group*)	0	0	0	0	0	0	0	0	19	11	9
Chlorite (layered silicate) (*chlorite group*)	0	0	0	5	0	0	0	0	17	5	5
Hematite (oxide)	0	0	0	4	4	0	0	0	0	0	0
RWP	18	17	16	18	18	16	16	16	9	16	16

Note: Zero= below the limit of quantification (< 3%) for XRD quantification using the PC software TOPAS

As a function of moraine age there is no trend in any of mineralogical components of the glacier till in all transect and depths (a) and (b) (Appendix. B, Fig 6 to 8). The mineralogical composition of the bulk glacier till is dominated by the presence of quartz and albite, while muscovite and chlorite are accessory minerals. Carbonates, dolomite and calcite are dispersed at an abundance of <9 % and <5 % respectively, (for all mineralogical data see Appendix. B, Table 19).

4.4. Discussion

4.4.1. Provenance of Sulfur and Inorganic Carbon

The sulfur present in the till in the Midtre Lovénbreen glacier forefield is mostly sulfide (tabulated in Appendix B. Table 3) associated with the mineral pyrite (FeS_2). Hereafter this will be referred to as $TS_{sulfide}$ or sulfide. Of the source rocks found in the catchment area those that can contain more substantial proportions of pyrite are conglomerates (Borin et al., 2010; Mapelli et al., 2010; Ansari, 2016). Most of the other rocks can also contain traces of pyrite. As shown by as small amounts of sulfides were present in sandstones, and the low-grade metaphoric rocks such as psammites, mica schists and phyllites (Fig. 4.5). The latter two source rocks are the primary lithological units in Midtre Lovénbreen glacier catchment (Harland et al., 1997) and thus the major constituents in the both types of forefield till. Therefore, together with the conglomerate these source rocks provide the largest potential source of sulfide.

Neither sulfate minerals, nor sulfate itself, re-precipitated as efflorescent salts were detected in the source rocks, or associated with the glacial tills, indicating an absence of evaporite minerals such as gypsum or anhydrite. This is not surprising, as geological studies have found no evidence for sulfate containing evaporites in the Proterozoic and Paleozoic basin of this region (Birkenmajer, 1990; Czerny, 1992; Dallmann, 1999). Furthermore, efflorescent salts containing sulfate (i.e. Mg^{2+} or Ca^{2+} SO_4^{2-}) that are often found in High-Arctic forefields (i.e., Finsterwalderbreen; 77°28’ N, 15° 18’ E; Cooper et al., 2002) are most often re-dissolved and washed downstream throughout the melt season (Cooper et al., 2002). Taking this into account explains the absence of the sulfate in our till samples, as these were all collected late in the melt season with no snow cover left during sampling.

The $TS_{sulfide}$ concentrations 0.02 to 0.16 wt% in the soil fraction of the glacial till (Fig. 4.6 & 4.7) are comparable to those in terrestrial arable and bog soils 0.01-0.1 (wt %) (Blume et al., 2010). Given the fact glacial soils are primarily mineral and skeletal and not more mature organic rich soils, this further suggests it is parent material that is the source of $TS_{sulfide}$. It is therefore perhaps unexpected that the $TS_{sulfide}$ concentration in the soil size fraction (subglacial till $\bar{x}$ of 0.07 ±0.03 wt%) is marginally elevated compared to the parent material fractions (subglacial till $\bar{x}$ of 2-7mm = 0.05±0.04 and >7mm 0.04±0.02 wt%). One reason that could account for the difference in $TS_{sulfide}$ observed between size fractions is bacterial sulfate reduction (BSR). Bacterial sulfate reduction may prevail in forefield soils where the ground

conditions are reducing, as the soils are waterlogged, akin to in bog soils, due to underlying impermeable permafrost. On the contrary, where it has been shown that glacial forefield soils are anoxic they were associated with anoxic sulfide oxidation and not BSR (Wadham et al., 2007). Wadham et al., (2007) conclude that a reason for this may be because anoxia is not as widespread compared to the adjacent subglacial environment where the overlying ice restricts the flow of oxygen to the glacial sediments. Inspection of the subglacial till in Tr1, showed no visual evidence of iron sulfides e.g. pyrite or rust-coloured surface coatings that would potentially indicate BSR. Such coatings are a good indication of BSR as commonly observed in subglacial till (Tranter et al., 1993). Furthermore, it is unlikely that the enriched $TS_{sulfide}$ in the soil size fraction is due to its subglacial provenance, as both tills were characterized by similar trends in $TS_{sulfide}$ (Fig. 4.6 & 4.7). With negligible organic matter inputs (necessary for BSR) at young moraine ages, and no evidence of pedogenic iron formation by BSR or iron mobility (Chapter 5. Fig.5 & 6). The data therefore suggests that the observed relatively higher values of $TS_{sulfide}$ in the soil fractions are probably primarily due to density settling and minerals grain size sorting. Due to its high density of 5 g/cm^3 pyrite grains, when compared to other common mineral components (e.g. quartz grains with a density 2.65 g/cm^3), these are more easily environmental gravitationally sorted, or by sieving. Consequently, pyrite grains or sediment containing pyrite, often ends up in the smaller grain size fractions (Robb, 2013) such as the <2 mm soil fraction. Sieving of the till most likely accounted for this observation, as there was no significant difference between the sampled depths, 0-15 and 15-30cm, that would suggest gravitational sorting by density (see Table 8 in Appendix B). These results support a lack of evidence of BSR produced sulfide in our surficial and newly deglaciated Arctic forefield soils (e.g. Wadham et al., 2007 and see also later).

Source rocks in the catchment of Midtre Lovénbreen contain between 0.01 to 10% TIC. Those source rocks containing TIC are conglomerates, psammites (with calcite matrixes), mica schists and phyllites (containing disseminated calcite), and dolostones comprising of calcite and dolomite (Fig. 4.5). Therefore, these source rocks likely make up the soil parent material and could be the source of the TIC variations observed in the soil fractions. The δ^{13}C-TIC isotopic signatures of these source rocks are characteristic of marine carbonates (~0 ‰). Parent material and soil samples in the subglacial till ($\bar{x}$ -1.4‰ from 0-113 y) are concurrent with the δ^{13}C-TIC signatures of the source rocks (Fig. 4.8). Principally the δ^{13}C-TIC subglacial till mix of source rocks reflects the signature of the mica schist (-1.4‰), and therefore disseminated calcite and not dolomite that had a signature of +4.3 to 4.4. This is unsurprising, as mica schist and phyllite

are the dominant lithological rock types in the catchment of Midtre Lovénbreen (Glasser et al., 2001). This is evidence that there has been little fractionation between the carbonate ion and $CaCO_3$ and that of the PDB standard (Craig, 1957; Coleman, 2012), and therefore no pedogenic carbonate formation (e.g. C3 plant -27 + soil CO_2 +5 + 10 ‰ the equilibrium fraction during $CaCO_3$ formation from soil CO_2 = -12‰; Cerling, 1984). Consequently, hereinafter TIC will be referred to as $TIC_{crustal}$ as it is derived from a lithogenic origin.

Qualitative X-ray diffraction identified that the soil samples reflected the source rock carbonate minerology as both calcite and dolomite were identified. Although, quantitative XRD was unable to precisely quantify their concentrations in the soil samples, as they were below the threshold for complex mineralogical mixtures <3% (Tamer, 2013). As TIC reflects primarily disseminated calcite (as discussed above), the TIC expressed as calcite equivalent gives in most cases concentrations similar to the limit of quantification for complex mineralogical mixtures <3%. Due to the heterogeneous nature of our glacial till samples, some carbonate 'nuggets' are observed. This was not surprizing as carbonates as primarily disseminated calcite, and calcite in general was ubiquitous in the parent material and the soil samples. As calcite is abundant in Midtre Lovénbreen forefield, it is likely to exert a major control on the soil weathering regime, its formation, and in turn the CO_2 sink or source potential. This has been evidenced in other silicate dominated deglaciating catchments where traces of calcite combined with the presence of Ca and alkalinity dominates the solute flux of proglacial meltwaters (Anderson et al., 2000; White et al., 1999; Jacobson et al., 2000).

4.4.2. TS and TIC gradients in different types of glacial till

Of the two till types present in Midtre Lovénbreen, a $TIC_{crustal}$ depletion with age is only evident in the subglacial debris in transect Tr1 and in this chronosequence this was true for all size fractions and for both depths (Fig. 4.6 & 4.7). In contrast, $TS_{sulfide}$ was depleted within all subglacial tills samples and in part also in the supraglacial till within the soil fraction (2 mm) and <7 mm non-size fractioned samples. This implies that there is an inherent difference between the chemical weathering of sulfides and carbonates in each till type. A finding that is similar to a study done in the foreland of Glacier Bay, Alaska conducted by Anderson et al. (2000). Their study showed that in a catchment made up of metasediments containing carbonates and sulfides, inorganic carbonate variations in the till residuals seemed independent of moraine age over roughly a century of deglaciation. However, in the same study carbonate

dissolution in forefield waters were shown to be dependent upon the moraine age. These contrasting results were explained by their distributed point sampling approach at specific aged moraines. An approach like this, however, is unlikely to be effective in highly heterogeneous glacier tills, reflecting the insensitivity to variation in the thickness of a leached zone. Such a carbonate leach zone measurement approach was adopted by Goldthwait et al., 1966; Ugolini, 1968 in the Bench glacier forefield. They found this to be effective, as evidenced by a rapid depletion in carbonates with moraine age. The results from this study that used a sampling strategy more akin to that of Anderson et al., 2000 match those in the Goldthwait et al., 1966; Ugolini, 1968 studies better. The fact that this thesis study results are contradictory to those of Anderson et al., 2000 may (a) arise either because their till samples were collected below the surface at depths ranging from 10 to 53 cm compared to 0-15 and 15-30cm in this study. In addition, (b) Anderson et al., 2000 study used a distributed point sampling approach, while this thesis study sampled along chronosequences, clearly separated into either predominately subglacial or supraglacial till soils. It is this difference in sampling approach, along one till type, that probably accounts for the observed difference in TIC between studies, and less so the fact different depths were sampled. If the sampling depth determined the difference between the two studies, there would be a lack of similarity. The results of this thesis study show, in all but one case, no significant difference (p value >0.05 Appendix B. Table. 8) between surface (0-15 cm) and subsurface (15-30 cm) samples. If it is primarilysampling approach (b) that is responsible for the contrasting results between studies, use of this approach in Glacier Bay, Alaska should yield a depletion in TIC as a function of age.

Glaciers, by virtue of their nature, are characterized by a wide range of forces, e.g. changes in climate, glacier hydrology and its bed conditions. It is these that lead to a multitude of possible modes by which glacial till is eroded, transited and weathered, prior to its deposition in a glacial forefield (Benn and Evans, 2014; Tranter et al., 1993). The identifiable subglacial and supraglacial tills' character in our forefield, visible as discrete transects (e.g. Glasser et al., 2001; Fig 4.3) were separable by their grain size distribution (Fig. 4.4) which decreased with size, or was bimodal, as shown in other studies (Boulton, 1978; Benn and Evans., 2014).

Intriguingly, it has been shown that the Midtre Lovénbreen forefield till is either isovolumetric in the stable moraine complex, or, that in part of the forefield physical denudation occurs at a uniform rate (e.g. Irvine-Fynn et al., 2011). It is highly plausible therefore, that the evidenced 20% change in both the soil sample sized fraction (<2 mm), and parent material fraction (>7

mm) as a function of age, would infer substantial chemical and physical weathering in the subglacial till (Fig. 4.4.). These results are concurrent with a depleted TIC and TS in all grain size fractions. However, only if it is assumed that the weathering products move and collect further down the soil profile, or that chemical weathering has little effect on the soil volume. Conversely, the supraglacial till either remained fairly constant in the 2-7 mm parent material fraction, or else it changed by 10% in the >7 mm and <2 mm grain sized fractions at older moraine ages >29 y, respectively. This suggests that more limited chemical and physical weathering had occurred; a result that agrees with the lack of changes in TS and TIC concentrations observed in this till type.

The difference in the concurrent evolution of TS and TIC and grain sized fraction gradients in both the subglacial and supraglacial tills may therefore be due to the changes in physical and chemical properties that each till type experiences during glacial to proglacial transit. Both till types primarily consisted of phyllite, mica schist, sandstones and psammite. However, only the supraglacial till is typically well-lithified, and was observed to have undergone little physical weathering during its glacial transit (Boulton, 1978; Glasser et al., 2001). As such, this till type is less prone to chemical weathering once deposited in the forefield. Conversely, the subglacial till is more prone, as during transit it is susceptible to mechanical breakdown by attrition and physical weathering of the mineral surface by processes such as abrasion (Föllmi et al., 2009; Benn and Evans, 2014). Transit, resulted in a subglacial till that consisted of a higher proportion of phyllites and mica schist and fewer psammites and sandstones (Glasser et al., 2001). Due to the higher proportion of these rocks within the till fabric, a greater degree of chemical weathering may be achieved as their mineral structures are brittle and easily fractured. Also, the subglacial till clearly has a higher abundance of smaller grain sized fractions (Fig. 4.4). This till characteristic would certainly enhance chemical weathering, as the increased surface area due to higher physical weathering during transit, is a fundamental kinetic control on sulfide and calcite weathering rates (McKibben and Barnes, 1986; Morse and Arvidson et al., 2002; Sjöberg, 1976). It is also feasible that subglacial till surface roughness e.g. cracks and dislocation loops in mineral surfaces, enhance its forefield weathering potential (MacInnis and Brantley, 1992).

The results of this thesis chapter suggest that chemical weathering during the tills subglacial transit was minimal. Both TS and TIC were present at similar concentrations (both at TS 0.13 and TIC 0.2 wt%) in the < 2 mm fraction in both supraglacial and subglacial soils at zero-years-

old. This is evidence that this grain size was rapidly evacuated from the subglacial environment and deposited in the glacial forefield. Till with a long residence time in the subglacial domain quickly, and comprehensively, exhausted sulfides and carbonates (Tranter et al., 1993). Intriguingly, TIC concentrations in the subglacial till parent material fraction >7 mm are roughly an order higher (1-1.7 wt%) at young moraine ages, relative to those measured in the supraglacial (0.12 wt%). It is suspected that these values are a sign of the carbonate 'nugget' effect that can originate from subglacial glaciofluvial till sorting (Tranter et al., 1993).

In summary, this part of Chapter number 4 provides the first evidence for differential chemical weathering of TS and TIC in supraglacially and subglacially-derived tills. Because of this finding, subsequent studies would benefit from identification and separation of the till types. Such a geomorphological *a priori* separation would enable a much better constraint of the chemical weathering progression, and in turn soil development processes in glacial forefields. A difference in physical weathering regimes during their residence in either sub- or supra-glacial systems is the most probable rational for the observed chemical gradients in Midtre Lovénbreen. However, microscopic studies and quantification of specific surface areas using techniques such as BET to allow a comparison between the <2 mm fractions from supraglacial and subglacial till collected from one glacial forefield, could help further elucidate this issue. In addition, it may be that using tills from sub- and supra-glacial environments in dissolution experiments, carried out under forefield environmental analogue conditions, would help compare their chemical weathering rates.

4.4.3. Evidence of sulfide oxidation driving carbonate dissolution

With increasing moraine age, the till samples become $TS_{sulfide}$ depleted, and this is coincident with a similar trend in $TIC_{crustal}$, suggesting a correlation between sulfide oxidation and carbonate dissolution (SOCD) (Fig. 4.6 & 4.7). These coupled trends are primarily evident in the subglacial till chronosequence. As such, only the subglacial till will be further discussed. The process of SOCD is defined as a coupled reaction where sulfuric acid is produced from the oxidation of sulfides and rapidly dissolves proximal carbonates. SOCD is most commonly found in subglacial realms, and only more recently has it been discovered to also play a major role in forefield weathering arenas (Tranter et al., 1993; Anderson et al., 2000; Wadham et al., 2001; Wadham et al., 2007; Dixon et al., 2016). The aqueous analytes of SOCD in rivers

flowing through glacial forefield dominate the melt water flux (Anderson et al., 2000; Wadham et al., 2001). In this study, SOCD can also be inferred for the observed trends in the forefield soils. The pH changes with the depletion in TS and $TIC_{crustal}$ with moraine age (Appendix. B. Fig. 1). In addition, as shown later in Chapter 5, the relative abundance of chemolithoautotrophs, such as iron or sulfur oxidizers (genera *Acidithiobacillus, Thiobacillus, Gallionella, Sulfurimonas*) also decrease with increased moraine age (see, Chapter 5. Fig 5.9). Finally, as discussed above iron extraction data showed that at young moraine ages high concentrations of iron oxides prevailed. Consequently, it is possible that these are a product of iron sulfide oxidation (see, Chapter 5. Fig 5.6).

To determine whether weathering along our chronosequences was dominated by SOCD, a mass balance calculation was conducted. The measured TS and TIC concentrations were tested to see which predicted reaction pathway stoichiometries best matched their concentrations. To do such a mass balance calculation, several criteria were met and some assumptions were made.

Firstly, weak organic acids were ruled out as possible sources of carbonate dissolution because of the sparse vegetation and dominance of chemolithoautotrophs microbes at younger moraine ages. This has been shown in Bradley et al., (2016) (Joshua J. Blacker as co-author) in Midtre Lovénbreen forefield. It has also been suggested by Hodkinson et al., (2003) for several high Arctic proglacial areas. Moreover, there is little evidence for sesquioxide translocation down the soil profile, although further work would be needed to prove this (Appendix B. Fig. 5 & Appendix C. Fig. 3). Secondly, the potential reaction pathway and controlling parameters were determined. The sulfide oxidation depends on the species, redox conditions, pH (Nordstrom, 1982), abundance and activity of enzymatic iron and sulfur oxidizing bacteria (Crundwell, 2003; Singer and Stumm, 1970). In Midtre Lovénbreen, pyrite has been identified (e.g. in this study, and Borin et al., 2007), and subsequently used as the sulfide species. In aerated and unconsolidated surface tills within a forefield, O_2 is the obvious oxidizing agent. However, subsurface tills can be poorly drained and anoxic, yet sulfide oxidation can persist using Fe^{3+} and / or NO_3^- as the oxidizing agents (Wadham et al., 2007; Moses and Herman, 1991; Bottrell and Tranter, 2002). In forefield studies that sampled proglacial waters, anoxic tills were inferred to be widespread (Wadham et al., 2007; Hindshaw et al., 2016; Nauer et al., 2012). Anoxia is primarily controlled by hydrometerological and prevailing groundwater conditions (Cooper et al., 2002). Therefore, till sampled from 0-30 cm depth in this study could be reducing, and thus sulfide oxidation under anoxia are considered (Table 4.4. Reaction no. 3).

In Midtre Lovénbreen no depletion of NO_3^- was evidenced (samples from this study remained constant at ~0.3 µg/g over the chronosequence; Appendix B. Fig. 10), and was therefore disregarded. In the same region, young samples have an abundance of iron and sulfur oxidizing bacteria (discussed above and in chapter 5). Microbial activity is likely to be responsible for sulfide oxidation under oxic and anoxic conditions. Such a process has been also inferred from visual observations of iron oxide staining on isolated conglomerate clasts in the Midtre Lovénbreen forefield (Borin et al., 2007).

The reaction products from SOCD are inferred to be HCO_3^- and CO_2 because of the pH range measured (pH =6.5-8.3; Appendix B. Fig. 4.1). Iron minerals present in the forefield (Chapter 5. Fig. 5.7) were dominated by $Fe(OH)_3$, Fe_2O. Dissolved iron ($Fe^{2+/3+}$) was also included due to its presence in Midtre Lovénbreen and in glacial-forefield systems in general (Anderson et al., 2000; Wadham et al. 2001; Raiswell et al., 2009). An added complication was the fact the sampled tills were visibly freeze-thaw active soils, (also evidenced by Hodkinson et al., 2003), meaning they could be open or closed to, and in or out of equilibrium with the atmosphere. At the time of sampling no isotopic evidence of pedogenic carbonates (Fig. 4.8) or efflorescent salts containing sulfate were observed. Thus, it was reasonable to assume that carbon and sulfate species produced from carbonate weathering remained in either the aqueous or gaseous phase. It must also be remembered that forefields are dynamic environments, and temporal and spatial variations in pH, $_PCO_2$, temperature and moisture can cause the species to interconvert. Perturbations in one part of this evolving system could lead to a significant redistribution of the species. Nevertheless, in this chapter the potential for weathering of bulk soils and rocks in a glacial forfied to act as a CO_2 sink and source is discussed. This study focuses on the fact that carbon and sulfur species are formed over years, up to ~ 1 century, rather than seasonal changes. This is based on the discussion above, and that sulfide oxidation in forefields proceeds via several different reaction pathways (Anderson et al., 2000; Wadham et al. 2001; Raiswell et al., 2009). Based on the fact that speficic reactions can regulate the proton yield, and thus the amount of carbonate dissolved, several SOCD reaction scenarios were considered, Table 4.4.

Table 4.4. Potential reaction pathways for sulfide oxidation and carbonate dissolution SOCD that may occur in the soils in the Midtre Lovénbreen forefield.

Reaction no.	Theoretical Reaction Equation	Reaction Stoichiometry (mole:mole)
	Sulfide oxidation-acid production	
1	$4FeS_2 + 15O_2 + 14H_2O \rightarrow 4Fe(OH)_3 + 8H_2SO_4$	1:2
2	$4FeS_2 + 15O_2 + 8H_2O \rightarrow 2Fe_2O_3 + 16H^+ + 8SO_4^{2-}$	1:4
3	$FeS_2 + 14Fe^{3+} + 8H_2O \rightarrow 15Fe^{2+} + 2SO_4^{2-} + 16H^+$	1:16
	Carbonate dissolution	
a	$CaCO_3 + H_2SO_4 \rightarrow CO_2 + H_2O + Ca^{2+} + SO_4^{2-}$	1:1
b	$2CaCO_3 + H_2SO_4 \rightarrow 2Ca^{2+} + SO_4^{2-} + 2HCO_3$	2:1

Note: reaction stoichiometry in reactions 1-3 are the ratio of FeS_2: proton active species and in reactions a & b $CaCO_3$: proton active species.

A stoichiometric mass balance was calculated for each of the equations tabulated in Table 4.4. This was determined as the ratio of moles of acid to carbonate (as in Anderson et al., 2000) and suggests an SOCD reaction pathway, where O_2 is used as the oxidant to produce ferric oxide and CO_2 (reaction 2a), this best fits the measured concentrations and their stoichiometry in each of the scenarios in Table. 4.4 & 4.5. Sufficient acidity is generated from sulfide oxidation to deplete all available calcite via this pathway. Therefore, other possible proton supplies (e.g., carbonic acid or weak organic acids from biological inputs) likely play a minor role.

Table 4.5. Stoichiometric mass balance results from the predicted SOCD reactions and their stoichiometry in Table 4.4 compared to the measured concentrations of $TS_{sulfide}$ and $TIC_{carbonate}$

Scenario	Total Sulfur (expressed as sulfide) (mol/kg)	Total Inorganic Carbon ($TIC_{crustal}$) (mol/kg)	Theoretical Reactions					
			1, a	2, a	3, a	1, b	2, b	3, b
Max	0.039	0.0195	-0.12	-0.04	0.43	-0.31	-0.24	0.23
Min	0.007	0.0040	-0.03	-0.01	0.07	0.07	0.05	0.03
$Mol^{-} kg\, a^{-1}$	0.03	0.131	-0.07	-0.02	0.32	-0.21	-0.15	0.19

Note: Tabulated results show the data from Tr1 <2mm. For all mass balance results plotted as a function of moraine age see Appendix. B. Fig. 9. Values closest to zero denote the measured concentrations of $TS_{sulfide}$ and $TIC_{crustal}$ and their reaction stoichiometry that are closest to their theoretical stoichiometry (highlighted in grey). $Mol^{-} kg\, a^{-1}$ is calculated from slope of the line from linear regression analyses (see Appendix. B. Table. 5).

These results, though not conclusive, suggest that anoxic sulfide oxidation within the top 30 cm of soils is unlikely or limited. In these particular soils this is unsurprising, since they are porous tills and soils, and oxygen can easily diffuse into them. Further support of this, is the

fact that there is little difference between surface and subsurface reactive iron concentrations (Appendix C. Fig. C.3). Interestingly, in other deglaciated forefields in Svalbard, Dryadbreen (Hindshaw et al., 2016) and Finsterwarderbreen (Wadham et al., 2007), evidence of both anoxic and oxic SOCD has been identified, but in both cases through processes in subglacial river effluents. One reason is that different SOCD reactions occur both temporally and spatially deeper down in the soil or glacial till profile, where changes in hydrological and redox conditions may be present. In addition, meltwater measurements usually show the integrated effects of all possible SOCD reactions over an entire forefield or delineated area, at predefined time-steps, over a selected period of measurement, typically a melt season. This is in contrast to this study, where the data from weathered, bulk soils, along chronosequences, show the integrated effects of SOCD at the depth sampled at a specific point in time and space. In other words, this accounts for the overall weathering period of the samples at a specific location and age. It is therefore evident, both approaches (proglacial meltwater and chronosequence soil measurements) provide different but complementary angles to our understanding of SOCD and chemical weathering in glacial forefields.

4.4.4. Evidence of silicate weathering?

The weathering results described in Section 4.3.3.1. revealed that the elements most easily mobilised during the chemical weathering of silicates (Na, Ca, Mg and K), and those that in principal should be enriched (e.g., Al), remained mostly unchanged along the 113 year chronosequenses studied (Fig. 4.9). Moreover, that silicate weathering in Midtre Lovénbreen is independent of glacial till type e.g. supra-and sub-glacial. Mineralogical results are consistent with those of the weathering indices, showing no significant transformation of primary minerals with age, e.g., feldspars to secondary minerals and sheet- and phyllosilicates (Appendix B. Fig. 6, 7 & 8). However, indices indicated that all soils can be considered weathered, even the freshest exposed ones. This is a finding that could agree with the presence of traces of secondary weathering minerals, chlorite and kaolinite (Appendix B. Table. 19 & 22), a consequenec of their removal from the parent rocks due to mechanical abrasion. It is likely that these minerals are from lithogenic and not pedogenic origins, as the metasedimentary rocks, mica and phyllite, within the soil parent material, contain primary chlorite (Table. 4.3), while the conglomerates and sandstones can contain kaolinite in their rock matrixes. Consequently, sorting of the source rocks' derived mineral grains, within these forefield-forming soils, could result in a 'pseudo' chemical weathering trend, such as the

plagioclase-muscovite one, described above (Fig. 4.9.a & 4.12). The apparent difference between the subglacial (Tr1) and supraglacial (Tr2) tills' elemental oxide compositions (Fig. 4.12), could in part arise by their mode of glacial transit, and subsequent level of physical weathering and sorting, prior to their deposition in the forefield (discussed below).

Pseudo-chemical weathering trends, such as those inferred from the weathering indices' results of the grain size fractionated bulk soil samples (Fig. 4.9.a & 4.12), have been observed in other soils that were formed through chemical weathering of glacial till parent materials (Nesbitt and Young, 1996; Nesbitt and Young, 1997). These trends result from the preferential physical sorting of source rocks, either in the forefield by soil mechanical processes e.g., cryoturbation (Nesbitt and Young, 1997) or during glacial transit (Boulton, 1978; Benn and Evans., 2014). In turn, the abundance and type of source rocks in glacial tills and thus its chemical and mineralogical composition are affected. Soils forming from glacial till may be operationally sorted, affecting chemical and mineralogical composition, by soil grain size fractionation during sieving. Sieving can cause the breakdown of sedimentary rocks, meaning finer soil grain fractionation over-concentrates aluminous clays. Weathering index values are not representative of natural settings, being typically higher than in reality. Conversely, feldspars are found in larger, sand-sized particles, and thus derive less weathered values (Nesbitt and Young, 1996). Even though incongregant weathering plagioclase (albite) is apparent in Fig. 4.10, 4.11 & 4.12, there is little confidence in this observed chemical weathering trend, as physical processes, environmental and/or sieving, can also give rise to these data trends.

As discussed previously, source-rock sorting accounts for the observed trends (Fig. 4.10, 4.11 & 4.12) and may arise due to their transit through the glacial system, and the tills' physical weathering. Sandstones, psammites, and to a lesser degree weakly cemented conglomerates, are more prone to physical deterioration under freeze-thaw action and hydrological attrition during subglacial glacial transit (Nicholson and Nicholson, 2000; Benn and Evans., 2014). This is similar in the foliated, fine-grained phyllites (unlike higher grade mica schists), because they have a higher muscovite content which is more prone to weakening due to their inherent anisotropic properties (Table. 4.3). These rock types are more likely to fracture into smaller segments during physical weathering (Shea, W.T. and Kronenberg., 1993) such as in the subglacial domain. Rock-mineral properties predispose forefield-forming soils to silicate weathering, and, in part, explain the observed physical and chemical difference between subglacial and supraglacial tills. Note: rock-mineral properties of a glacial till in the context of

forefield soil formation is also discussed previously in Section 4.2 for carbonates and sulfide minerals.

If forefield silicate weathering is reflected in the chemical weathering indices, the rate of it is extremely slow, as shown by the small relative change in weathering indices values (Fig. 4.10, 4.11 & 4.12). In the Midtre Lovénbreen forefield, this is in part due to the presence of sedimentary carbonates within the till. Carbonates such as calcite reacts orders of magnitude faster than Ca silicate e.g., plagioclase. Carbonate dissolution buffers the soil solution's acidity for sulfide weathering. This is a common trait in environments where mechanical erosion is less intense, as the most reactive mineral phases are depleted from accessible portions of the exposed rocks first (Stallard and Emmond, 1983; Drever and Zorbist, 1992; White et al., 1999). Further retardation of silicate weathering rates could be caused by the slow onset of microbial and vegetation assemblage in Midtre Lovénbreen (Hodkinson et al., 2003; Bradley et al., 2016), discussed below.

Slow rates of silicate weathering in high-Arctic glacial forefields is not uncommon. Three independent studies where proglacial meltwaters and bulk sediments chemistries were assessed are in the high-Arctic forelands of the Bench glacier, south-central Alaska (Anderson et al., 2000), Finsterwalderbreen, Svalbard (Wadham et al., 2001), and Werenskiold glacier (Kabala and Zapart., 2012). These studies inferred that silicate weathering is <10% over the first century. In contrast, similar studies of forefields in the European Alps, over the first 150-years of deglaciation, show it to be somewhat variable. In the Morterasch glacier, Switzerland, mica (biotite) was transformed into vermiculite, and after less than a decade of glacier retreat, pedogenic kaolinite and smectites were present in the clay fractions of the forland soils (Mavris et al., 2010; Mavris et al., 2011). This change was not easily explained because there was no detectable decrease in the plagioclase content (Mavris et al., 2010).

In glacial forefield soil and till samples, differences in lithology and mineralogy could partially account for the silicate weathering observed between forefields. For example, Midtre Lovénbreen forefield comprises of metasediments consisting of primarily mica as muscovite, while the foreland of the Morterasch glacier has a primary grantic lithology containing mica as biotite. Mica as muscovite, unlike biotite, exhibits very little chemical variation (ion substitution) from its ideal chemical formula, $KAl_2(AlSi_3O_{10})(OH)_2$, due to its dioctahedral structure. Subsequently muscovitve is significantly more resistant to chemical alteration than biotite that has a trioctahedral structure (Tischendorf et al., 2007).

Interestingly however, the Damma glacier forefield Morterasch in Switerzerland has a granitic lithology (Bernasconi et al., 2011), yet the evidence suggests a significant difference in silicate weathering. Lithology, and in turn a soil's parent material, may not be as influential in forefield soil development as other factors. For instance, mineral abundance, inferring silicate to clay transformation, was shown in the Morterasch forefield, as discussed previously. Conversely, little evidence of silicate weathering in the Damma forefield was found (i.e., no trend in CIA (range 50-65) as a function of age); although, the amount of clay content of minerals did increase with age. Despite the accumulation of clay, the authors of this study suggest that silicate weathering, clay mineral genesis is an unlikely explanation. Instead, because a clay mineral fraction was present in the immature soils as early as 2-18 years-old, and there was an observed development of a vegetation community with soil age, the accumulation of clays was due to biological stabilization of the fine fraction of 57-79-yrs.

Silicate weathering regimes in forefield soils seems to be driven by the stage that fauna and flora also establishes. In Alpine forefields, colonisation with vascular plants, including *oxyria digyna* (commonly known as mountain or Arctic sorrel), proceeds after only a decade of deglaciation, and these communities become fully established after ~ 30 years (Burga, 1999; Bernasconi et al., 2011). Conversely, vascular plant colonisation in the high-Arctic Midtre Lovénbreen forefield begins only after ~ 60 years (e.g. *Saxifraga*) and is still sparse after >113 years (Hodkinson et al., 2003). In these settings, *Oxyria digyna* becomes established after ~ 150 years (Hodkinson et al., 2003), revealing that biological colonization, and particularly the establishment of vegetation, may be the crucial catalyst for soil formation in forefields. This is because, microbial and vegetation colonization can help reduce soil erosion as plant-rhizosphere root development anchors clay fines within a soil (Bernasconi et al., 2011). Also, early plant coloniser exudate, muslicage soil particle 'gluing' polysaccharide compounds, help soil aggregation (Galloway,. et al., 2018; Joshua Blacker co-authored). The combined effect of a reduction in soil erosion, improved soil structure, and increased soil water retention, as organic matter accumulates, and mineral weathering proceeds, means that soil fertility, and its role as a habitat is improved (Borin et al., 2007). The earlier a plant and microbe evolution occurs in forefield, the faster the soil devlops, and in turn enhances silicate weathering rates. Key nutrients are released to the soils by mineral weathering, and this further facilites forefield soil ecosytem evolution (Bernasconi et al., 2011). Biological weathering in forefield soils includes localised mineral weathering, by the addition of organic acid exudates from plant roots

and fungi hyphae, raising the rhizosphere PCO_2 (Drever, 1994; Bonneville et al., 2016). It has been hypothesised that in landscapes with limited erosion, biological-driven processes dominate the initial stages of weathering, which then facilitates biological processes over the long-term (Brantley et al., 2011). The contrasting rates of vegetation assemblages between Arctic and European Alpine studies and the observed levels of silicate weathering certainly support this hypothesis.

4.4.5. Carbonate *vs*. silicate weathering in glacial forefields and its implications for CO_2 dynamics

The empirical relationships recorded in the chronosequence samples in the Midtre Lovenbreen forefield show evidence that SOCD dominates the weathering regime, especially in the early stages, while silicate weathering is more limited. The observed trends in soil elemental, chemical and mineralogy compositions support other studies that assessed the changes in proglacial meltwater effluents, which drain forefields. Collectively these spatiotemporal trends suggest that SOCD-type weathering regimes may be common in high-Arctic glacial forefields containing sulfide and carbonates. (e.g. Anderson et al., 2000; Wadham et al., 2001). The question is therefore, how the prevalence of this weathering regime in forefields may have implications on carbon-cycle and climatic changes?

The world has undergone numerous interglacial cycles, and is currently responding to unprecedented levels of warming-induced deglaciation. Forefields provide the environmental conditions, and a chemically reactive substrate, subglacial till, that if containing accessory carbonates and sulfides, promotes SOCD. Such reactions can be a potential source of CO_2 to the atmosphere. In transport-limited terrestrial sediments, like the soils forming in forefield moraine complexes, the contribution of SOCD on short timescales has been little researched (Martin, 2016). Plant assemblage is slow in Arctic forefields (e.g. Hodkinson et al., 2003), and is a potenital CO_2 sink feedback (Harden et al. 1992), as a result, deglaciation may be accelerated. In turn, the lack of biologically enhanced silicate weathering slows soil-development (See, Chapter 5). Taken together, these results imply that Arctic glacial forefields at young moraine ages are a net CO_2 source to the atmosphere.

To test this, a forefield carbon balance model is needed that combines all known major facets of biogeochemical CO_2 sinks and source. All of the current models focus on microbiological

inputs and outputs (e.g. Bradley et al., 2016). So far, such models do not include the influence of rock-water interactions and pedogenic processes, or the development of vegetation assemblages. Moreover, an in-depth process-based understanding, that bridges long-term bulk soil mineral residual observations with short-term seasonal and diurnal chemical reactions, is also lacking. In principle, glacial till mineral weathering can generate above atmospheric levels PCO_2 either by a localised and/or abundant supply of sulphuric acid driving carbonate weathering, which is a direct source of CO_2 (Tranter et al., 1993). Alternatively, in a diurnal-seasonal, freeze-thaw active soil system like Midtre Lovénbreen, SOCD in unfrozen liquid soil pockets could also raise the soil PCO_2 and outgas upon thaw (Wadham et al., 2001). This is possible as we found no evidence for newly formed pedogenic carbonates. Therefore, depending on the prevailing soil-water PCO_2, CO_2 could be released directly into the atmosphere or hydrosphere. Due to the fast reaction kinetics of this reaction it may be possible to derive a better understanding of the soil forming processes by conducting *in-situ* studies that measure physical and chemical changes in the bulk till and its effluent. A shift from bulk soil analysis to micro and nano-scale chemical soil measurements would further reveal the level of localised biotic (and abiotic) silicate weathering.

4.5. Conclusion

In Midtre Lovénbreen the transport-limited forefield tills consisted of a mix of sedimentary and metasedimentary rocks derived primarily from subglacial and supraglacial domains. The fact that the primary forefield lithology was low grade mica schists and phyllites was reflected in the abundance, and chemical composition, of both till types. These rock types contained sulfide and carbonate mineral traces. With moraine age, only subglacial tills tended to be depleted in TS and TIC, while in the supraglacial till a marked depletion was only evident in TS in the <2 mm fraction. Furthermore, chemical and mineralogical differences between till soil types, as well as parent material fractions, were apparent. Subglacial till chemistries were more clearly separated by grain size, and had a higher concentration of easily mobilised elemental oxides in the larger fractions. Conversely, the supraglacial tills showed scattered grain size distributions, and there was no clear evidence of a relationship to their chemical composition. This was most likely due the variation in weathering that each till type was subjected to during their glacial transit, and to some extent since exposure.

The results in this chapter have revealed that TS and TIC became depleted in the 0-15cm surface of subglacial tills, and that this change could be accounted for by sulfide oxidation, that is able to supply sufficient protons to deplete the carbonates after less than 113 years of deglaciation. This reaction could also be linked to the changes observed in iron mineral abundance along the chronosequences. Mass balance results are also consistent with the relative abundance of sulfide oxidizing microbes found along the chronosequence (work by collaborators at the Uni of Bristol). Finally, the decrease in soil pHs with moraine age, further supported the occurrence of SOCD in the newly forming soils.

In contrast to SOCD, silicate weathering in the Midtre Lovénbreen forefield soils and its parent material was found to be very limited. With increased moraine age, the weathering indices showed that both mobile and immobile elemental oxides from silicate minerals remained at similar stochiometric ratios; whilst primary and secondary mineral modal abundance was constant. When elemental oxides were plotted on a ternary diagram, stoichiometric compositional changes were evident. These could be interpreted as a chemical weathering-induced enrichment in immobile aluminium and potassium, and as depletion in calcium and sodium in mobile elemental oxides, which infers plagioclase weathering. A more likely interpretation though, is instead of pedogenic weathering, these changes reflect the sorting of metasedimentary source rocks within the glacial till. Not only was it found that soil and parent material chemical compositions sort per grain size fraction, but that higher concentrations of easily mobilised elemental oxides in larger grain size fractions existed. Each grain size fraction seemed to correspond to specific source rocks, and their chemical compositions, and thus modal abundance in the bulk. Larger grain size fractions corresponded to mica-schists rich in Ca and Na-bearing feldspar minerals, namely anorthite and albite, whereas smaller grains sizes consisted of greater proportions of aluminium and potassium oxide rich psammites and phyllite source rocks. Therefore, a silicate chemical weathering signal was not evident from the background heterogeneity of chemical composition of the glacial till material.

The results of chemical weathering indices indicated that silicate was very limited, and was coincident with mineralogical modal abundance and type analyses. Primary silicate minerals were uncorrelated with moraine age, and almost at steady state. A low abundance of secondary clay minerals were measured at roughly <10 % chlorite and kaolinite, representing <3 % of the total bulk soil mineralogy. The presence of these minerals reflected their constituents in the

metasedimentary source rocks that make up the parent material glacial till. This is most probably due to a lithogenic origin, rather than *in-situ* pedogenic primary silicate weathering.

Where sulfide and carbonate minerals in a forefield till are accessible for weathering in developing soils, SODC probably plays a key role in controlling soil pH. Acidity produced by sulfide oxidation seemed to be buffered by lithogenic carbonates present, this process potential CO_2 source. The longevity of this process seems to be at the cost of retarded silicate weathering, a potential atmospheric sink of CO_2. Furthermore, it is apparent that this process has slowed soil development through a lack of nutrient availability and therefrom, heterotrophic abundance and assemblage. This may result in lower CO_2 drawdown from the atmosphere and attribute lower levels of bio-enhanced weathering. Where carbonates were exhausted in moraine ages of 50 and 113 years, silicate weathering was more likely to procced, as this coincides with the establishment of high-order vascular plant species which enhance weathering. Elemental oxide ratios and mineralogical changes did not show measurable evidence of silicate weathering. The fact that few plants are present at older ages, indicates nutrient acquisition may occur by localised bio-mining essential for their metabolism; although at a lower level than the baseline chemical heterogeneity of the forefield till-forming soils.

These results suggest that forefields comprising only accessory carbonates and sulfides within their tills, and primitive ecosystems, could also be potential CO_2 sources over glacial-inter-glacial periods in deglaciated terrain less than a century old, as silicate weathering and heterotrophs are limited.

4.6. References

Abbey, S. 1980. Studies in “standard samples” for use in the general analysis of silicate rocks and minerals. *Geostandards Newsletter,* 4**,** 163-190.

Anderson, S. P., Drever, J. I., Frost, C. D. & Holden, P. 2000. Chemical weathering in the foreland of a retreating glacier. *Geochimica Et Cosmochimica Acta,* 64**,** 1173-1189.

Anderson, S.P., Drever, J.I. and Humphrey, N.F., 1997. Chemical weathering in glacial environments. Geology, 25(5), pp.399-402.

Anesio, A. M., Hodson, A. J., Fritz, A., Psenner, R. & Sattler, B. 2009. High microbial activity on glaciers: importance to the global carbon cycle. *Glob Chang Biol,* 15**,** 955-960.

Anesio, A. M., Sattler, B., Foreman, C., Telling, J., Hodson, A. & Tranter, M. 2010. Carbon fluxes through bacterial communities on glacier surfaces. *Ann Glaciol,* 51**,** 32-40.

Ansari, A. H. 2016. Stable isotopic evidence for anaerobic maintained sulphate discharge in a polythermal glacier. *Polar Science,* 10**,** 24-35.

Benn, D. and Evans, D.J., 2014. *Glaciers and glaciation*. Routledge.

Bernasconi, S. M., Bauder, A., Bourdon, B., Brunner, I., Bunemann, E., Christl, I., Derungs, N., Edwards, P., Farinotti, D., Frey, B., Frossard, E., Furrer, G., Gierga, M., Goransson, H., Gulland, K., Hagedorn, F., Hajdas, I., Hindshaw, R., Ivy-Ochs, S., Jansa, J., Jonas, T., Kiczka, M., Kretzschmar, R., Lemarchand, E., Luster, J., Magnusson, J., Mitchell, E. a. D., Venterink, H. O., Plotze, M., Reynolds, B., Smittenberg, R. H., Stahli, M., Tamburini, F., Tipper, E. T., Wacker, L., Welc, M., Wiederhold, J. G., Zeyer, J., Zimmermann, S. & Zumsteg, A. 2011. Chemical and Biological Gradients along the Damma Glacier Soil Chronosequence, Switzerland. *Vadose Zone Journal,* 10**,** 867-883.

Berner, R. A., Lasaga, A. C. & Garrels, R. M. 1983. The carbonate-silicate geochemical cycle and its effect on atmospheric carbon dioxide over the past 100 million years. *American Journal of Science,* 283**,** 641-683.

Birkenmajer, K. 1990. Geology of the Hornsund area, Spitsbergen. *Explanations to the map,* 1.

Bish, D. L. & Howard, S. 1988. Quantitative phase analysis using the Rietveld method. *Journal of Applied Crystallography,* 21**,** 86-91.

Blum, J.D., Gazis, C.A., Jacobson, A.D. and Chamberlain, C.P., 1998. Carbonate versus silicate weathering in the Raikhot watershed within the High Himalayan Crystalline Series. Geology, 26(5), pp.411-414.

Blume, H.-P., Brümmer, G. W., Horn, R., Kandeler, E., Kögel-Knabner, I., Kretzschmar, R., Stahr, K., Wilke, B.-M., Thiele-Bruhn, S. & Welp, G. 2010. Scheffer/Schachtschabel. *Lehrbuch der,* 4.

Bluth, G. J. & Kump, L. R. 1994. Lithologic and climatologic controls of river chemistry. *Geochimica et Cosmochimica Acta,* 58**,** 2341-2359.

Borin, S., Ventura, S., Tambone, F., Mapelli, F., Schubotz, F., Brusetti, L., Scaglia, B., D'acqui, L. P., Solheim, B., Turicchia, S., Marasco, R., Hinrichs, K. U., Baldi, F., Adani, F. & Daffonchio, D. 2010. Rock weathering creates oases of life in a High Arctic desert. *Environmental Microbiology,* 12**,** 293-303.

Bottrell, S.H. and Tranter, M., 2002. Sulphide oxidation under partially anoxic conditions at the bed of the Haut Glacier d'Arolla, Switzerland. *Hydrological Processes*, *16*(12), pp.2363-2368.

Boulton, G. S. 1978. Boulder shapes and grain-size distributions of debris as indicators of transport paths through a glacier and till genesis. *Sedimentology,* 25**,** 773-799

Bradley, J.A., Singarayer, J.S. and Anesio, A.M., 2014, November. Microbial community dynamics in the forefield of glaciers. In Proc. R. Soc. B (Vol. 281, No. 1795, p. 20140882). The Royal Society.

Bradley, James A., et al. "Microbial dynamics in a High Arctic glacier forefield: a combined field, laboratory, and modelling approach." *Biogeosciences* 13.19 (2016): 5677.

Bray, A.W., Oelkers, E.H., Bonneville, S., Wolff-Boenisch, D., Potts, N.J., Fones, G. and Benning, L.G., 2015. Geochimica et cosmochimica acta, 164, pp.127-145.

Brown, G. H. 2002. Glacier meltwater hydrochemistry. *Applied Geochemistry,* 17**,** 855-883.

Burga, C. A. 1999. Vegetation development on the glacier forefield Morteratsch (Switzerland). *Applied Vegetation Science,* 2**,** 17-24.

Calmels, D., Gaillardet, J., Brenot, A. and France-Lanord, C., 2007. Sustained sulfide oxidation by physical erosion processes in the Mackenzie River basin: climatic perspectives. Geology, 35(11), pp.1003-1006.

Canfield, D.E., Raiswell, R., Westrich, J.T., Reaves, C.M. and Berner, R.A., 1986. The use of chromium reduction in the analysis of reduced inorganic sulfur in sediments and shales. Chemical geology, 54(1-2), pp.149-155.

Caughey, M.E., Barcelona, M.J., Powell, R.M., Cahill, R.A., Grøn, C., Lawrenz, D. and Meschi, P.L., 1995. Interlaboratory study of a method for determining nonvolatile organic carbon in aquifer materials. Environmental Geology, 26(4), pp.211-219.

Cerling, T. E. 1984. The stable isotopic composition of modern soil carbonate and its relationship to climate. *Earth and Planetary Science Letters,* 71**,** 229-240.

Coleman, D. C. 2012. *Carbon isotope techniques*, Academic Press.

Cooper, R. J., Wadham, J. L., Tranter, M., Hodgkins, R. & Peters, N. E. 2002. Groundwater hydrochemistry in the active layer of the proglacial zone, Finsterwalderbreen, Svalbard. *Journal of Hydrology,* 269**,** 208-223.

Craig, H., 1957. Isotopic standards for carbon and oxygen and correction factors for mass-spectrometric analysis of carbon dioxide. Geochimica et cosmochimica acta, 12(1-2), pp.133-149.

Crocker, R. L. & Major, J. 1955. Soil Development in Relation to Vegetation and Surface Age at Glacier Bay, Alaska. *Journal of Ecology,* 43**,** 427-448.

Crundwell, F.K., 2003. How do bacteria interact with minerals?. *Hydrometallurgy*, *71*(1), pp.75-81.

Czerny, J. 1992. *Geological Map of the SW Part of Wedel Jarlsberg Land Spitsbergen*, Institute of Geology and Mineral Deposits, University of Mining and Metallurgy.

Dallmann, W. K. 1999. *Lithostratigraphic Lexicon of Svalbard. Upper Palaeozoic to Quaternary bedrock*, Committee on the Stratigraphy of Svalbard / Norsk
Polarinstitutt.

Drever, J.I., 1994. The effect of land plants on weathering rates of silicate minerals. Geochimica et Cosmochimica Acta, 58(10), pp.2325-2332.

Drever, J.I. and Zobrist, J., 1992. Chemical weathering of silicate rocks as a function of elevation in the southern Swiss Alps. Geochimica et Cosmochimica Acta, 56(8), pp.3209-3216.

Dulski, P. 2001. Reference Materials for Geochemical Studies: New Analytical Data by ICP-MS and Critical Discussion of Reference Values. *Geostandards Newsletter,* 25**,** 87-125.

Ellis, S. and Mellor, A., 1995. Soils and environment. Taylor & Francis US.

Fao, I. 2006. Working Group, WRB (2007). *World reference base for soil resources*.

Fedo, C. M., Nesbitt, H. W. & Young, G. M. 1995. Unraveling the effects of potassium metasomatism in sedimentary rocks and paleosols, with implications for paleoweathering conditions and provenance. *Geology,* 23**,** 921-924.

Gardner, L.R., 1980. Mobilization of Al and Ti during weathering—isovolumetric geochemical evidence. Chemical Geology, 30(1-2), pp.151-165.

Garrels, R. M. & Christ, C. L. 1965. Solutions, minerals, and equilibria.

Gibbs, M.T. and Kump, L.R., 1994. Global chemical erosion during the last glacial maximum and the present: sensitivity to changes in lithology and hydrology. Paleoceanography, 9(4), pp.529-543.

Glasser, N. F. & Hambrey, M. J. 2001. Styles of sedimentation beneath Svalbard valley glaciers under changing dynamic and thermal regimes. *Journal of the Geological Society,* 158**,** 697-707.

Goldthwait, R. P., Loewe, F., Ugolini, F., Decker, H., Delong, D., Trautman, M., Good, E., Merrell Iii, T. & Rudolph, E. 1966. Soil development and ecological succession in a deglaciated area of Muir Inlet, Southeast Alaska. Research Foundation and the Institute of Polar Studies, The Ohio State University.

Gonfiantini, R., Stichler, W. and Rozanski, K., 1995. Standards and intercomparison materials distributed by the International Atomic Energy Agency for stable isotope measurements (No. IAEA-TECDOC--825).

Group, I. W. 2006. WRB, 2006. *World reference base for soil resources*.

Hagen, J. O. & Liestøl, O. 1990. Long-term glacier mass-balance investigations in Svalbard. *Annals of Glaciology,* 14**,** 102-106.

Hagen, J. O., Melvold, K., Pinglot, F. & Dowdeswell, J. A. 2003. On the net mass balance of the glaciers and ice caps in Svalbard, Norwegian Arctic. *Arctic, Antarctic, and Alpine Research,* 35**,** 264-270.

Hambrey, M. J., Murray, T., Glasser, N. F., Hubbard, A., Hubbard, B., Stuart, G., Hansen, S. & Kohler, J. 2005. Structure and changing dynamics of a polythermal valley glacier on a centennial timescale: Midre Lovenbreen, Svalbard. *Journal of Geophysical Research-Earth Surface,* 110.

Harland, W. B., Anderson, L. M., Manasrah, D., Butterfield, N. J., Challinor, A., Doubleday, P. A., Dowdeswell, E. K., Dowdeswell, J. A., Geddes, I. & Kelly, S. R. 1997. The geology of Svalbard.

Hindshaw, R. S., Heaton, T. H. E., Boyd, E. S., Lindsay, M. R. & Tipper, E. T. 2016. Influence of glaciation on mechanisms of mineral weathering in two high Arctic catchments. *Chemical Geology,* 420**,** 37-50.

Hodkinson, I. D., Coulson, S. J., Harrison, J. & Webb, N. R. 2001. What a wonderful web they weave: spiders, nutrient capture and early ecosystem development in the high Arctic – some counter-intuitive ideas on community assembly. *Oikos,* 95**,** 349-352.

Hodkinson, I. D., Coulson, S. J. & Webb, N. R. 2003. Community assembly along proglacial chronosequences in the high Arctic: vegetation and soil development in north-west Svalbard. *Journal of Ecology,* 91**,** 651-663.

Hodkinson, I. D., Webb, N. R. & Coulson, S. J. 2002. Primary community assembly on land – the missing stages: why are the heterotrophic organisms always there first? *Journal of Ecology,* 90**,** 569-577.

Hodson, A., Anesio, A. & Tranter, M. 2008. Glacial ecosystems. *Ecol Stud,* 78**,** 41-67.

Hodson, A., Mumford, P., Kohler, J. & Wynn, P. M. 2005. The High Arctic glacial ecosystem: new insights from nutrient budgets. *Biogeochemistry,* 72**,** 233-256.

Hodson, A., Murnford, P. & Lister, D. 2004. Suspended sediment and phosphorus in proglacial rivers: bioavailability and potential impacts upon the P status of ice-marginal receiving waters. *Hydrological Processes,* 18**,** 2409-2422.

Huggett, R. J. 1998. Soil chronosequences, soil development, and soil evolution: a critical review. *CATENA,* 32**,** 155-172.

Irvine-Fynn, T. & Hodson, A. 2010a. Biogeochemistry and dissolved oxygen dynamics at a subglacial upwelling, Midtre Lovénbreen, Svalbard. *Annals of Glaciology,* 51**,** 41-46.

Irvine-Fynn, T. D. L., Barrand, N. E., Porter, P. R., Hodson, A. J. & Murray, T. 2011. Recent High-Arctic glacial sediment redistribution: A process perspective using airborne lidar. *Geomorphology,* 125**,** 27-39.

Irvine-Fynn, T. D. L. & Hodson, A. J. 2010b. Biogeochemistry and dissolved oxygen dynamics at a subglacial upwelling, Midtre Lovenbreen, Svalbard. *Annals of Glaciology,* 51**,** 41-46.

Irvine-Fynn, T. D. L., Moorman, B. J., Sjogren, D. B., Walter, F. S. A., Willis, I. C., Hodson, A. J., Williams, J. L. M. & Mumford, P. N. 2005. Cryological processes implied in Arctic proglacial stream sediment dynamics using principal components analysis and regression. *Cryospheric Systems: Glaciers and Permafrost,* 242**,** 83-98.

Jacobson, A.D. and Blum, J.D., 2000. Ca/Sr and 87Sr/86Sr geochemistry of disseminated calcite in Himalayan silicate rocks from Nanga Parbat: Influence on river-water chemistry. Geology, 28(5), pp.463-466.

Kabala, C. and Zapart, J., 2012. Initial soil development and carbon accumulation on moraines of the rapidly retreating Werenskiold Glacier, SW Spitsbergen, Svalbard archipelago. Geoderma, 175, pp.9-20.

Kump, L. R., Brantley, S. L. & Arthur, M. A. 2000. Chemical Weathering, Atmospheric CO2, and Climate. *Annual Review of Earth and Planetary Sciences,* 28**,** 611-667.

Langmuir, D., Hall, P. & Drever, J. 1997. *Environmental Geochemistry*, Prentice Hall, New Jersey.

Lerman, A., Wu, L. & Mackenzie, F. T. 2007. CO2 and H2SO4 consumption in weathering and material transport to the ocean, and their role in the global carbon balance. *Marine Chemistry,* 106**,** 326-350.

Macinnis, I. N. & Brantley, S. L. 1992. The role of dislocations and surface morphology in calcite dissolution. *Geochimica et Cosmochimica Acta,* 56**,** 1113-1126.

McCrea, J.M., 1950. On the isotopic chemistry of carbonates and a paleotemperature scale. The Journal of Chemical Physics, 18(6), pp.849-857.

Mangerud, J., Bolstad, M., Elgersma, A., Helliksen, D., Landvik, J. Y., Lønne, I., Lycke, A. K., Salvigsen, O., Sandahl, T. & Svendsen, J. I. 1992. The last glacial maximum on Spitsbergen, Svalbard. *Quaternary Research,* 38**,** 1-31.

Mapelli, F., Marasco, R., Rizzi, A., Baldi, F., Ventura, S., Daffonchio, D. & Borin, S. 2010. Bacterial Communities Involved in Soil Formation and Plant Establishment Triggered by Pyrite Bioweathering on Arctic Moraines. *Microbial Ecology,* 61**,** 438-447.

Martin, J.B., 2017. Carbonate minerals in the global carbon cycle. Chemical Geology, 449, pp.58-72.

Mavris, C., Egli, M., Plotze, M., Blum, J. D., Mirabella, A., Giaccai, D. & Haeberli, W. 2010. Initial stages of weathering and soil formation in the Morteratsch proglacial area (Upper Engadine, Switzerland). *Geoderma,* 155**,** 359-371.

Mavris, C., Plotze, M., Mirabella, A., Giaccai, D., Valboa, G. & Egli, M. 2011. Clay mineral evolution along a soil chronosequence in an Alpine proglacial area. *Geoderma,* 165**,** 106-117.

Moses, C.O. and Herman, J.S., 1991. Pyrite oxidation at circumneutral pH. Geochimica et Cosmochimica Acta, 55(2), pp.471-482.

Midgley, N. G., Glasser, N. F. & Hambrey, M. J. 2007. Sedimentology, structural characteristics and morphology of a Neoglacial high-Arctic moraine-mound complex: Midre Lovenbreen, Svalbard. *Glacial Sedimentary Processes and Products,* 39**,** 11-22.

Nesbitt, H. and Young, G.M., 1982. Early Proterozoic climates and plate motions inferred from major element chemistry of lutites. Nature, 299(5885), pp.715-717.

Nesbitt, H.W. and Young, G.M., 1996. Petrogenesis of sediments in the absence of chemical weathering: effects of abrasion and sorting on bulk composition and mineralogy. Sedimentology, 43(2), pp.341-358.

Nesbitt, H.W., Young, G.M., McLennan, S.M. and Keays, R.R., 1996. Effects of chemical weathering and sorting on the petrogenesis of siliciclastic sediments, with implications for provenance studies. The Journal of Geology, 104(5), pp.525-542.

Nicholson, D.T. and Nicholson, F.H., 2000. Physical deterioration of sedimentary rocks subjected to experimental freeze–thaw weathering.

Nordstrom 1, D. K. 1982. Aqueous Pyrite Oxidation and the Consequent Formation of Secondary Iron Minerals. *In:* KITTRICK, J. A., FANNING, D. S. & HOSSNER, L. R. (eds.) *Acid Sulfate Weathering.* Madison, WI: Soil Science Society of America.

Oliva, P., Viers, J. & Dupré, B. 2003. Chemical weathering in granitic environments. *Chemical Geology,* 202**,** 225-256.

Parker, A., 1970. An index of weathering for silicate rocks. Geological Magazine, 107(6), pp.501-504.

Price, J.R. and Velbel, M.A., 2003. Chemical weathering indices applied to weathering profiles developed on heterogeneous felsic metamorphic parent rocks. Chemical Geology, 202(3), pp.397-416.

Raiswell, R., Benning, L.G., Davidson, L., Tranter, M. and Tulaczyk, S., 2009. Schwertmannite in wet, acid, and oxic microenvironments beneath polar and polythermal glaciers. Geology, 37(5), pp.431-434.

Rietveld, H. 1969. A profile refinement method for nuclear and magnetic structures. *Journal of applied Crystallography,* 2**,** 65-71.

Schumacher, B.A., 2002. Methods for the determination of total organic carbon (TOC) in soils and sediments. Ecological Risk Assessment Support Center, 2002, pp.1-23.

Shea, W.T. and Kronenberg, A.K., 1993. Strength and anisotropy of foliated rocks with varied mica contents. *Journal of Structural Geology*, *15*(9-10), pp.1097-1121.

Singer, P.C. and Stumm, W., 1970. Acidic mine drainage: the rate-determining step. *Science*, *167*(3921), pp.1121-1123.

Serreze, M.C. and Barry, R.G., 2011. Processes and impacts of Arctic amplification: A research synthesis. Global and Planetary Change, 77(1), pp.85-96.

Sjöberg, E.L., 1976. A fundamental equation for calcite dissolution kinetics. Geochimica et Cosmochimica Acta, 40(4), pp.441-447.

Stallard, R.F. and Edmond, J.M., 1983. Geochemistry of the Amazon: 2. The influence of geology and weathering environment on the dissolved load. Journal of Geophysical Research: Oceans, 88(C14), pp.9671-9688.

Svendsen, H., Beszczynska-Moller, A., Hagen, J. O., Lefauconnier, B., Tverberg, V., Gerland, S., Orbaek, J. B., Bischof, K., Papucci, C., Zajaczkowski, M., Azzolini, R., Bruland, O., Wiencke, C., Winther, J. G. & Dallmann, W. 2002. The physical environment of Kongsfjorden-Krossfjorden, an Arctic fjord system in Svalbard. *Polar Research,* 21**,** 133-166.

Tamer, M. 2013. Quantitative Phase Analysis Based on Rietveld Structure Refinement for Carbonate Rocks.

Tischendorf, G., Förster, H.-J., Gottesmann, B. & Rieder, M. 2007. True and brittle micas: composition and solid-solution series. *Mineralogical Magazine,* 71**,** 285-320.

Torres, M. A., West, A. J. & Li, G. 2014. Sulphide oxidation and carbonate dissolution as a source of CO2 over geological timescales. *Nature,* 507**,** 346-349.

Tranter, M. 2003. Geochemical weathering in glacial and proglacial environments. *Treatise on geochemistry,* 5**,** 189-205.

Tranter, M., Brown, G., Raiswell, R., Sharp, M. & Gurnell, A. 1993. A conceptual model of solute acquisition by Alpine glacial meltwaters. *Journal of Glaciology,* 39**,** 573-581.

Tranter, M. & Wadham, J. L. 2014. 7.5 - Geochemical Weathering in Glacial and Proglacial Environments. *In:* TUREKIAN, H. D. H. K. (ed.) *Treatise on Geochemistry (Second Edition)*. Oxford: Elsevier.

Ugolini, F. Soil development and alder invasion in a recently deglaciated area of Glacier Bay, Alaska. Proc Symp Northwest Sci Assoc, 1968.

Wadham, J. L., Cooper, R. J., Tranter, M. & Bottrell, S. 2007. Evidence for widespread anoxia in the proglacial zone of an Arctic glacier. *Chemical Geology,* 243**,** 1-15.

Wadham, J. L., Cooper, R. J., Tranter, M. & Hodgkins, R. 2001. Enhancement of glacial solute fluxes in the proglacial zone of a polythermal glacier. *Journal of Glaciology,* 47**,** 378-386.

Wadham, J.L., Bottrell, S., Tranter, M. and Raiswell, R., 2004. Stable isotope evidence for microbial sulphate reduction at the bed of a polythermal high Arctic glacier. Earth and Planetary Science Letters, 219(3), pp.341-355.

West, A. J., Galy, A. & Bickle, M. 2005. Tectonic and climatic controls on silicate weathering. *Earth and Planetary Science Letters,* 235**,** 211-228.

White, A.F., Blum, A.E., Schulz, M.S., Bullen, T.D., Harden, J.W. and Peterson, M.L., 1996. Chemical weathering rates of a soil chronosequence on granitic alluvium: I.

Quantification of mineralogical and surface area changes and calculation of primary silicate reaction rates. Geochimica et Cosmochimica Acta, 60(14), pp.2533-2550.

White, A.F., Bullen, T.D., Schulz, M.S., Blum, A.E., Huntington, T.G. and Peters, N.E., 2001. Differential rates of feldspar weathering in granitic regoliths. Geochimica et Cosmochimica Acta, 65(6), pp.847-869.

White, A.F., Bullen, T.D., Vivit, D.V., Schulz, M.S. and Clow, D.W., 1999. The role of disseminated calcite in the chemical weathering of granitoid rocks. Geochimica et Cosmochimica Acta, 63(13), pp.1939-1953.

White, D. M., Hodkinson, I. D., Seelen, S. J. & Coulson, S. J. 2007. Characterization of soil carbon from a Svalbard glacier-retreat chronosequence using pyrolysis–GC/MS analysis. *Journal of Analytical and Applied Pyrolysis,* 78**,** 70-75.

Wynn, P. M., Hodson, A. & Heaton, T. 2006. Chemical and isotopic switching within the subglacial environment of a High Arctic glacier. *Biogeochemistry,* 78**,** 173-193.

Wynn, P. M., Hodson, A. J., Heaton, T. H. E. & Chenery, S. R. 2007. Nitrate production beneath a High Arctic Glacier, Svalbard. *Chemical Geology,* 244**,** 88-102.

Chapter 5. Results: Organic Carbon Dynamics in Arctic Glacier Forefields

Abstract

Soil formation and ecosystem development is highly dependent on the organic carbon dynamics, and in turn this is highly susceptible to changes in environmental and biological conditions. Despite this, few studies have been conducted in the Arctic where the climate is warming and glaciers are receding. Deglaciating landscapes creating forefields provide a unique opportunity to study organic carbon dynamics during the early stages of soil development. Forefields are ideal natural laboratories to better understand spatial and age-resolved processes that occur on short (annual) to long-term (decadal, centennial) timescales. By comparing three different dynamic Arctic forefields, one in the High-Arctic, Svalbard and two Sub-Arctic, Alpine glacier forefields in N-Sweden this study attempted to quantify whether organic carbon accumulates as a function of moraine age and determine if this was consequence of geochemical and biological processes. Combining a multitude of geochemical and field data, the aim was to critically evaluate what soil forming processes dominate and what factors may have facilitated soil organic carbon (SOC) accumulation and turnover. Stable carbon isotope studies complemented these analyses, and helped identify the provenance and potential cycling of soil carbon in these forefield s. Study results showed that in all forefields the total organic carbon (TOC) accumulated with moraine age, and that this was driven by organic carbon inputs derived primarily from modern photosynthetic carbon from C3 plants. Only limited weathering induced-organo-mineral stabilization that facilitated carbon accumulation was evidenced, despite a century of regional climatic warming that could be expected to enhance this process. Instead, organic carbon stabilization seems to have been achieved by a cascade of processes connected to a) slow forefield biological evolution, specifically of the soil saprophyte community b) that was constrained by a lack of availability to less biodegradable forms of plant litter inputs to the soil. Differences in these processes (a & b) in Arctic forefields, (such as this study), and European-Alpine and other high-altitude forefield studies, likely account for the observed contrast in soil organic carbon (SOC) accumulation, a^{-1} rates; whereby Arctic SOC a^{-1} rates are significantly lower. It is therefore postulated, that the extreme prevailing polar climate may still slow bio-enhanced mineral weathering, and in turn SOC accumulation in Arctic glacial forefields. Whereas in others, with milder climates, it is more of a control. Interestingly, differential rates in SOC accumulation were evidenced, even between Arctic forefields. In the high-Arctic forefield they were roughly three times higher (2.2 $g.m^{-2}$) than those in the two sub-Arctic, Alpine forefields (0.6-0.7 $g.m^{-2}$). This highlights, that although all Arctic forefields studied tend to accumulate TOC with time, their rates are to some extent controlled by more localised soil-forming factors. Further studies are needed to assess organic carbon dynamics at a seasonal and wider annual temporal resolution, to document if the difference between the timing at which sampling was conducted could be accountable for the observed differences in rates between these forefields.

5.1. Introduction

The global mass of atmospheric CO_2 is 760 GT of carbon, growing at 3.5 $GT.y^{-1}$ (1 GT = 10^{15} g). It is strongly controlled by the 3060 GT of carbon in the terrestrial pool, of which 2500 GT is found in soils. Soil organic carbon accounts for 1550 GT, with soil inorganic carbon accounting for the remaining 950 GT (Lal, 2008). Vast quantities of organic carbon stored in high latitude boreal and tundra soils and permafrost (Schuur et al., 2008; Schuur et al., 2009) are susceptible to degradation, and this thought to be a problematic, as they may release vast amounts of greenhouse gases (e.g. CO_2 or methane) as the Arctic climate changes (Chapin III et al., 2009). A strong warming trend in the Arctic has led to an increase in ecosystem productivity (Epstein et al., 2012; Guay et al., 2014), and changes in the soil organic carbon dynamics. This is of concern as plants and microbes, and their metabolic enzymatic functions, are highly temperature and moisture sensitive. They enhance soil fertility and biomass growth, but at the cost of SOC mineralization which could increase levels of CO_2 emission to the atmosphere (Lehmann and Kleber, 2015). Conversely, biomass growth can facilitate SOC storage from plant-derived carbon inputs to soils if it exceeds the rate of SOC decomposition (Davidson and Janssens, 2006). Determining this soil carbon balance (input, storage, and output) has been the subject of numerous studies. However, of the vast body of literature on this topic has focused on its fate in frozen soils (permafrost) (Schuur et al., 2015, and references therein). Only over the past two decades has the importance of understanding soil ecosystem carbon balance during soil formation re-emerged as part of large interdisciplinary projects e.g., Critical Zone Observatories or the Big Link Project (Bernasconi et al., 2011a; Banwart et al., 2012; Banwart et al., 2017). These projects employed a holistic and multidisciplinary approach, treating the soils as a reactive layer fundamental to regulating critical zone functions. By doing so they have contributed to a significant advancement in quantifying processes based on empirical relationships and understanding process-based relationships about a soils role in the critical zone. In general, furthering our understanding of the carbon dynamics in lower-latitude Alpine forefields (Alexander and Burt, 1996; Egli et al., 2001; He and Tang, 2008; Bernasconi et al., 2011; Dümig et al., 2011; Bockheim and Haus, 2014;).

In these Alpine forefield soil formation studies, it was documented that soil formation and ecosystem development occurred as a function of exposure age (Alexander and Burt, 1996; Egli et al., 2001; He and Tang, 2008; Bernasconi et al., 2011; Dümig et al., 2011; Bockheim and Haus, 2014;). A principle driving factor was shown to be bio-enhanced mineral weathering

that facilitates organo-mineral, organic carbon stabilization. To this end, forefield fauna and flora mining led to accelerated primary to secondary mineral conversion. Since biological activity is intrinsically linked to the temperature during the short Alpine summer growing season, rates of carbon turnover increased, and this led to more organic carbon degradation to low weight organic compounds. A new paradigm for forefield soil formation was carbon turnover, producing low weight organic compounds. These promote organo-mineral complexation with newly exposed and reactive mineral surfaces (Dümig et al., 2011; Dümig et al., 2012). It seems that the co-evolution of both mineral weathering and forefield ecosystem development facilitates rapid soil organic matter (SOM) and SOC accumulation in newly forming forefield soils (Dümig et al., 2011; Dümig et al., 2012). Yet, it is the sensitivity of forefield ecosystems and their fragile carbon stocks in these soils, as organo-mineral stabilization products (e.g. micro aggregates), that makes them vulnerable to the extreme changes in Alpine climatic conditions (Smittenberg et al., 2012).

It has been suggested that studies conducted at lower-latitude, but often high altitude, can be used as analogues for similar processes in Arctic forefields (i.e. Smittenberg et al., 2012). Results from these non-high-Arctic forefields are unlikely to be applicable because the weather is more extreme, resulting in a shorter growing season (Karlsen et al., 2014). In addition, this causes clear differences in both plant and microbiological community assemblage, and the degree of weathering, as a function of age in Arctic forefields, compared to those in high altitude Alpine settings (Bradley et al., 2016b; Hodkinson et al., 2003; Kabala and Zapart, 2012). Such differences will affect key soil forming processes (Jenny, 1941) and SOM dynamics, which have been postulated to be primarily an ecosystem property (Schmidt et al., 2011). Based on these assumptions, soil formation through combined mineral weathering and organic carbon dynamics are potentially quite different in Alpine vs. Arctic glacial forefields.

In glacier forefields it has so far been documented that SOM and SOC can be derived from three sources: (i) autochthonous primary production (e.g., ecosystem flora and fauna), (ii) allochthonous material (external animal, insects and pyrogenic material) that tend to be more aliphatic, photosynthetic carbon-based compounds and are often termed ‘modern’ carbon and (iii) ‘ancient’ carbon associated with permafrost paleosols and lithological, diagenetic kerogen consisting of primarily aromatic carbon (Bradley et al., 2014 and references therein). In terrestrial Arctic ecosystems with prevailing cold climates it has been suggested that these organic material inputs to SOC, accumulate due to low primary productivity and organic

carbon degradation (Kirschbaum, 2000; Schlesinger and Andrews, 2000). Short-term experimental studies certainly concur with this (Hobbie, 1996), but also indicate substrate quality as an important factor, as plants tend to be woody, and nutrient poor. In these one year experiments, plant litter from *Salix polaris* had mass losses of 12.7 % (measured in Svalbard, 78 °N), and mosses 0-8 % (Asbisko, Northern Sweden 68 °N) (Robinson et al., 1995; Hobbie, 1996). Despite these slower decomposition rates, biomass assemblage with a simple trophic structure (Hodkinson et al., 2003; Bradley et al., 2016a; Bradley et al., 2016b) (compared to warmer and more humid climates) resulted in appreciable SOC turnover during a century of soil formation in Arctic forefields. This was particular evident under Arctic warming trends, and evidenced in regional and annual to decadal changes (Serreze and Barry, 2011; Førland et al., 2012). In light of the organic carbon turnover times, and under Arctic warming, this could further enhance SOC decomposition in a High-Arctic (Kabala and Zapart, 2012). This suggests, like other forefields (e.g. Alpine), that SOC accumulation could be concurrent with mineral weathering and pedogenic stabilization with time.

In soils, the organic matter is a continuum of different heterogeneous organic carbon-based compounds, each with different chemical and physical properties (Lehman and Kleber, 2015). As a result, SOM residence time at each stage of the decomposition continuum depends on its distribution between litter, pores, aggregates and on mineral surfaces (Kleber and Johnson, 2010; Schmidt et al., 2011). Chemical preservation consists of organo-mineral interactions, carbon adsorption onto mineral surfaces, clay minerals, iron oxides and biological exudates (often resistant to enzymatic breakdown), which often leads to physical preservation through aggregate formation (Tisdall and Oades, 1982; Six et al., 2002; Kleber et al., 2007). While physical protection involves saprophyte disconnection to carbon due to pore space size, freeze-thaw action (Schmidt et al., 2011), and mineral, protein or chemical precipitates at the mineral surface (Kleber et al., 2007). These functions, combined with abiotic factors that control chemical oxidation and leaching, e.g., temperature and moisture, control the SOM pool turnover rate (Lehman and Kleber, 2015). Consequently, since SOM comprises roughly 58 % SOC (Pribyl, 2010), changes to these controls can induce SOC turnover on short-term timescales (hourly, diurnally, monthly, annually). However, SOC changes may respond slowly under a polar climate, meaning long-term changes (decade to century) may be missed in short-term experimental studies. A chronosequence approach, in deglaciating landscapes, enables annual, decadal to centennial time-scale determination of processes that control the carbon dynamics during soil formation, with time being the independent variable. In this study, a

space-time, chronological approach is used, and it is hypothesised that: Arctic forefields, with a prevailing polar climate with low primary productivity, and subsequently low organic carbon degradation, accumulate SOC with age because of soil forming processes.

To investigate this, two different Arctic forefield locations, characterized by different polar climates with geographical characteristics and ecologies, were selected for comparison: (a) the High-Arctic, Midtre Lovénbreen, in Svalbard was contrasted to (b) two sub-Arctic forelands of the Storglaciären and Rabot's glacier forefields in N-Sweden. These three forefields, and their newly developing soils, have continually formed over the last century, post deglaciation.

The aim of this study was therefore, to gain an integrated understanding of soil organic carbon dynamics and minerals' weathering during ecosystem evolution in newly developing Arctic forefield soils.

To achieve the aim, the following objectives were set:

- Bulk soil samples at two soil depths, 0-15cm and 15-30cm, and their elemental (including organic carbon) and mineralogical concentrations should be quantified (including iron species, namely poorly crystalline ferrihydrite and poorly soluble iron oxides). These data sets, plotted as a function of age, will infer the strength of the empirical relationship between soil organic carbon and mineral weathering products.
- Bulk soil sample $\delta\,^{13}C$ isotopic signatures are to be measured to determine the source and pathway of organic carbon in each of soils on the forefield chronosequences. In addition, a carbon budget should be formulated to provide further validation of the isotopic data, and to calculate the relative proportion of soil organic carbon derived-vegetation, microbial (autotrophic and heterotrophic) biomass and lithogenic kerogen.
- To put the study results and their interpretation into a wider context, by comparing the soil measurements to other glacial and non-glacial forefield studies, literature and ecological, biogeochemical, metrological and climate data.

5.2. Study Sites and Methods (see Chapter 4 for Midtre Lovénbreen study site info, section 4.2.1 and 4.2.3 for the sampling scheme used)

Storglaciären (67°54'N, 18°34'E) and Rabot's glacier (67°55′N, 18°30′E) in sub-Arctic Sweden are classified as small valley glaciers of about 3 km^2 in (planar) area. Storglaciären is located on the east side of the Kebnekaise massif, while Rabot's glacier is on the west side Fig. 5.1. Their forefields are 0.5 km^2 and 1 km^2, respectively, with an elevation decrease of roughly 115m and 80m from their glacier snouts to the terminal moraine (aged 1910). These topographic, elevation changes result in the Storglaciären forefield having a steeper slope relief (Avg. slope 27%), while Rabot's glacier had a gentler slope (Avg. slope 12%). In both forefields, several braided river systems have incised into the inner moraines and the pronounced terminal moraine (Karlén, 1973; Jahn, 1991). These streams have formed since the Little Ice Age (LIA) glacier maximum, in response to a regional warming of ~1°C in both annual and summer temperatures that began 1910 and continued into the mid-1930s (Holmlund and Jansson, 2002).

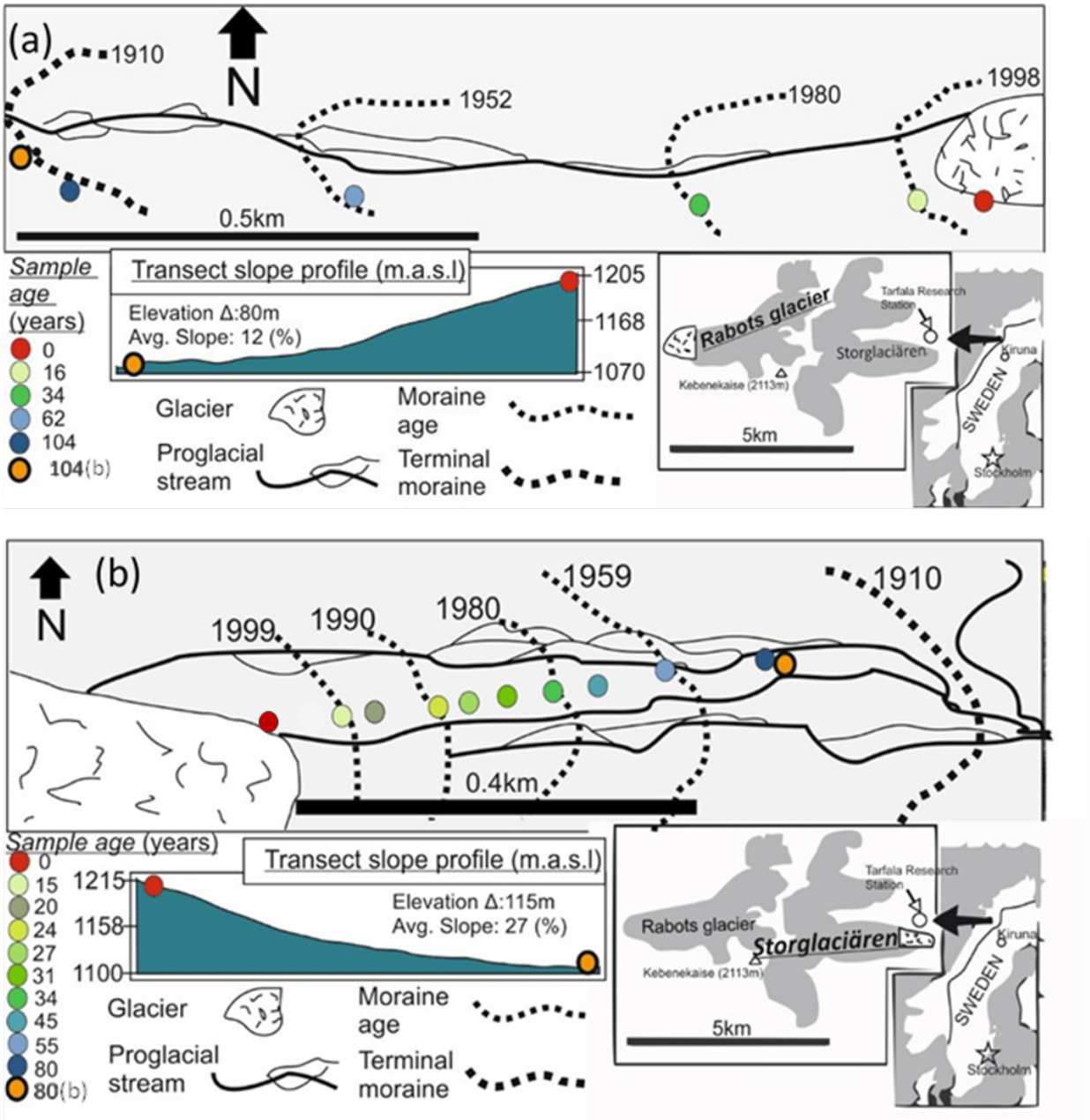

Figure 5.1. A schematic map of (a) Rabot's glacier and (b) Storglaciären forefields situated on opposite sides of the highest mountain in Sweden, Kebenkaise. Literature dated glacier moraine deposits and proglacial streams are delineated in the scheme (see key). Sampled sites are shown as coloured dots and their ages are shown in the key.

The mean annual air temperature (1965–2014) at the Tarfala Research Station (TRS) (1130 m a.s.l and 0.5 km away from Storglaciären) is −3.5 ± 0.9 °C. The average summer temperature (1946–2014) is 5.9 ± 1.2 °C with maximum temperatures up to 20–25 °C, while the mean winter temperature (1965–2014) is −6.6 ± 1.1 °C, with minimum temperatures of −25 °C (Grudd et al., 1996; updated with unpublished data from the TRS). The mean annual precipitation at TRS has been estimated as 1997-450 mm, of which 400–600 mm falls between June and August (Dahlke et al., 2012). The Kebnekaise massif in which the Storglaciären and

Rabot's glacier forefields are situated in part of the late Precambrian Seve belt of the Scandinavian Caledonides (Andréasson and Gee, 1989). Storglaciären forefield is underlain by bedrock strata consisting primarily of Tarfala Amphibolites (Fig.5 .2).

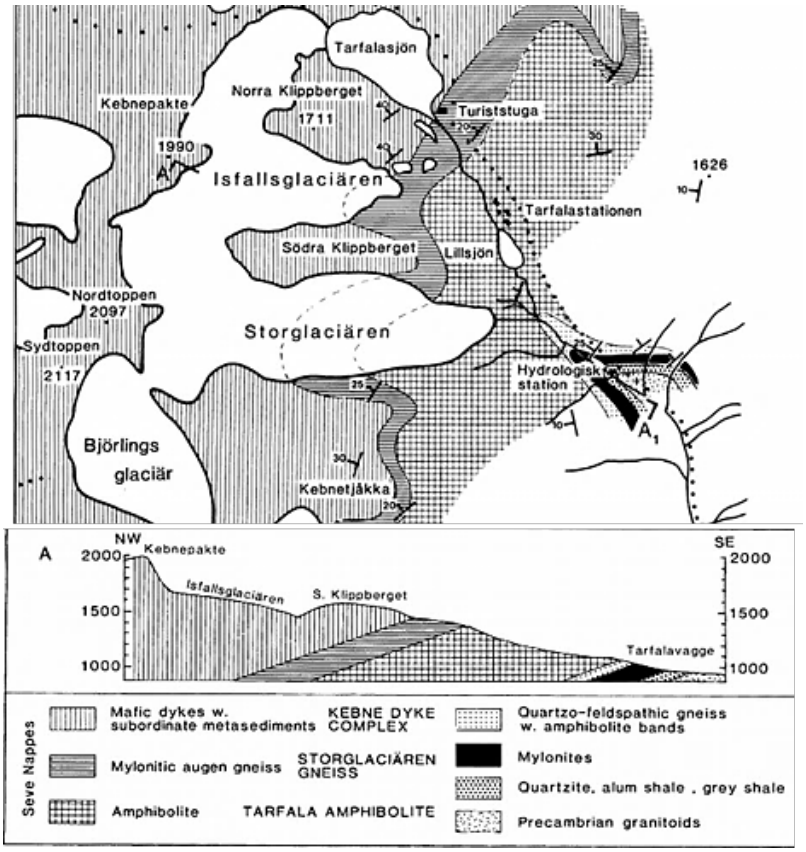

Figure 5.2. Geology of the Tarfala valley, obtained from (Andréasson and Gee, 1989)

In both Storglaciären and Rabot's glacier forefields, the newly exposed surfaces (age 0-24 years) consisted of ground that was mostly devoid of vegetation apart from lichens on certain larger rock surfaces. Mosses, sphagnum (grasses and mainly *Salix* species) were present as carpets or micro-niche communities only in soils from 27-years onward. Such vegetation became well-established after 45-years-of exposure (Fig. 5.3. & Fig.5 .4). The soils in the forefields were characteristically not layered, and had no horizons, and typically include a high stone content derived from their glacier till, especially in the surface layers. Consequently, these skeletal minerals soils are classified as Leptosols and Regosols (FAO, 2006). The soils present were effected by cryoturbation processes (Jahn, 1991) that in part resulted from an annual active layer thaw depth of discontinuous permafrost to a mean depth of 1.5 to 1.6m (Bolin Centre for Climate Research, 2013).

5.2.1. Sampling

Sites in the Storglaciären and Rabot's glacier forefields were sampled in June 2014 along a 0.5 km and 1 km transect that propagated away from the glacier snouts to their LIA terminal moraines. At each sampled site along a predefined transect, three individual samples were taken within a 10 m radius of the set location, to maximise the site and forefield representativeness. This scheme enabled an adequate and reproducible space-for-time approach aimed at understanding biogeochemical gradients during soil formation while the forefield ecosystem develops. As explained in Chapter 4 this was the approach already used in the Midtre Lovénbreen forefield, and similar approaches have been used in the High-Alpine Damma Glacier forefield (Bernasconi et al., 2011) which is also a valley glacier with similar geomorphological characteristics to those in Storglaciären and Rabot's. Prior to sampling, each site was photographed, notes were taken describing the site characteristics and its GPS coordinates were recorded, (Table. 5.1). Bulk samples were excavated from the soil at a depth of between 0-15 cm with sample sizes being roughly 30 cm^3. Firstly, a trowel was sterilised (using ethanol whips), introduced to the site's soil, and then used to collect the soil samples; this way both clean geochemical/mineralogical samples, but also microbiological and carbon samples could be collected. Any obvious overlying vegetation was removed, and samples were placed in sterile whirl-pack bags which were shaken for ~ 5-minutes for homogenisation. In addition, un-weathered source rocks, representative of the glacier catchment lithology's were collected. As already explained in chapter 4 the *in-situ* soil moisture (using a Theta Kit Moisture Meter), soil strength (using a soil penetrometer: Humboldt Mfg. Co. H-4195), and the temperature (using a HannaHI-76305: interface unit: model: pH 210) were measured at each site. Sampled sites were then backfilled. On return to the Tarfala station laboratory (usually maximum 2-4 hours later) an aliquot (200g) was removed, while the remaining sample was frozen at -20°C for shipping back to the University of Leeds. Each sampled sub-aliquot was analysed for its pH and conductivity after reacting with deionized water in a 1:2.5 soil: solution ratio. The soil water mixtures were shaken and reacted for ~ 30 min and then left to settle for ~ 60 min. prior to measuring the pH in supernatant using a glass electrode (VWR, model: 622-1759) and a pH meter (Hanna, model: pH 210) that was calibrated just prior to use, using NIST standard buffer solutions at 19 °C. In addition, the conductivity was measured with a meter (Hanna, model: pH 210). Finally, each of aliquot was air-dried, and the dry sample soil colour was noted according to the Munsell Soil Colour Chart (Munsel 2009).

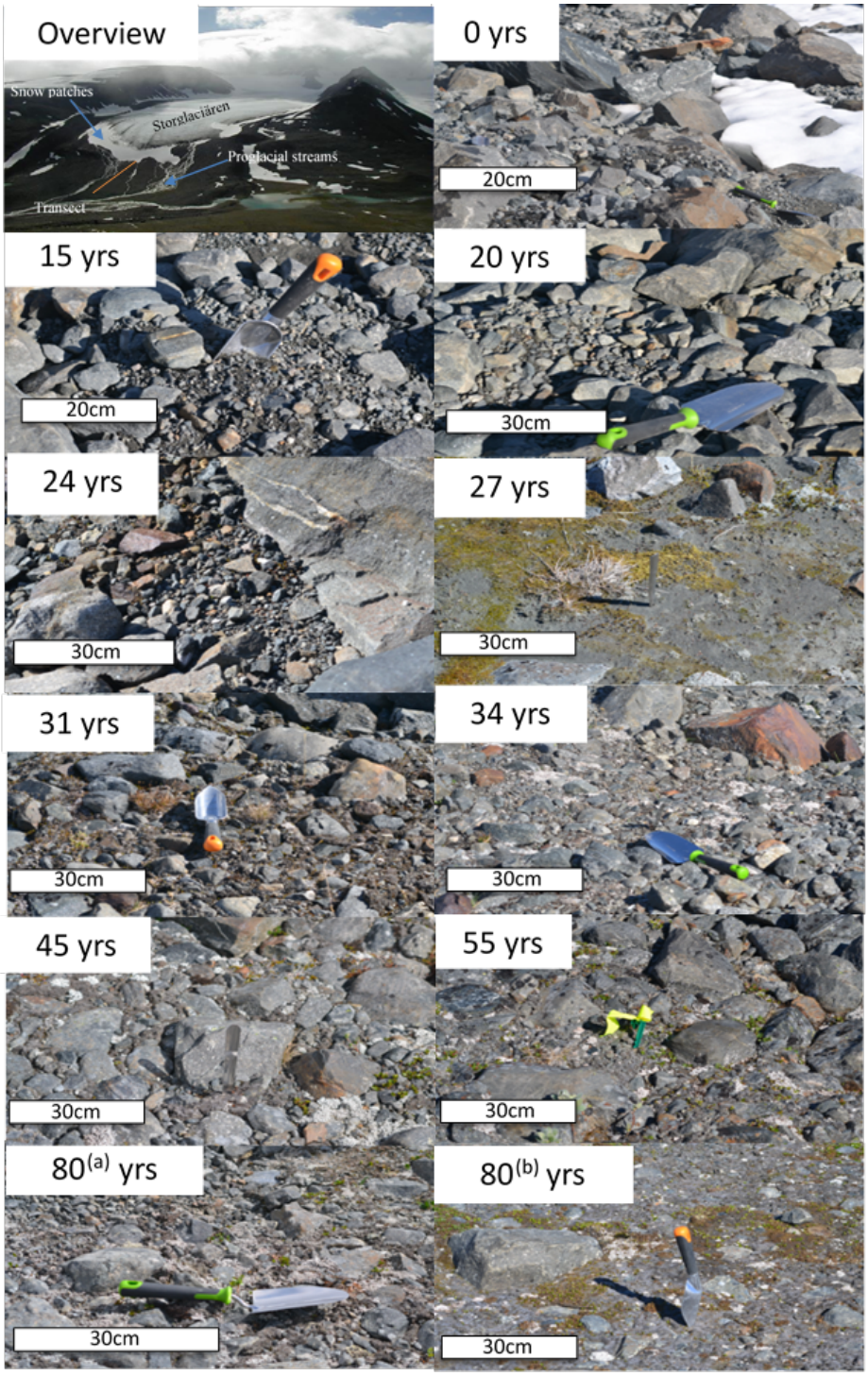

Figure 5.3. Photographic mosaic of the sampled sites in the Storglaciären forefield. Note: at site zero snow patches were still present, young sites (0 to 24-years) were devoid of vegetation apart from lichens on larger rocks. Significant vegetation establishment started at / after ~ 27-year site as evidenced through an abundance of mosses, sphagnum, lichens and grass tussocks. Thereafter, species became more diverse, however, the absolute abundance of mosses decreased from the 27-year-old site onward while the relative abundance of sphagnum, grasses and vascular plants of the *Saxifraga* genus increased with age. At site 80(b) considerable moss and sphagnum carpets and vascular plant *Saxifraga* species dominated the vegetation coverage. The overview photo included an aerial photograph (facing east), showing the forefield, key landscape features and the transect sampled as delineated and labelled.

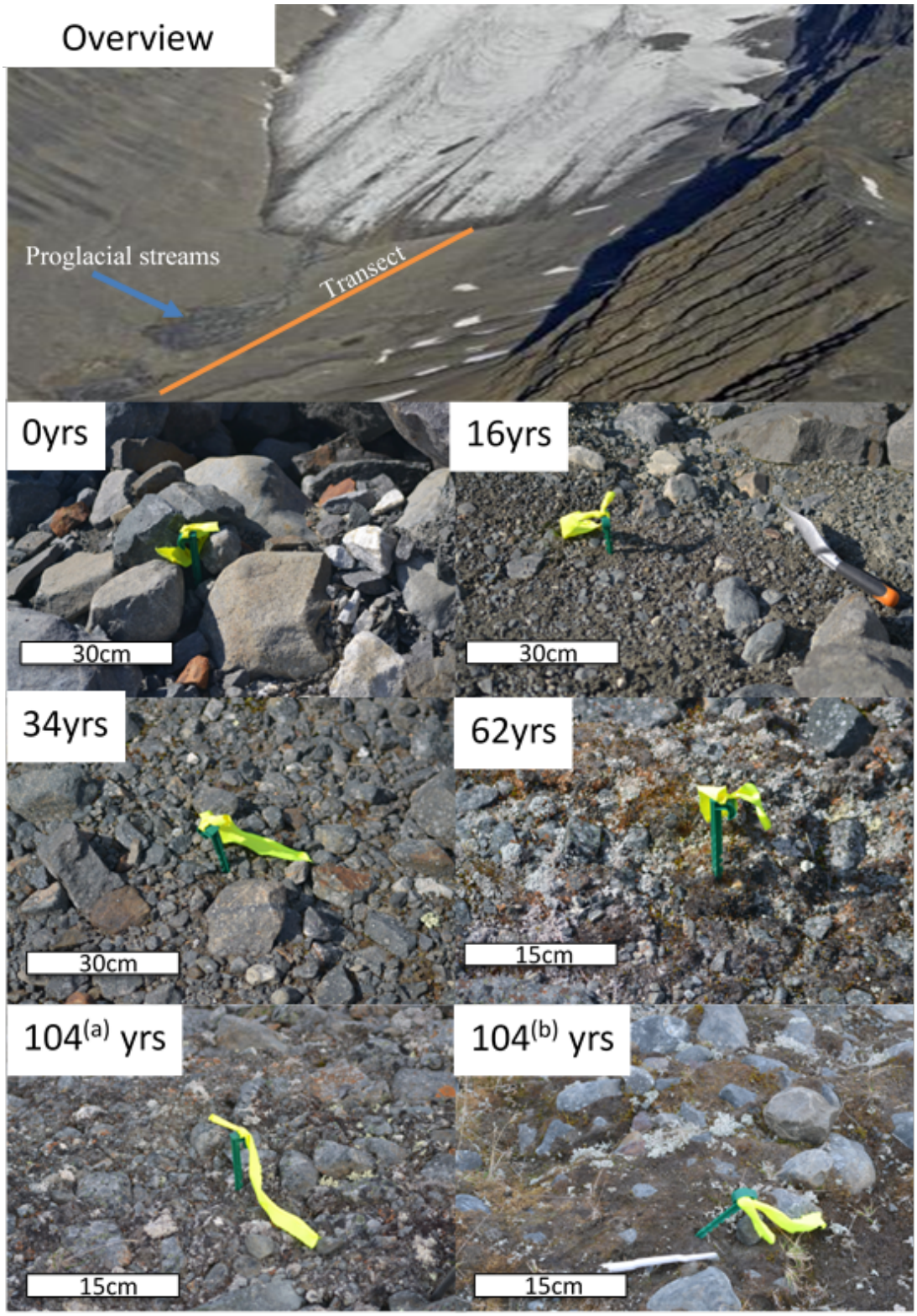

Figure 5.4. Photograph mosaic of each of the sampled moraine age sites in the forefield of Rabot's glacier, Sweden. Note: at young sites vegetation is absent, mosses, sphagnum and lichens are present at/after 34-years site; thereafter they increase in relative abundance. At site 104(b) ground conditions were waterlogged and unlike other sites we sampled a thick organic matter layer as well as abundant vascular plants (e.g. *saxifraga* and grasses) were observed. The overview photo shows an aerial view (facing west) of the forefield, as well as key landscape features and the transect sampled.

Evaluations of the glaciers termini positions and age were made using land and aerial photographs sourced from: Rabot's = (Brugger, 1992; Brugger et al., 2005; Brugger and Pankratz, 2015); Storglaciären = (Koblet et al., 2010). Moraines deposited over the last decade were dated using satellite imagery (S) from Landsat 4, 5 (TM) and 7 (ETM) and Quickbird. Sampled sites in between known moraine ages were obtained by pro-rata distance between two known ages (Figure.5.1. & Table.5.1).

Table 5.1. Chronological information and GPS coordinates for the sampled moraines and ages from Midtre Lovénbreen, Svalbard, and Storglaciären and Rabot's glacier, Sweden. Sample site ages were determined by delineation of the glacier snout using historic aerial photographs as it retreated (Hodkinson et al., 2002). Moraines deposited over the last decade were dated using satellite imagery (S). Unknown ages were estimated by pro-rata distance (P) between two known ages assuming a linear rate of retreat over the last century: Midtre Lovénbreen = 14m a^{-1} (Hambrey et al., 2005), Storglaciären and Rabot's = 4 to10 m a^{-1} (Holmlund et al., 1996).

Moraine site age (years)	Dating approach	Midtre Lovénbreen	Storglaciären	Rabot's glacier
0 (glacial snout)	S	78°53'48.134 N 12°3'4.504 E	67° 54'11.2716" N 18° 36' 14.22" E	67° 54' 25.6284" N 18° 26' 51.0792" E
2	S	78°53'48.942 N 12°3'5.902 E	*	*
3	S	78°53'49.615 N 12°3'6.951 E	*	*
5	P	78°53'50.894 N 12°3'9.048 E	*	*
13	P	78°53'55.327 N 12°3'16.388 E	*	*
15	L	*	67° 54' 11.2608" N 18° 36' 15.678" E	*
16	L	*	*	67° 54' 24.6456" N 18° 26' 43.98" E
20	P	*	67° 54' 11.4876" N 18° 36' 17.8848" E	*
21	L	78°53'59.845 N 12°3'26.525 E	*	*
24	L	*	67° 54' 11.772" N 18° 36' 21.9744" E	*
27	L	*	67° 54' 12.024" N 18° 36' 23.6664" E	*
31	L	*	67° 54' 12.6216" N 18° 36' 24.8904" E	*
34	L	*	67° 54' 12.582" N 18° 36' 28.7568" E	67° 54' 25.164" N 18° 26' 2.6376" E
40	L	78°54'6.709 N 12°3'39.109 E	*	*
45	P	*	67° 54' 13.3128" N 18° 36' 30.1428" E	*

50	L	78°54'11.149 N 12°3'46.449 E	*	*
55	L	*	67° 54' 13.7736" N 18° 36' 34.9848" E	*
62	L	*	*	67° 54' 24.588" N 18° 26' 27.9348" E
80	P	*	(a) 67° 54' 15.0012" N 18° 36' 41.6376" E (b) 67° 54' 14.8104" N 18° 36' 41.9148" E	*
104	L	*	*	(a) 67° 54' 24.8004" N 18° 25' 39.4176" E (b) 67° 54' 28.4112" N 18° 25' 39.018" E

5.2.2. Chemical Analyses

Upon return of the samples to the Leeds' laboratories, and prior to any sub-sampling for chemical analyses, each was vigorously shaken for homogenization for ~ 5 min. Then ~ 200 g were weighed-out and sieved, to either >7 mm, 7-2 mm or ≤2 mm fractions. All size fractions were then dried at 40 °C for 48 h and re-weighed to evaluate relative soil moisture content. Samples were then crushed to a homogeneous powder using an agate disk-crushing mill. Finally, if needed, samples were sieved to <63 μm and the remnants re-crushed to achieve a uniform, homogenous powder.

In all crushed powders, aliquots were used to measure total organic carbon (TOC) contents and carbon isotopic composition of each bulk soil samples, as well as the patent and source rocks. These measurements were carried out at the Geo Forschung's Zentrum (GFZ) in Germany. Prior to analyses, any possible inorganic carbon from mineral carbonates were removed by treating the powders with 10% HCl at room temperature for 24 h. Once CO_2 effervescence had stopped, samples were centrifuged, washed (to remove remnant acids) and dried again at 40 °C to avoid loss of volatile organic carbon (Caughey et al., 1995). For analyses, samples were combusted in sealed tubes with CuO at 900 °C for 2 h to convert all organic matter to CO_2. The TOC was measured using an elemental analyser (Carlo-Erba NC2500), whilst $\delta^{13}C_{org}$ was analysed using a mass spectrometer (DELTAplusXL ThermoFisher). The limit of detection was <0.01 TOC (wt%) and $\delta^{13}C_{org}$ <0.05‰; analytical accuracy was $\delta^{13}C_{org}$ 0.3‰, and TOC 0.02 wt% (95% con. limit), see Appendix. C. Table.1 & 2 for TOC and $\delta^{13}C_{org}$ data and SD of replicates. The $^{13}C/^{12}C$ of samples was reported relative to the $^{13}C/^{12}C$ of the Pee Dee Belemite (PDB) standard in delta (δ) per mille (‰) using Eq. 5.1.:

$$\partial^{13}\mathrm{C} = \left(\frac{^{13}\mathrm{C}/\,\partial^{12}\mathrm{C}_{sample}}{^{13}\mathrm{C}/\,\partial^{12}\mathrm{C}_{PDB}} - 1 \right) 1000 \qquad \text{Equation 5.1}$$

Soil organic stocks were calculated according to the following equation (Mavris et al., 2010):

$$SOC_{stocks} = C\rho d(1 - \mathrm{RM}) \qquad \text{Equation 5.2}$$

where SOC_{stock} denotes the organic carbon abundance (kg/m^2), C, the organic carbon concentration (kg/t), d, the thickness of the layer sampled (m), RM the mass proportion of rock fragments >2 mm, and ρ the soil density (t/m^3). We used an average dry bulk density of glacier till of 1.4 g.cm^{-3} in Midtre Lovénbreen (He and Lee, 2008), and assumed a similar soil parent material and level of weathering over a century, and a density of 1.1 g.cm^{-3} for samples from Storglaciären and Rabot's (Fuchs, 2013)(for SOC_{stock} sensitivity analysis to different soil bulk densities Appendix C, Table 3).

All iron species in the crushed powers were quantified using an operationally defined iron extractions procedure (Poulton and Canfield, 2005) (unless otherwise stated). Extractions were performed under oxic conditions in constantly agitated 15 ml centrifuge tubes (polyethylene: Sarstedt: Ref. 60.732.001), except for the boiling HCl step, that was performed in glass test tubes. The samples were subjected to a series of sequential extractions that progressively removed more and more stable iron species. Step 1) was an ascorbic acid treatment that targets poorly crystalline ferrihydrite (Raiswell et al., 2010). Step 2) is reaction with a sodium dithionite solution (50 g.l^{-1}) buffered to pH 4.8 with 0.35 M acetic acid / 0.2 M sodium citrate to extract 'reducible' crystalline iron oxides (goethite, hematite and akaganeite). Together extractions 1&2 are termed the highly reactive Fe fraction (Fe_{HR}). Step 3) A 0.2 M ammonium oxalate solution (pH 3.2) was used to extract magnetite. However, as the dithionite extraction was performed before the oxalate extraction (as suggested by Poulton and Canfield, 2005 magnetite, Fe may be ~ 4 % underestimated. Step 4) Reaction with a concentrated 12 N boiling hydrochloric acid (HCl) extraction, (5 ml HCl reacted for 1 min.), used to quantify Fe remaining from certain sheet-silicate minerals (nontronite, chlorite, glauconite, biotite). Extractions 3 & 4 are termed the poorly reactive Fe fractions (Fe_{PR}). The total Fe (Fe_{total}) in the

powders was analysed using X-ray florescence spectroscopy (see below and chapter 4). Step 5) This represents the difference between total Fe and the sum of each of the extraction phases, and is termed the unreactive iron fraction (Fe_u), plus pyrite Fe. This fraction consists of residual silicate iron, specifically from pyroxenes and amphiboles, which are essentially unreactive towards dissolved sulfide, (Poulton and Canfield, 2005). Each of the extract solutions were analysed for their dissolved Fe concentration using atomic absorbance spectroscopy (High Resolution Continuum Source Contra AA 700 Atomic unit). An analytical accuracy of < 0.16 (wt%) 95% confidence, and a limit of detection of 0.05 (wt%) were achieved for all extraction fractions. For data precision and blanks see Appendix C, Tables 4-7.

In all powdered samples, major (Si, Al, Fe, Mg, Mn, Ca, Na, K, Ti, P) and minor elemental concentrations (Ba, Co, Cr, Cu, Ga, Ni, Pb, Rb, S, Sr, V, Y, Zn and Zr) were analysed using X-ray florescence spectroscopy (XRF) (Pan-analytical, *model*: Axios) on fused glass pellets that were prepared using a 1:6 ratio of sample: fluxona plus 0.7 g of ammonium nitrate. Samples were dissolved in platinum crucibles by heating them on a five-stage, melting stage. The temperature ranged from 450 to 1100 °C over a 30 min. melting period, and removed volatile species that are included in the, loss on ignition (LOI). On the final heat stage, the molten solution was cast into a platinum form that was left to cool before being re-weighed, cooled and analysed. For major elements the data is reported as oxides in *wt%*, while minor and trace elements are reported as elements in ppm. The standard reference material, Granit GM (Abbey, 1980; Dulski, 2001) was used, and the analytical accuracy was ± <0.06 (*wt* %) 95.0% confidence limit for most element oxides, and ± <8.83 ppm, 95.0% confidence limit. For the XRF data minor and trace elements and analytical precision see Appendix C, Table 8, unless otherwise stated.

Microbe classes and their relative abundance were identified and quantified using an optical microscopy at the University of Bristol. Under an auto-fluorescent light using functional dyes and photosynthetic pigmentation allowed their cell to be counted. A negative control was a sample with no visible stained or auto-fluorescing cells Thirty random grids (each 104 μm2/ were counted per sample. Cell morphologies were measured and cell volume was estimated and converted to carbon content per Bratbak and Dundas 1984.

5.2.3. Statistics

All data processing was conducted with either the SPSS (IMB®) or the Microsoft Excel® software. To examine the relationships between moraine age (independent variable) and dependent variables such as chemical concentrations, both simple and multiple regression analyses were conducted. Simple regression was used to identify the pattern (e.g., linear or nonlinear) of the relationship with each dependent variable. Data normality was checked using a Shapiro-Wilk test and Z scores and histograms to select appropriate parametric or non-parametric statistical tests. For the statistical comparison of means, using their sum of squares, a test for homogeneity of variances is required, Levene's test was used. If the variance level from this test was >0.05, a one-way ANOVA test was used to test independent data sets for their statistical significance (significance level 0.05) on one dependent variable and two or more (independent variables) groups. Data with unequal variances (Levene's test <0.05) were tested for their significance using the Welch's ANOVA test.

5.3. Results

5.3.1. Basic geochemical debris properties and soil classification

Over a century of deglaciation, a change in pH was evident (Appendix C, Table 9, & Fig. 1). In Midtre Lovénbreen and Rabot's glacier forefield, an inverse relationship between pH and moraine age along the transects was observed, with 70% (R^2 0.7, p value < 0.05) of the pH variability being accounted for by moraine age. The decrease in pH with age from 8.3 to 7.5 in Midtre Lovénbreen and 6.7 to 6.3 in Rabot's glacier was contrary to the lack of correlation between pH and moraine age in the samples from the Storglaciären transect. In this transect the pH remained roughly stable at 6.5. However, one significant deviation was observed at 20 years, where the pH was closer to neutral, 7.6 ± 0.5, and in the 24 year old soils where the pH was more acidic at 6.0 ±1 and the 27 year-old soils where the pH was 6.4 ±1. The soil moisture contents in the Midtre Lovénbreen transect soils (Appendix C, Fig.1) decreased exponentially from 100 % moisture at the DE glaciated forefield interface, with values of 10%, and often below the limit of detection, further away from the glacier (Appendix C, Fig.1). In the soils from the Rabot's forefield, a similar decrease, albeit linear was evident as a function of moraine age. In the Storglaciären samples, where the relief was steeper, no correlation between soil

moisture and moraine age was evident. In a similar fashion, no correlation between soil strength and moraine ages was observed in the Storglaciären samples, yet significant variability between soil strength values was evident (Appendix C, Fig.1). Again, this contrasted with the strong positive correlation ($R^2 = 0.87$) that was statistically significant (p value < 0.05), in the Rabot's forefield soils, which was characterized by more consistent variability between sites.

5.3.2. Total Organic Carbon (TOC)

Total organic carbon increased as a function of moraine age in the forefield of Midtre Lovénbreen. This is exhibited by a strong positive linear correlation ($R^2 = 0.95$, p value <0.01) (Fig. 5.5.; for all correlation coefficients see Appendix C, Table 10). This relationship was present in all of the three transects (Tr1, Tr2 and Tr3) both in the surface (0-15cm) and subsurface (15-30cm) bulk soils sampled (see Appendix C, Fig.2 and Section 4). The TOC was initially low (0.06 wt%) at the glaciers snout (zero-years-old) and it increased more than fivefold to 0.33 wt% in the sample from the 113 year-old moraine. Unlike Midtre Lovénbreen, the TOC in the bulk soils in the top 0-15cm of Storglaciären and Rabot's forefields seem less dependent on moraine age (Fig. 2). Only a weak positive relationship ($R^2 = 0.42$; black dashed line of best fit) was observed, yet a significant correlation (p value < 0.05) was present in the Storglaciären samples. Although, this relationship becomes weaker, it remains significant ($R^2 = 0.21$, p value = <0.05; green dashed line of best fit) if TOC outliers 0.26 ± 0.1 and 0.34 ± 0.2 associated with the moraine ages 27 and 80 years respectively, are excluded (see Appendix A, Section A.1, for justification for the removal of these sites). In the Rabot's glacier soils, the positive linear relationship is more dependent on moraine age than Storglaciären, with a correlation coefficient of $R^2 = 0.66$ and significance of p = <0.05. However, the range in TOC values over the similar deglaciation period was smaller. In the zero-year-old samples, the TOC was within the uncertainty 0.02 wt % (± 0.02) of the analyses, but it increased and reached an asymptotic concentration of 0.13 wt % at the 104 year-old moraine. In contrast, the TOC in Storglaciären soils ranged from 0.01 (=LD) to 0.57 (wt%), the largest range of TOC of the three forefields. Overall, it was notable that in all forefields, considerably more TOC variability was observed in samples from the older moraines.

5.3.3. Organic $\delta^{13}C$ ($\delta^{13}C_{org}$)

Stable carbon isotopic values ($\delta^{13}C_{org}$ relative to PDB) revealed in the samples from Midtre Lovénbreen that the $\partial^{13}C_{org}$ was characterised by a relatively large isotopic change from heavier $\partial^{13}C_{org}$ of -18‰ in 0 year-old samples (glacier snout) to lighter values of -25‰ in the 113 year-old moraine soils (Fig. 5.5). This negative linear relationship with moraine age has a correlation coefficient of R^2 0.76 that is statistically significant (p value < 0.01). This trend was valid for all three transects (Tr1, Tr2 and Tr3) both in the surface (0-15cm) and subsurface (15-30cm) bulk soils sampled (see, Appendix C, Fig.2). In contrast, only a smaller, 3-4 per mill ‰ $\delta^{13}C_{org}$, isotopic shift was observed with age in Storglaciären (-23‰ to -26‰) and Rabot's glacier (-21‰ to -25‰) samples. In these forefields, although the $\partial^{13}C_{org}$ do have similar asymptotic values like in Midtre Lovénbreen, yet they are less dependent on moraine age as evidenced by the weaker linear negative correlations observed (ST = R^2 0.46, RB = R^2 0.50). However, these relationships are statically significant in both N-Swedish forefields (ST p value <0.01, RB p value <0.05). Linear regression analysis allowed an average annual isotopic change of roughly twice the values of 0.045 $\delta^{13}C_{org}$ ‰ a^{-1} to be calculated for soils in Midtre Lovénbreen forefield and values of 0.017 and 0.024 $\delta^{13}C_{org}$ ‰ a^{-1} for Storglaciären and Rabot's glacier, respectively.

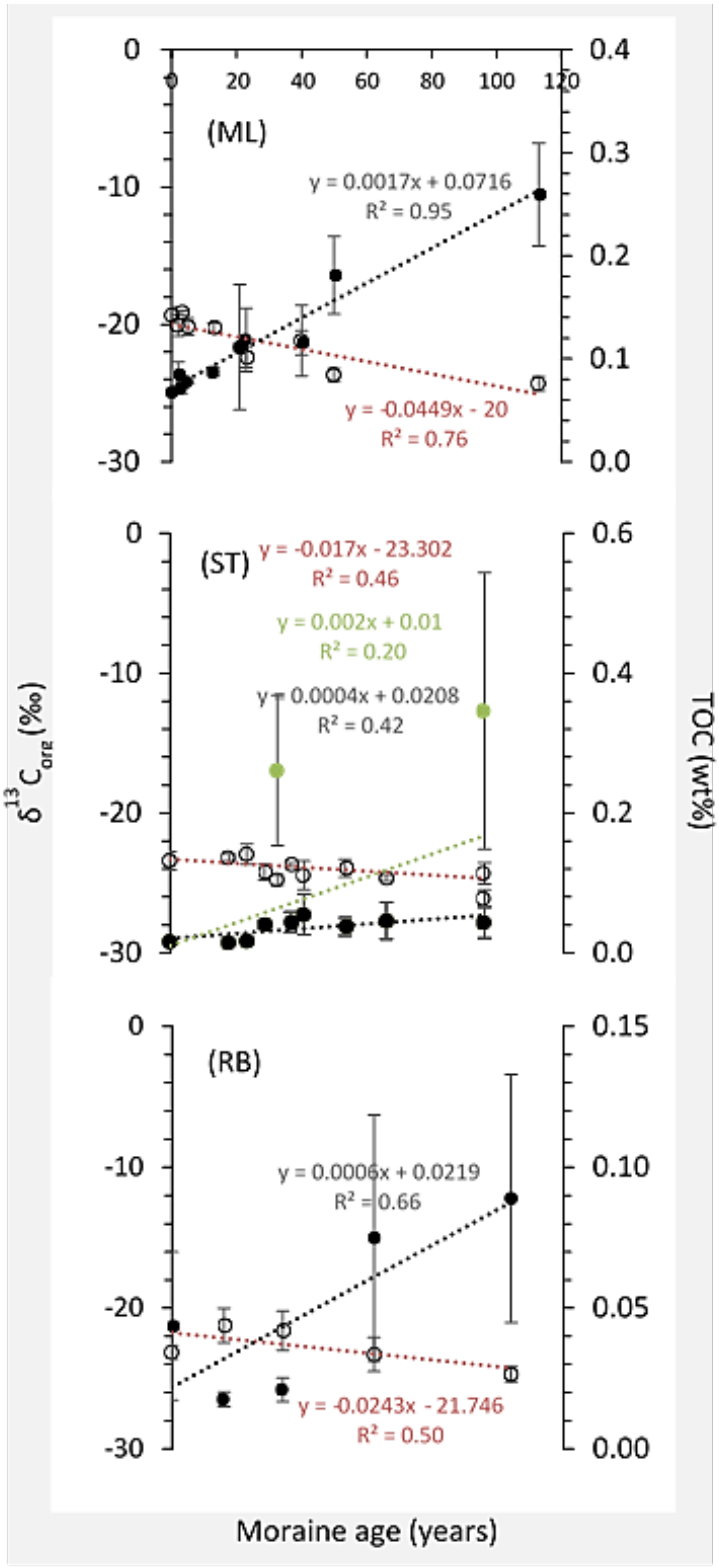

Figure 5.5. Average isotopic $\delta^{13}C_{org}$ (‰) (white circles) and TOC (black points) plotted as a function of moraine age in Midtre Lovénbreen (ML), Storglaciären (ST) and Rabot's glacier (RB) forefields. Uncertainty bars represent 1σ of triplicate samples at each moraine age. Note: in plot of ST samples, the outlier TOC values were included in the linear regression analysis (green points and line) although these TOC outliers corresponded to soils from ages 27 and 80(b)-years, where moss carpets, grass swards and *saxifrage* vascular plants (80(b) only) were present (see Fig. 5.3).

5.3.4. Chemical Weathering Index of Alteration (CIA) and reactive iron fractions

Overall, it can be said that the changes in major element composition of the bulk glacier-debris soil samples revealed weak signs of chemical weathering and associated alterations in soil mineralogy. Easily leachable base cations (i.e., Ca, Na and K) associated with primary mineral weathering remain, in general, unaltered over a century of weathering. The CIA values change only slightly from a value that infers an unaltered / fresh character (≤50) to values that indicate just incipient weathering (50-60). As discussed in chapter 4 deglaciation and debris exposure in Midtre Lovénbreen once corrected for Ca in carbonates revealed only weak weathering at >50 years. In the freshly exposed soils in Storglaciären and Rabot's glacier forefields, on average, considerably lower (~40) CIA values were observed, reflecting both the fresh unweathered character of the newly exposed material (Fig. 5.6a). Also, likely reflecting the fact that the CIA approach may not be entirely suitable for the more complex lithologies in the N-Swedish catchment compared to Svalbard. However, with increasing age in Storglaciären CIA value of =>50 were observed at certain ages where vegetation of micro-niche environments was present. For example, soils from age 27 years' exposure had a CIA value of 76 ± 37.3, while soils from age 80 also showed highly weathered CIA values of 75 ± 29.7. These two sampling sites were explained previously to be outliers in terms of TOC (see above and Appendix A, Section A.1.), yet they show high degrees of change in terms of chemical weathering. Finally, in the soils from Rabot's, the CIA value at the earliest ages also indicated a very unweathered character (CIA <50), and with exposure age only relatively weak changes in chemical weathering index values were observed (i.e., at 62 years, CIA = 53.5 ± 11.5 and at 104 years CIA = 61.8 ± 27).

When assessing if the iron speciation in the various chronosequences and transects in the three glacial forefield soils affected by exposure age, a regression analysis of the Fe_{HR} fractions, derived from *in-situ* weathering, revealed, in all cases, no correlation. Indicating that this type of weathering was not dominant in these soils (for all data from ML, see Appendix C, Fig. 3). The data showed that ferrihydrite, the most indicative of pedogeneic processes, remained at a roughly constant concentration in Midtre Lovénbreen soils. Although, in Storglaciären soils some site-specific variations were observed at young ages. These variations were within the range of natural variabilities (Fig. 5.6b). In contrast, more significant changes were observed in Rabot's soils samples, with an increase at the >104 year-old moraine, being one order of magnitude higher than the average. However, this highest age moraine sample, in the Rabot's

transect, was waterlogged, and was characterized by a thicker organic layer (Fig. 5.4.); making this sample a periodic histosol, in contrast to the other sample soils along this transect which were all classified as Leptosols and Regosols.

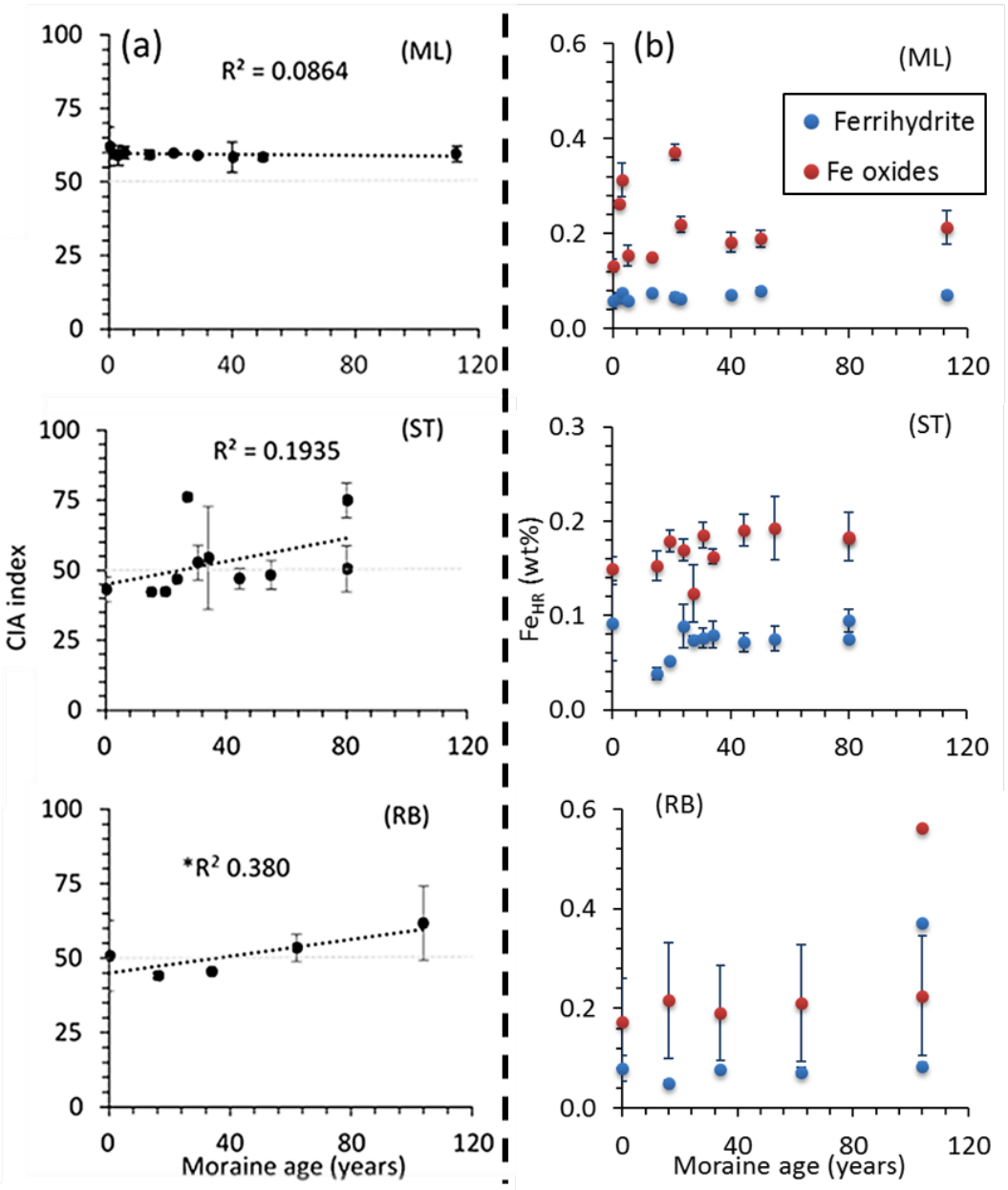

Figure 5.6. Plots **(a)** of the average CIA values and **(b)** highly reactive iron phases (Fe_{HR}) showing both ferrihydrite and Fe oxides as a function of moraine age for Midtre Lovénbreen (ML), Storglaciären (ST) and Rabot's glacier (RB). Uncertainty bars represent 1σ of triplicate samples from the same aged site. Dashed grey horizontal lines (CIA plots only) represent the value of nominally 'fresh' unweathered metasedimentary samples, while the dotted black lines are calculated linear regression line. It is worth noting that the CIA values < 50 in the ST and RB soils may indicate local variations in weathering but possibly also point to issues with the applicability of the CIA index as defined in the literature (Pri) to the rocks in the two N-Swedish catchments, where not all rocks were metasediments.

Interestingly, when comparing the changes in iron chemistries between the three glacial forefields (and not along each chronosequence or transect), major differences were observed. These differences were due primarily to variations in the relative abundance of the different iron fractions. One typical example was, the fraction Fe_u, which was 7 times higher in soils from Storglaciären and Rabot's glacier compared to Midtre Lovénbreen (Fig. 5.7). In the soils in the transects in Storglaciären and Rabot's glacier, the Fe_u was likely associated with pyroxenes and amphiboles (Andréasson and Gee, 1989). Literature data indicates that the source rocks in the local lithologies contain such minerals in abundance. When combined with the fact that the Fe_u extraction step (Poulton and Canfield, 2005) targets Fe primarily form such Fe containing silicates, this supports data that showed the Fe_u in these transects was derived from the silicate's primary rock type which was present in lithological units in the Tarfala Valley that underlay Storglaciären and Rabot's glaciers (Fig. 5.6b). Other more reactive phases than Fe_u, but still considered the poorly reactive iron fractions Fe_{PR} (magnetite and Fe bound in sheet-silicates), also show a large difference between Midtre Lovénbreen, Storglaciären and Rabot's. Sheet-silicate iron is usually associated with the mineral biotite, which is present in the gneisses and amphibolites in Storglaciären and Rabot's (Andréasson and Gee, 1989 and Fig. 5.2).

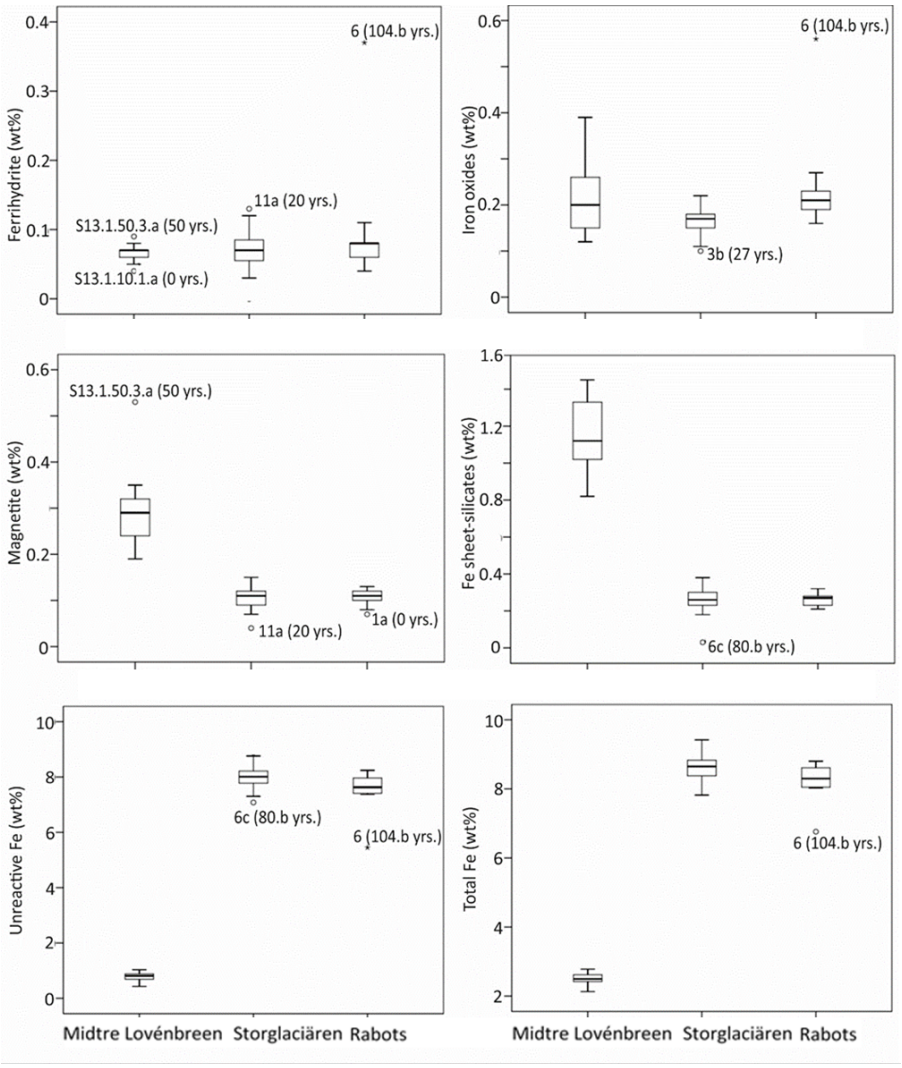

Figure 5.7. Box and whisker plots of operationally defined Fe fractions for each of the glacier forefields. Interquartiles are set as 1st = 25 % and 3rd =75% of the sample size and the interquartile range (IR) is the difference between the 3rd and 1st interquartile values. Minimum and maximum (whiskers) are those values within the sample size that exclude outliers. Outliers were set as > than the critical value calculated as follows: mild outliers = 1.5*IR (circles) and extreme outliers 3*IR (stars)

5.4. Discussion

5.4.1. TOC and $\delta^{13}C_{org}$

The accumulation of organic matter is considered the most important aspect of soil formation in a succession sequence (Viereck, 1966). Results from this study showed that TOC, in general, increased as a function of moraine age (Fig. 5.5). Other Arctic and non-Arctic forefields also observed an age dependent accumulation of TOC over similar, century long timescales of deglaciation and soil development (Stork, 1963; Kabala and Zapart, 2012; Mavris et al., 2010; Bernasconi et al., 2012). In European Alpine forefields, plant assemblages, and in turn ecosystem evolution, was found to be the primary driver of TOC accumulation (Dumid et al.,

2011; D' Amcio et al., 2014; Cohen et al., 2007). In the few Arctic forefield studies, TOC accumulation was inferred through changes in above ground percentage coverage (e.g. Hodkinson et al., 2003), however the drivers of the below ground TOC accumulation in the bulk soil are still unclear. Autochthonous plant assemblages often provide considerable input of organic matter to soils, and this could be a driver of TOC accumulation. In the current study, bulk soils were measured for their $\delta^{13}C_{org}$ isotopic composition and plotted as a function of moraine age (Fig. 5.5). A strong inverse relationship with moraine age is observed. To further aid the identification of the isotopic endmembers, and possible organic carbon sources, in addition to possible non-linear isotopic fraction processes (Faure and Mensing, 2005) an isotope mixing model $\delta^{13}C_{org}$ vs. 1/TOC (1/wt%) was used (Fig. 5.8; for all forefield transect see, Appendix C, Fig. 4). Using this approach, straight lines representing a simple mixing of two endmembers, were derived. If an exponential line was found, this would have indicated that the data would have been the consequence of a single isotopic fractionation process (Faure & Mensing, 2005). In the bulk soil analyses in this study, all mixing lines exhibited straight trends and strong linear relationships (R^2 0.59-0.94) that were significant (p value <0.001) (Appendix C, Table 10). Based on these trends, and thus treating the observed data as a binary mixture of two endmembers, the separate organic carbon-based sources lead to the observed TOC pool accumulations. To do this, several assumptions had to be made: (i) the two end members were the main contributors of organic material to the bulk soil and (ii) few secondary isotope changes affected the bulk soil after its deposition. Such changes to the latter are usually detectable only by compound specific analyses and are generally negligible with respect to the isotopic composition of the bulk sediment. The data clearly shows that TOC accumulates with age in all forefields. This means that the data shows that endmembers likely represent: (a) the organic carbon provenance at young ages and (b), what organic carbon pool(s) are responsible for TOC accumulation after roughly a century of deglaciation. Such assumptions have possible pitfalls, below is discussed the rationale behind constraining the two endmembers identified, and the differences between forefields.

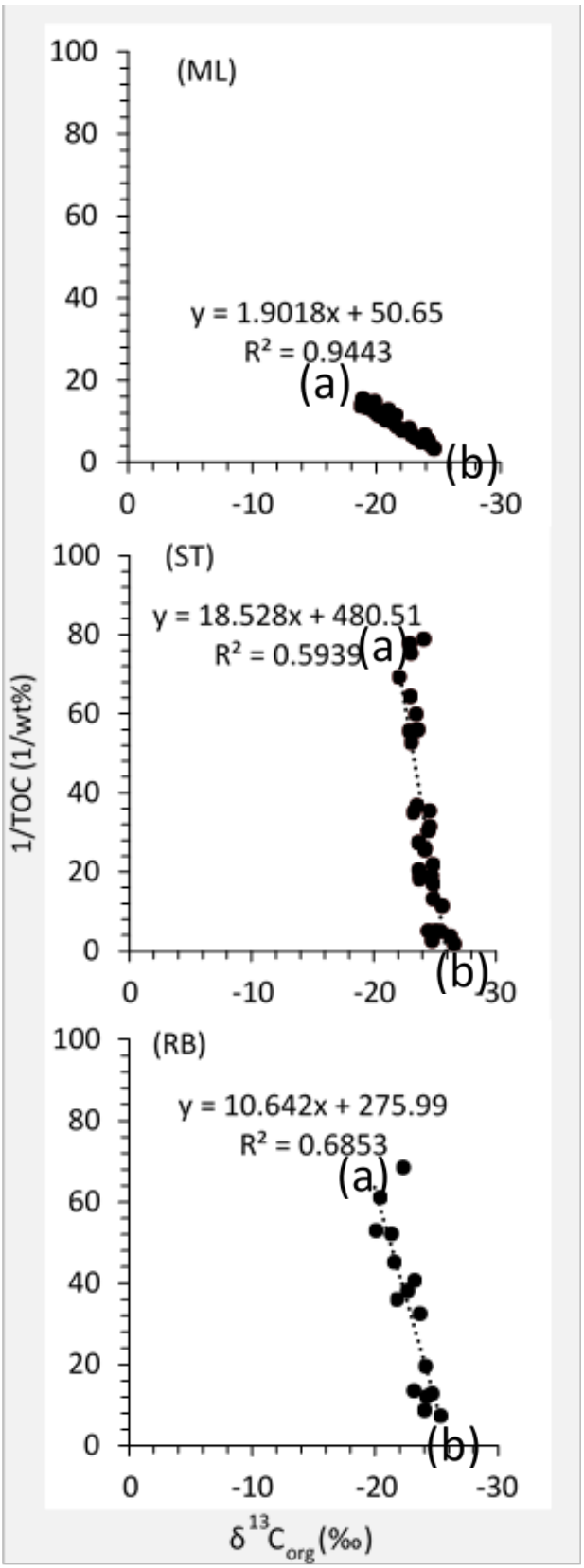

Figure 5.8. Isotopic δ13Corg (‰) *vs.*1/TOC of the soils from the Midtre Lovénbreen (ML), Storglaciären (ST) and Rabot's glacier (RB) forefield. All isotopic mixing lines cross the x axis between -25 and -28. The notation (a) represents soils at zero-years-old, while (b) is soils from the 113-year-old moraine. For the 95% prediction intervals for mean of the samples, see Appendix C. Fig.5.

Those found in Midtre Lovénbreen 0.07 TOC wt.% are significantly higher (p value > 0.05) than at Storglaciären 0.01 TOC wt.% and Rabot's 0.02 TOC wt.%, which are both at the LD and within uncertainty, and thus highly unreliable. Furthermore, $\delta^{13}C$ values reveal that TOC in Midtre Lovénbreen was comparatively $\delta^{13}C$-enriched -18.7‰, compared to Rabot's -20‰ and Storglaciären -23‰. These differences between TOC and $\delta^{13}C$ isotopes arise from the source and age of organic carbon. In Midtre Lovénbreen, where vegetation is absent at zero-years, $\delta^{13}C$ values are typical of diagenetic kerogen with an algal origin $\delta^{13}C$ -17.7-22.8‰ (Spiker and Hatcher, 1984; Hayes, 1993). In Midtre Lovénbreen the kerogen likely originates from coal, and in part, sandstones, and conglomerates, which are all part of the source rocks within the glacial catchment. These were all present in the glacial till (TOC, 0.3 wt% and 0.1wt%, respectively, Appendix C, Table 2). The low isotopic scatter at 0 years-old is characteristic of kerogen, whereby labile organic compounds (e.g., carbohydrates) are preferential removed to more diagenetic-stable 'recalcitrant' species (Spiker and Hatcher, 1984; Petsch et al., 2000). Consistent with $\delta^{13}C$ and source rock-TOC results are an observed high relative abundance of aromatic carbon compounds compared to polysaccharide, proteins and phenols at young ages in Midtre Lovénbreen (White et al., 2007). Moreover, as mentioned above, the Permo-Carboniferous rocks in the geological basin Midtre Lovénbreen contain bituminous, kerogen in the coal seams that are primarily anthracitic in nature (Dineley, 1958). Ancient carbon evidenced in other forefields is often assumed to be organic matter from beneath glaciers or paleosol remnants (Bardgett et al., 2007). The results from this study have shown geological, diagenetic organic carbon is an additional source to consider in soils developing from metasedimentary glacial tills.

In Storglaciären and Rabot's forefields, initial carbon contents are negligible and $\delta^{13}C_{org}$ at young moraine ages are $\delta^{13}C$ 4.3 to 1.3‰ heavier than in Midtre Lovénbreen. This was expected, as the glacier's catchment contains primarily high grade metamorphic and subordinate metasedimentary rocks (Andréasson and Gee, 1989) containing no organic matter (Burt, 1977). Instead, modern photosynthetic organic carbon accounts for endmember (a) in the forefields of Storglaciären and Rabot's (Fig. 5.8). Possible sources are allochthonous inputs from a glacier's ice-surface, Aeolian, meteoritic and ornithological and mammalian excrement (Bradley et al., 2014). In addition to autochthonous sources, biological communities such as algae (White et al., 2007) and endolithic organisms such as lichen, or microbial biomass may contribute to the observed increase (Rime et al., 2016). An isotopic shift from $\delta^{13}C_{org}$-depleted values -24‰ in Storglaciären and -23‰ in Rabot's, at the glacier-forefield interface, to more

enriched values -22.2‰ in Storglaciären and -20‰ in Rabot's. These progressively depleted at older ages, showing that there are two separate organic carbon inputs, and are suspected to be from a range of glaciogenic organic carbons inputs. For example, supraglacial cryoconite or algae or Aeolian derived C3 photosynthetic biomass. Such sources typically have lighter $\delta^{13}C_{org}$ values (Lutz et al., 2015), and proglacial tills are often saturated with water and subjected to mixing (i.e., high SD of TOC in Rabot's) at the glacier-forefield interface. Organic carbon delivery by this pathway has been observed in other forefields (Bradly et al., 2014; Rime et al 2016). In this study, the transects away from the glacier-forefield interface, in the vadose zone soils, have $\delta^{13}C_{org}$ depleted values with a wide isotopic scatter that increase chronologically. Organic carbon, derived from a multitude of sources, reflects the observed trends (Fig. 5.8). For Storglaciären and Rabot's glacier, microbial supraglacial sources (Lutz et al., 2015), combined with C3 plant substrates with different types of residual plant matter and isotopic values (O'Leary, 1981; O'Leary, 1988; Ziegler and Lüttge, 1998), could explain the observed trends.

Extrapolation of the linear regression models showed a clear pathway towards endmember (b) that is typical of C3 photosynthetic organisms (-27‰; Craig, 1953; O'Leary, 1981; O'Leary, 1988)(Appendix C, Fig.4). This provides evidence that photosynthetic C3 plant carbon dominates the total organic carbon pool and drives its accumulation in the bulk soil at higher exposure ages. Unsurprisingly, these results are consistent with an increase in vegetation ground cover, diversity and abundance, as evidenced in all three transects (Fig.5.3 & 5.4), and as supported by independent ecological studies (Hodkinson et al., 2003; Stork, 1963). The difference between TOC and isotopic scatter along the mixing lines in each forefield likely derives from the differences of type of C3 plants in the forefields (O'Leary, 1988; Ehleringer, 1991). This can be also enhanced by differential rates of degradation in the different plant species (Schmidt et al., 2011). It is plausible that this was because only 24 plant species were present in the forefield in Midtre Lovénbreen (Hodkinson et al., 2003), as evidenced by the narrow range of isotopic scatter along the mixing line. On the contrary, in Storglaciären 43 species have been documented (Stork, 1963) resulting in a wider isotopic scatter. Comparing with Alpine glacial forefields, e.g., in the Damma glacier, Switzerland, where the diversity and abundance of plant species is much greater after only a decade of deglaciation (vascular *Salix* is established) (Bernasconi et al., 2011), a wider and plant dominated isotopic scatter is not surprising (-25.5 to -28.5‰; Smittenberg et al., 2012).

5.4.2. Carbon budget, organic carbon accumulation and possible mechanisms for stabilization or losses

A carbon budget for the soils in the Midtre Lovénbreen forefield was used with the aim of quantifying the relative fractions of three known organic pools making up the measured TOC: (i) total microbial biomasses ($OC_{microbe}$) (autotrophic + heterotrophic), (ii) kerogen ($OC_{kerogen}$) and (iii) organic carbon of photosynthetic C3 plant origin (OC_{plant}). The $OC_{microbe}$ along the chronosequence was taken from microbial biomass counts (taken from an aliquot of the samples in this study; Bradley et al., 2016). $OC_{kerogen}$ concentrations in 0 year-old samples matched TOC values (0.079 wt%) and $\delta\ ^{13}C_{org}$ value of -18.7 indicating diagenetic kerogen, as vegetation was absent (Spiker and Hatcher, 1984; Hayes et al., 1997). At older ages, $OC_{kerogen}$ decreased by 20% (assuming a linear decrease) over the first 27 years of glacier retreat (our study was 29 years)(White et al., 2007). Subsequently, a correction factor was used as follows:

$$OC_{kero,corr} = \sum_{a=0}^{a=29} [OC_{kerogen}] \times 0.0005 \qquad \text{Equation 5.3}$$

For the remaining site ages, $OC_{kerogen}$ remains at a constant abundance. Using TOC concentrations along transects Tr1 (data in Appendix C, Table 1), Eq 5.4 was rearranged to determine OC_{plant} as follows:

$$OC_{plant} = TOC - OC_{microbe} - OC_{kero,\ corr} \qquad \text{Equation 5.4}$$

It is important, however, that these results are used cautiously. Firstly, because it was suggested that the presence of aromatic hydrocarbon precursors (AHP) compounds have not been derived from kerogens (White et al., 2007). AHP are generally considered not to come from lignin / coals, and thus we presume they mean plant origin. Secondly, the source of AHP remains identified in their bulk soil samples, thus using the evidence of sedimentary carbon we assign it to diagenetic kerogen (evidence discussed above, Section 5.4.1). Thirdly, all variables are subject to temporal change, particularly OC_{plant} and $OC_{microbe}$ that represent the average community biomass at that point in time.

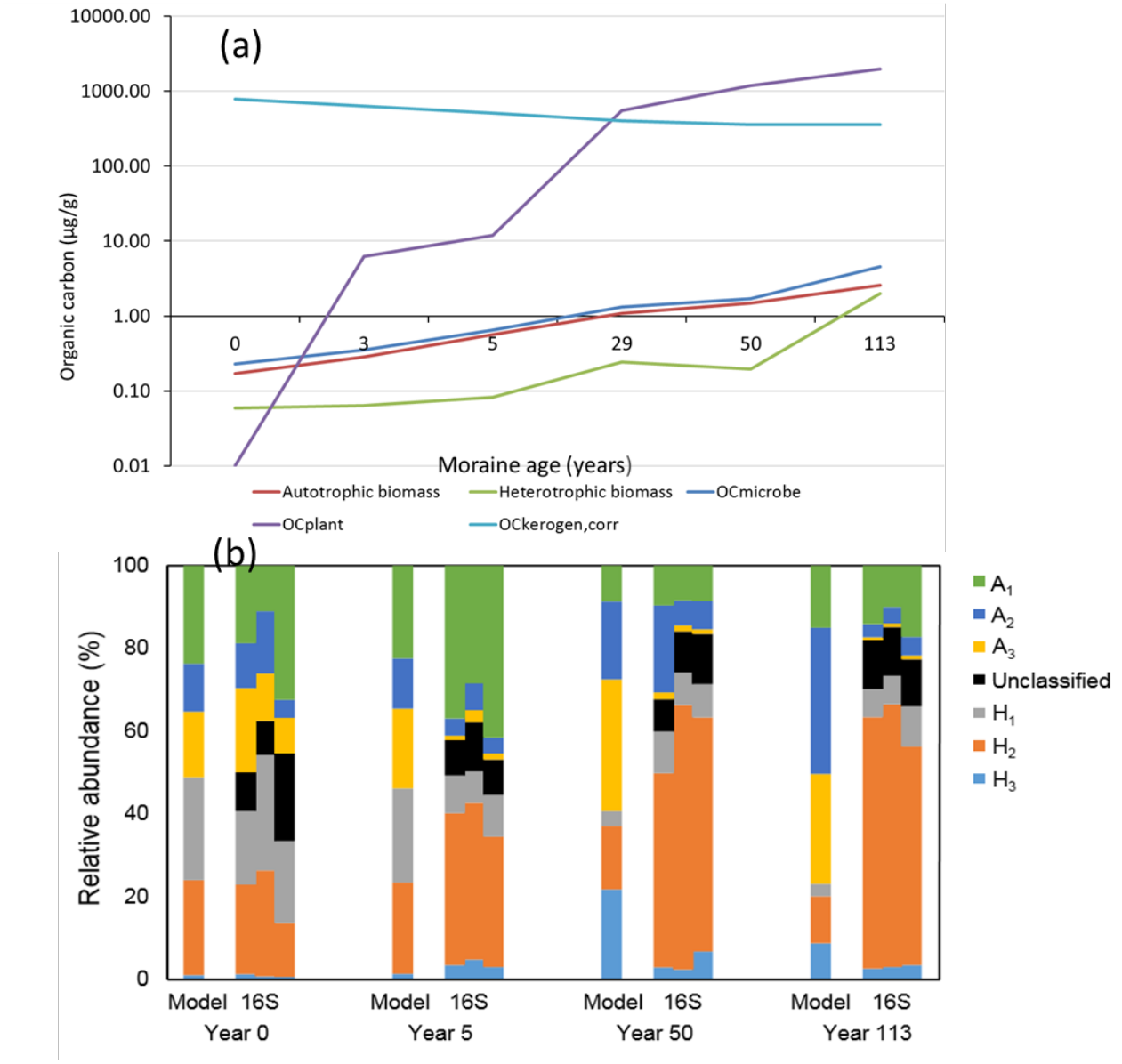

Figure 5.9. Plot **(a)** absolute organic carbon fraction concentrations on a Log 10 scale as a function of moraine age for each of the organic carbon pools. OC_{plant} and $OC_{kerogen,corr}$ were calculated using Equation. b.3. & 4. The sum of autotrophic and heterotrophic microbes equates to $OC_{microbe}$. For all used data sets see, Table 13. **(b)** the relative abundance C, compared of microbial diversity from model output and genomic analyses at 0-, 5-, 50-, and 113 year-old soil in Midtre Lovénbreen forefield (figure from Bradley et al., 2016). Note: the considerable shift in microbial population from A_1 Chemolithoautotrophs, such as known iron or sulfur oxidizers (genera *Acidithiobacillus, Thiobacillus, Gallionella, Sulfurimonas*) to H_2, general soil heterotrophic microorganisms (mainly members of *Alphaproteobacteria*, *Actinobacteria*,*Bacterioidetes,andAcidobacteria*).

Carbon budget results agree with those from the $\delta^{13}C_{org}$ mixing models, that OC_{plant} fraction of the TOC pool drives the accumulation of organic carbon in Midtre Lovénbreen (Fig. 5.9a & Table 5.2). Kerogen is the dominant source of carbon in young soils and microbial processes and plant colonization dominates at later ages. This result supports the findings of White et al.,

2007, on samples from the same forefield in Midtre Lovénbreen, where they measured a shift in carbon species within the soil carbon pool from a presumed algal kerogen source to an organic carbon lignin-based substrate from plant litter inputs. Collectively, these results suggest 'negative priming' is in action (e.g., Kuzyakov et al., 2000), whereby at >50 years, soil organic matter mineralisation of the kerogen carbon is reduced due to the addition of a new substrate, vascular plants (Hodkinson et al., 2003). This coincides with the divergence of microbes to the more easily available substrate, as evidenced by a community switch from chemolithoautotrophs, and a low abundance of heterotrophs at young ages, to a population where 68% of the microbial community is soil heterotrophs at >50 year-old soil (Bradley et al 2016).

The relative proportions of microbial biomass in TOC, ranges from 0.03 ± 0.01 to 0.18 ± 0.05%. This is roughly one order of magnitude lower than those found in the Damma glacier forefield (0.33 to 1.85%; Bernasconi et al., 2011) or Morteratsch (3.7 to 6.3%) and Riedgletscher forefields (3.9 to 6.7%; Conen et al., 2007), over a similar century long deglaciation time scale. In terms of soil formation and ecosystem development, firstly, a low prevailing microbial biomass would reduce the size of the liable organic pool. Secondly, this would lead to a decrease in metabolic-enzymatic oxidation of resistant organic carbon compounds i.e., plant-derived phenols, lignin that are observed to accumulate with age in Midtre Lovénbreen (White et al., 2007) and nutrient cycling. Thirdly, it could retard the formation of soil structures due to reduced soil enzymatic proteins and organic polymers that help create soil aggregates and stabilize soil organic carbon (Tisdall and Oades, 1982; Stockmann et al., 2013).

Table 5.2 Carbon budget results for each of major organic carbon proportion relative to the total organic carbon pool; total microbial biomasses, autotrophic + heterotrophic ($OC_{microbe}$), kerogen ($OC_{kerogen}$) and photosynthetic C3 plant origin (OC_{plant})

Soil age (years)	$OC_{microbe}$/TOC (%)	$OC_{microbe}$/TOC ±	OC_{plant}/TOC (%)	OC_{plant}/TOC ±	$OC_{Kerogen}$/TOC (%)
0	0.03	0.01	0.00	0.01	99.9
3	0.05	0.01	0.87	0.01	99.1
5	0.08	0.00	1.53	0.00	98.4
29	0.11	0.03	46.53	0.03	53.4
50	0.09	0.04	65.13	0.04	34.8
113	0.18	0.05	75.55	0.05	24.3

Note: ± = 1σ of triplicate samples at a moraine age. No standard deviation is available for kerogen.

5.4.2.1. Evidence for organo-mineral complexes

Iron-bearing minerals are abundant in each of glacier forefield catchment lithological units. This is evidenced by the fact all samples contained Fe-bearing sheet-silicates, magnetite and unreactive iron as sulfides (Fig. 5.7; and Appendix B, Table 3). This is further validated, as the soil parent materials contained a total Fe elemental concentration >2 wt% (Appendix B, Tables 12 & 14). Consequently, chemical weathering and transformation of these primary iron containing mineral phases during pedogenesis could result in organo-mineral complexation. The possibility of this process being dominant in the analysed transects was assessed here. Iron organo-mineral complexes contribute to physical and chemical organic carbon stabilization during pedogenesis, through mixed electrostatic particle aggregation, mineral sorption and co-precipitation processes (Kleber et al 2007; Schmidt et al., 2011; Lalonde et al., 2012). Therefore, in new soil forming processes such reactions and interactions could be important, and are considered herein.

Two of the most common minerals that are often characteristic of pedogenic iron formation, and interact with organic matter, are: ferrihydrite (poorly crystalline iron oxide) and iron oxides (crystalline), termed reactive iron phases (Fe_{HR}) (Vodyanitskii and Shoba, 2016). Iron extractions revealed that these phases were present in all of the developing soils in all of the forefields. High iron oxide concentrations were documented at young ages in Midtre Lovénbreen (~0.4 wt%) compared to the average (0.2 wt%). This may reflect their formation through subglacial or subaerial sulfide oxidation, as also predicted by the stoichiometric mass balance calculation in Chapter 4, Table 4.5. Other than sulfide oxidation, there was limited evidence of changes in Fe speciation that would suggest pedogenic iron formation. In general, Fe_{HR} remained relatively constant along the transects (Fig.5.6, and Appendix C, Fig. 6). These results are not surprising, because the bulk soil pH's measured (0-15cm depth, at the point of sampling) were not low enough to cause significant mineral-bound Fe translocation. The pH values varied between slightly alkaline, to weakly acidic $\bar{x}$ 7.6, 6.7 and 6.5, respectively, in Midtre Lovénbreen, Storglaciären and Rabot's; Appendix C, Fig.1. In addition, no soil horizon formation was yet evident in any of the transects. Such soil layering would also indicate aggregation and Fe leaching and its chelation during transformation. Such processes further support the fact that new pedogenic iron mineral formation was very limited, and that iron concentrations primarily reflect the catchment lithology of the parent material. Due to this very limited pedogenic iron, and near-neutral prevailing soil pH, the lack of a relationship between

TOC and any of the Fe_{HR} phases is not surprising (Fig. 5.10; for data including outlier see Appendix C, Fig. 7). The lack of organo-mineral interactions is evidenced by the absence of a correlation between loosely-bound P or Fe-bound P species with reactive iron phases (Appendix C, Tables14, 15 & Fig. 8).

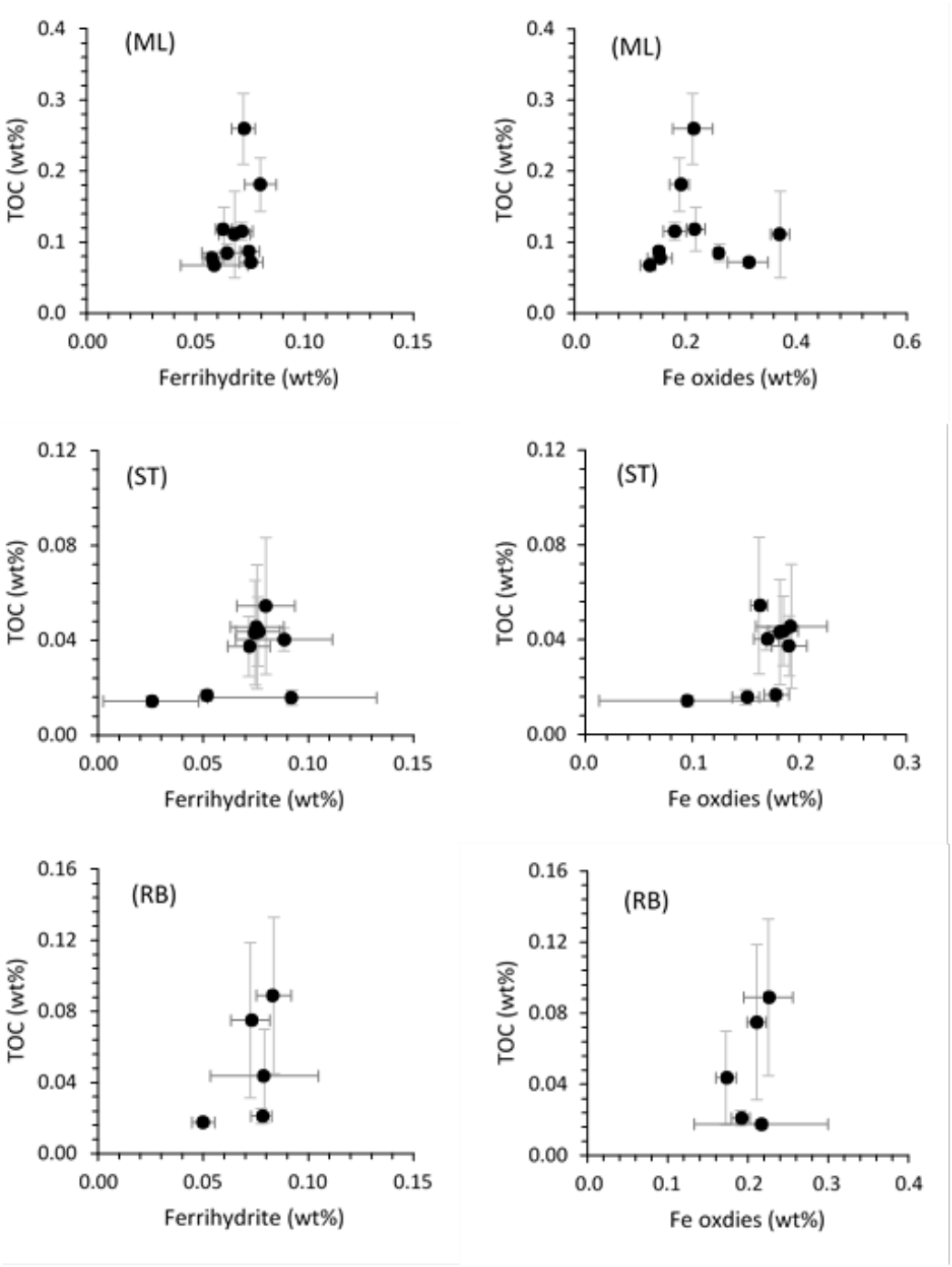

Figure 5.10. TOC as a function of Ferrihydrite and Fe oxides for ML, RB and ST. Uncertainty bars represent 1σ of triplicate samples at a moraine age site. Note: Outliers from ST at sites 27 and 80(b) have been removed, for plots include these see, Appendix C. Fig.C.5.

Evidence of other secondary weathering products that facilitate organic carbon stabilization are very limited. Pedogenic clay mineral formation is negligible and principally lithogenic, consequently their abundance is very low, as shown by the chemical weathering index of alteration, where predominantly incipient (CIA = <60) to 'fresh' (CIA = <50) values are present (see Fig. 5.6a & Chapter 4.4 for a more in-depth discussion). Where chemical weathering is observed, it consists of the near-complete removal of comparatively soluble carbonates (expressed as TIC), to silicates, as a function of time (see Chapter 4, Figs. 4.6 & 4.7). Cement aggregation is a transient form of physical organic matter stabilization, where the lack of secondary weathering products retards soil formation (Tisdall and Oades, 1982). Furthermore, a soil devoid of pedogenic smectites may explain the fall in soil moisture away from the glacial forefield interface, vadose zone in the flat relief forefields (Blume et al., 2015)(Appendix C, Fig. 1b). Interestingly, site-specific examples of enhanced weathering and pedogenesis are observed ST at 27 and 80(b) years-old. Here CIA values are high, and concurrent with this are high concentrations of reactive iron phases and TOC (Fig. 5.6.)(Appendix C, Fig. 7).

In this study, the apparent lack of abiotic organo-mineral associations, after a century of deglaciation, is related to low-level weathering of primary minerals. Despite limited evidence of organo-mineral carbon stabilization over this soil-forming timescale, soil binding agents in the form of polysaccharide mucilage have been observed on each forefield in this study. These transient soil particle 'gluing' agents were exuded from earlier plant colonisers in the forefield at mostly older moraine ages (Galloway et al., in prep; co-authored by Joshua Blacker). Further work is needed to quantify their contribution to the soil accumulation observed.

5.4.3 Biological and environmental factors that control organic carbon accumulation

If organo-mineral association, leading to organic carbon stabilization, is minimal in Arctic glacier forefields, the organic carbon accumulation observed is a consequence of other biological or environmental factors. In cold regions, such as the Arctic, a prevailing polar climate limits not only forefield abiotic weathering but also the activity and efficiencies of the heterotrophic and soil saprobic microbial community (Chapters 4 and 5; Kabala and Zapart, 2011; Bradley et al., 2016b). This is also seen by the few macro-gaunal species, and a low abundance of soil saprobic fauna (Hodkinson et al., 2001; Bradley et al., 2016b). Consequently, a lower metabolic-enzymatic rate of organic matter decomposition occurs, limiting biomass

growth (Bradley et al., 2016b; Bradley et al., 2017). Empirical evidence supports these results because SOC does not only accumulate, but the OM-bound P also increases as a function of age (Appendix C, Fig. 9 & Tables 13 and 14).

In the oligotrophic Arctic forefield environments studied here, it is expected that key nutrients would be scavenged. However, organic matter litter bag experiments in Midtre Lovénbreen exhibited no mass loss over a two-year period, supporting a short-term lack of substrate biodegradation (Hodkinson et al., 2003). Long-term SOC stabilization may therefore be due to differential digestion of organic material by reindeer grazing and the fact they preferentially select nutrient-rich plants leaving behind predominately more stable organic matter (Ritchie et al., 1998). Reindeer populations present in of the forefields can further affect carbon substrate quality by trampling, hindering low order vegetation growth and aggregate formation (Cooper and Wookey, 2003). Results from this study suggest this is plausible since, a low $\delta^{13}C$ isotopic scatter between endmembers could suggest more stable carbon forms make up the soil TOC residual. It is apparent from the White et al., 2007 study, and in Midtre Lovénbreen, that primarily plant-derived phenolic compounds associated with lignin accumulate as a function of age along the same chronosequence. Therefore, if soil TOC comprises of more complex and stable forms of OC compounds (i.e. lignin) in the bulk soil, perhaps this is the reason why TOC accumulates as a function of age. Similar results are present in Antarctica, where low concentrations of OC comprise of more 'recalcitrant' TOC (Pires et al., 2017).

As opposed to the high-Arctic low altitude Midtre Lovénbreen setting, The sub-Arctic and higher altitude forefields of Storglaciären and Rabot's in the Tarfala valley, benefit from somewhat milder climatic conditions. The higher average ground surface temperatures and higher precipitation, result in a longer growing season that clearly benefits valley soils and the development of new ecosystems upon glacial retreat (Holmlund and Jansson, 2002). In the Tarfala valley, there is a high allochthonous pollen input (Lutz et al., 2015), a great and diverse abundance of above-ground biomass (Fig. 5.3 & 5.4; Stork, 1963), and a soil TOC of up to 50% has been measured (Fuchs et al., 2015). Despite these factors, the average rate of SOC accumulation over similar soil forming timescales in Storglaciären and Rabot's are lower than in High-Arctic forefields, Midtre Lovénbreen (Table. 5.3), and another Arctic forefield Werenskiold (Kabala and Zapart, 2012). A soil system where heterotrophic respiration is higher than net primary productivity, depleting organic stocks could account for SOC accumulation. Determining if this is applicable to Stor and Rabot's glaciers' forefield

ecosystems would require either carbon isotope labelling or measurement of soil respiration. Our evidence suggests that this process is unlikely because the $\delta\ ^{13}C_{org}$ values associated with C3 plant and TOC accumulation along the transects (Fig. 5.8), indicate that the forefield ecosystems are in a phase of primary, albeit spatially variable, plant productivity. Instead, we argue that soil profile translocation processes could be responsible for the observed trends. These could include chelation or physical erosion of the substrate due to freeze-thaw, water and Aeolian processes (katabatic winds).

Fungal species (inc. mycorrhiza) are present in the Tarfala valley (Coleine et al., 2015). Due to their efficient spore dispersal of ~1000 m per decade, they are also likely to occur in the Storglaciären and Rabot's glacier forefields' soils (Peay et al., 2016). As plant communities tend to be micro-niches in both forefields, bio-enhanced weathering (and chelation) via fungi is unlikely to be widespread in Storglaciären over the 27 years tested, Fig. 5.3. The surface soil strength measurements revealed a significant transition ($R^2 = 0.87$ $p = <0.05$) from a loose soil at young ages to a well-compacted soil with moraine age in the Rabot's forefield soils, (Appendix C, Fig. 1). At young ages, nearest the glacier terminus, a dynamic phreatic zone was dominated by loosely compacted soils (<0.5 $kg.cm^{-2}$) with high soil moisture; these soils were recently deposited together with larger glaciogenic till and glaciofluvial gravels (Appendix C, Fig. 1b). In this forefield, spring snowmelt and episodic intensive rainfall events are likely to infiltrate and flush out glacier till substrates due to their macroporous and stony structure (Espeby, 1990; Jansson et al., 2005). Such erosive processes would result in the loss of the loose-particulate fractions, as well as the flushing-away of loose organic matter. The difference between the organic accumulation processes in the high-Arctic and sub-Arctic Alpine forefields may be due to such seasonal annual processes. In North Sweden, the annual precipitation is ~ 60 % higher (1000 mm) (Holmlund and Jansson, 2002) than in the high-Arctic, Midtre Lovénbreen forefield (300-400 mm) (Førland et al., 2011). In addition, soil collected early in the melt-season in June in the Storglaciären and Rabot's glacier forefields, compared to those collected in August in the high-Arctic Midtre Lovénbreen melt-season, may allow for a slightly more prolonged period of TOC stock replenishment.

Somewhat less cohesive but more stable soils (>0.5 to < 1.5 $kg.cm^{-2}$), and compacted soils (>1.5 $kg^{-}cm^{2}$), were found at progressively older ages in the Rabot's forefield. The bulk soils had lower moistures, being from a vadose zone away from the glacier and till surface. Here, organic matter could be preserved as soil-crusts, that in turn could impede water infiltration

and soil-water flushing of organic carbon laden substrates. Soil development and organic carbon preservation may instead suffer from retarded aggregate formation, due to water redistribution by sheet flow over the surface (Tisdall & Oades, 1982). In Storglaciären, no correlation was observed between soil age, moisture and strength. The reason for the random distribution of these values was most likely due to the steep slope relief which enhances subsequent frequent re-mobilization of the glacier soils and till (Fig. 5.1).

5.4.3. Soil organic carbon stocks: a comparison with global forefields

It is argued that soil processes, or lack of them, as discussed in Sections 5.4.1 to 5.4.3, could derive the annual average rates of SOC accumulation of 2.2, 0.7 and 0.6 g C m^2 a^{-1} in the Midtre Lovénbreen, Storglaciären and Rabot's glaciers respectively. These values are low compared to studies from a range of different climatic biomes at lower latitudes (Table 5.3).

Table 5.3. Soil organic carbon stocks for forefields from this study and others from around the globe over roughly a century of deglaciation.

Locale Forefield name	*Latitude* (°)	Lithology	Deglaciation period (years)	SOC (g C m^2 a^{-1})	Regression model (*r* & p value)
High-Arctic					
*Midtre Lovénbreen	79, N	Metased	0 to 113	2.2	Linear (0.9, <0.001)
[1]Werenskiold	77, N	Metased	1 to 80	4.4	Log10 (0.8, <0.05)
Sub-Arctic					
*Storglaciären	67, N	High g. meta	0 to 80	0.6	Linear (0.52, <0.05)
			0 to >80(b)	*2.5*	*Linear (0.40, <0.05)*
*Rabot's	67, N	High g. met	0 to 104	0.7	Linear (0.65, <0.05)
			0 to >104(b)	*5*	*Exp (0.67, <0.05)*
European Alps					
[2]Morteratsch	48, N	Granitic	0 to 128	7 to 36	Logistic (0.74 <0.05)
[3]Damma	46, N	Granitic	0 to 136	20	Linear (n/a)
China, Tibetan plateau					
[4]Hailuogou	29, N	Metased	0 to 183	28	Logistic (0.95 <0.001)

Note: Studies with the following notation represent their citation: *Our studies ML, ST and RB conducted in 2013, 2014, and 2014 respectively; [1.] Kabala and Zapart, 2012 [2.] Mavris et al., 2010, [3.] Smittenberg et al., 2012 and [4.] He and Tang, 2008. Forefields ST and RB have additional regression analysis values below that that show all the sampled sites including the excluded outliers (for justification outlier removal, see Appendix A, Section A.1).

In the European Alps, values for the rates of SOC accumulation are 20 g C m^2 a^{-1} in the Damma (Smittenberg et al., 2012) and 7- 36 g C m^2 a^{-1} in the Morteratsch, Switzerland (Mavris et al.,

2010). Similar values to these were observed in the high altitude, low latitude Hailuogou Forefield, Tibetan plateau, China (19 g C m^2 a^{-1}). Other non-forefield land use change studies focusing on decadal to centennial timescales, report rates of SOC accumulation of between 20 and 40 g C m^2 a^{-1} (Post and Kwon, 2000; Franzluebbers and Follett, 2005; Fabrizzi et al., 2005). By comparison of similarity, the Arctic forefield study done in Werenskiold, also in Svalbard (Kabala and Zapart, 2012), measured an SOC accumulation rate of 4.4 g C m^2 a^{-1}. The difference between SOC accumulation rates in forefields residing in different climatic biomes is highlighted by the results from comparative biogeographical and ecological studies. For example, substantial biological productivity, and variations in diversity and biomass were observed after only a decade of deglaciation in European and Tibetan forefields (Bernasconi et al., 2011; Mavris; 2010; He and Tang, 2008). This was evident in part from the faster colonization and establishment of higher order plant species including vascular plants (see, Appendix A, Fig. 2 for photographic evidence). These European and Tibetan forefields exhibit logarithmic or exponential growth functions that become flatter towards an asymptotic value after roughly a century of deglaciation. Such data were interpreted as meaning that their soil ecosystem was progressing to, or had reached almost, steady-state conditions. Conversely, the Arctic forefields assessed in this study exhibited growth functions that clearly indicate that soil development has begun, but that steady-state conditions have not yet been reached. The contrast between these studies is perhaps unsurprising given the range in timescale of global soils which reach steady-state over centuries to thousands of years (Egli et al., 2001; He and Lee 2008).

In one of the chronosequences in the Midtre Lovénbreen forefield, and based on literature values (Hodkinson et al., 2003), an ~ 2000 year of exposure since deglaciation can be used to test if this is something to be expected in high-Arctic settings. Extrapolating each of the TOC trend lines from the 113 year-old moraine to the ~ 2000 year-old moraine ridge in Midtre Lovénbreen, indicates a linear accumulation of TOC between these ages (Fig. 11) (Hodkinson et al., 2003). If the regression of the ice-sheet has also been linear between these ages (unlikely, but good 1st assumption), it follows that the TOC has continually accumulated at the same rate over ≥ 2000-years.

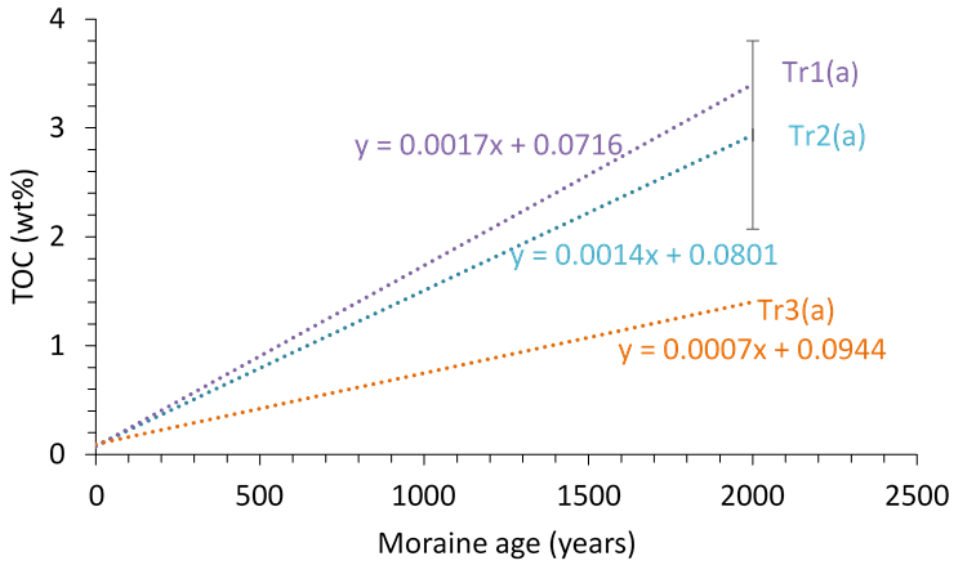

Figure 5.11. TOC concentrations along Tr1, Tr2 and Tr3 in the Midtre Lovebreen forefield extrapolated to 2000-years-old assuming a linear relationship between TOC and moraine age. The error bar represents 1σ of the average of triplicate TOC measurements analysed in the 2000-years-old samples. Note: TOC raw data for all transects and moraine ages is tabulated in Appendix B, Table. B.1..

Intriguingly, differences in TOC accumulation are observed between Tr1, Tr2 and Tr3 over the 2000 years of soil formation. Although not conclusive, the range in TOC between transects is potentially due to localised topographical and hydrogeological variations. In contrast to TR3 that is approximately 25m away from a proglacial stream that runs parallel to it, Tr1 and Tr2 are situated away from any water features. It could be expected that in Arctic forefields, such as Midtre Lovenbreen where the soils are immature and the vegetation is limited, both key mechanism for organic carbon stabilization, hydrological flushing porous glacial tills could remove plant derived particulate organic carbon. It is entirely plausible soil carbon removal related to hydrogeological processes may explain the difference in TOC accumulation occurred since, similar processes have been recorded in other Arctic forefield settings.

Inorganic carbon removal during the first 10-years of deglaciation is greater than the amount of soil organic carbon accumulated defining the early stages of soil formation and deglaciation as a CO_2 efflux to the atmosphere. Only after 10-years does soil organic carbon compensate for the inorganic carbon removed and thereafter it remains approximately proportional.

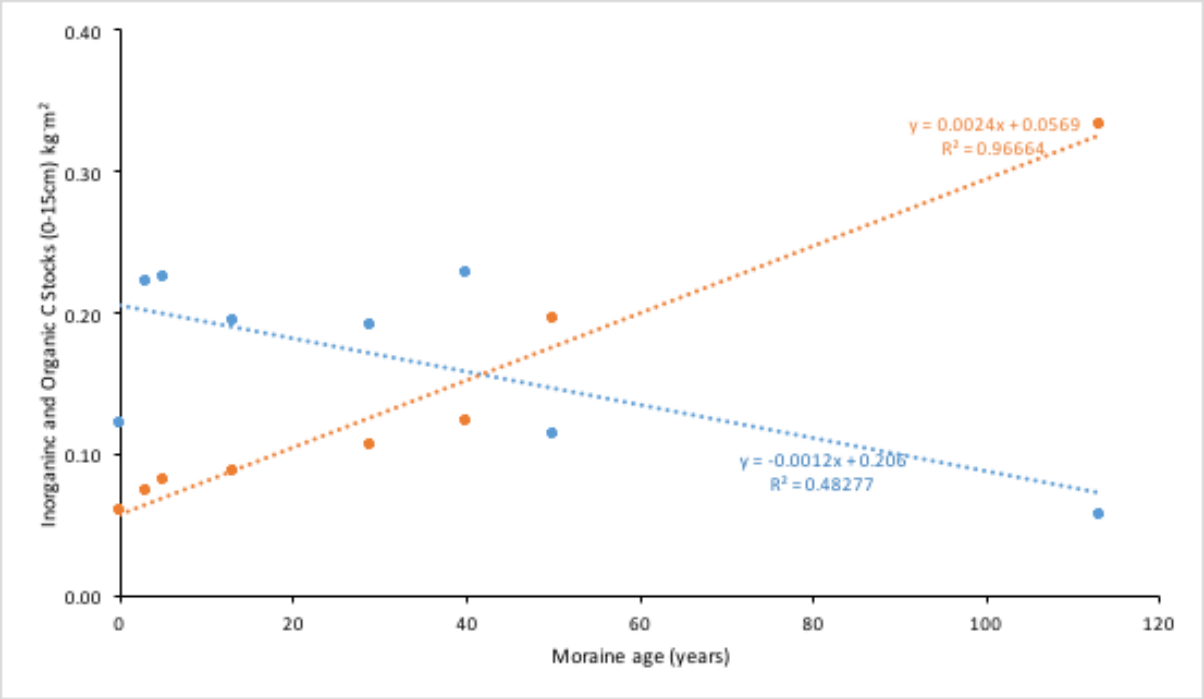

Figure 5.12. Inorganic and organic carbon concentrations plotted as a function of moraine age over approximately a century deglaciation and soil formation. Note: orange points denote organic carbon stock, while blue points are inorganic carbon stocks.

5.5. Conclusion

This study started by trying to test the hypothesis: Arctic forefields with a prevailing polar climate, low primary productivity and low organic carbon degradation accumulate SOC with age. The data, however, revealed a lack of empirical relationships to support pedogenic weathering related processes. No clear evidence was found for organo-mineral complexes or stabilization of organic carbon. In summary the result from this study showed:

- The TOC, and thus SOC accumulation in Arctic forefields, occurs as a linear function of time, and this was driven primarily by photosynthetic C3 plant carbon inputs to the near-surface bulk soil as evidenced by the asymptotic trends in each forefield after roughly a century of accumulation as typical of C3 plants ($\delta^{13}C_{org}$ -27 ‰). High initial concentrations of TOC 0.07 (wt%) and low $\delta^{13}C_{org}$ -18.7 ‰ values in the forefield of High-Arctic, Midtre Lovénbreen were due to organic carbon associated with kerogen residing in diagenetic metasediments. The absence of kerogen in sub-Arctic forefields, Storglaciären and Rabot's, meant TOC concentration at the point of initial deglaciation

were negligible, coincident with the relative higher $\delta^{13}C_{org}$ ~21. ‰ compared to those in Midtre Lovénbreen. A TOC and organic carbon $\delta^{13}C_{org}$ mixing model showed a low isotopic scatter in Midtre Lovénbreen with ages that would indicate the SOC comprised of few and well-mixed plants and their parts, or selective organic matter degradation. Conversely, sub-Arctic alpine forefields, had a wider isotopic scatter that implied a greater array of plant signals make up the prime SOC pool. Carbon budget calculations for the chronosequences in Midtre Lovénbreen are consistent with the $\delta^{13}C_{org}$ results, revealing that TOC accumulation was overwhelmingly driven by plant-derived organic carbon soil addition into the recently deglaciation and developing soils. A century of TOC accumulation in the bulk soils implies that the carbon signatures are a consequence of either intrinsic or extrinsic preservation mechanism in the soils.

- A low degree of silicate mineral weathering, and conversely a depletion of carbonates (Chapter 4.4.2 and 4.4.3), led to the finding that chemical and physiochemical stabilization of organic carbon was limited. The lack of silicate weathering was supported by the low levels of clay formation. Although clay minerals were identified in the parent material tills, and of lithogenic origin, they were detected in soils only at very low abundance, inferring no weathering related clay formation. This is consistent with the incipient slow chemical weathering trends in all Arctic forefields. Furthermore, highly reactive, and poorly reactive, iron concentrations remained unchanged with age, supporting the fact that the largest part of the total iron was lithogenic, and not pedogenically derived. It was unsurprising that the regression analysis of highly reactive iron phases in all forefields showed no correlation with TOC. The absence of secondary weathering products within the forefield soils, together with the depletion in TIC associated with carbonates, would hinder soil aggregated formation which is usually a key process for soil development. Despite this, recent work in Midtre Lovénbreen has shown that at older moraine ages, where ample plant coloniser species were present, and their polysaccharide exudates likely have facilitated the transient ‘gluing’ of soil particles together. High-resolution microscopic analyses, species specific organic analyses, and grain-size fractionation of the soil-fines, would help assess how the limited chemical weathering is linked to organic carbon stabilization at the micro and nanometre scale. The lack of organo-mineral complexation during the initial soil formation in Arctic glacier forefields, may, in part, explain the slower accumulation of SOC compared to other forefields studies where these are present.

- Due the intrinsic and extrinsic factors discussed above, the SOC accumulation rate in g C m^2 a^{-1} in Arctic soils is roughly one order of magnitude slower than in European and Tibetan, but lower-latitude and higher altitude forefield soils. Interestingly, comparing Arctic settings we observed a three-time lower SOC rate, and a weaker linear correlation with moraine age in the Sub-Arctic, alpine forefields compared to the High-Arctic forefield in Svalbard. This may be due to either the different sampling times during the summer melt-season, or due to external inputs. The difference in sampling during the melt-season may also be enhanced by slope differences, and thus by substrate flushing, which may have had more time to replenish the SOC stocks lost over winter.

This shows, that although all the Arctic forefields studied accumulate TOC, their rates were strongly related to local soil-forming factors. Measurements of dissolved organic carbon and particulate carbon, as continual time-series over a melt season in these forefields, would help to reveal if this is the case. Although these findings provide a new understanding of Arctic forefield organic carbon dynamics, further studies are needed to bridge the gap between the effect of short-term changes in seasonality and SOC turnover on longer-term time scales.

5.6. References

Abbey, S. 1980. Studies in "standard samples" for use in the general analysis of silicate rocks and minerals. *Geostandards Newsletter,* 4**,** 163-190.

Alexander, E. & Burt, R. 1996. Soil development on moraines of Mendenhall Glacier, southeast Alaska. 1. The moraines and soil morphology. *Geoderma,* 72**,** 1-17.

Andréasson, P.-G. & Gee, D. G. 1989. Bedrock geology and morphology of the Tarfala area, Kebnekaise Mts., Swedish Caledonides. *Geografiska Annaler. Series A. Physical Geography***,** 235-239.

Andrianaki, M., Bernasconi, S. M. & Nikolaidis, N. P. 2017. Chapter Eight - Quantifying the Incipient Development of Soil Structure and Functions Within a Glacial Forefield Chronosequence. *In:* STEVEN, A. B. & DONALD, L. S. (eds.) *Advances in Agronomy.* Academic Press.

Banwart, S., Menon, M., Bernasconi, S. M., Bloem, J., Blum, W. E. H., De Souza, D. M., Davidsdotir, B., Duffy, C., Lair, G. J., Kram, P., Lamacova, A., Lundin, L., Nikolaidis, N. P., Novak, M., Panagos, P., Ragnarsdottir, K. V., Reynolds, B., Robinson, D., Rousseva, S., De Ruiter, P., Van Gaans, P., Weng, L., White, T. & Zhang, B. 2012. Soil processes and functions across an international network of Critical Zone Observatories: Introduction to experimental methods and initial results. *Comptes Rendus Geoscience,* 344**,** 758-772.

Banwart, S. A., Bernasconi, S. M., Blum, W. E. H., De Souza, D. M., Chabaux, F., Duffy, C., Kercheva, M., Krám, P., Lair, G. J., Lundin, L., Menon, M., Nikolaidis, N. P., Novak,

M., Panagos, P., Ragnarsdottir, K. V., Robinson, D. A., Rousseva, S., De Ruiter, P., Van Gaans, P., Weng, L., White, T. & Zhang, B. 2017. Chapter One - Soil Functions in Earth's Critical Zone: Key Results and Conclusions. *In:* STEVEN, A. B. & DONALD, L. S. (eds.) *Advances in Agronomy.* Academic Press.

Bardgett, R. D., Richter, A., Bol, R., Garnett, M. H., Bäumler, R., Xu, X., Lopez-Capel, E., Manning, D. a. C., Hobbs, P. J., Hartley, I. R. & Wanek, W. 2007. Heterotrophic microbial communities use ancient carbon following glacial retreat. *Biology Letters,* 3**,** 487-490.

Bernasconi, S. M., Bauder, A., Bourdon, B., Brunner, I., Bunemann, E. & Chris, I. 2011a. Chemical and biological gradients along the Damma glacier soil chronosequence, Switzerland. *Vadose Zo J,* 10**,** 867.

Bernasconi, S. M., Bauder, A., Bourdon, B., Brunner, I., Bunemann, E., Christl, I., Derungs, N., Edwards, P., Farinotti, D., Frey, B., Frossard, E., Furrer, G., Gierga, M., Goransson, H., Gulland, K., Hagedorn, F., Hajdas, I., Hindshaw, R., Ivy-Ochs, S., Jansa, J., Jonas, T., Kiczka, M., Kretzschmar, R., Lemarchand, E., Luster, J., Magnusson, J., Mitchell, E. a. D., Venterink, H. O., Plotze, M., Reynolds, B., Smittenberg, R. H., Stahli, M., Tamburini, F., Tipper, E. T., Wacker, L., Welc, M., Wiederhold, J. G., Zeyer, J., Zimmermann, S. & Zumsteg, A. 2011b. Chemical and Biological Gradients along the Damma Glacier Soil Chronosequence, Switzerland. *Vadose Zone Journal,* 10**,** 867-883.

Blume, H.P., Brümmer, G.W., Fleige, H., Horn, R., Kandeler, E., Kögel-Knabner, I., Kretzschmar, R., Stahr, K. and Wilke, B.M., 2015. Scheffer/Schachtschabel soil science. Springer.

Bockheim, J. G. & Haus, N. W. 2014. Distribution of organic carbon in the soils of Antarctica. *Soil Carbon.* Springer.

Bradley, J., Anesio, A. & Arndt, S. 2017. Microbial and biogeochemical dynamics in glacier forefields are sensitive to century-scale climate and anthropogenic change. *Frontiers in Earth Science,* 5.

Bradley, J., Singarayer, J. & Anesio, A. 2014. Microbial community dynamics in the forefield of glaciers. *Proc R Soc B Biol Sci,* 281**,** 20140882.

Bradley, J. A., Anesio, A. M. & Arndt, S. 2016a. Bridging the divide: a model-data approach to Polar and Alpine microbiology. *FEMS Microbiology Ecology,* 92**,** fiw015-fiw015.

Bradley, J. A., Arndt, S., Šabacká, M., Benning, L. G., Barker, G. L., Blacker, J. J., Yallop, M. L., Wright, K. E., Bellas, C. M., Telling, J., Tranter, M. & Anesio, A. M. 2016b. Microbial dynamics in a High Arctic glacier forefield: a combined field, laboratory, and modelling approach. *Biogeosciences,* 13**,** 5677-5696.

Brugger, K. 1992. A comperative study of the response of Rabots Glaciär and Storglaciären to recent climate change in Sweden. *PhD Diss. Dept. of Geology and Geophysics, University of Minnesota, USA*.

Brugger, K. A. & Pankratz, L. 2015. Changes in the Geometry and Volume of Rabots glaciär, Sweden, 2003–2011: Recent Accelerated Volume Loss Linked to More Negative Summer Balances. *Geografiska Annaler: Series A, Physical Geography,* 97**,** 265-278.

Brugger, K. A., Refsnider, K. A. & Whitehill, M. F. 2005. Variation in glacier length and ice volume of Rabots Glaciär, Sweden, in response to climate change, 1910–2003. *Annals of Glaciology,* 42**,** 180-188.

Burt, D. 1977. Mineralogy and petrology of skarn deposits. *Soc Italiana Mineral Petrol Rendiconti,* 33**,** 859-873.

Caughey, M. E., Barcelona, M. J., Powell, R. M., Cahill, R. A., Grøn, C., Lawrenz, D. & Meschi, P. L. 1995. Interlaboratory study of a method for determining nonvolatile organic carbon in aquifer materials. *Environmental Geology,* 26**,** 211-219.

Chapin Iii, F., Stuart., Mcfarland, J., David Mcguire, A., Euskirchen, E. S., Ruess, R. W. & Kielland, K. 2009. The changing global carbon cycle: linking plant–soil carbon dynamics to global consequences. *Journal of Ecology,* 97**,** 840-850.

Coleine, C., Selbmann, L., Ventura, S., D'acqui, L. P., Onofri, S. & Zucconi, L. 2015. Fungal Biodiversity in the Alpine Tarfala Valley. *Microorganisms,* 3**,** 612-624.

Conen, F., Yakutin, M. V., Zumbrunn, T. & Leifeld, J. 2007. Organic carbon and microbial biomass in two soil development chronosequences following glacial retreat. *European Journal of Soil Science,* 58**,** 758-762.

Cooper, E. J. & Wookey, P. A. 2003. Floral herbivory of Dryas octopetala by Svalbard reindeer. *Arctic, Antarctic, and Alpine Research,* 35**,** 369-376.

Craig, H. 1953. The geochemistry of the stable carbon isotopes. *Geochimica et Cosmochimica Acta,* 3**,** 53-92.

Craig, H. 1957. Isotopic standards for carbon and oxygen and correction factors for mass-spectrometric analysis of carbon dioxide. *Geochimica et cosmochimica acta,* 12**,** 133-149.

Dahlke, H. E., Lyon, S. W., Stedinger, J., Rosqvist, G. & Jansson, P. 2012. Contrasting trends in floods for two sub-arctic catchments in northern Sweden-does glacier presence matter? *Hydrology and Earth System Sciences,* 16**,** 2123.

Davidson, E. A. & Janssens, I. A. 2006. Temperature sensitivity of soil carbon decomposition and feedbacks to climate change. *Nature,* 440**,** 165-173.

Dineley, D. 1958. A review of the Carboniferous and Permian rocks of the west coast of Vestspitsbergen. *Nors. Geolog. Tidsskr,* 38**,** 197-217.

Drever, J. I. 1994. The effect of land plants on weathering rates of silicate minerals. *Geochimica et Cosmochimica Acta,* 58**,** 2325-2332.

Dulski, P. 2001. Reference Materials for Geochemical Studies: New Analytical Data by ICP-MS and Critical Discussion of Reference Values. *Geostandards Newsletter,* 25**,** 87-125.

Dungait, J. A., Hopkins, D. W., Gregory, A. S. & Whitmore, A. P. 2012. Soil organic matter turnover is governed by accessibility not recalcitrance. *Global Change Biology,* 18**,** 1781-1796.

Dümig, A., Smittenberg, R. and Kögel-Knabner, I., 2011. Concurrent evolution of organic and mineral components during initial soil development after retreat of the Damma glacier, Switzerland. Geoderma, 163(1), pp.83-94.

Dümig, A., Häusler, W., Steffens, M. and Kögel-Knabner, I., 2012. Clay fractions from a soil chronosequence after glacier retreat reveal the initial evolution of organo–mineral associations. Geochimica et Cosmochimica Acta, 85, pp.1-18.

Egli, M., Fitze, P. & Mirabella, A. 2001. Weathering and evolution of soils formed on granitic, glacial deposits: results from chronosequences of Swiss alpine environments. *CATENA,* 45**,** 19-47.

Ehleringer, J. R. 1991. 13C/12C fractionation and its utility in terrestrial plant studies. *Carbon isotope techniques,* 1**,** 187.

Epstein, H. E., Raynolds, M. K., Walker, D. A., Bhatt, U. S., Tucker, C. J. & Pinzon, J. E. 2012. Dynamics of aboveground phytomass of the circumpolar Arctic tundra during the past three decades. *Environmental Research Letters,* 7**,** 015506.

Espeby, B. 1990. Tracing the origin of natural waters in a glacial till slope during snowmelt. *Journal of Hydrology,* 118**,** 107-127.

Fabrizzi, K., Rice, C., Schlegel, A., Sweeney, D., Peterson, D. & Thompson, C. Effect of different management practices on soil carbon sequestration in Kansas. Third USDA Symposium on Greenhouse Gases and Carbon Sequestration in Agriculture and Forestry, 2005.

Fao, I. 2006. Working Group, WRB (2007). *World reference base for soil resources*.
Faure, G. & Mensing, T. M. 2005. *Isotopes: principles and applications*, John Wiley & Sons Inc.
Førland, E. J., Benestad, R., Hanssen-Bauer, I., Haugen, J. E. & Skaugen, T. E. 2012. Temperature and precipitation development at Svalbard 1900–2100. *Advances in Meteorology,* 2011.
Franzluebbers, A. J. & Follett, R. F. 2005. Greenhouse gas contributions and mitigation potential in agricultural regions of North America: Introduction. Elsevier.
Fuchs, M. Soil Organic Carbon Inventory and Permafrost Mapping in Tarfala Valley, Northern Sweden. A first estimation of the belowground soil organic carbon storage in a sub-arctic high alpine permafrost environment. AGU Fall Meeting Abstracts, 2013. 0697.
Grudd, H., Xe, Kan & Schneider, T. 1996. Air Temperature at Tarfala Research Station 1946-1995. *Geografiska Annaler. Series A, Physical Geography,* 78**,** 115-120.
Guay, K. C., Beck, P. S. A., Berner, L. T., Goetz, S. J., Baccini, A. & Buermann, W. 2014. Vegetation productivity patterns at high northern latitudes: a multi-sensor satellite data assessment. *Global Change Biology,* 20**,** 3147-3158.
Hambrey, M. J., Murray, T., Glasser, N. F., Hubbard, A., Hubbard, B., Stuart, G., Hansen, S. & Kohler, J. 2005. Structure and changing dynamics of a polythermal valley glacier on a centennial timescale: Midre Lovenbreen, Svalbard. *Journal of Geophysical Research-Earth Surface,* 110.
Hayes, J. 1993. Factors controlling 13C contents of sedimentary organic compounds: Principles and evidence. *Marine Geology,* 113**,** 111-125.
He, L. & Tang, Y. 2008. Soil development along primary succession sequences on moraines of Hailuogou Glacier, Gongga Mountain, Sichuan, China. *Catena,* 72**,** 259-269.
Hobbie, S. E. 1996. Temperature and plant species control over litter decomposition in Alaskan tundra. *Ecological Monographs,* 66**,** 503-522.
Hodkinson, I. D., Coulson, S. J., Harrison, J. & Webb, N. R. 2001. What a wonderful web they weave: spiders, nutrient capture and early ecosystem development in the high Arctic – some counter-intuitive ideas on community assembly. *Oikos,* 95**,** 349-352.
Hodkinson, I. D., Coulson, S. J. & Webb, N. R. 2003. Community assembly along proglacial chronosequences in the high Arctic: vegetation and soil development in north-west Svalbard. *Journal of Ecology,* 91**,** 651-663.
Holmlund, P. & Jansson, P. 2002. *Glaciological research at Tarfala research station*, Stockholms universitet.
Holmlund, P., Karl, Xe, N, W., Xf, Rn, Grudd, H., Xe & Kan 1996. Fifty Years of Mass Balance and Glacier Front Observations at the Tarfala Research Station. *Geografiska Annaler. Series A, Physical Geography,* 78**,** 105-114.
Jahn, A. 1991. Slow Soil Movement in Tarfala Valley, Kebnekaise Mountains, Swedish Lapland. *Geografiska Annaler. Series A, Physical Geography,* 73**,** 93-107.
Jansson, C., Espeby, B. & Jansson, P.-E. 2005. Preferential water flow in a glacial till soil. *Hydrology Research,* 36**,** 1-11.
Jenny, H. 1941. Factors of Soil Formation. *Soil Science,* 52**,** 415.
Kabala, C. & Zapart, J. 2012. Initial soil development and carbon accumulation on moraines of the rapidly retreating Werenskiold Glacier, SW Spitsbergen, Svalbard archipelago. *Geoderma,* 175–176**,** 9-20.
Kaiser, C., Meyer, H., Biasi, C., Rusalimova, O., Barsukov, P. & Richter, A. 2007. Conservation of soil organic matter through cryoturbation in arctic soils in Siberia. *Journal of Geophysical Research: Biogeosciences,* 112**,** n/a-n/a.

Karlén, W. 1973. Holocene glacier and climatic variations, Kebnekaise mountains, Swedish Lapland. *Geografiska Annaler. Series A. Physical Geography*, 29-63.

Karlsen, S., Elvebakk, A., Høgda, K. & Grydeland, T. 2014. Spatial and Temporal Variability in the Onset of the Growing Season on Svalbard, Arctic Norway — Measured by MODIS-NDVI Satellite Data. *Remote Sensing,* 6, 8088.

Kirschbaum, M. U. F. 2000. Will changes in soil organic carbon act as a positive or negative feedback on global warming? *Biogeochemistry,* 48, 21-51.

Kleber, M. & Johnson, M. G. 2010. Advances in understanding the molecular structure of soil organic matter: implications for interactions in the environment. *Advances in agronomy,* 106, 77-142.

Kleber, M., Sollins, P. & Sutton, R. 2007. A conceptual model of organo-mineral interactions in soils: self-assembly of organic molecular fragments into zonal structures on mineral surfaces. *Biogeochemistry,* 85, 9-24.

Koblet, T., Gärtner-Roer, I., Zemp, M., Jansson, P., Thee, P., Haeberli, W. & Holmlund, P. 2010. Reanalysis of multi-temporal aerial images of Storglaciären, Sweden (1959–99) – Part 1: Determination of length, area, and volume changes. *The Cryosphere,* 4, 333-343.

Lalonde, K., Mucci, A., Ouellet, A. and Gélinas, Y., 2012. Preservation of organic matter in sediments promoted by iron. Nature, 483(7388), pp.198-200.

Lal, R. 2008. Carbon sequestration. *Philosophical Transactions of the Royal Society B: Biological Sciences,* 363, 815-830.

Lehmann, J. & Kleber, M. 2015. The contentious nature of soil organic matter. *Nature,* 528, 60-68.

Lutz, S., Anesio, A. M., Field, K. & Benning, L. G. 2015. Integrated 'Omics', Targeted Metabolite and Single-cell Analyses of Arctic Snow Algae Functionality and Adaptability. *Frontiers in Microbiology,* 6.

Mavris, C., Egli, M., Plotze, M., Blum, J. D., Mirabella, A., Giaccai, D. & Haeberli, W. 2010. Initial stages of weathering and soil formation in the Morteratsch proglacial area (Upper Engadine, Switzerland). *Geoderma,* 155, 359-371.

O'leary, M. H. 1981. Carbon isotope fractionation in plants. *Phytochemistry,* 20, 553-567.

O'leary, M. H. 1988. Carbon isotopes in photosynthesis. *Bioscience,* 38, 328-336.

Oliva, P., Viers, J. & Dupré, B. 2003. Chemical weathering in granitic environments. *Chemical Geology,* 202, 225-256.

Peay, K. G., Kennedy, P. G. & Talbot, J. M. 2016. Dimensions of biodiversity in the Earth mycobiome. *Nat Rev Micro,* 14, 434-447.

Petsch, S. T., Berner, R. A. & Eglinton, T. I. 2000. A field study of the chemical weathering of ancient sedimentary organic matter. *Organic Geochemistry,* 31, 475-487.

Pires, C., Schaefer, C., Hashigushi, A., Thomazini, A. & Mendonça, E. 2017. Soil organic carbon and nitrogen pools drive soil C-CO2 emissions from selected soils in Maritime Antarctica. *Science of The Total Environment,* 596, 124-135.

Post, W. M. & Kwon, K. C. 2000. Soil carbon sequestration and land-use change: processes and potential. *Global Change Biology,* 6, 317-327.

Poulton, S. W. & Canfield, D. E. 2005. Development of a sequential extraction procedure for iron: Implications for iron partitioning in continentally derived particulates. *Chemical Geology,* 214, 209-221.

Raiswell, R., Vu, H. P., Brinza, L. & Benning, L. G. 2010. The determination of labile Fe in ferrihydrite by ascorbic acid extraction: Methodology, dissolution kinetics and loss of solubility with age and de-watering. *Chemical Geology,* 278, 70-79.

Rime, T., Hartmann, M., Stierli, B., Anesio, A. M. & Frey, B. 2016. Assimilation of microbial and plant carbon by active prokaryotic and fungal populations in glacial forefields. *Soil Biology and Biochemistry,* 98**,** 30-41.

Ritchie, M. E., Tilman, D. & Knops, J. M. 1998. Herbivore effects on plant and nitrogen dynamics in oak savanna. *Ecology,* 79**,** 165-177.

Robinson, C., Wookey, P., Parsons, A., Potter, J., Callaghan, T., Lee, J., Press, M. & Welker, J. 1995. Responses of plant litter decomposition and nitrogen mineralisation to simulated environmental change in a high arctic polar semi-desert and a subarctic dwarf shrub heath. *Oikos***,** 503-512.

Schlesinger, W. H. & Andrews, J. A. 2000. Soil respiration and the global carbon cycle. *Biogeochemistry,* 48**,** 7-20.

Schmidt, M. W., Torn, M. S., Abiven, S., Dittmar, T., Guggenberger, G., Janssens, I. A., Kleber, M., Kögel-Knabner, I., Lehmann, J. & Manning, D. A. 2011. Persistence of soil organic matter as an ecosystem property. *Nature,* 478**,** 49-56.

Schrumpf, M., Kaiser, K., Guggenberger, G., Persson, T., Kögel-Knabner, I. & Schulze, E.-D. 2013. Storage and stability of organic carbon in soils as related to depth, occlusion within aggregates, and attachment to minerals. *Biogeosciences,* 10**,** 1675-1691.

Schuur, E., Mcguire, A., Schädel, C., Grosse, G., Harden, J., Hayes, D., Hugelius, G., Koven, C., Kuhry, P. & Lawrence, D. 2015. Climate change and the permafrost carbon feedback. *Nature,* 520**,** 171-179.

Schuur, E. A., Bockheim, J., Canadell, J. G., Euskirchen, E., Field, C. B., Goryachkin, S. V., Hagemann, S., Kuhry, P., Lafleur, P. M. & Lee, H. 2008. Vulnerability of permafrost carbon to climate change: Implications for the global carbon cycle. *BioScience,* 58**,** 701-714.

Schuur, E. A., Vogel, J. G., Crummer, K. G., Lee, H., Sickman, J. O. & Osterkamp, T. 2009. The effect of permafrost thaw on old carbon release and net carbon exchange from tundra. *Nature,* 459**,** 556-559.

Serreze, M. C. & Barry, R. G. 2011. Processes and impacts of Arctic amplification: A research synthesis. *Global and Planetary Change,* 77**,** 85-96.

Six, J., Conant, R., Paul, E. A. & Paustian, K. 2002. Stabilization mechanisms of soil organic matter: implications for C-saturation of soils. *Plant and soil,* 241**,** 155-176.

Smittenberg, R. H., Gierga, M., Göransson, H., Christl, I., Farinotti, D. & Bernasconi, S. M. 2012. Climate-sensitive ecosystem carbon dynamics along the soil chronosequence of the Damma glacier forefield, Switzerland. *Global Change Biology,* 18**,** 1941-1955.

Spiker, E. C. & Hatcher, P. G. 1984. Carbon isotope fractionation of sapropelic organic matter during early diagenesis. *Organic Geochemistry,* 5**,** 283-290.

Stockmann, U., Adams, M. A., Crawford, J. W., Field, D. J., Henakaarchchi, N., Jenkins, M., Minasny, B., Mcbratney, A. B., De Courcelles, V. D. R. & Singh, K. 2013. The knowns, known unknowns and unknowns of sequestration of soil organic carbon. *Agriculture, Ecosystems & Environment,* 164**,** 80-99.

Stork, A. 1963. Plant Immigration in front of Retreating Glaciers, with Examples from the Kebnekajse Area, Northern Sweden. *Geografiska Annaler,* 45**,** 1-22.

Tisdall, J. M. & Oades, J. M. 1982. Organic matter and water-stable aggregates in soils. *Journal of Soil Science,* 33**,** 141-163.

Tranter, M. & Wadham, J. L. 2014. 7.5 - Geochemical Weathering in Glacial and Proglacial Environments. *In:* TUREKIAN, H. D. H. K. (ed.) *Treatise on Geochemistry (Second Edition).* Oxford: Elsevier.

Viereck, L. A. 1966. Plant Succession and Soil Development on Gravel Outwash of the Muldrow Glacier, Alaska. *Ecological Monographs,* 36**,** 182-199.

Vodyanitskii, Y. N. & Shoba, S. 2016. Ferrihydrite in soils. *Eurasian Soil Science,* 49**,** 796-806.

Wagai, R. and Mayer, L.M., 2007. Sorptive stabilization of organic matter in soils by hydrous iron oxides. Geochimica et Cosmochimica Acta, 71(1), pp.25-35.

White, D. M., Hodkinson, I. D., Seelen, S. J. & Coulson, S. J. 2007. Characterization of soil carbon from a Svalbard glacier-retreat chronosequence using pyrolysis–GC/MS analysis. *Journal of Analytical and Applied Pyrolysis,* 78**,** 70-75.

Ziegler, H. & Lüttge, U. 1998. Carbon Isotope Discrimination in Cyanobacteria of Rocks of Inselbergs and Soils of Savannas in the Neotropics*. *Botanica Acta,* 111**,** 212-215.

Chapter 6. Outlook and Work in Progress

This thesis delves into a newly emerging area of research: soil formation in currently understudied Arctic glacial forefields. Newly deglaciated areas in the Arctic are temperature sensitive landscapes that are important to study. As shown in this thesis, depending on their mineralogy and organic carbon state, such new soils can act as potential atmospheric CO_2 sinks or sources. Understanding such processes are crucial since CO_2 is intrinsically linked to the earth's climate that is currently undergoing unprecedented changes. Furthermore, the work in this thesis has revealed that as crustal inorganic carbon depletes as a function of moraine age, organic carbon accumulates. The balance between these biogeochemically controlled atmospheric CO_2 sinks and sources need further work to determine if they counteract one another. Based on the results from this study a simple comparison is possible but caution should be taken as these biogeochemical reactions may vary both spatially, i.e. depth within the soil and glacial till profile amongst other less accessible, re-worked areas of the forefield, but also temporally. The sampling methodology used in this thesis provides a snapshot in time, therefore, seasonal and diurnal changes have invariably been overlooked.

This work has also highlighted that to gain further insight into chemical weathering and soil forming processes in forefields, it is important to investigate glacial forefields and the soils that form there in various and different environments and locations. Like any other landscape where soils form, glacial forefields' soil formation obeys the first principle of soil-forming factors that were formulated first by Hans Jenny in 1941. He showed that difference in climate, biota, topography, parent material, time and management result in differences in a forefields soils development and in turn in their inorganic and organic carbon dynamics.

On the other hand, unlike carbonate and silicate mineral weathering, no Arctic glacial forefield studies have been conducted that quantify short-term, seasonal changes, in soil organic carbon dynamics. This is a concern, since this study (as with many other Arctic forefield studies) only provides a snapshot of the real evolution of a possibly highly dynamic soil organic carbon pool. Soil organic carbon, and associated soil organic matter, have been shown in non-Arctic polar environments to respond to diurnal and seasonal biotic changes induced by seasonal warming and cooling. That said, the results from this study combined with those from White et al., (2007) tend to suggest that Arctic forefield soil development is progressively a stable carbon

sink. This is evidenced by the profiles of soil organic carbon, which accumulated due a complex cascade of predominantly climatic and biotic related carbon stabilization processes. In any case, to validate this interpretation, new studies in Arctic glacial forefield settings are needed, akin to those conducted in many European studies. These have successfully measured short-term and highly variable temporal changes in soil and ecosystem organic carbon dynamics in response to soil forming and ecosystem factors. Measurements *in-situ*, and in the laboratory, could be useful for determining the residence time of soil organic carbon in Arctic forefields. Such soil CO_2 emission data could come from ^{14}C isotopic labelled tracers, the use of CO_2 gas chambers to measure the soils CO_2 flux, or dissolved organic, inorganic carbon soil pore water measurements and the speciation of soil organic compounds.

There is limited evidence to support organo-mineral interactions and soil organic carbon stabilization, and these results were also supported by the lack of pedogenic clay, and highly reactive iron phase formation and the low degree of chemical weathering of the silicate mineral fractions. The lack of empirical relationships between soil organic carbon and highly reactive iron phases that may sorb organic carbon, could result from the fact that in this study the TOC and iron phase chemistry values of the <2 mm soil fraction were used. Organic carbon is often preferentially retained in, or sorbed to, clay and iron mineral surfaces in silt sized particles (a size which often contains the highest abundance of reactive iron phases). Consequently, empirical relationships between organic carbon and such minerals may have been masked. Future studies should look for organo-mineral relationships in the particle size range of clay and silt in particular. This would require particle size fractionation, and a separation step that was outside the scope of this study.

The use of chemical weathering indices revealed that weathering was limited to lower levels than the background variability of the parent material, glacial till. Yet, very low levels of silicate weathering are likely to occur due to the presence pioneer species: endolithic lichens, and vascular plant with rhizosphere root networks, which suggests localised bio-mining nutrient acquisition is occurring to enable their metabolic processes. Microscopic analyses such as XPS microprobe, or scanning electron microscopy of silicates mineral surfaces, may elucidate the extent of localised elemental and mineralogical chemical weathering-induced changes. Data that may be important for understanding the indirect effects of silicate-based nutrient release for kick-starting soil and ecosystem development, and their role in the carbon cycle.

Future Arctic forefield-based soil studies would benefit from the collection of soil bulk densities, where possible, in addition to specific surface area analyses and particle and grain-size of fractions less than <2 mm. Firstly, bulk density could be used as an independent measure of chemical weathering and is useful for upscaling. Secondly, normalization to either bulk density or initial BET specific surface area would allow a better comparison of forefield field and laboratory studies. This would allow measurement of soil silicate chemical weathering rates that have slow reaction kinetics compared to say, carbonate and sulfide minerals. Finally, as mineral reactivity is strongly controlled by its specific surface area, to reveal subtle mineral changes by chemical weathering in heterogeneous mineral mixtures such as glacial till metasediments, smaller particle and grain sizes such as those in silt and clay fractions should be analysed. Interestingly, the results of grain size fractionation, < 2 mm, and parent material 2-7 mm and >7 mm from subglacial-till-forming soils, all show clear TS and TIC trends as a function of moraine age. This provided evidence of the extent of SOCD sulfide and carbonate depletion in this till type. Future studies evaluating SOCD in subglacial till may therefore benefit from testing a wide range of grain sizes depending on the research question.

The thesis highlighted that additional work was carried out as a collaborator on two other papers during my PhD as follows;

One study was done with colleagues at the Institute of Biology at the University of Leeds. This work has recently been published in the *New Phytologist* with the authors and title being: *Galloway, A. F., Pedersen, M. J., Merry, B., Marcus, S. E.,* ***Blacker, J.,*** *Benning, L. G., Field, K. J. and Knox, J. P. (2018), Xyloglucan is released by plants and promotes soil particle aggregation. New Phytol, 217: 1128–1136. doi:10.1111/nph.14897.*

In this work, we investigated the role of polysaccharide plant secretion in soil particle aggregation. We found that at old moraine ages, Xyloglucan was secreted by plants and this ‘glued’ together soil particles, indicating that indeed there is a possible form of organic carbon stabilization. This mechanism of soil particle aggregation may facilitate stable aggregate formation, albeit this may be more of a transient stabilization mechanism, which would protect organic carbon contained within soil aggregates. Such carbon-based “glue” can, however, be lost via the formation of water-dispersible aggregates which leads to the internal organic carbon protection to cease.

The other study was done with colleagues at the Faculty of Geography at the University of Bristol. This work has been published in the journal *Biogeosciences* with the authors and title being: *Bradley, J.A., Arndt, S., Sabacká, M., Benning, L.G., Barker, G.L.,* ***Blacker, J.J.,*** *Yallop, M.L., Wright, K.E., Bellas, C.M., Telling, J. and Tranter, M., 2016. Microbial dynamics in a High Arctic glacier forefield: a combined field, laboratory, and modelling approach. Biogeosciences, 13(19), p.5677.*

In this work, we investigated soil development following glacier retreat. The soil's development was characterized using a novel integrated field, laboratory and modelling approach in Svalbard. We found community shifts in bacteria which were responsible for driving cycles in carbon and nutrients. Allochthonous inputs were also important in sustaining bacterial production. This study showed how an integrated model–data approach can improve understanding and obtain a more holistic picture of soil development in an increasingly ice-free future world.

Chapter 7. Conclusion

This thesis describes the work carried out to test the hypothesis, aims and objectives in Chapter 1. Section 1.2.

Few Arctic forefields have been studied previously for their role in soil formation and in the carbon cycle. The complementary sets of data collected and analysed during this thesis provide a new European pan-Arctic insight into soil forming processes, chemical weathering and organic carbon dynamics in response to deglaciation in newly emergent forefields. Two of the Arctic glacial forefields studied were in the sub-Arctic, Swedish Lapland (67°N; Storglaciären and Rabot's glacier), which are more akin to lower latitude Alpine environments. These were contrasted to the High-Arctic, Midtre Lovénbreen forefield, on the Norwegian archipelago, Svalbard (79°N).

The strength of this work lies in the combined, and complementary, use of bulk chemical and mineralogical techniques, with the addition of elemental and isotopic, inorganic and organic, carbon analyses and a range of *in-situ* ancillary soil measurements. Furthermore, the large size and number of soil samples obtained (ML = 193, ST = 40 and RB = 17) enabled capture of surficial soil compositions in each forefield that were statistically significant and representative of the soil forming processes in it. In addition, the methodological trial of sampling of either, supra- or subglacial tills, as transects led to the clear distinction of chemical and mineralogical gradient trends in primarily subglacial tills. This is an interesting finding, since other studies have previously overlooked till type differentiation when sampling. Yet, this approach was particularly advantageous for revealing chemical gradients in these forefields' soils that form in a dynamic environment, from multi-provenance heterogeneous glacial tills. However, it was evident that soil and till compositional heterogeneities may still mask extremely subtle chemical gradient changes with time, as only very limited silicate weathering was evidenced. The forefields selected for study also benefited from a wealth of existing soil related literature to draw on where such knowledge for Arctic forefields is currently sparse. Also, each had their own unique geographical setting with soil forming over similar timescales, ideal for a comparative study. Overall, this somewhat holistic approach, allowed the evaluation of empirical relationships with multitude of variables, to test the defined hypothesis and develop a more confident interpretation of the study results.

In the Midtre Lovénbreen forefield, compositional changes of bulk soil chemistries were studied as a function of age. These were dominated by a depletion in TS and TIC associated with accessory sulfides and carbonates. This depletion was a result of sulfide oxidation coupled to carbonate dissolution. The finding was also validated by a multitude of inter-annual independent soil samples, and its parent material measurements, that supported one another. Stoichiometric mass balance calculations showed that soil TS and TIC contents matched the predicted reaction stoichiometry of SOCD sulfide oxidation coupled to carbonate dissolution. This result agreed with the presence of often relatively high iron oxide concentrations, a product of iron sulfide oxidation, at young to old moraine ages. This is in addition to the relative abundance of microbial sulfur and iron oxidisers in soils, which were most prevalent at young moraine ages. A decrease in soil pH with moraine age, resulting from acid-base neutralisation of soil sulfides and carbonate, SOCD weathering, dominated the soil samples. Again, this is an important finding, since this reaction is a potential transient release of sedimentary carbon to the atmosphere, as sulfate has a long residence time (10M y) relative to Ca^{2+} (1M y) in the ocean.

Compared to the important sulfide and carbonate changes observed, limited evidence for silicate mineral weathering was found in all forefields except in the oldest exposed soils. This result is significant as weathering of calcium and magnesium silicates by acid would produce a net decrease in atmospheric CO_2 levels in the long term. The bulk chemical compositional changes shown by the variations in chemical indices of alteration (CIA etc.) showed no relationship with soil development or moraine age. Instead, bulk soil CIA values remained at a constant value. This result was concurrent with little soil change in mineralogical compositional trends. Plotting ternary diagrams, the soils, and their parent material fractions and source rocks, revealed stoichiometric changes in mobile and immobile elemental oxide that could be interpreted as a product of chemical weathering. Nevertheless, these soils' elemental chemical changes were not related to a true chemical weathering, rather they reflected variations (and sorting) in the metasedimentary source rocks and parent materials. These trends support the fact that silicate weathering was limited over the century of sampled Arctic soil transects. These results corroborate that such incipient soils in Arctic settings do not contribute substantially as an atmospheric CO_2 sink through silicate weathering.

Despite the absence of evidence for major chemical silicate weathering, when assessing the fate of the carbon and nutrient stocks in these newly formed soils, the data revealed that the

total organic carbon, and thus the soil organic carbon accumulation, occurred as a linear function of time. Stable carbon isotopes $\delta^{13}C_{org}$ revealed that the principal drivers of accumulation was modern photosynthetic C3 plant carbon added to the near-surface bulk soil. This suggests that developing Arctic forefield soils initiate progressive storage of carbon-based photosynthetic biomass on the long-term. It should be also mentioned that in the forefield of Midtre Lovénbreen, organic carbon was present in the youngest samples, yet this carbon was due to residual rock kerogen in the soils parent material. This was evidenced by the low $\delta^{13}C_{org}$ (-18.7 ‰) isotopic signature that is typical of kerogen. Consequently, because negligible other soil organic carbon sources were found at young moraine ages, they are unlikely to be a sink of atmospheric CO_2.

In summary, in young subglacial till-based moraine soils the rapid depletion of accessory sulfide and carbonates minerals in the initial, and up to about 60 years of exposure, reflects widespread SOCD processes. This process clearly defines young forefield soils as a potential transient CO_2 source to the atmosphere. Since potential CO_2 sinks, namely calcium silicate mineral weathering and soil organic carbon accumulation, are retarded, and limited to the older moraine soils, this can be used to infer a slow evolutionary onset of autotrophic and heterotrophic microbial community colonization processes during the first centenary of new soil formation in Arctic forefields. A finding that agrees with Arctic forefield fauna and flora studies. Combining this new knowledge with information from other proglacial meltwater chemistries studies, shows that with increased glacial retreat, initial SOCD will predominate, and only later will silicate weathering take over, when primary sulfide and carbonate minerals are exhausted. Collectively, the results from the studies in this thesis suggest that Arctic warming-induced deglaciation causing the continual expansion of terrestrial landmasses has potential widespread implications for the carbon cycle. Extrapolating to the past, such processes are likely to have also dominated weathering, soil formation and thus CO_2 cycling during the many glacial–interglacial cycles that have waxed and waned throughout the Earth's history. For example, deglaciation since the last maximum (~ 20k years-ago) resulted in as much as ~ 28% of the Northern Hemisphere's emergence as ice-free land. In most rock, making-up vast cratons in the Northern Hemisphere, carbonate and sulfide minerals are common, as most lithologies are made up of low to medium grade metamorphic and metasedimentary rocks. Glacial till that is pre-processed (ground) during its subglacial transit, is inherently more reactive, and once deposited quickly in a forefield, its reaction kinetics can be sped up. This is compared to supraglacial settings where the weathering kinetics are much

slower. Although high-Arctic forefield ecosystem development is slow, relative to Alpine forefields, microbial communities at young moraine ages are primarily dominated by chemolithotrophs, that are specially adapted for iron sulfide-based metabolism and these may act as bio-enhancers for the weathering of these minerals in the early stages of soil formation post deglaciation.

Appendix A.

Table. A.1. International panel on climate change in Emissions scenarios

RCP 8.5 – High emissions: This RCP is consistent with a future with no policy changes to reduce emissions. It was developed by the International Institute for Applied System Analysis in Austria and is characterised by increasing greenhouse gas emissions that lead to high greenhouse gas concentrations over time. This future is consistent with: a) Three times today's CO2 emissions by 2100 b) rapid increase in methane emissions c) increased use of croplands and grassland which is driven by an increase in population d) a world population of 12 billion by 2100 e) lower rate of technology development f) heavy reliance on fossil fuels g) high energy intensity h) no implementation of climate policies.
RCP 2.6 – Low emissions: This RCP is developed by PBL Netherlands Environmental Assessment Agency. Here radiative forcing reaches 3.1 W/m^2 before it returns to 2.6 W/m^2 by 2100. To reach such forcing levels, ambitious greenhouse gas emissions reductions would be required over time. This future would require: a) declining use of oil b) low energy intensity c) a world population of 9 billion by year 2100 d) use of croplands increase due to bio-energy production e) more intensive animal husbandry f) methane emissions reduced by 40 per cent g) CO_2 emissions stay at today's level until 2020, then decline and become negative in 2100 h) CO_2 concentrations peak around 2050, followed by a modest decline to around 400 ppm by 2100.

Table. A.2. General biogeochemical reactions that contribute to the carbon cycle in glacial forefields.

Silicate weathering (CO_2 sink) $2CO_2 + 3H_2O + CaAl_2Si_2O_8 \rightarrow Ca^{+2} + 2HCO_3^- + Al_2SiO_5(OH_4)$ Eq. A.1. Draws down atmospheric CO_2 and reacts with water to produce carbonic acid (H_2CO_3) that reacts with anorthite. The products Ca^{+2} and 1 HCO_3^- ultimately precipitate as $CaCO_3$ that is then captured by diagenisis in the lithosphere and thus acting as CO_2 sink, exerting a negative feedback on a warming climate (Berner et al., 1983).
Sulfide oxidation (such as, pyrite) (acid production, enhances weathering rates) $4FeS_2 + 15O_2 + 14H_2O \rightarrow 4Fe^{3+} + 8H_2SO_4$ Eq. A.2. Typically, a microbial-meditated reaction that enhances weathering rates through the production of sulfuric acid. Occurs under anoxia using Fe^{3+} and NO_3^- as oxidizing agents.
Carbonate dissolution by sulfuric acid (derived from, Equation A.2.) (potential CO_2 source) $CaCO_3 + H_2SO_4 \rightarrow CO_2\,(g) + H_2O + Ca^{2+} + SO_4^{2-}$ Eq.A.3. $2CaCO_3 + H_2SO_4 \rightarrow 2Ca^{2+} + SO_4^{2-} + 2HCO_3$ Eq. A.4 $Ca^{2+} + 2CH_2O + SO_4^{2-} \rightarrow H_2S + 2HCO_3^- + Ca^{2+} \rightarrow H_2S + CaCO_3 + CO_2 + H_2O$ Eq. A.5 A high pCO_2 soil system above that of atmospheric levels <3.5 and subsequent soil CO_2 to the atmosphere may arise from the input of protons into the soil system, to give a short-lived reduction in pH. For example, when acidic snowmelts either or if localized acidity generation by lithological

sulfide oxidation is neutralized by carbonates. If open to the atmosphere CO_2 this can be an instantaneous CO_2 source to the atmosphere Eq. A.3. or if in soil solution it can be introduced to the hydrosphere and thus on the timescale of diagenetic carbonate formation one mole of HCO_3 is locked up as carbonate rock while the other can be potential released back into the atmosphere as CO_2 gas Eq. A.4. The CO_2 released from these reactions is balanced on the timescale of the sulfate residence time in the oceans (10^7) Eq. A.5 (Claypool et al., 1980). These scenarios are believed to be transient CO_2 source in other environments such as carbonate cave systems and continental shelves, but particularly in glacial-forefields, since when water inputs interact with highly chemically reactive subglacial rock flour within the soils parent material it has a great capacity for adsorbing protons. A soils pCO_2 (aq) can become higher, if soil pores and cavities have only limited opportunity for the solution to degas.

The importance of this reaction as a potential CO_2 source in various carbonate and sulfide containing lithology has been highlighted by Wadham et al., 2001; Wadham et al., 2007; Lerman et al., 2007; Torres et al., 2014; Hindshaw et al., 2016; Anderson et al., 2000 and recently reviewed in Martin, 2016.

The biological pump and soil carbonate precipitation (CO_2 sink)

$$2CO_2 + H_2O + CaCO_3 \rightleftarrows Ca^{2+} + 2HCO_{3\,(aq)}^- \qquad \text{Eq. A.6.}$$

$$2CO_2 + H_2O + CaCO_3 \rightleftarrows Ca^{2+} + 2CO_{2(g)} + H_2O \qquad \text{Eq. A.7.}$$

$$Ca^{2+} + 2HCO_3^- + \rightarrow CaCO_3 + \psi(CO_2 + H_2O) + (1- \psi)\,(CH_2O + O_2) \qquad \text{Eq. A.8.}$$

The reactions Eq. A.6. &A.7 can be a transient sink of CO_2 via the biological pump Eq. A.8. however, ultimately there is no net change. Note: in equation A.8 ψ is the fractional stoichiometry.

A Low-pCO_2 systems in soil pore spaces results in soil calcite precipitation and this is a short-term transient CO_2 sink that could impact the carbon cycle at short interglacial-glacial timescales (10^2 to 10^5yrs) thereafter it is carbon neutral (Martin, 2016).

Low-pCO_2 systems could be common in glacial environments when a large supply of reactive, comminuted rock is brought into contact with relatively pure water. The glacial forefield analogue is when large quantities of dilute supra glacial quick-flow meltwaters mix with sediment-laden delayed flow at the glacial-forefield interface during the melt season. Given these circumstances, the rate of proton consumption is greater than the rate of gaseous diffusion of CO_2 into solution, and (CO_2) (aq) remains below open-system values.

Organic carbon oxidation (CO_2 source)

$$CH_2O + O_2 \rightleftarrows H_2O + CO_2 \qquad \text{Eq. A.9}$$

Requires prevailing oxic conditions although oxidation is microbial-meditated under anoxic soil conditions, See Eq. 2.4 Note: CH_2O is the general formula for organic matter

Note: Grey boxes are potential CO_2 sinks (although in the case of carbonation of carbonates it is ultimately carbon neutral on glacial-interglacial timescales), blue boxes are potential CO_2 sources (although this depends on the fate of the sulfate with a general residence time of 10^7). The orange box is a potential non-carbon based proton source for mineral weathering. All aqueous carbon species readily interconvert depending on the prevailing environmental conditions.

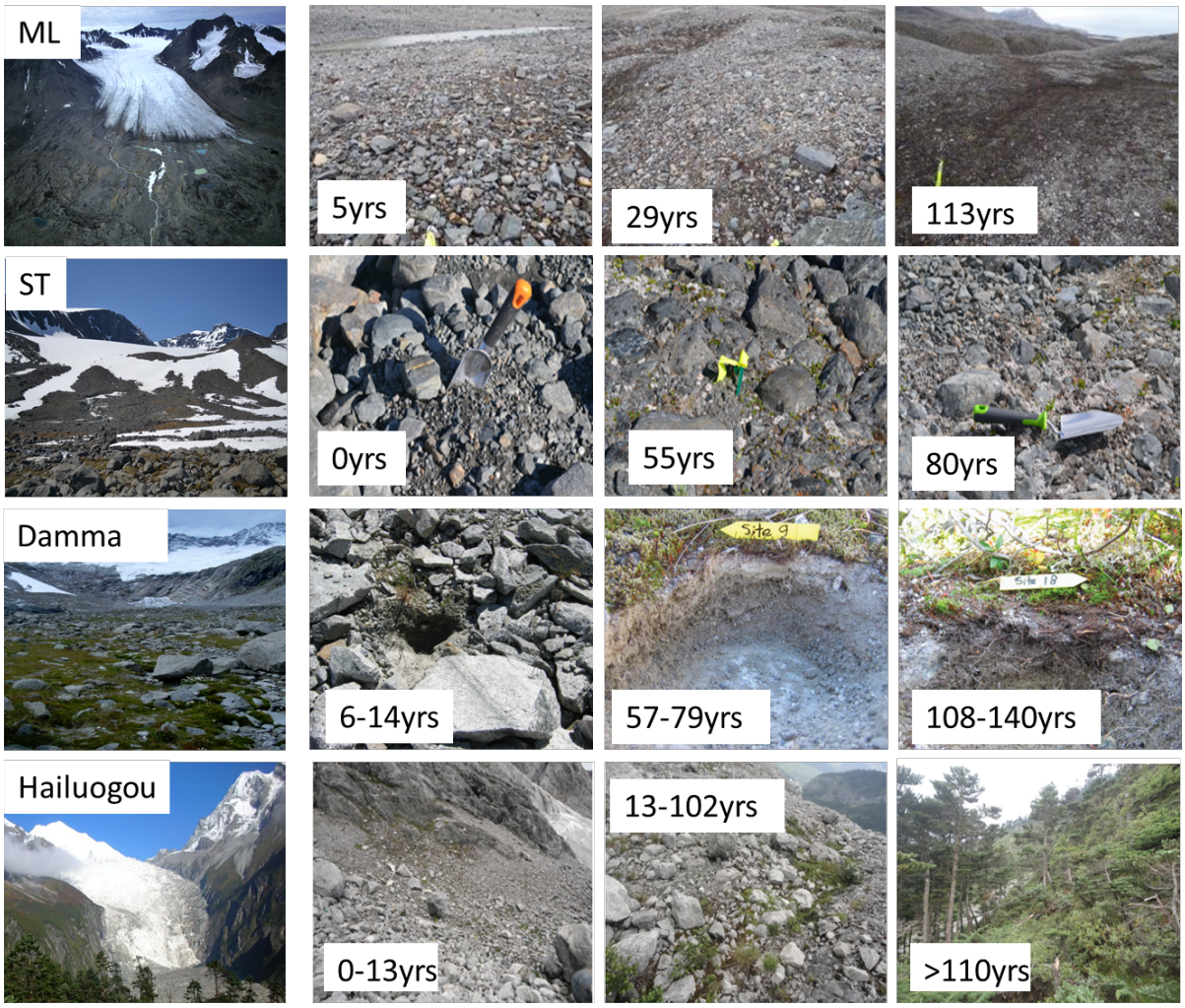

Figure. A.1. Photographic mosaic highlighting the contrast in vegetation types and extents at similar soil ages from forefields in different locale. Midtre Lovénbreen (ML) is high Arctic forefield, where vegetation is assemblage coverage is low until 113-years and species type present are of a low trophic level, mainly bryophytes, lichens and only dispersed vascular > 60 years. In Storglaciären forefield (ST) attributes are like Midtre Lovénbreen, however, vegetation coverage onset is sooner 27-years and the species diversity is greater. The Damma glacier, situated in the Swiss Alps, Europe has notable vascular plant assemble after roughly a decade and significant shrub coverage after half a century. Vegetation in the foreland of Hailuogou glacier, Tibetan Plateau, China is present as isolated pockets of shrubs and grass forbs as early as a decade of soil development, while at a >110-year-old site a pine forest is full established.

A.1. Critical evaluation of the formula used to calculate soil organic carbon stocks and a justification for the removal of extreme outliers

To calculate soil organic carbon, the following equation was used

$$SOC_{stocks} = C\rho d(1 - \mathrm{RM}) \qquad \text{Equation A.10.}$$

where SOC_{stock} denotes the org. C abundance (kg/m^2), C the organic C concentration (kg/t), d the thickness of layer the layer sampled (m), (RM) the mass proportion of rock fragments above >2mm and ρ = soil density (t/m^3). We use an average dry bulk density of glacier till of 1.4 g$^-$cm^3 in Midtre Lovénbreen (He and Lee, 2008) assuming a similar metasedimentary soil parent material and level of weathering over a century and 1.1 g$^-$cm^3 in Storglaciären and Rabot's (Fuchs, 2013) obtained from the same forefield (see, Chapter 2. section XX for details and SOC_{stock} sensitivity analysis Appendix B. Table.3). The term RM assumes the soil organic carbon resides within the <2mm fraction. In principle, this assumption is justified in some soils as their capacity to store organic C appears to be determined largely by its mass proportion of fine particles (Oades, 1988; Carter et al., 2003; Yang et al., 2016). Silt and particularly high charge surfaced clay minerals with a high specific surface area enhance organic carbon through sorption and aggregate formation (Oades, 1988). However, from plotting TOC g/kg as a function of RM it is observed that in Storglaciären this assumption unjustified as 40% of the mass proportion >2mm contains outlier high TOC values ranging from 2-6wt%. These values correspond to sites 27 and 80b-years-old. Vegetation micro niche communities consisting of moss carpets and grass forbs present at these ages (Fig. A.2) likely account for the high TOC values observed. Moss and grass material at these sites could be incorporated into the soil volume. In Rabot's glacier the extreme outlier observed at a site greater than 104-years-old (Fig. A.2.) owes to its soil type, a histosol and subsequently it is characterised by a high soil organic carbon content like the one observed. Site could be aged anywhere from 104 to 20,000-years-old, the last glacial maximum. The outliers from sites at Storglaciären 27 and 80b-years and Rabot's glacier, are statistically significantly different outliers, and therefore data analyses are conducted with their removal, however, analyse including these sites can be found in Appendices B and C.

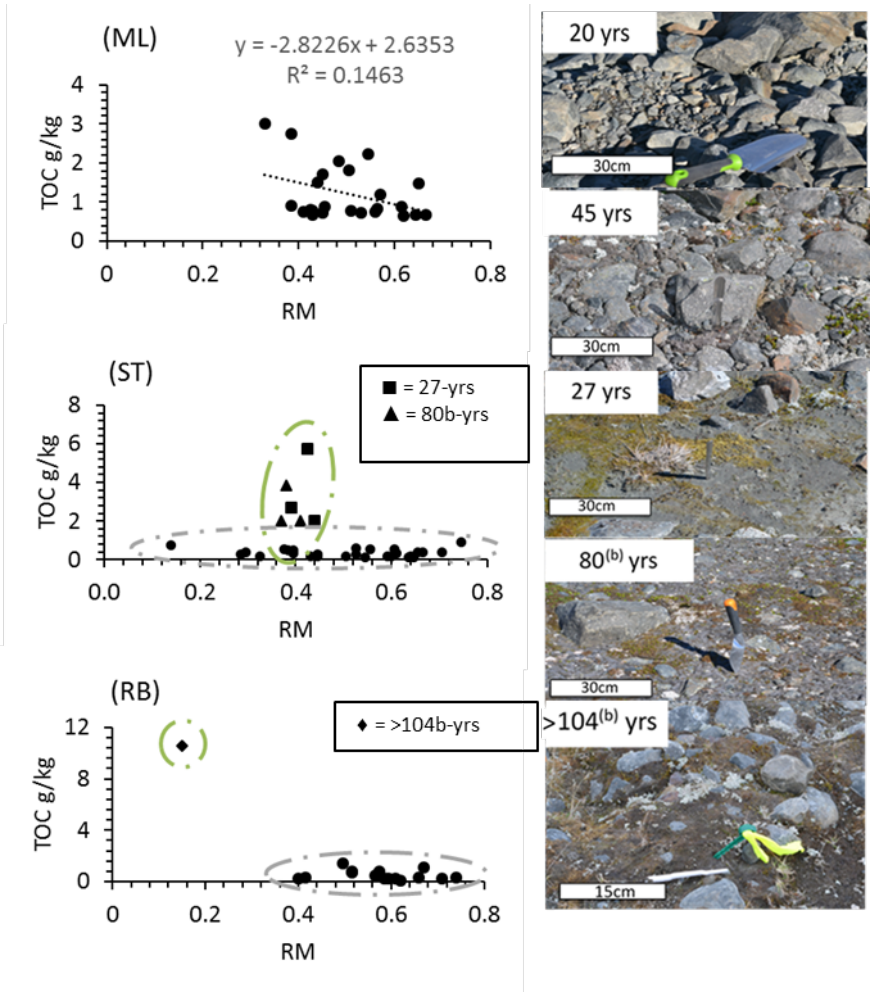

Figure. A.2. Total organic carbon as a function of the mass proportion of rock fragments >2mm in bulk soils at a depth of 0-15cm from Midtre Lovénbreen (ML), Storglaciären (ST) and Rabot's (RB) glacial forefields. The green circles delineate extreme outlier sites that correspond to sites 27 and 80b-years in ST and >104-years in Rabot's. These sites consisted of vegetation micro niche communities and a histosol soil type, observable in photographs on the right-hand-side, relative to other sites along the same transects, for instance sites 20 and 45-years in ST.

A.2. Geometric Surface Area

The particle size distribution data were used to calculate geometric surface areas for each grain size fraction (Table C.16) assuming that the particles were smooth spheres with a density of 1.6 g cm^{-3} using the formula

$$A_{GEOM,i} = 6 / \rho \, . \, d$$

Where $A_{GEOM,i}$ refers to the geometric surface area of the ith fraction (m^2/g); ρ stands for the density of the solid (g cm^{-3}) and; d_i represents the spherical diameter of the ith fraction(cm).

The $A_{GEOM,i}$ were then combined to generate a total geometric surface area A_{GEOM} for the bulk soil using

$$A_{GEOM} = \Sigma \, x_i \cdot A_{GEOM,i} /100$$

where x_i refers to the mass percentage of the ith fraction in whole sample

The results of the total geometric surface area A_{GEOM} are tabulated in Table A.3

Table A.3 Geometric surface area for the mass percentage of the grain size fractions 2mm, 2-7mm and 7mm

		Geometric Surface Area (m^2g^{-1})		
	Moraine age (years)	<2mm	2-7mm	>7mm
Tr1 (subglacial till)	0	0.3	0.5	0.7
	3	0.4	0.5	0.5
	5	0.4	0.3	0.8
	13	0.4	0.6	0.5
	29	0.3	0.7	0.4
	40	0.4	0.5	0.4
	50	0.4	0.5	0.5
	113	0.5	0.5	0.2
Tr2 (supraglacial till)	0	0.3	0.3	1.3
	5	0.2	0.2	1.5
	13	0.3	0.3	1.0
	29	0.2	0.3	1.6
	40	0.2	0.4	1.3
	50	0.2	0.3	1.5
	113	0.2	0.2	1.7

In the subglacial till the geometric surface areas at young moraine ages are generally greater in the 7mm grain size fraction than the <2mm and 2-7mm. With increasing moraine ages this trend becomes more evenly distributed and switches to smaller grain sizes have the highest geometric surface area. An increase in geometric surface area with a decrease in grain size would indicate physical weathering is occurring as a function of moraine age and soil formation. In contrast, the geometric surface areas in the supraglacial till was consistently highest in the largest 7mm grain size fraction. A result that would suggest a lack of physical weathering as function of moraine age. Since physical weathering is intrinsically to chemical weathering rates (White & Brantley, 2003), the increase in geometric surface area with moraine age observed agrees with evidenced low degree of chemical weathering in subglacial till, compared to the negligible degree in the supraglacial till.

Appendix B.

Table. B.1. pH, TS and TIC data for all the sampled soils from the field campaigns 2013 and 2015 in Midtre Lovénbreen plus δ^{13}C-TIC (‰) relative to VPDB data for Tr1

Sample no.	Grain size fraction	Moraine age	pH	Total Sulfur	Total Inorganic Carbon (TIC)	δ^{13}C–TIC
#	(mm)	(years)	#	(wt.%)	(wt.%)	(‰)
2013						
TR1						
Subglacial 0-15 cm						
S13.1.10.1.a	<7	0	8.5	0.141	0.36	-2.1
S13.1.10.2.a	<7	0	8.1	0.112	0.22	-2.1
S13.1.10.3.a	<7	0	8.4	0.207	0.28	-2
S13.1.11.1.a	<7	2	8	0.081	0.21	-1.3
S13.1.11.2.a	<7	2	8	0.083	0.26	-1.6
S13.1.11.3.a	<7	2	8.1	0.142	0.18	-1.4
S13.1.20.1.a	<7	3	8.2	0.137	0.2	-2
S13.1.20.2.a	<7	3	8.1	0.13	0.26	-2.2
S13.1.20.3.a	<7	3	8	0.117	0.25	-1.6
S13.1.30.1.a	<7	5	7.9	0.245	0.18	-1.9
S13.1.30.2.a	<7	5	7.7	0.114	0.23	-1.6
S13.1.30.3.a	<7	5	7.5	0.093	0.2	-1.5
S13.1.31.1.a	<7	13	7.9	0.076	0.17	-1.5
S13.1.31.2.a	<7	13	7.4	0.093	0.21	-1.5
S13.1.31.3.a	<7	13	7.5	0.104	0.18	-1
S13.1.32.1.a	<7	21	7.9	0.068	0.13	-1.1
S13.1.32.2.a	<7	21	8	0.079	0.13	-1.6
S13.1.32.3.a	<7	21	7.4	0.062	0.2	-0.2
S13.1.40.1.a	<7	29	7.5	0.095	0.12	-1.9
S13.1.40.2.a	<7	29	7.5	0.057	0.29	1.7
S13.1.40.3.a	<7	29	7.5	0.048	0.15	-0.9
S13.1.41.1.a	<7	40	7.7	0.118	0.25	-0.9
S13.1.41.2.a	<7	40	7.3	0.105	0.21	-1.8
S13.1.41.3.a	<7	40	7.6	0.141	0.25	-2
S13.1.50.1.a	<7	50	7	0.053	0.13	-0.9
S13.1.50.2.a	<7	50	7.2	0.076	0.09	-1.7
S13.1.50.3.a	<7	50	7.3	0.104	0.08	-1.4
S13.1.60.1.a	<7	113	7	0.059	0.12	-1.3
S13.1.60.2.a	<7	113	7	0.046	0.14	-1.3
S13.1.60.3.a	<7	113	7.1	0.033	0.14	-1.5

TR1						
Subglacial						
15-30 cm						
S13.1.10.1.b	<7	0	7.9	0.193	0.37	-
S13.1.10.2.b	<7	0	7.6	0.158	0.65	-
S13.1.10.3.b	<7	0	7.6	0.133	0.44	-
S13.1.11.1.b	<7	2	8	0.102	0.33	-
S13.1.11.2.b	<7	2	8.1	0.137	0.28	-
S13.1.11.3.b	<7	2	7.9	0.117	0.27	-
S13.1.20.1.b	<7	3	7.6	0.139	0.29	-
S13.1.20.2.b	<7	3	8	0.141	0.45	-
S13.1.20.3.b	<7	3	7.8	0.196	0.33	-
S13.1.30.1.b	<7	5	8	0.119	0.17	-
S13.1.30.2.b	<7	5	7.8	0.115	0.19	-
S13.1.30.3.b	<7	5	7.5	0.107	0.3	-
S13.1.31.1.b	<7	13	7.4	0.074	0.22	-
S13.1.31.2.b	<7	13	7.6	0.09	0.24	-
S13.1.31.3.b	<7	13	7.8	0.066	0.2	-
S13.1.32.1.b	<7	21	7.8	0.041	0.19	-
S13.1.32.2.b	<7	21	7.3	0.035	0.2	-
S13.1.32.3.b	<7	21	7.4	0.085	0.26	-
S13.1.40.1.b	<7	29	7.6	0.052	0.2	-
S13.1.40.2.b	<7	29	7.5	0.045	0.18	-
S13.1.40.3.b	<7	29	7.8	0.037	0.2	-
S13.1.41.1.b	<7	40	7.3	0.142	0.23	-
S13.1.41.2.b	<7	40	7.2	0.144	0.25	-
S13.1.41.3.b	<7	40	7.2	0.055	0.34	-
S13.1.50.1.b	<7	50	7.5	0.073	0.22	-
S13.1.50.2.b	<7	50	7.4	0.058	0.24	-
S13.1.50.3.b	<7	50	7.2	0.044	0.2	-
S13.1.60.1.b	<7	113	7	0.049	0.22	-
S13.1.60.2.b	<7	113	7.2	0.053	0.26	-
S13.1.60.3.b	<7	113	6.9	0.069	0.2	-
TR2						
Supraglacial						
0-15 cm						
S13.2.10.1.a	<7	0	7	0.172	0.27	-
S13.2.10.2.a	<7	0	7.5	0.167	0.26	-
S13.2.10.3.a	<7	0	7.5	0.146	0.37	-
S13.2.11.1.a	<7	2	8.2	0.123	0.32	-
S13.2.11.2.a	<7	2	8.1	0.172	0.3	-
S13.2.11.3.a	<7	2	7.9	0.135	0.28	-
S13.2.20.1.a	<7	3	7.8	0.123	0.22	-
S13.2.20.2.a	<7	3	8	0.106	0.22	-

S13.2.20.3.a	<7	3	7.5	0.151	N/A	-
S13.2.30.1.a.	<7	5	7.7	0.058	0.37	-
S13.2.30.2.a.	<7	5	7.4	0.055	0.21	-
S13.2.30.3.a.	<7	5	7.8	0.052	0.13	-
S13.2.31.1.a	<7	13	7.7	0.132	0.28	-
S13.2.31.2.a	<7	13	7.2	0.036	0.32	-
S13.2.31.3.a	<7	13	7.6	0.105	0.39	-
S13.2.32.1.a	<7	21	7.5	0.112	0.15	-
S13.2.32.2.a	<7	21	7.7	0.067	0.26	-
S13.2.32.3.a	<7	21	7.8	0.083	N/A	-
S13.2.32.1.a	<7	25	7.3	N/A	0.25	-
S13.2.33.2.a	<7	25	7	N/A	0.16	-
S13.2.33.3.a	<7	25	7.4	N/A	N/A	-
S13.2.40.1.a	<7	29	7.5	N/A	N/A	-
S13.2.40.2.a	<7	29	7.1	0.088	0.1	-
S13.2.40.3.a	<7	29	7	0.101	0.17	-
S13.2.41.1.a	<7	40	7.2	0.132	0.22	-
S13.2.41.2.a	<7	40	7.1	0.094	0.24	-
S13.2.41.3.a	<7	40	7.1	0.096	N/A	-
S13.2.50.1.a	<7	50	7.3	N/A	0.18	-
S13.2.50.2.a	<7	50	7.1	0.043	0.26	-
S13.2.50.3.a	<7	50	7	0.042	N/A	-
S13.2.51.1.a	<7	73	7	N/A	0.28	-
S13.2.51.2.a	<7	73	6.9	0.081	0.19	-
S13.2.51.3.a	<7	73	7	0.079	0.34	-
S13.2.60.1.a	<7	113	7.2	0.085	0.3	-
S13.2.60.2.a	<7	113	6.8	0.07	0.27	-
S13.2.60.3.a	<7	113	6.7	0.075	0.47	-
S13.2.70.1.a	<7	~2000	7	0.085	1	-
S13.2.70.2.a	<7	~2000	6.3	0.079	1.19	-
S13.2.70.3.a	<7	~2000	6.4	0.09	0.94	-
TR2 Supraglacial 15-30 cm						
S13.2.10.1.b	<7	0	6.7	0.076	0.26	-
S13.2.10.2.b	<7	0	7.5	0.156	0.22	-
S13.2.10.3.b	<7	0	7.9	0.174	0.3	-
S13.2.11.1.b	<7	2	8	0.158	0.15	-
S13.2.11.2.b	<7	2	8.1	0.098	0.24	-
S13.2.11.3.b	<7	2	8	0.087	N/A	-
S13.2.20.1.b	<7	3	7.9	N/A	0.18	-
S13.2.20.2.b	<7	3	7.7	0.136	0.14	-
S13.2.20.3.b	<7	3	7.8	0.136	0.31	-
S13.2.30.1.b	<7	5	7.1	0.131	0.23	-

S13.2.30.2.b	<7	5	7	0.106	0.25	-
S13.2.30.3.b	<7	5	7.3	0.104	0.3	-
S13.2.31.1.b	<7	13	7.8	0.132	0.33	-
S13.2.31.2.b	<7	13	7.5	0.132	0.35	-
S13.2.31.3.b	<7	13	7.9	0.099	0.2	-
S13.2.32.1.b	<7	21	8	0.14	0.26	-
S13.2.32.2.b	<7	21	7.7	0.074	0.24	-
S13.2.32.3.b	<7	21	7.7	0.086	0.31	-
S13.2.33.1.b	<7	25	7.6	0.121	0.16	-
S13.2.33.2.b	<7	25	8	N/A	N/A	-
S13.2.33.3.b	<7	25	7.5	0.085	N/A	-
S13.2.40.1.b	<7	29	7.7	N/A	N/A	-
S13.2.40.2.b	<7	29	7.3	N/A	0.16	-
S13.2.40.3.b	<7	29	7.6	0.079	0.11	-
S13.2.41.1.b	<7	40	7.2	0.072	0.26	-
S13.2.41.2.b	<7	40	7	0.035	0.3	-
S13.2.41.1.b	<7	40	7.3	0.051	0.18	-
S13.2.60.1.b	<7	50	7.4	0.119	0.28	-
S13.2.60.2.b	<7	50	7.1	0.087	0.29	-
S13.2.60.3.b	<7	50	7	0.05	0.22	-
S13.2.50.1.b	<7	73	6.9	0.073	0.94	-
S13.2.50.2.b	<7	73	7	0.031	1.25	-
S13.2.50.3.b	<7	73	7	0.034	1.18	-
S13.2.51.1.b	<7	113	6.7	0.03	0.31	-
S13.2.51.2.b	<7	113	6.9	0.066	0.29	-
S13.2.51.3.b	<7	113	7	0.047	0.27	-
TR3						
Supraglacial						
0-15 cm						
S13.3.10.1.a	<7	0	7.1	0.079	0.31	-
S13.3.10.2.a	<7	0	8.1	0.119	0.37	-
S13.3.10.3.a	<7	0	8	0.124	0.28	-
S13.3.11.1.a	<7	2	7.8	0.111	0.01	-
S13.3.11.2.a	<7	2	8	0.148	0.47	-
S13.3.11.3.a	<7	2	8	0.109	0.17	-
S13.3.20.1.a	<7	3	8	0.052	0.32	-
S13.3.20.2.a	<7	3	7.8	0.16	0.28	-
S13.3.20.3.a	<7	3	8.2	0.093	0.3	-
S13.3.30.1.a	<7	5	7.8	0.107	0.32	-
S13.3.30.2.a	<7	5	7.7	0.037	0.18	-
S13.3.30.3.a	<7	5	7.9	0.062	0.18	-
S13.3.31.1.a	<7	13	8.1	0.137	0.29	-
S13.3.31.2.a	<7	13	8	0.118	0.3	-
S13.3.31.3.a	<7	13	8	0.064	0.36	-

S13.3.32.1.a	<7	21	7.7	0.092	0.44	-
S13.3.32.2.a	<7	21	7.9	0.116	0.4	-
S13.3.32.3.a	<7	21	7.9	0.081	0.14	-
S13.3.40.1.a	<7	29	8.1	0.079	0.35	-
S13.3.40.2.a	<7	29	7.4	0.112	0.21	-
S13.3.40.3.a	<7	29	7.5	0.124	0.27	-
S13.3.41.1.a	<7	40	7.1	0.145	0.47	-
S13.3.41.2.a	<7	40	7.4	0.084	0.56	-
S13.3.41.3.a	<7	40	7	0.121	0.35	-
S13.3.50.1.a	<7	50	7.3	0.108	0.16	-
S13.3.50.2.a	<7	50	7.4	0.06	0.21	-
S13.3.50.3.a	<7	50	7	0.055	0.38	-
S13.3.60.1.a	<7	113	7.2	0.108	0.44	-
S13.3.60.2.a	<7	113	6.9	0.048	0.74	-
S13.3.60.3.a	<7	113	7.1	0.041	0.97	-
TR3						
Supraglacial						
15-30 cm						
S13.3.10.1.b	<7	0	8.2	0	0.26	-
S13.3.10.2.b	<7	0	7.5	0.101	0.26	-
S13.3.10.3.b	<7	0	7.7	0.124	0.44	-
S13.3.11.1.b	<7	2	7.9	0.147	0.43	-
S13.3.11.2.b	<7	2	8	0.123	0.26	-
S13.3.11.3.b	<7	2	7.6	0.14	0.27	-
S13.3.20.1.b	<7	3	7.9	0.154	0.53	-
S13.3.20.2.b	<7	3	8.1	0.127	0.34	-
S13.3.20.3.b	<7	3	7.5	0.111	0.4	-
S13.3.30.1.b	<7	5	7.4	0.088	0.24	-
S13.3.30.2.b	<7	5	7.8	0.097	0.37	-
S13.3.30.3.b	<7	5	7.8	0.117	0.17	-
S13.3.31.1.b	<7	13	7.5	0.094	0.43	-
S13.3.31.2.b	<7	13	7.6	0.066	0.54	-
S13.3.31.3.b	<7	13	7.7	0.111	0.18	-
S13.3.32.1.b	<7	21	7.7	0.025	0.33	-
S13.3.32.2.b	<7	21	7.5	0.122	0.39	-
S13.3.32.3.b	<7	21	7.9	0.112	0.32	-
S13.3.40.1.b	<7	29	7.5	0.106	0.36	-
S13.3.40.2.b	<7	29	7.4	0.086	0.38	-
S13.3.40.3.b	<7	29	7.3	0.052	0.34	-
S13.3.41.1.b	<7	40	7	0.08	0.37	-
S13.3.41.2.b	<7	40	7	0.069	0.41	-
S13.3.41.3.b	<7	40	7.3	0.06	0.49	-
S13.3.50.1.b	<7	50	7.5	0.043	0.37	-
S13.3.50.2.b	<7	50	7.2	0.034	0.3	-

S13.3.50.3.b	<7	50	7	0.065	0.47	-
S13.3.60.1.b	<7	113	6.9	0.092	0.31	-
S13.3.60.2.b	<7	113	7	0.055	0.78	-
S13.3.60.3.b	<7	113	7	0.028	0.33	-
2015						
TR1						
Subglacial 0-15 cm						
S15.24	<2	0	8.2	0.092	0.15	
S15.27	<2	3	8	0.124	0.24	
S15.30	<2	5	7.6	0.095	0.23	
S15.33	<2	13	7.3	0.084	0.21	
S15.36	<2	29	7.4	0.071	0.22	
S15.39	<2	40	7.1	0.032	0.22	
S15.42	<2	50	7.1	0.054	0.11	
S15.45	<2	113	6.9	0.022	0.05	
S15.23	2-7	0	8	0.075	0.23	
S15.26	2-7	3	8.1	0.099	0.32	
S15.29	2-7	5	7.9	0.101	0.45	
S15.32	2-7	13	7.4	0.08	0.34	
S15.35	2-7	29	7.5	0.031	0.19	
S15.38	2-7	40	7.3	0.028	0.02	
S15.41	2-7	50	7.2	0.021	0.35	
S15.44	2-7	113	7.1	0.003	0.07	
S15.22	>7	0	8	0.049	1.64	
S15.25	>7	3	7.8	0.029	0.17	
S15.28	>7	5	7.7	0.032	0.79	
S15.31	>7	13	7.3	0.04	1.12	
S15.34	>7	29	7.3	0.031	0.23	
S15.37	>7	40	7.4	0.099	0.53	
S15.40	>7	50	7.2	0.018	0.28	
S15.43	>7	113	7.2	0.035	0.04	
TR2						
Supraglacial						
0-15 cm						
S15.3	<2	0	7.8	0.134	0.2	
S15.6	<2	5	7.9	0.122	0.16	
S15.9	<2	13	7	0.163	0.2	
S15.12	<2	29	7.6	0.065	0.13	
S15.15	<2	40	7.4	0.132	0.15	
S15.18	<2	50	7.5	0.082	0.4	
S15.21	<2	113	7.1	0.03	0.23	
S15.2	2-7	0	7.7	0.038	0.31	
S15.5	2-7	5	7.6	0.198	0.44	

S15.8	2-7	13	7.7	0.067	0.34
S15.11	2-7	29	7.5	0.034	0.49
S15.14	2-7	40	7.5	0.073	0.31
S15.17	2-7	50	7.2	0.079	0.36
S15.20	2-7	113	7.5	0.084	0.45
S15.1	>7	0	7.8	0.045	0.13
S15.4	>7	5	7.9	0.026	0.27
S15.7	>7	13	7.5	0.063	0.25
S15.10	>7	29	7.6	0.13	0.08
S15.13	>7	40	7.7	0.037	0.67
S15.16	>7	50	7.2	0.055	0.22
S15.19	>7	113	7.3	0.134	0.37

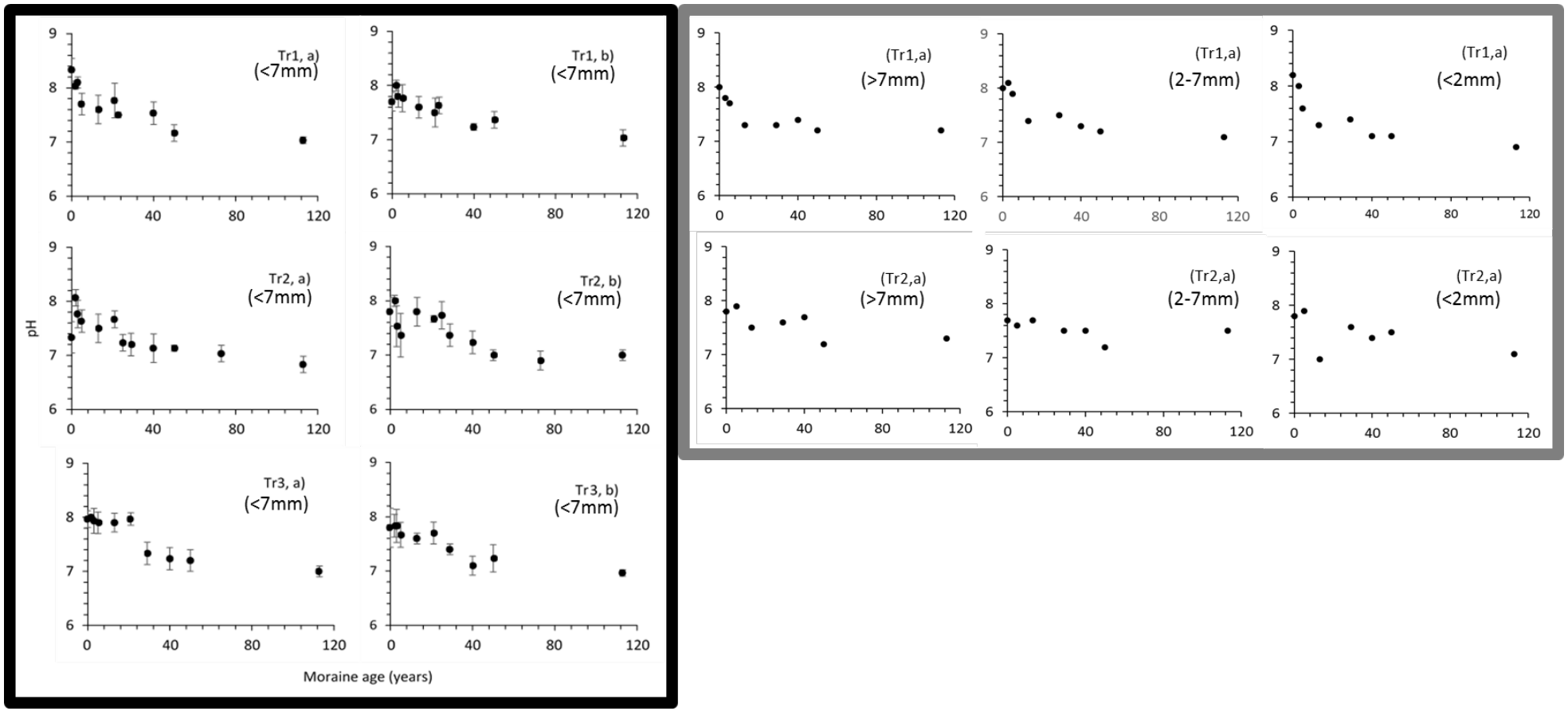

Figure. B.1. pH as a function of moraine age from the 2013 (black box) and 2015 (grey box) field season each transect and at both depths (a) 0-15cm and (b) 15-30cm and for grain size fractions <7, >7, 2-7, and <2mm. Symbols on the 2015 plots denote the $\bar{x}$ of three replicate pH values of samples collected at each moraine age along a 10-meter travers and bars repersent 1σ sd, while the symbols on the 2013 plots are indivual sampled site.

Table. B.2 TS and TIC (TC) precision and limit of detection

	TS (wt %)	TC (wt %)
	0.030	2.03
	0.027	2.04
	0.029	2.06
	0.030	2.04
	0.029	2.02
Mean	0.029	2.04
SD 1σ	0.001	0.01
95% confidence limit	0.002	0.02
Certified ref value	0.029± 0.004	2.02 ± 0.06
	0.030	2.06
	0.028	2.04
	0.031	2.03
	0.030	2.03
	0.028	2.00
Mean	0.029	2.03
SD 1σ	0.0012	0.02
95% confidence limit	0.0014	0.02
Certified ref value	0.029± 0.004	2.02 ± 0.06
	0.030	2.00
	0.028	1.97
	0.029	1.97
	0.030	1.98
	0.031	2.00
Mean	0.03	1.98
Sd 1σ	0.001	0.016
95% confidence limit	0.001	0.020
Certified ref value	0.029± 0.004	2.02 ± 0.06
	0.030	2.06
	0.028	2.03
	0.027	2.04
	0.028	2.09
	0.029	2.08
	0.030	2.10

Mean	0.029	2.07
SD 1σ	0.001	0.028
95% confidence limit	0.001	0.03
Certified ref value	0.029± 0.004	2.02 ± 0.06
Blank	0.0082	0.038
Blank	0.0061	0.029
Blank	0.0071	0.032
Blank	0.0081	0.027
Blank	0.0059	0.001
Blank	0.0003	0.001
Blank	0.0001	0.002
Blank	0.0001	0.022
Blank	0.0002	0.016
Blank	0.0010	0.018
SD 1σ	0.004	0.014
Mean	0.004	0.019
Limit of detection	0.01	0.06
Limit of quant	0.04	0.15

Note: Certified reference material was a soil (LECO#Pt. No. 502-620)

Table. B.3. Pyrite extraction data compared with those from total sulfur (TS) analyses

Sample no. #	Total Sulfur (wt. %)	Sulfur in Pyrite* (P) (wt. %)	TS - P (wt. %)
S13.1.10.1.a	0.141	0.124	0.016
S13.1.10.2.a	0.112	0.082	0.030
S13.1.11.1.a	0.081	0.071	0.010
S13.1.11.2.a	0.083	0.068	0.015
S13.1.31.1.a	0.076	0.070	0.005
S13.1.31.2.a	0.093	0.088	0.005
S13.1.50.3.a	0.104	0.091	0.013
S13.1.20.1.a	0.137	0.122	0.015
S13.1.20.2.a	0.130	0.094	0.036
S13.1.10.2.b	0.158	0.029	0.129
S13.1.10.3.b	0.133	0.068	0.065
S13.1.31.1.b	0.074	0.034	0.040
S13.1.31.2.b	0.090	0.107	-0.016
S13.1.31.3.b	0.066	0.050	0.015
replicates			
S13.1.11.3.a	0.104	0.076	0.028
S13.1.11.3.a	0.142	0.129	0.013
S13.1.11.3.a	0.128	0.120	0.009
S13.1.20.3.a	0.081	0.110	-0.029
S13.1.20.3.a	0.116	0.125	-0.009
S13.1.20.3.a	0.112	0.116	-0.004
S13.1.20.3.a	0.123	0.125	-0.003
S13.1.20.3.a	0.117	0.133	-0.016

Table. B.4. TS and TIC data for all source rocks collected in the 2015 field campaign, plus TIC-δ^{13}C (‰) relative to VPDB data for Tr1, depth (a).

Sample no.	Source rock	TS	TIC	δ^{13}C–TIC
#	#	(wt%)	(wt%)	(‰)
S15.47	Dolomite (1)	0.005	10.54	2.7
S15.48	Dolomite (2)	0.002	10.09	4.3
S15.52	Dolomite (3)	0.005	10.69	4.4
S15.50	Conglomerate	0.1	2.83	-1.8
S15.49	Sandstone	0.032	0.01	-0.1
S15.51	Psammite (1)	0.023	2.93	-2.4
S15.54	Psammite (2)	0.012	0.04	-3.1
S15.55	Psammite (3)	0.035	0.41	-10.6
S15.56	Mica schist (1)	0.03	0.12	-1.4
S15.46	Mica schist (2)	0.034	0.1	-1.4
S15.57	Phylite	0.026	0.12	-3.8

Table. B.5. Regression analyses and Pearson's r correlation coefficients for TS and TIC in the bulk soil as a function of moraine age in Midtre Lovénbreen at the depths 0-15 and 30cm from all transects sampled.

Variables (dep vs. indep.)	Transects (no.)	Depth (cm)	Regression model	Exponent (x^e)	R_2	*r* value	Critical *r* value	Sig. level (p value) (α)	*n*
TS vs. Moraine age	Tr1	0-15	exponential decay	-0.009	0.57	0.75	0.46	0.01	30
		15-30	exponential decay	-0.010	0.30	0.55	0.46	0.01	30
	Tr2	0-15	exponential decay	-0.005	0.20	0.45	0.45	0.01	32
		15-30	exponential decay	-0.009	0.54	0.73	0.45	0.01	32
	Tr3	0-15	exponential decay	-0.010	0.49	0.70	0.46	0.01	30
		15-30	exponential decay	-0.010	0.61	0.78	0.46	0.01	30
TIC vs. Moraine age	Tr1	0-15	exponential decay	-0.003	0.15	0.38	0.36	0.01	30
		15-30	exponential decay	-0.006	0.41	0.64	0.46	0.01	30
	Tr2	0-15	N/A	-	N/A	N/A	0.46	0.01	31
		15-30	N/A	-	N/A	N/A	0.45	0.01	32
	Tr3	0-15	N/A		N/A	N/A	0.46	0.01	30
		15-30	N/A	-	N/A	N/A	0.46	0.01	30

Note: df = *n*-2 and N/A represent no correlation

Table. B.6. Regression analyses and Pearson's r correlation coefficients for TS and TIC in separate grain size fractions as a function of moraine age in Midtre Lovénbreen from Tr1 and Tr2.

Variables (dep vs. indep.)	Transects (no.)	Grain size fraction (mm)	Regression model	Exponent (x^e)	R_2	*r* value	Critical *r* value	Sig. level (p value) (α)	*n*
TS vs. Moraine age	Tr1	<2	exponential decay	-0.014	0.83	0.91	0.83	0.01	8
		<2 - 7	exponential decay	-0.032	0.97	0.98	0.83	0.01	8
		>7	N/A	-	N/A	N/A	-	-	8
	Tr2	<2	N/A	-	N/A	N/A	-	-	7
		<2 - 7	N/A	-	N/A	N/A	-	-	7
		>7	N/A	-	N/A	N/A	-	-	7
TIC vs. Moraine age	Tr1	<2	exponential decay	-0.013	0.75	0.87	0.83	0.01	8
		<2 - 7	Linear	-	0.53	0.73	0.71	0.05	8
		>7	exponential decay	-0.024	0.60	0.77	0.71	0.05	8
	Tr2	<2	N/A	-	N/A	N/A	-	-	7
		<2 - 7	N/A	-	N/A	N/A	-	-	7
		>7	N/A	-	N/A	N/A	-	-	7

Note: df = *n*-2 and N/A represent no correlation

Table. B.7. A compassion of 2013 and 2015 TS and TIC till concentrations (wt%) from Tr1 and Tr2 at the depth 0-15cm.

				2013		2015	
Grain size fraction (mm)	Depth (cm)	Transect #	Moraine age (years)	TS (wt. %)	TIC (wt. %)	TS (wt. %)	TIC (wt. %)
<7mm	0-15	Tr1	0	0.153	0.46	0.063	0.13
<7mm	0-15	Tr1	3	0.128	0.36	0.091	0.22
<7mm	0-15	Tr1	5	0.151	0.22	0.068	0.20
<7mm	0-15	Tr1	13	0.091	0.25	0.067	0.22
<7mm	0-15	Tr1	29	0.066	0.32	0.044	0.18
<7mm	0-15	Tr1	40	0.121	0.29	0.026	0.12
<7mm	0-15	Tr1	50	0.077	0.18	0.034	0.16
<7mm	0-15	Tr1	113	0.046	0.22	0.014	0.05
<7mm	0-15	Tr2	0	0.162	0.3	0.051	0.12
<7mm	0-15	Tr2	5	0.055	0.24	0.064	0.11
<7mm	0-15	Tr2	13	0.091	0.14	0.082	0.15
<7mm	0-15	Tr2	29	0.094	0.14	0.02	0.12
<7mm	0-15	Tr2	40	0.107	0.23	0.054	0.12
<7mm	0-15	Tr2	50	0.042	0.24	0.034	0.16
<7mm	0-15	Tr2	113	0.077	0.35	0.017	0.10

NOTE: The TS and TIC from 2013 is from the till sieved to <7mm while these concentrations from the 2015 samples are the weighted average concentration from the <2mm + 2-7mm that derives the <7mm fraction.

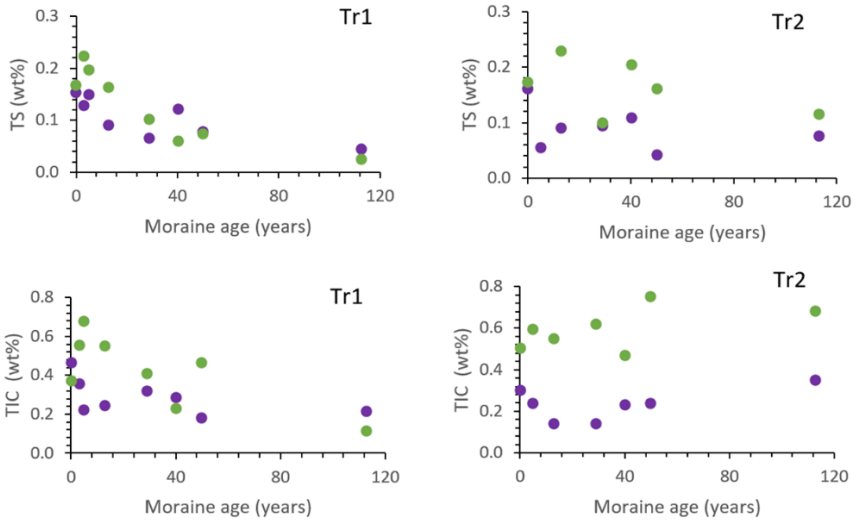

Figure. B.2. A comparison of TIC and TS between the years 2013 (purple dots) and 2015 (green dots) plotted as a function of the moraine age; independent T-test results (P values) are shown in Appendix B. Table. 9 and data is tabulated in Appendix B. Table. 7

Table. B.8. Two tail paired t-test for TS and TIC conc. 0-15 and 15-30cm collected in 2013
H_0 = means ($\bar{x}$) are equal between the two depths sampled 0-15 and 15-30cm
$H_1 \neq$ means ($\bar{x}$) are unequal between the two depths sampled 0-15 and 15-30cm

TS	Tr1		Tr2		Tr3	
	0-15cm	*15-30cm*	*0-15cm*	*15-30cm*	*0-15cm*	*15-30cm*
Mean	0.10	0.09	0.10	0.09	0.10	0.09
Variance	0.00	0.00	0.00	0.00	0.00	0.00
t Stat	0.85		0.24		0.79	
P(T<=t) two-tail	0.40		0.81		0.44	
t Critical two-tail	2.05		2.00		2.05	

TIC	Tr1		Tr2		Tr3	
	0-15cm	*15-30cm*	*0-15cm*	*15-30cm*	*0-15cm*	*15-30cm*
Mean	0.19	0.27	0.26	0.33	0.34	0.37
Variance	0.00	0.01	0.01	0.08	0.03	0.01
t Stat	-4.64		-1.36		-0.85	
P(T<=t) two-tail	0.00		0.18		0.40	
t Critical two-tail	2.05		2.03		2.05	

Note: α level is <0.05

Table. B.9. Independent T Test for TS & TIC concentrations between 2013 and 2015.
H_0 = means ($\bar{x}$) are equal between the two concentrations of either TS or TIC sampled in 2013 and 2015.
$H_1 \neq$ means ($\bar{x}$) are unequal between the two concentrations of either TS or TIC sampled in 2013 and 2015.

(TS)	Tr1		Tr2	
Levene's Test for Equality of Variances	0.484			
	2013	2015	2013	2015
Mean	*0.15*	*0.06*	*0.16*	*0.05*
df	11.00		10.00	
t Stat	2.74		2.22	
P(T<=t) one-tail	0.01		0.03	
t Critical one-tail	1.80		1.81	
P(T<=t) two-tail	0.02		0.05	
t Critical two-tail	2.20		2.23	

Note: α level is <0.05

(TIC)	Tr1		Tr2	
Levene's Test for Equality of Variances	0.452			
	2013	*2014*	*2013*	*2014*
Mean	0.26	0.16	0.22	0.13
df	12.00		6.00	
t Stat	2.98		2.88	
P(T<=t) one-tail	0.01		0.01	
t Critical one-tail	1.78		1.94	
P(T<=t) two-tail	0.01		0.03	
t Critical two-tail	2.18		2.45	

Table. B.10. Analytical precision of the XRF measurements for elemental major oxides, minor and trace elements

No.	SiO_2 (%)	TiO_2 (%)	Al_2O_3 (%)	Fe_2O_3 (%)	MnO (%)	MgO (%)	CaO (%)	Na_2O (%)	K_2O (%)	P_2O_5 (%)	LOI (%)	Sum (%)
CRM value	**73.4**	**0.212**	**13.55**	**2.01**	**0.043**	**0.28**	**0.95**	**3.78**	**4.76**	**0.062**	**0.63**	
1	73.5	0.199	13.45	1.94	0.041	0.29	0.93	3.78	4.81	0.061	0.63	99.65
2	73.5	0.197	13.38	1.93	0.042	0.28	0.93	3.91	4.82	0.061	0.63	99.68
3	73.5	0.196	13.38	1.93	0.043	0.29	0.93	3.9	4.81	0.061	0.63	99.66
4	73.4	0.198	13.38	1.94	0.043	0.28	0.93	3.96	4.81	0.061	0.63	99.66
5	73.5	0.197	13.44	1.93	0.043	0.31	0.96	3.81	4.84	0.06	0.63	99.76
6	73.5	0.199	13.45	1.93	0.043	0.3	0.96	3.81	4.85	0.061	0.63	99.71
7	73.5	0.197	13.44	1.93	0.043	0.3	0.95	3.87	4.86	0.062	0.63	99.77
Mean	73.49	0.198	13.42	1.93	0.043	0.29	0.94	3.86	4.83	0.061	0.63	99.70
STDEV	0.03	0.001	0.03	0.005	0.001	0.01	0.01	0.07	0.02	0.001	0	0.05
95% confidence limit	0.03	0.001	0.03	0.005	0.001	0.01	0.01	0.06	0.02	0.001	0	0.05

Table. B.11. Analytical precision of the XRF measurements for elemental minor and trace elements (continued from, Table 18)

No. #	Ba (ppm)	Cr (ppm)	Ga (ppm)	Nb (ppm)	Ni (ppm)	Rb (ppm)	Sr (ppm)	V (ppm)	Y (ppm)	Zn (ppm)	Zr (ppm)
CRM value	**340**	**10**	**15**	**21**	**6.8**	**260**	**133**	**12**	**26**	**32**	**149**
1	331	10	16	22	10	264	137	12	26	34	136
2	330	13	16	21	10	259	136	10	29	32	137
3	332	11	16	22	10	261	135	15	28	33	136
4	347	10	16	20	10	265	138	16	28	33	137
5	331	13	17	19	10	271	141	12	28	30	142
6	353	10	16	20	10	274	140	14	28	30	142
7	330	12	18	20	10	275	141	12	27	30	146
Mean	336.29	11.29	16.43	20.57	10.00	267	138.29	13	27.71	31.71	139.43
STDEV	9.55	1.38	0.79	1.13	n/a	6.35	2.43	2.08	0.95	1.70	3.91
95% confidence limit	8.83	1.28	0.73	1.05	n/a	5.87	2.25	1.93	0.88	1.58	3.62

Table. B.12. XRF data: major elemental oxide concentrations from the 2013 and 2015 field season

Sample no.	Grain size fraction	Moraine age	SiO_2	TiO_2	Al_2O_3	Fe_2O_3	MnO	MgO	CaO	Na_2O	K_2O	P_2O_5	LOI	Sum
#	(mm)	Years	(%)	(%)	(%)	(%)	(%)	(%)	(%)	(%)	(%)	(%)	(%)	(%)
2013														
TR1														
Subglacial 0-15 cm														
S13.1.10.1.a	<7	0	76.83	0.49	9.32	3.05	0.06	1.06	1.67	2.01	2.13	0.08	2.85	100
S13.1.10.2.a	<7	0	74.57	0.54	10.5	3.37	0.06	1.17	1.56	2.3	2.47	0.09	2.92	100
S13.1.10.3.a	<7	0	73.13	0.54	10.45	3.46	0.06	1.24	1.78	2.79	2.45	0.09	3.15	99
S13.1.11.1.a	<7	2	71.52	0.62	11.61	3.75	0.06	1.3	1.61	2.9	2.8	0.1	3.11	99
S13.1.11.2.a	<7	2	72.2	0.59	11.31	3.72	0.06	1.33	1.8	2.48	2.67	0.1	3.24	99
S13.1.11.3.a	<7	2	72.93	0.57	11.18	3.84	0.06	1.23	1.47	2.42	2.64	0.09	2.93	99
S13.1.20.1.a	<7	3	75.42	0.56	10.58	3.56	0.06	1.25	1.57	2.15	2.5	0.09	2.28	100
S13.1.20.2.a	<7	3	75.24	0.55	10.4	3.54	0.06	1.23	1.69	2.13	2.46	0.09	2.61	100
S13.1.20.3.a	<7	3	73.7	0.59	11.19	3.56	0.06	1.25	1.5	1.99	2.61	0.1	3.04	100
S13.1.30.1.a	<7	5	76.27	0.52	10.07	3.51	0.06	1.23	1.5	2.19	2.31	0.1	2.24	100
S13.1.30.2.a	<7	5	73.78	0.61	11.28	3.72	0.06	1.32	1.69	2.15	2.68	0.09	2.62	100
S13.1.30.3.a	<7	5	74.16	0.59	10.77	3.45	0.06	1.17	1.72	2.01	2.53	0.09	3.02	100
S13.1.31.1.a	<7	13	71.12	0.64	11.76	3.96	0.06	1.33	1.49	3.03	2.98	0.1	2.96	99
S13.1.31.2.a	<7	13	73.86	0.57	10.71	3.63	0.06	1.2	1.53	2.35	2.52	0.1	2.98	100
S13.1.31.3.a	<7	13	73.06	0.61	11.1	3.85	0.06	1.27	1.57	2.16	2.68	0.1	3.07	100
S13.1.32.1.a	<7	21	74.62	0.57	10.81	3.43	0.05	1.16	1.32	2.04	2.55	0.1	2.99	100
S13.1.32.2.a	<7	21	74.62	0.56	10.78	3.62	0.06	1.1	1.18	2.13	2.43	0.1	2.99	100
S13.1.32.3.a	<7	21	73.12	0.62	11.2	3.79	0.06	1.25	1.44	2.12	2.73	0.1	3.22	100
S13.1.40.1.a	<7	29	76.05	0.53	10.58	3.38	0.05	1.17	1.2	2.22	2.55	0.09	2.18	100

S13.1.40.2.a	<7	29	73.9	0.52	10.56	3.46	0.06	1.4	2.24	2.24	2.47	0.11	3.04	100
S13.1.40.3.a	<7	29	74.42	0.56	10.93	3.42	0.05	1.16	1.26	2.24	2.51	0.11	3	100
S13.1.41.1.a	<7	40	74.04	0.56	10.66	3.52	0.06	1.2	1.68	2.1	2.52	0.09	3.09	100
S13.1.41.2.a	<7	40	73.49	0.6	11.05	3.5	0.06	1.24	1.78	2.1	2.6	0.09	3.01	100
S13.1.41.3.a	<7	40	71.84	0.61	11.05	3.98	0.07	1.3	1.84	2.59	2.78	0.1	3.17	99
S13.1.50.1.a	<7	50	74.66	0.59	11.05	3.57	0.06	1.29	1.29	2.14	2.65	0.1	2.6	100
S13.1.50.2.a	<7	50	74.53	0.63	11.39	3.62	0.06	1.28	1.1	2.23	2.71	0.11	2.35	100
S13.1.50.3.a	<7	50	75.04	0.58	10.96	3.26	0.05	1.1	0.97	2.22	2.5	0.11	2.83	100
S13.1.60.1.a	<7	113	74.39	0.61	10.92	3.79	0.06	1.31	1.19	1.84	2.65	0.12	3.14	100
S13.1.60.2.a	<7	113	72.99	0.64	11.84	3.78	0.06	1.29	1.28	2.13	2.93	0.11	2.95	100
S13.1.60.3.a	<7	113	72.85	0.62	10.98	3.68	0.06	1.21	1.22	2.41	2.65	0.11	3.72	100
TR1														
Subglacial														
15-30 cm														
S13.1.10.1.b	<7	0	75.8	0.52	9.9	3.45	0.06	1.28	1.91	2.07	2.33	0.09	2.58	100
S13.1.10.2.b	<7	0	75.06	0.55	10.23	3.58	0.06	1.32	1.9	2.06	2.44	0.09	2.72	100
S13.1.10.3.b	<7	0	72.14	0.56	10.72	3.86	0.07	1.4	2.07	2.57	2.68	0.09	3.2	99
S13.1.11.1.b	<7	2	71.58	0.63	11.6	3.96	0.06	1.36	1.82	2.43	2.86	0.1	3.14	100
S13.1.11.2.b	<7	2	73.2	0.57	11.11	3.64	0.06	1.24	1.7	2.19	2.6	0.09	3.06	99
S13.1.11.3.b	<7	2	75.09	0.54	10.23	3.39	0.05	1.11	1.48	2.08	2.37	0.09	2.99	99
S13.1.20.1.b	<7	3	74.19	0.58	10.83	3.69	0.06	1.34	1.82	2.11	2.6	0.1	2.68	100
S13.1.20.2.b	<7	3	73.63	0.59	10.96	3.7	0.06	1.39	1.91	2.17	2.64	0.1	2.85	100
S13.1.20.3.b	<7	3	71.92	0.6	10.94	3.81	0.06	1.27	1.88	2.67	2.73	0.1	3.16	99
S13.1.30.1.b	<7	5	77.31	0.53	9.79	3.17	0.05	1.05	1.37	1.69	2.22	0.09	2.73	100
S13.1.30.2.b	<7	5	78.41	0.5	9.15	3.29	0.04	1.04	1.14	1.42	2.11	0.11	2.79	100
S13.1.30.3.b	<7	5	74.65	0.55	10.2	3.42	0.06	1.16	1.67	2.16	2.44	0.09	3.02	99
S13.1.31.1.b	<7	13	73.93	0.58	10.97	3.69	0.06	1.17	1.49	2.08	2.63	0.09	2.92	100
S13.1.31.2.b	<7	13	73.23	0.59	10.88	4.02	0.06	1.25	1.56	2.23	2.72	0.1	2.92	100

S13.1.31.3.b	<7	13	74.66	0.56	10.86	3.64	0.06	1.11	1.31	1.93	2.44	0.1	2.94	100
S13.1.32.1.b	<7	21	72.24	0.63	11.63	3.96	0.06	1.27	1.39	2.21	2.91	0.11	3.2	100
S13.1.32.2.b	<7	21	72.74	0.63	11.58	3.88	0.06	1.23	1.36	2.14	2.74	0.11	3.14	100
S13.1.40.1.b	<7	29	74.44	0.59	11.11	3.66	0.06	1.23	1.28	2.17	2.67	0.1	2.7	100
S13.1.40.2.b	<7	29	73.73	0.61	11.74	3.74	0.05	1.32	1.31	2.28	2.81	0.1	2.31	100
S13.1.40.3.b	<7	29	73.35	0.58	11.25	3.86	0.05	1.23	1.32	2.3	2.64	0.1	2.89	100
S13.1.41.1.b	<7	40	71.58	0.61	11.04	4.12	0.07	1.37	1.82	2.66	2.87	0.1	3.05	99
S13.1.41.2.b	<7	40	73.46	0.58	10.8	3.67	0.07	1.23	1.8	1.98	2.55	0.09	3.21	99
S13.1.41.3.b	<7	40	74.08	0.59	10.71	3.57	0.06	1.16	1.34	1.98	2.52	0.1	3.52	100
S13.1.50.1.b	<7	50	73.86	0.59	11.12	3.77	0.06	1.32	1.54	2.12	2.69	0.1	2.81	100
S13.1.50.2.b	<7	50	72.99	0.62	11.68	3.8	0.06	1.31	1.52	2.16	2.88	0.1	2.89	100
S13.1.50.3.b	<7	50	72.29	0.62	11.26	3.89	0.06	1.3	1.34	2.53	2.76	0.11	3.25	99
S13.1.60.1.b	<7	113	73.82	0.62	11.15	3.86	0.06	1.37	1.27	1.92	2.68	0.11	3.13	100
S13.1.60.2.b	<7	113	73	0.64	11.38	3.93	0.06	1.32	1.5	1.94	2.83	0.11	3.28	100
S13.1.60.3.b	<7	113	71.93	0.63	11.53	4.11	0.06	1.32	1.44	2.55	2.86	0.11	2.96	99
TR2														
Supraglacial														
0-15 cm														
S13.2.10.1.a	<7	0	74.06	0.56	11.06	3.63	0.06	1.3	1.65	2.26	2.69	0.09	2.64	100
S13.2.10.2.a	<7	0	73.81	0.57	10.8	3.55	0.06	1.31	1.84	2.14	2.62	0.1	3.22	100
S13.2.10.3.a	<7	0	76.7	0.56	9.88	3.15	0.05	1.02	1.34	1.84	2.28	0.11	2.81	100
S13.2.11.1.a	<7	2	73.96	0.55	10.81	3.51	0.06	1.18	1.6	2.18	2.56	0.09	3	99
S13.2.11.2.a	<7	2	74.05	0.56	10.69	3.53	0.06	1.2	1.63	2.07	2.52	0.1	3.08	99
S13.2.11.3.a	<7	2	72.91	0.58	11.09	3.84	0.06	1.26	1.71	2.14	2.66	0.1	3.18	100
S13.2.20.1.a	<7	3	74.32	0.55	11.33	3.61	0.05	1.3	1.54	2.36	2.77	0.1	2.06	100
S13.2.20.2.a	<7	3	73.56	0.55	11.3	3.63	0.06	1.21	1.43	2.17	2.62	0.09	2.93	100
S13.2.30.1.a.	<7	5	73.77	0.57	11.01	3.64	0.06	1.15	1.48	2.09	2.61	0.1	3.03	100
S13.2.30.2.a.	<7	5	74.23	0.62	11.06	3.89	0.06	1.19	1.04	1.92	2.65	0.11	2.98	100

S13.2.30.3.a.	<7	5	74.97	0.61	10.64	3.52	0.05	1.11	1.22	1.85	2.49	0.12	3.16	100
S13.2.31.1.a	<7	13	71.24	0.59	11.48	3.86	0.06	1.28	1.84	2.78	2.84	0.1	3.17	99
S13.2.31.2.a	<7	13	71.05	0.61	11.51	3.98	0.07	1.34	1.81	2.78	2.9	0.1	3.08	99
S13.2.31.3.a	<7	13	73.12	0.59	10.97	3.52	0.06	1.22	1.73	2.31	2.59	0.09	3.16	99
S13.2.32.1.a	<7	21	73.28	0.66	11.44	3.79	0.06	1.22	1.25	2.16	2.89	0.11	2.73	100
S13.2.32.2.a	<7	21	77.59	0.48	9.19	3.07	0.05	0.92	1.08	1.86	2.15	0.1	3.06	100
S13.2.32.3.a	<7	21	74.81	0.53	9.98	3.42	0.06	1.07	1.65	2.7	2.4	0.1	2.59	99
S13.2.33.2.a	<7	25	78.72	0.46	9.03	2.89	0.05	0.86	1.12	1.79	2.04	0.1	2.54	100
S13.2.40.2.a	<7	29	74.51	0.66	11.99	4.2	0.07	1.31	0.81	2.13	2.85	0.11	3.03	102
S13.2.40.3.a	<7	29	74.84	0.61	11.01	3.74	0.06	1.3	1.09	2.04	2.66	0.11	2.53	100
S13.2.41.1.a	<7	40	76.06	0.58	10.45	3.49	0.05	1.15	0.98	2.03	2.47	0.11	2.62	100
S13.2.41.2.a	<7	40	73.71	0.6	11.11	3.7	0.06	1.15	1.38	2.23	2.72	0.1	2.83	100
S13.2.50.1.a	<7	50	75.28	0.55	10.69	3.34	0.06	1.06	1.15	1.97	2.52	0.1	3.01	100
S13.2.50.2.a	<7	50	74.2	0.58	10.63	3.63	0.06	1.27	1.42	1.89	2.48	0.11	3.42	100
S13.2.50.3.a	<7	50	73.52	0.61	11.09	3.54	0.06	1.26	1.56	1.9	2.62	0.11	3.43	100
S13.2.51.1.a	<7	73	75.95	0.49	9.94	3.17	0.05	1.08	1.44	2.24	2.33	0.09	2.81	100
S13.2.51.2.a	<7	73	76.35	0.49	9.98	3.1	0.05	1.05	1.13	2.12	2.4	0.09	2.9	100
S13.2.51.3.a	<7	73	76.48	0.48	9.82	2.78	0.05	1.05	1.6	2.11	2.23	0.09	2.94	100
S13.2.60.1.a	<7	113	78.55	0.45	9.21	2.9	0.05	1.1	1.31	2.07	2.14	0.08	2.14	100
S13.2.60.2.a	<7	113	76.96	0.45	9.26	2.77	0.04	1.09	1.48	2.06	2.21	0.08	3.59	100
S13.2.70.1.a	<7	~2000	68.79	0.63	9.7	3.01	0.06	1	0.94	1.62	2.17	0.13	11.97	100
S13.2.70.2.a	<7	~2000	54.02	0.53	7.95	2.23	0.05	0.74	0.69	1.56	1.74	0.11	30.02	100
S13.2.70.3.a	<7	~2000	57.21	0.47	7.71	2.4	0.06	0.95	1.11	1.97	1.76	0.12	25.65	99
TR2														
Supraglacial														
15-30 cm														
S13.2.10.1.b	<7	0	73.78	0.56	11.32	3.67	0.06	1.25	1.55	2.31	2.72	0.1	2.68	100
S13.2.10.2.b	<7	0	72.81	0.58	11.35	3.88	0.06	1.22	1.55	2.24	2.67	0.1	3.04	100

S13.2.10.3.b	<7	0	73.26	0.59	10.86	4.15	0.06	1.22	1.73	1.82	2.57	0.1	3.19	100
S13.2.11.1.b	<7	2	72.1	0.59	11.55	4.02	0.06	1.24	1.61	2.29	2.86	0.1	3.12	100
S13.2.11.2.b	<7	2	73.02	0.44	12.42	3.08	0.04	0.96	1.37	3.18	2.71	0.08	2.3	100
S13.2.11.3.b	<7	2	72.9	0.54	11.65	3.58	0.06	1.17	1.53	2.48	2.72	0.09	2.79	100
S13.2.20.1.b	<7	3	74.4	0.53	11.02	3.54	0.06	1.19	1.6	2.39	2.65	0.1	2.51	100
S13.2.20.2.b	<7	3	73.3	0.57	11.16	3.72	0.06	1.23	1.66	2	2.57	0.1	3.14	99
S13.2.20.3.b	<7	3	73.44	0.59	11.11	3.78	0.06	1.34	1.81	2.19	2.73	0.1	2.83	100
S13.2.30.1.b	<7	5	74.59	0.58	10.73	3.72	0.06	1.26	1.46	2.13	2.65	0.1	2.72	100
S13.2.30.2.b	<7	5	71.8	0.6	11.28	3.78	0.06	1.27	1.7	2.88	2.81	0.11	2.98	99
S13.2.30.3.b	<7	5	73.91	0.58	11.06	3.69	0.06	1.3	1.65	2.16	2.69	0.1	2.8	100
S13.2.31.1.b	<7	13	73.25	0.57	10.84	3.58	0.06	1.23	1.77	2	2.6	0.11	3.44	99
S13.2.31.2.b	<7	13	72.81	0.59	11.09	3.7	0.07	1.25	1.81	2.11	2.68	0.09	3.23	99
S13.2.31.3.b	<7	13	73.65	0.57	11.32	3.74	0.06	1.24	1.58	2.26	2.73	0.1	2.75	100
S13.2.32.1.b	<7	21	75.38	0.54	10.46	3.79	0.06	1.05	1.17	1.85	2.37	0.11	2.84	100
S13.2.32.2.b	<7	21	74.35	0.54	10.57	3.41	0.06	1.14	1.62	2.25	2.45	0.1	3.03	100
S13.2.32.3.b	<7	21	76.37	0.47	9.4	4.36	0.06	0.93	1.15	1.63	2.17	0.16	2.9	100
S13.2.33.1.b	<7	25	75.14	0.56	10.27	3.54	0.06	1.11	1.47	1.94	2.49	0.1	2.84	100
S13.2.33.2.b	<7	25	74.4	0.61	11	3.78	0.06	1.16	1.21	1.87	2.6	0.1	2.83	100
S13.2.33.3.b	<7	25	74.24	0.51	10.99	3.35	0.06	1.1	1.51	2.33	2.55	0.1	2.75	99
S13.2.40.1.b	<7	29	74.4	0.62	11.02	3.87	0.06	1.29	1.34	1.96	2.69	0.11	2.64	100
S13.2.40.2.b	<7	29	75.41	0.57	10.67	3.47	0.05	1.14	1.12	1.97	2.48	0.1	2.63	100
S13.2.40.3.b	<7	29	75.32	0.57	10.53	3.56	0.06	1.26	1.45	2.04	2.5	0.1	2.62	100
S13.2.41.1.b	<7	40	74.45	0.61	10.74	3.82	0.06	1.16	1.32	2.06	2.62	0.11	2.82	100
S13.2.41.2.b	<7	40	74.43	0.6	10.79	3.61	0.06	1.15	1.2	2.06	2.57	0.11	3.05	100
S13.2.41.1.b	<7	40	75	0.55	10.6	3.59	0.06	1.08	1.36	1.96	2.44	0.1	2.83	100
S13.2.60.1.b	<7	50	77.73	0.43	9.39	2.91	0.05	1.11	1.75	2.15	2.23	0.08	2.18	100
S13.2.60.2.b	<7	50	78.03	0.43	8.97	2.69	0.04	0.94	1.45	1.94	2.05	0.08	2.51	99
S13.2.60.3.b	<7	50	77.58	0.43	9.35	2.91	0.04	1.1	1.75	2.11	2.22	0.08	2.44	100

S13.2.50.1.b	<7	73	65.81	0.79	12.94	4.21	0.05	2.23	3.24	1.64	3.26	0.15	5.69	100
S13.2.50.3.b	<7	73	61.99	0.82	13.18	4.38	0.06	2.6	4.63	1.51	3.42	0.15	7.28	100
S13.2.51.1.b	<7	113	75.13	0.55	10.36	3.57	0.06	1.13	1.4	2.05	2.44	0.1	2.92	100
S13.2.51.2.b	<7	113	75.28	0.53	10.22	3.2	0.05	1.07	1.32	2.22	2.34	0.09	3.15	99
S13.2.51.3.b	<7	113	77.51	0.43	9.06	2.66	0.05	0.98	1.81	2.09	2.1	0.08	2.81	100
TR3														
Supraglacial														
0-15 cm														
S13.3.10.1.a	<7	0	71.9	0.62	11.52	3.84	0.06	1.35	1.94	2.17	2.71	0.1	3.24	99
S13.3.10.2.a	<7	0	72.88	0.59	11.28	3.85	0.06	1.44	2.04	2.32	2.63	0.1	2.81	100
S13.3.10.3.a	<7	0	74.58	0.57	10.46	3.59	0.06	1.16	1.58	1.93	2.42	0.11	3.12	100
S13.3.11.1.a	<7	2	75.24	0.53	10.11	3.58	0.06	1.08	1.63	1.79	2.24	0.12	3.13	100
S13.3.11.2.a	<7	2	71.55	0.62	11.49	4.05	0.07	1.42	1.96	2.19	2.76	0.11	3.22	99
S13.3.11.3.a	<7	2	64.33	0.94	16.57	4.4	0.05	1.84	1.29	2.34	4.21	0.14	3.41	100
S13.3.20.1.a	<7	3	71.34	0.59	10.86	4.04	0.07	1.31	1.93	2.94	2.64	0.12	3.26	99
S13.3.20.3.a	<7	3	73.46	0.6	11.26	3.74	0.06	1.39	1.71	2.21	2.62	0.11	2.85	100
S13.3.30.1.a	<7	5	79.15	0.5	8.47	2.87	0.05	0.95	1.13	1.86	1.92	0.12	2.54	100
S13.3.30.2.a	<7	5	75.15	0.55	10.47	3.73	0.06	1.14	1.48	1.95	2.49	0.11	2.86	100
S13.3.30.3.a	<7	5	74.98	0.58	10.27	3.69	0.06	1.26	1.71	1.9	2.45	0.12	2.98	100
S13.3.31.3.a	<7	13	75.47	0.53	10.05	3.45	0.07	1.09	1.6	1.79	2.32	0.1	3.12	100
S13.3.31.3.a	<7	13	66.36	0.9	14.12	5.11	0.09	1.69	2.14	2.45	3.59	0.17	2.81	99
S13.3.31.3.a	<7	13	74.16	0.55	10.58	3.66	0.06	1.37	1.99	2.23	2.44	0.1	2.86	100
S13.3.32.3.a	<7	21	77.67	0.49	9.29	2.88	0.05	0.96	1.25	2	2.09	0.09	2.68	99
S13.3.32.3.a	<7	21	74.61	0.59	9.85	3.48	0.06	1.11	1.26	2.95	2.29	0.11	2.76	99
S13.3.32.3.a	<7	21	76.04	0.53	9.83	3.34	0.06	1.09	1.26	2.21	2.27	0.1	2.76	99
S13.3.40.1.a	<7	29	74.89	0.53	10.26	3.55	0.06	1.22	1.32	2.51	2.31	0.11	2.67	99
S13.3.40.2.a	<7	29	78.13	0.47	9.15	3.28	0.06	1.1	1.39	1.92	2.08	0.1	2.31	100
S13.3.40.3.a	<7	29	77.07	0.48	9.62	3.16	0.05	1.15	1.77	2.01	2.36	0.09	2.25	100

S13.3.41.3.a	<7	40	66.48	0.87	14.7	4.36	0.05	1.76	1.01	2.66	3.58	0.13	3.85	99
S13.3.41.3.a	<7	40	70.7	0.74	12.75	3.67	0.05	1.46	1.25	2.42	3.14	0.12	3.22	100
S13.3.41.3.a	<7	40	74.35	0.57	10.15	3.66	0.08	1.15	1.5	2.37	2.44	0.14	2.96	99
S13.3.50.1.a	<7	50	73.63	0.55	10.2	3.77	0.06	1.14	1.14	2.97	2.43	0.13	3.26	99
S13.3.50.2.a	<7	50	75.93	0.61	10.32	3.68	0.05	1.36	1.13	1.99	2.31	0.14	2.49	100
S13.3.50.3.a	<7	50	75.58	0.55	9.97	3.62	0.06	1.29	1.91	1.7	2.4	0.15	2.78	100
S13.3.60.1.a	<7	113	76.27	0.51	9.77	3.24	0.06	1.18	1.38	2.34	2.31	0.11	2.41	100
S13.3.60.2.a	<7	113	71.25	0.61	10.35	3.68	0.05	1.95	3.11	1.69	2.52	0.12	4.66	100
S13.3.60.3.a	<7	113	70.04	0.51	8.95	3.24	0.05	2	5.15	1.54	2.14	0.1	6.3	100
TR3														
Supraglacial														
15-30 cm														
S13.3.10.1.b	<7	0												
S13.3.10.2.b	<7	0	75.28	0.53	9.83	3.8	0.08	1.19	1.6	1.75	2.32	0.12	3.52	100
S13.3.10.3.b	<7	0	84.75	0.68	12.74	4.61	0.08	1.61	2.4	2.41	3.06	0.13	-12.47	100
S13.3.11.1.b	<7	2	72.98	0.58	10.62	3.75	0.07	1.21	1.67	2.66	2.51	0.12	3.17	99
S13.3.11.2.b	<7	2	73.5	0.67	10.79	3.69	0.05	1.2	1.21	2.2	2.67	0.13	3.1	99
S13.3.11.3.b	<7	2	72.23	0.63	11.55	3.87	0.06	1.27	1.62	2.21	2.82	0.1	2.99	99
S13.3.20.1.b	<7	3	73.85	0.56	10.51	3.77	0.07	1.18	1.86	1.93	2.42	0.11	3.21	99
S13.3.20.2.b	<7	3	74.28	0.56	10.51	3.79	0.07	1.28	1.87	1.98	2.49	0.12	3.04	100
S13.3.20.3.b	<7	3	74.15	0.55	10.44	3.66	0.07	1.31	2.1	2.07	2.48	0.12	3.06	100
S13.3.30.1.b	<7	5	71.85	0.62	11.05	4.14	0.08	1.36	2.11	2.28	2.73	0.11	3.16	99
S13.3.30.2.b	<7	5	74.65	0.58	10.63	3.77	0.08	1.3	1.59	1.87	2.56	0.12	2.85	100
S13.3.30.3.b	<7	5	75.89	0.55	9.79	3.63	0.06	1.25	1.69	1.76	2.34	0.12	2.92	100
S13.3.31.3.b	<7	13	71.07	0.63	11.54	3.99	0.07	1.38	2.05	2.62	2.83	0.1	3.13	99
S13.3.32.3.b	<7	21	73.73	0.55	10.4	3.9	0.07	1.17	1.75	2.02	2.43	0.11	3.28	99
S13.3.32.3.b	<7	21	74.77	0.47	9.8	3.22	0.05	1.16	2.12	2.56	2.34	0.09	2.9	99
S13.3.32.3.b	<7	21	75.11	0.53	10.16	3.51	0.06	1.12	1.61	1.91	2.34	0.11	3.05	100

S13.3.40.1.b	<7	29	75.51	0.53	9.99	3.56	0.07	1.08	1.5	1.87	2.35	0.11	2.96	100
S13.3.40.2.b	<7	29	76.36	0.51	9.88	3.41	0.06	1.26	1.43	2.12	2.29	0.1	2.58	100
S13.3.40.1.b	<7	29	73.91	0.59	10.88	3.6	0.06	1.32	2.06	2.17	2.59	0.1	2.72	100
S13.3.41.2.b	<7	40	74.6	0.6	10.31	3.54	0.06	1.18	1.52	2.12	2.43	0.13	3.01	100
S13.3.41.3.b	<7	40	74	0.57	10.47	3.59	0.06	1.2	1.81	1.96	2.45	0.1	3.25	99
S13.3.41.3.b	<7	40	74.92	0.57	10.55	3.59	0.06	1.18	1.34	1.82	2.49	0.11	3.02	100
S13.3.50.1.b	<7	50	75.12	0.54	10.25	3.44	0.05	1.16	1.42	1.88	2.4	0.11	3.29	100
S13.3.50.2.b	<7	50	75.94	0.53	9.8	3.52	0.05	1.3	1.82	1.65	2.34	0.17	2.89	100
S13.3.50.3.b	<7	50	75.48	0.63	10.27	3.74	0.06	1.39	1.36	1.87	2.41	0.15	2.65	100
S13.3.60.1.b	<7	113	73.44	0.57	10.12	3.73	0.06	1.25	1.89	2.35	2.45	0.16	3.4	99
S13.3.60.2.b	<7	113	72.86	0.61	10.65	3.74	0.05	1.49	2.36	1.69	2.57	0.13	3.85	100
S13.3.60.3.b	<7	113	73.04	0.64	11.03	3.92	0.06	1.42	1.85	1.65	2.71	0.14	3.55	100
2015														
TR1														
Subglacial 0-15 cm														
S15.24	<2	0	67.7	0.9	10.53	4.57	0.06	1.7	1.18	2.14	3.49	0.13	3.12	99
S15.27	<2	3	71.7	0.68	11.62	3.98	0.06	1.37	1.53	2.09	2.89	0.1	3.02	100
S15.30	<2	5	70.15	0.72	11.38	4.21	0.06	1.51	1.37	2.12	3.12	0.1	3.35	100
S15.33	<2	13	72.36	0.66	11.61	3.86	0.06	1.32	1.27	2.24	2.85	0.11	2.86	99
S15.36	<2	29	73.14	0.6	9.68	3.68	0.06	1.26	1.25	2.11	2.67	0.1	3.17	100
S15.39	<2	40	71.86	0.68	10.45	3.97	0.06	1.35	1.21	1.98	2.85	0.11	3.62	100
S15.42	<2	50	71.92	0.68	11.71	3.69	0.06	1.28	1.11	2.71	2.77	0.12	3.44	99
S15.45	<2	113	74.53	0.64	9.28	3.74	0.06	1.21	0.86	1.76	2.56	0.13	3.25	100
S15.23	2-7	0	74.6	0.55	9.31	3.45	0.06	1.15	1.45	2.31	2.36	0.09	2.6	100
S15.26	2-7	3	75.03	0.49	10.32	3.33	0.05	1.27	1.72	2.23	2.15	0.09	2.89	100
S15.29	2-7	5	73.36	0.54	9.12	3.51	0.07	1.35	2.19	2.06	2.37	0.09	3.58	100
S15.32	2-7	13	77.17	0.43	8.32	2.98	0.06	1.25	1.64	1.98	2.02	0.08	2.93	100
S15.35	2-7	29	79.31	0.41	9.15	2.63	0.06	0.84	1.21	2.25	1.8	0.07	2.21	100

S15.38	2-7	40	77.36	0.44	9.24	2.8	0.05	0.87	1.43	2.33	2.11	0.1	2.28	100
S15.41	2-7	50	76.17	0.43	7.81	2.81	0.05	0.99	2.1	2.22	2.16	0.08	3.1	100
S15.44	2-7	113	79.97	0.39	11.9	2.66	0.06	0.93	1.5	1.71	1.81	0.08	2.6	100
S15.22	>7	0	69.44	0.39	9.94	2.89	0.12	1.1	7.05	1.49	1.77	0.07	7.61	100
S15.25	>7	3	77.03	0.58	10.53	3.21	0.07	1.11	1.21	2.28	2.07	0.1	2.05	100
S15.28	>7	5	77.69	0.32	10.58	2.72	0.07	1.98	2.63	1.21	1.87	0.06	4.22	100
S15.31	>7	13	68.11	0.45	7.57	3	0.15	1.05	5.79	2.52	2.17	0.14	5.66	100
S15.34	>7	29	75.92	0.45	8.48	3.01	0.06	1.04	1.31	2.69	2.32	0.1	2	100
S15.37	>7	40	77.57	0.53	14.5	2.69	0.04	0.96	2.42	1.05	2.14	0.08	3.58	100
S15.40	>7	50	79.78	0.32	12.08	2.37	0.05	0.91	1.5	2.04	2.02	0.06	2.14	100
S15.43	>7	113	76.76	0.42	12.86	3.11	0.05	1.01	0.9	2.68	2.31	0.13	1.8	100
TR2														
Supraglacial														
0-15 cm														
S15.3	<2	0	75.39	0.53	11.89	3.17	0.06	1.11	1.3	2.15	2.5	0.09	2.69	100
S15.6	<2	5	73.2	0.64	11.52	3.31	0.05	1.27	1.21	2.07	2.82	0.1	3.13	99
S15.9	<2	13	73.2	0.61	11.97	3.69	0.06	1.23	1.32	2.15	2.71	0.1	2.96	99
S15.12	<2	29	73.62	0.64	11.7	3.78	0.06	1.21	1.02	2.02	2.73	0.11	2.81	100
S15.15	<2	40	77.39	0.47	10.95	3.1	0.05	1.05	1.08	1.97	2.25	0.09	2.53	100
S15.18	<2	50	73.33	0.54	10.97	3.35	0.05	1.43	1.96	1.84	2.49	0.1	4.07	100
S15.21	<2	113	71.95	0.67	10.3	3.99	0.06	1.38	1.41	1.83	2.76	0.12	3.81	100
S15.2	2-7	0	77.89	0.35	10.48	2.64	0.05	0.86	1.75	2.23	2.12	0.08	2.5	100
S15.5	2-7	5	75.97	0.41	9.14	2.86	0.06	1.1	1.92	2.16	2.14	0.07	3.33	99
S15.8	2-7	13	74.93	0.49	8.99	2.99	0.06	1	2	2.09	2.46	0.09	3.31	100
S15.11	2-7	29	76.76	0.37	9.99	2.58	0.09	0.9	2.39	2.19	1.98	0.06	3.36	100
S15.14	2-7	40	79.01	0.37	9.74	2.63	0.04	0.96	1.84	1.76	1.93	0.1	2.64	100
S15.17	2-7	50	77.22	0.43	8.05	2.94	0.05	1.09	1.82	1.94	2.03	0.09	2.89	100
S15.20	2-7	113	74.86	0.46	7.87	3.54	0.06	1.32	2.19	1.97	1.92	0.09	3.71	99

S15.1	>7	0	83.03	0.26	9.98	1.88	0.04	0.53	0.94	1.9	1.93	0.06	1.39	100
S15.4	>7	5	74.23	0.33	6.99	2.51	0.05	0.7	1.83	3.23	2.76	0.06	2.15	100
S15.7	>7	13	76.8	0.48	10.54	2.91	0.07	0.94	1.29	2.54	2.32	0.09	2.28	100
S15.10	>7	29	77.32	0.49	10.81	2.93	0.05	0.91	0.91	2.3	2.43	0.07	1.61	100
S15.13	>7	40	72.08	0.43	8.5	3.31	0.06	1.9	2.47	2.44	2.4	0.08	3.97	100
S15.16	>7	50	81.67	0.32	8.6	2.46	0.05	0.69	1.39	1.68	1.67	0.09	2.12	100
S15.19	>7	113	78.15	0.41	10.57	2.64	0.05	1.02	1.95	1.63	1.95	0.07	3.12	99

Note: Samples: S13.1.32.3.b, S13.2.20.3.a, S13.2.32.1.a, S13.2.33.3.a, S13.2.40.1.a, S13.2.41.3.a, S13.2.60.3.a, S13.2.50.2.b, S13.3.20.2.a are not available

Table. B.13. XRF data: minor and trace element concentrations from the 2013 and 2015 field season

Sample no. #	Grain (mm)	Moraine age (Years)	Ba (ppm)	Cr (ppm)	Ga (ppm)	Nb (ppm)	Ni (ppm)	Rb (ppm)	Sr (ppm)	V (ppm)	Y (ppm)	Zn (ppm)	Zr (ppm)
2013													
TR1													
Subglacial													
0-15 cm													
S13.1.10.1.a	<7	0	388	28	11	10	14	82	92	32	28	44	293
S13.1.10.2.a	<7	0	447	27	12	10	13	92	89	35	29	47	284
S13.1.10.3.a	<7	0	439	26	13	10	15	89	93	42	28	47	303
S13.1.11.1.a	<7	2	536	32	13	12	17	106	98	49	34	55	312
S13.1.11.2.a	<7	2	473	29	13	12	14	98	96	47	31	53	288
S13.1.11.3.a	<7	2	525	32	13	13	16	117	110	38	37	47	360
S13.1.20.1.a	<7	3	527	35	0	11	13	87	82	56	28	47	259
S13.1.20.2.a	<7	3	530	35	0	10	13	86	85	54	29	45	263
S13.1.20.3.a	<7	3	502	30	13	11	14	99	95	46	30	52	304
S13.1.30.1.a	<7	5	498	35	0	10	13	82	82	53	28	50	241
S13.1.30.2.a	<7	5	576	41	0	12	15	94	89	61	30	51	272
S13.1.30.3.a	<7	5	478	28	12	11	13	92	94	40	33	50	331
S13.1.31.1.a	<7	13	573	36	16	14	17	118	97	56	32	57	331
S13.1.31.2.a	<7	13	485	31	12	12	14	96	98	49	32	52	294
S13.1.31.3.a	<7	13	520	32	12	14	14	101	101	45	36	54	330
S13.1.32.1.a	<7	21	485	30	13	13	14	94	99	41	32	48	295
S13.1.32.2.a	<7	21	479	28	11	15	18	115	125	38	36	47	361
S13.1.32.3.a	<7	21	524	33	13	12	16	105	114	47	34	52	323

S13.1.40.1.a	<7	29	506	37	0	11	13	89	96	51	27	42	251
S13.1.40.2.a	<7	29	502	37	0	14	13	91	101	52	28	53	237
S13.1.40.3.a	<7	29	465	29	12	13	14	95	107	42	30	47	298
S13.1.41.1.a	<7	40	479	31	13	11	13	94	93	43	32	52	279
S13.1.41.2.a	<7	40	500	27	12	12	14	95	96	41	33	54	333
S13.1.41.3.a	<7	40	534	25	14	13	16	104	98	52	31	55	333
S13.1.50.1.a	<7	50	557	40	0	12	15	94	89	59	30	50	279
S13.1.50.2.a	<7	50	548	40	0	13	13	95	88	59	33	48	335
S13.1.50.3.a	<7	50	477	28	12	11	21	97	102	39	33	46	365
S13.1.60.1.a	<7	113	574	49	0	13	17	95	113	68	31	55	278
S13.1.60.2.a	<7	113	603	47	0	14	15	103	106	65	33	54	306
S13.1.60.3.a	<7	113	499	37	13	11	16	99	99	42	33	54	326
TR1													
Subglacial													
15-30 cm													
S13.1.10.1.b	<7	0	483	34	0	10	13	82	82	52	28	46	256
S13.1.10.2.b	<7	0	506	35	0	10	14	85	83	54	28	49	259
S13.1.10.3.b	<7	0	532	29	12	14	16	116	106	43	35	46	347
S13.1.11.1.b	<7	2	535	33	16	15	17	106	98	48	30	53	331
S13.1.11.2.b	<7	2	490	26	13	12	19	99	95	52	30	51	289
S13.1.11.3.b	<7	2	443	31	13	11	16	90	111	47	28	49	277
S13.1.20.1.b	<7	3	544	40	0	11	15	92	90	57	30	53	275
S13.1.20.2.b	<7	3	564	39	0	11	15	93	84	58	29	53	280
S13.1.20.3.b	<7	3	520	32	12	13	17	100	101	51	31	52	308
S13.1.30.1.b	<7	5	497	55	0	11	13	80	104	60	26	45	241
S13.1.30.2.b	<7	5	458	56	0	10	12	78	154	66	24	38	211
S13.1.30.3.b	<7	5	471	33	13	12	14	91	103	49	29	51	282
S13.1.31.1.b	<7	13	501	33	13	14	15	99	100	45	32	53	304

S13.1.31.2.b	<7	13	524	31	12	13	19	104	109	44	33	53	293
S13.1.31.3.b	<7	13	467	33	12	13	17	104	110	40	32	52	311
S13.1.32.1.b	<7	21	576	29	14	15	15	112	104	50	34	53	349
S13.1.32.2.b	<7	21	520	35	15	13	15	102	106	52	37	55	315
S13.1.40.1.b	<7	29	540	41	0	12	14	94	98	59	30	50	259
S13.1.40.2.b	<7	29	587	42	0	12	15	100	95	64	31	52	283
S13.1.40.3.b	<7	29	538	31	13	17	18	121	119	52	37	48	347
S13.1.41.1.b	<7	40	578	36	13	13	19	108	100	45	33	56	333
S13.1.41.2.b	<7	40	477	25	12	13	16	96	95	38	31	50	290
S13.1.41.3.b	<7	40	466	33	13	11	14	94	104	48	32	52	307
S13.1.50.1.b	<7	50	550	41	0	12	15	96	89	59	30	52	272
S13.1.50.2.b	<7	50	574	41	0	13	15	103	93	60	31	53	286
S13.1.50.3.b	<7	50	536	35	15	13	21	107	99	55	33	54	323
S13.1.60.1.b	<7	113	555	50	0	13	17	97	104	68	31	58	279
S13.1.60.2.b	<7	113	590	49	0	13	18	100	99	67	32	58	291
S13.1.60.3.b	<7	113	552	34	14	16	17	111	106	55	33	57	319
TR2													
Supraglacial													
0-15 cm													
S13.2.10.1.a	<7	0	557	37	0	12	14	96	86	57	29	50	270
S13.2.10.2.a	<7	0	567	39	0	11	14	93	82	56	30	51	274
S13.2.10.3.a	<7	0	447	29	11	10	13	87	90	45	31	46	319
S13.2.11.1.a	<7	2	503	32	14	13	14	98	101	45	31	53	301
S13.2.11.2.a	<7	2	482	28	14	12	15	97	103	38	28	48	287
S13.2.11.3.a	<7	2	559	26	13	14	19	120	113	44	35	47	346
S13.2.20.1.a	<7	3	526	33	0	12	14	99	99	55	29	48	260
S13.2.20.2.a	<7	3	511	30	15	12	16	106	114	45	31	48	297
S13.2.30.1.a.	<7	5	506	26	12	11	13	99	105	41	32	52	294

S13.2.30.2.a.	<7	5	509	32	13	12	16	103	90	51	35	58	319
S13.2.30.3.a.	<7	5	490	34	13	19	16	87	93	42	36	53	350
S13.2.31.1.a	<7	13	548	30	13	20	15	112	106	47	37	52	322
S13.2.31.2.a	<7	13	555	27	14	15	15	111	102	47	39	58	319
S13.2.31.3.a	<7	13	496	26	13	13	14	95	92	53	31	54	304
S13.2.32.1.a	<7	21	560	34	13	13	12	107	115	50	34	56	359
S13.2.32.2.a	<7	21	420	28	11	10	12	79	132	40	27	43	266
S13.2.32.3.a	<7	21	457	24	11	15	15	90	106	32	32	44	314
S13.2.33.2.a	<7	25	376	28	11	<10	11	76	127	36	26	40	267
S13.2.40.2.a	<7	29	545	38	15	21	18	110	102	50	36	59	357
S13.2.40.3.a	<7	29	563	44	0	13	14	95	96	59	30	77	290
S13.2.41.1.a	<7	40	517	40	0	11	14	87	80	56	29	48	289
S13.2.41.2.a	<7	40	534	30	13	12	18	103	110	45	32	52	307
S13.2.50.1.a	<7	50	477	25	12	13	12	94	105	38	32	48	316
S13.2.50.2.a	<7	50	462	33	11	14	17	94	94	47	33	56	302
S13.2.50.3.a	<7	50	482	31	12	12	16	98	107	43	33	50	332
S13.2.51.1.a	<7	73	438	22	11	13	13	88	94	39	30	49	267
S13.2.51.2.a	<7	73	449	25	12	14	12	90	90	38	28	42	264
S13.2.51.3.a	<7	73	418	23	12	11	11	81	91	37	26	39	283
S13.2.60.1.a	<7	113	401	43	0	8	10	74	78	43	23	36	208
S13.2.60.2.a	<7	113	417	29	0	9	10	75	81	42	22	33	210
S13.2.70.1.a	<7	~2000	494	51	0	11	14	80	82	64	27	57	337
S13.2.70.2.a	<7	~2000	329	27	10	11	11	60	72	36	25	36	321
S13.2.70.3.a	<7	~2000	316	32	10	11	12	61	78	40	24	41	271
TR2 Supraglacial 15-30 cm													
S13.2.10.1.b	<7	0	549	38	0	12	13	97	100	57	30	51	253

S13.2.10.2.b	<7	0	519	32	14	14	16	103	118	54	42	51	294
S13.2.10.3.b	<7	0	577	31	11	14	20	115	105	41	30	53	287
S13.2.11.1.b	<7	2	534	31	15	15	15	114	114	50	35	52	309
S13.2.11.2.b	<7	2	426	15	15	15	10	108	108	28	30	37	216
S13.2.11.3.b	<7	2	477	29	14	12	14	106	106	46	30	48	269
S13.2.20.1.b	<7	3	518	36	0	11	13	95	104	52	29	48	244
S13.2.20.2.b	<7	3	514	49	12	15	18	117	115	42	35	48	341
S13.2.20.3.b	<7	3	565	44	0	12	14	95	91	61	30	54	272
S13.2.30.1.b	<7	5	561	42	0	12	14	93	106	58	29	50	265
S13.2.30.2.b	<7	5	515	31	13	15	13	102	109	47	33	63	306
S13.2.30.3.b	<7	5	563	40	0	12	13	95	95	56	29	53	270
S13.2.31.1.b	<7	13	506	30	13	12	13	97	119	49	31	51	292
S13.2.31.2.b	<7	13	525	27	13	14	13	99	100	37	32	51	308
S13.2.31.3.b	<7	13	577	43	0	13	15	98	98	62	30	50	256
S13.2.32.1.b	<7	21	442	30	13	13	16	102	162	44	32	45	310
S13.2.32.2.b	<7	21	452	25	14	12	12	92	101	44	30	52	302
S13.2.32.3.b	<7	21	384	40	12	13	18	86	296	47	28	55	247
S13.2.33.1.b	<7	25	482	28	13	13	15	92	114	41	30	47	296
S13.2.33.2.b	<7	25	492	32	13	12	15	97	107	43	33	52	304
S13.2.33.3.b	<7	25	447	23	13	12	15	96	114	38	30	50	257
S13.2.40.1.b	<7	29	565	45	0	12	15	95	85	63	30	54	268
S13.2.40.2.b	<7	29	480	29	13	12	17	92	92	50	31	50	297
S13.2.40.3.b	<7	29	524	40	0	11	13	89	88	56	29	48	262
S13.2.41.1.b	<7	40	529	28	12	13	15	105	96	43	32	53	318
S13.2.41.2.b	<7	40	495	34	12	14	17	98	88	45	31	53	319
S13.2.41.1.b	<7	40	460	29	11	14	14	100	136	43	34	45	327
S13.2.60.1.b	<7	50	413	31	0	9	10	77	80	42	22	36	197
S13.2.60.2.b	<7	50	362	20	10	10	10	77	88	25	25	40	241

S13.2.60.3.b	<7	50	407	31	0	9	10	77	81	41	22	35	197
S13.2.50.1.b	<7	73	673	69	0	15	21	117	90	94	35	73	342
S13.2.50.3.b	<7	73	699	82	0	16	24	122	91	99	36	79	351
S13.2.51.1.b	<7	113	481	32	12	12	15	100	119	48	33	50	306
S13.2.51.2.b	<7	113	428	30	12	12	12	86	97	46	30	48	279
S13.2.51.3.b	<7	113	388	193	10	13	13	72	86	33	27	40	258
TR3													
Supraglacial													
0-15 cm													
S13.3.10.1.a	<7	0	512	31	14	14	16	101	113	37	34	55	325
S13.3.10.2.a	<7	0	505	37	0	12	14	94	103	58	29	51	277
S13.3.10.3.a	<7	0	439	34	12	12	14	92	145	41	32	50	299
S13.3.11.1.a	<7	2	427	35	12	12	15	96	204	46	32	48	302
S13.3.11.2.a	<7	2	553	34	13	12	15	105	139	50	36	52	324
S13.3.11.3.a	<7	2	785	50	21	18	16	145	100	76	45	62	446
S13.3.20.1.a	<7	3	491	40	13	13	18	102	165	51	33	53	306
S13.3.20.3.a	<7	3	527	43	0	12	14	94	131	63	31	49	280
S13.3.30.1.a	<7	5	361	22	10	11	14	72	86	38	29	43	405
S13.3.30.2.a	<7	5	515	58	0	12	19	89	131	61	28	51	259
S13.3.30.3.a	<7	5	557	50	0	12	15	87	158	63	31	50	308
S13.3.31.1.a	<7	13	439	29	11	12	13	85	137	49	29	47	285
S13.3.31.2.a	<7	13	715	49	18	18	24	133	185	70	47	73	545
S13.3.31.3.a	<7	13	511	42	0	11	14	86	124	58	28	46	250
S13.3.32.1.a	<7	21	392	24	10	11	12	93	103	35	34	38	370
S13.3.32.2.a	<7	21	410	39	12	13	18	87	118	43	33	45	384
S13.3.32.3.a	<7	21	409	31	10	13	15	87	126	40	29	44	282
S13.3.40.1.a	<7	29	455	31	11	14	15	96	132	47	34	45	296
S13.3.40.2.a	<7	29	424	38	0	9	12	74	114	49	24	36	219

S13.3.40.3.a	<7	29	495	35	0	10	12	81	88	52	25	47	235
S13.3.41.1.a	<7	40	675	42	19	18	17	134	104	70	50	57	483
S13.3.41.2.a	<7	40	580	34	16	14	14	112	103	53	40	53	473
S13.3.41.3.a	<7	40	461	37	12	12	14	90	140	48	35	48	319
S13.3.50.1.a	<7	50	498	37	13	13	16	112	147	37	37	54	341
S13.3.50.2.a	<7	50	463	45	0	12	15	85	108	61	31	47	310
S13.3.50.3.a	<7	50	529	53	0	11	17	84	120	64	28	54	262
S13.3.60.1.a	<7	113	401	29	11	13	15	86	96	38	30	45	255
S13.3.60.2.a	<7	113	566	56	0	12	19	88	94	72	30	57	288
S13.3.60.3.a	<7	113	501	49	0	10	19	77	92	65	25	59	239
TR3													
Supraglacial													
15-30 cm													
S13.3.10.1.b	<7	0											
S13.3.10.2.b	<7	0	520	51	0	11	15	82	170	64	27	52	247
S13.3.10.3.b	<7	0	568	46	0	12	15	93	135	63	29	54	270
S13.3.11.1.b	<7	2	445	40	12	11	16	91	166	46	31	54	294
S13.3.11.2.b	<7	2	486	41	13	13	17	98	93	54	34	54	324
S13.3.11.3.b	<7	2	519	32	15	14	16	107	114	47	31	52	319
S13.3.20.1.b	<7	3	469	35	14	12	15	94	172	46	29	50	289
S13.3.20.2.b	<7	3	505	47	0	11	14	89	153	61	29	50	250
S13.3.20.3.b	<7	3	506	44	0	11	14	88	133	58	29	48	260
S13.3.30.1.b	<7	5	540	36	12	13	19	106	133	47	32	58	324
S13.3.30.2.b	<7	5	600	52	0	12	16	91	129	68	29	56	270
S13.3.30.3.b	<7	5	520	49	0	11	14	83	172	61	27	50	246
S13.3.31.1.b	<7	13	558	29	13	13	13	105	112	48	36	54	328
S13.3.32.1.b	<7	21	490	39	12	16	18	112	181	49	37	49	314
S13.3.32.2.b	<7	21	454	24	11	12	13	89	107	35	27	46	249

S13.3.32.3.b	<7	21	423	32	12	12	15	89	140	37	29	53	268
S13.3.40.1.b	<7	29	423	35	12	13	16	90	157	47	29	48	272
S13.3.40.2.b	<7	29	466	36	0	10	12	80	86	54	28	41	251
S13.3.40.3.b	<7	29	552	37	0	11	15	91	93	60	29	51	283
S13.3.41.1.b	<7	40	497	34	11	15	16	101	110	41	36	48	415
S13.3.41.2.b	<7	40	473	28	13	13	15	93	131	54	30	50	297
S13.3.41.3.b	<7	40	473	38	12	14	15	95	115	52	34	55	281
S13.3.50.1.b	<7	50	500	32	10	14	14	107	110	43	32	48	308
S13.3.50.2.b	<7	50	490	49	0	11	14	83	113	62	27	51	237
S13.3.50.3.b	<7	50	524	50	0	12	15	88	122	64	32	52	357
S13.3.60.1.b	<7	113	453	43	13	14	15	92	134	49	33	53	310
S13.3.60.2.b	<7	113	575	56	0	12	18	92	113	76	29	58	273
S13.3.60.3.b	<7	113	573	58	0	13	18	96	119	76	30	69	274
2015													
TR1													
Subglacial													
0-15 cm													
S15.24	<2	0	696	50	19	15	21	128	101	67	44	65	476
S15.27	<2	3	570	35	14	10	16	112	93	51	38	54	349
S15.30	<2	5	585	43	17	10	18	120	92	62	38	59	344
S15.33	<2	13	553	36	15	10	13	106	100	51	37	52	362
S15.36	<2	29	497	35	14	11	15	103	109	39	32	49	321
S15.39	<2	40	555	37	15	12	16	114	95	56	35	58	352
S15.42	<2	50	530	33	15	10	15	106	99	53	37	51	413
S15.45	<2	113	507	35	14	11	15	102	87	49	34	53	331
S15.23	2-7	0	449	32	13	10	13	91	109	40	30	50	299
S15.26	2-7	3	427	28	12	10	10	98	106	42	31	39	274
S15.29	2-7	5	442	29	13	10	14	93	95	45	31	48	295

S15.32	2-7	13	402	25	10	10	11	83	97	42	26	42	232
S15.35	2-7	29	356	26	10	10	10	71	85	26	23	35	231
S15.38	2-7	40	417	26	12	10	10	85	107	33	28	42	263
S15.41	2-7	50	443	25	11	10	10	83	138	34	25	33	232
S15.44	2-7	113	371	23	10	10	10	73	79	34	23	32	251
S15.22	>7	0	334	22	10	10	10	68	96	35	31	378	228
S15.25	>7	3	404	28	11	10	11	82	117	44	32	44	346
S15.28	>7	5	285	18	10	10	10	71	66	22	22	30	201
S15.31	>7	13	412	22	13	10	10	86	225	40	30	41	201
S15.34	>7	29	448	23	12	10	10	87	138	34	29	33	250
S15.37	>7	40	333	34	10	10	15	91	75	48	28	58	229
S15.40	>7	50	385	17	11	10	10	77	101	29	24	27	206
S15.43	>7	113	453	16	15	10	10	90	114	31	31	34	292
TR2													
Supraglacial													
0-15 cm													
S15.3	<2	0	463	27	13	10	10	98	96	33	35	42	353
S15.6	<2	5	483	33	15	12	11	106	96	43	36	46	416
S15.9	<2	13	504	35	13	10	14	104	107	42	32	53	354
S15.12	<2	29	528	36	15	11	13	107	114	53	36	53	378
S15.15	<2	40	407	27	11	10	10	89	91	37	26	43	266
S15.18	<2	50	446	33	11	10	12	98	91	44	30	51	283
S15.21	<2	113	530	39	15	11	15	109	127	60	35	58	348
S15.2	2-7	0	391	18	12	10	10	85	100	35	26	33	217
S15.5	2-7	5	408	19	12	11	11	82	92	32	27	37	279
S15.8	2-7	13	456	23	13	10	10	95	112	35	29	43	312
S15.11	2-7	29	358	19	10	10	10	77	132	33	22	34	234
S15.14	2-7	40	345	20	10	10	10	78	88	30	22	34	213

S15.17	2-7	50	380	29	12	10	10	80	87	35	25	40	245
S15.20	2-7	113	2460	25	11	10	10	78	181	37	27	42	287
S15.1	>7	0	530	15	10	10	10	73	97	20	22	26	199
S15.4	>7	5	371	13	16	11	10	112	116	29	27	37	214
S15.7	>7	13	390	20	11	10	10	85	101	32	35	25	396
S15.10	>7	29	593	25	12	11	10	96	96	39	26	40	254
S15.13	>7	40	488	24	12	10	10	100	118	31	29	41	241
S15.16	>7	50	439	18	10	10	10	72	99	26	24	41	208
S15.19	>7	113	345	26	10	10	10	80	85	28	26	644	261

Note: Samples: S13.1.32.3.b, S13.2.20.3.a, S13.2.32.1.a, S13.2.33.3.a, S13.2.40.1.a, S13.2.41.3.a, S13.2.60.3.a, S13.2.50.2.b, S13.3.20.2.a are not available

Table. B.14. XRF data: source rock major element concentrations from the 2015 field season

Rock type	Sample no.	Moraine age	SiO_2	TiO_2	Al_2O_3	Fe_2O_3	MnO	MgO	CaO	Na_2O	K_2O	P_2O_5	LOI	Sum
#	#	(years)	(%)	(%)	(%)	(%)	(%)	(%)	(%)	(%)	(%)	(%)	(%)	(%)
Dolomite (1)	S15.47	N/A	10.57	0.01	0.48	4.95	0.53	15.37	26.52	0.05	0.05	0.03	41.48	100
Dolomite (2)	S15.48	N/A	20.14	0.08	1.71	1.06	0.05	15.99	23.40	<0.01	0.68	0.02	36.55	100
Dolomite (3)	S15.52	N/A	16.97	0.03	0.31	0.42	0.01	17.21	25.48	<0.01	0.12	0.02	39.44	100
Conglomerate	S15.50	N/A	57.39	0.61	8.08	2.97	0.09	1.81	12.94	1.89	1.57	0.16	12.06	100
Sandstone	S15.49	N/A	93.61	0.13	2.44	2.22	<0.01	0.07	0.20	<0.01	0.38	0.13	0.89	100
Psammite (1)	S15.51	N/A	69.32	0.09	2.77	0.68	0.14	0.25	13.61	1.33	0.16	0.03	11.48	100
Psammite (2)	S15.54	N/A	96.14	0.08	1.70	0.47	0.01	0.19	0.26	0.13	0.36	0.04	0.56	100
Psammite (3)	S15.55	N/A	94.71	0.02	0.39	0.41	0.01	0.05	1.95	<0.01	0.10	0.10	2.09	100
Mica schist (1)	S15.56	N/A	75.72	0.06	13.46	0.95	0.01	0.21	0.64	4.10	4.05	0.02	0.60	100
Mica schist (2)	S15.46	N/A	71.91	0.29	14.05	2.60	0.06	0.52	1.48	3.37	4.42	0.07	1.04	100
Phylite	S15.57	N/A	63.55	0.90	15.70	6.30	0.08	2.24	1.09	1.96	4.40	0.17	3.13	100

Table. B.15. XRF data: source rock minor and trace element concentrations from the 2015 field season

Rock type #	Sample no. #	Ba (ppm)	Cr (ppm)	Ga (ppm)	Nb (ppm)	Ni (ppm)	Rb (ppm)	Sr (ppm)	V (ppm)	Y (ppm)	Zn (ppm)	Zr (ppm)
Dolomite (1)	S15.47	18	10	10	10	10	10	229	10	10	59	10
Dolomite (2)	S15.48	1230	10	10	10	10	25	178	16	10	17	36
Dolomite (3)	S15.52	10	10	10	10	10	10	65	11	10	10	23
Conglomerate	S15.50	1013	44	10	10	12	69	375	70	38	35	399
Sandstone	S15.49	88	12	10	10	10	18	28	21	11	<10	73
Psammite (1)	S15.51	22	10	10	10	10	10	190	10	25	10	118
Psammite (2)	S15.54	99	10	10	10	10	14	11	10	11	10	190
Psammite (3)	S15.55	39	28	10	10	10	10	28	10	10	10	10
Mica schist (1)	S15.56	319	10	20	11	10	128	94	10	20	10	53
Mica schist (2)	S15.46	753	10	19	15	10	164	184	16	28	42	207
Phylite	S15.57	565	55	19	13	29	197	116	81	38	129	257

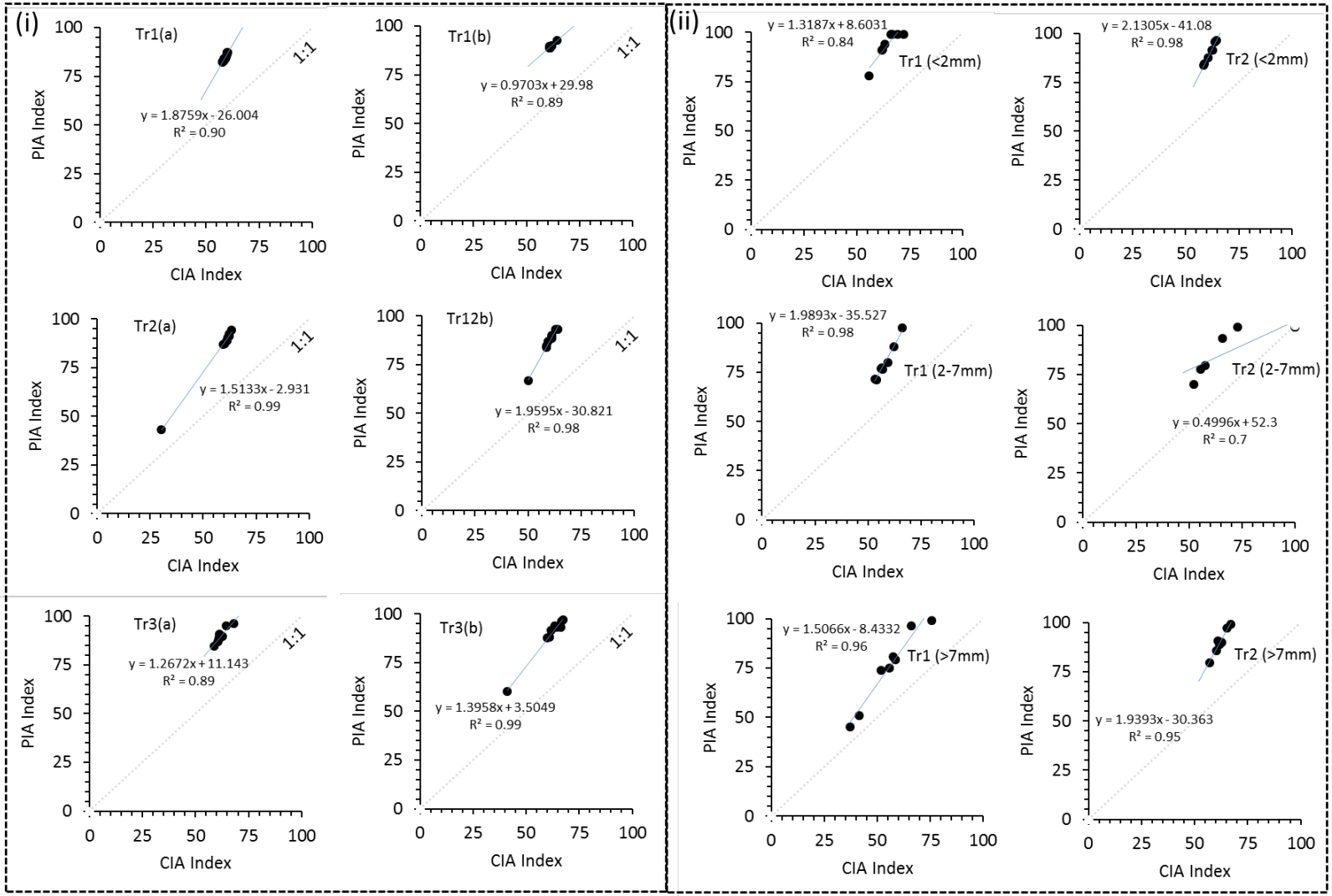

Figure. B.3. CIA *vs.* PIA plots showing data from 2013 (i) for all three transects at both depths 0-15cm (a) and 15cm (b) and 2015 (ii) grain size fractionated samples for only the transects Tr1 and Tr2. Note grey dotted line delineates the 1:1 ratio line and blue solid line is a linear best fit line.

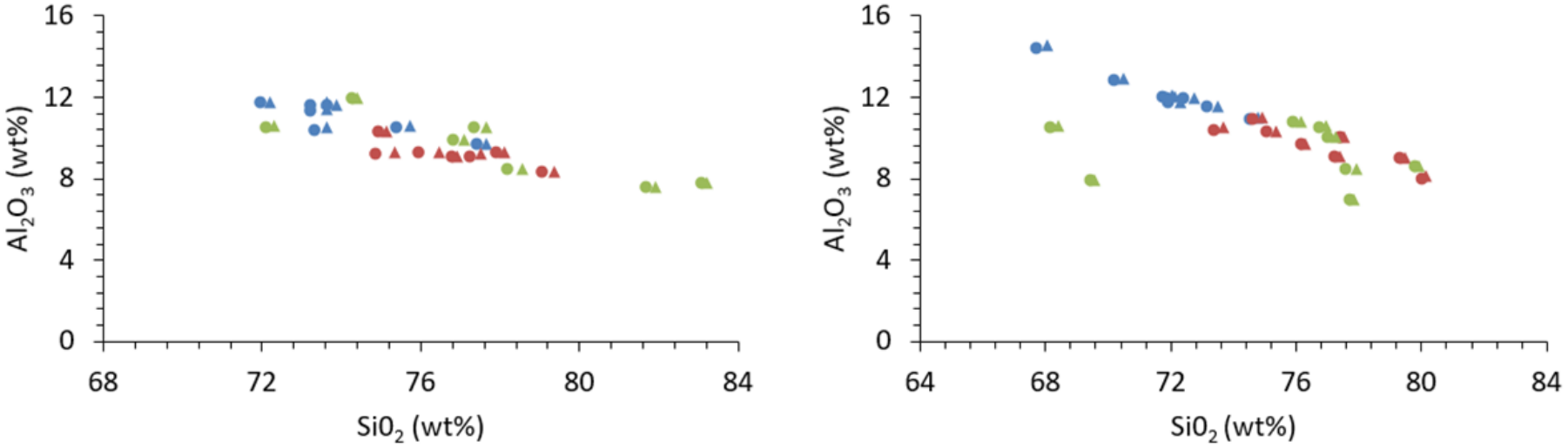

Figure. B.4. Difference between carbonate corrected (triangles) and carbonate uncorrected (circles) data points from the 2015. Sample colours represent weathered fractions (<2mm; blue) and the two parent material fractions (2 to 7mm; red; and >7mm; green). The top graph is Tr1 and the Tr2

Table. B.16. Weathering indices values for each of the source rocks within the glacier till from the glacial catchment of Midtre Lovebreen

Source rock type	Sample no.	CIA	PIA	WIP
Dolomite (1)	S15.47	-	-	-
Dolomite (2)	S15.48	-	-	-
Dolomite (3)	S15.52	-	-	-
Conglomerate	S15.50	63	85	36
Sandstone	S15.49	78	100	4
Psammite (1)	S15.51	55	60	14
Psammite (2)	S15.54	70	100	5
Psammite (3)	S15.55	69	100	1
Mica schist (1)	S15.56	52	79	74
Mica schist (2)	S15.46	54	84	73
Phylite	S15.57	64	100	63

Table. B.17. Moles calculation for molecular proportions of elemental oxides used in weathering indices

Moles Al_2O_3 =	wt% Al_2O_3	÷ 101.96
Moles CaO =	wt% CaO	÷ 56.08
Moles MgO	wt% MgO	÷ 40.3
Moles Na_2O =	wt% Na_2O	÷ 61.98
Moles K_2O =	wt% K_2O	÷ 94.20
Moles P_2O_5 =	wt% P_2O_5	÷ 141.95
Moles C =	wt% C	÷ 12.01
Moles CO_2 =	wt% CO_2	÷ 44.01

Table. B.18. Carbonate (cc; calcite, dol; dolomite, ap; apatite) corrections for silicate based weathering indices

Equation no.	Formula
Equation B.1	CaO* = mol CaO – mol C (cc)
Equation B.2	CaO* = mol CaO – mol C (cc) – (0.5 x mol C) (dol)
Equation B.3	CaO* = mol CaO – mol C (cc) – (0.5 x mol C) (dol) – (mol P_2O_5) (ap)

CaO* carbonate corrected CaO for silicate CaO only using Eq. A.1, where dolomite was absent. Where dolomite and calcite were present (see, Apendix). A. Table 23), Equ.A.2 was used. In as in all cases apatite was negligible <0.08 μmol (<11.2 μg/g) see Appendix B. Table. B.13 and thus Eq. A.3 was not used.

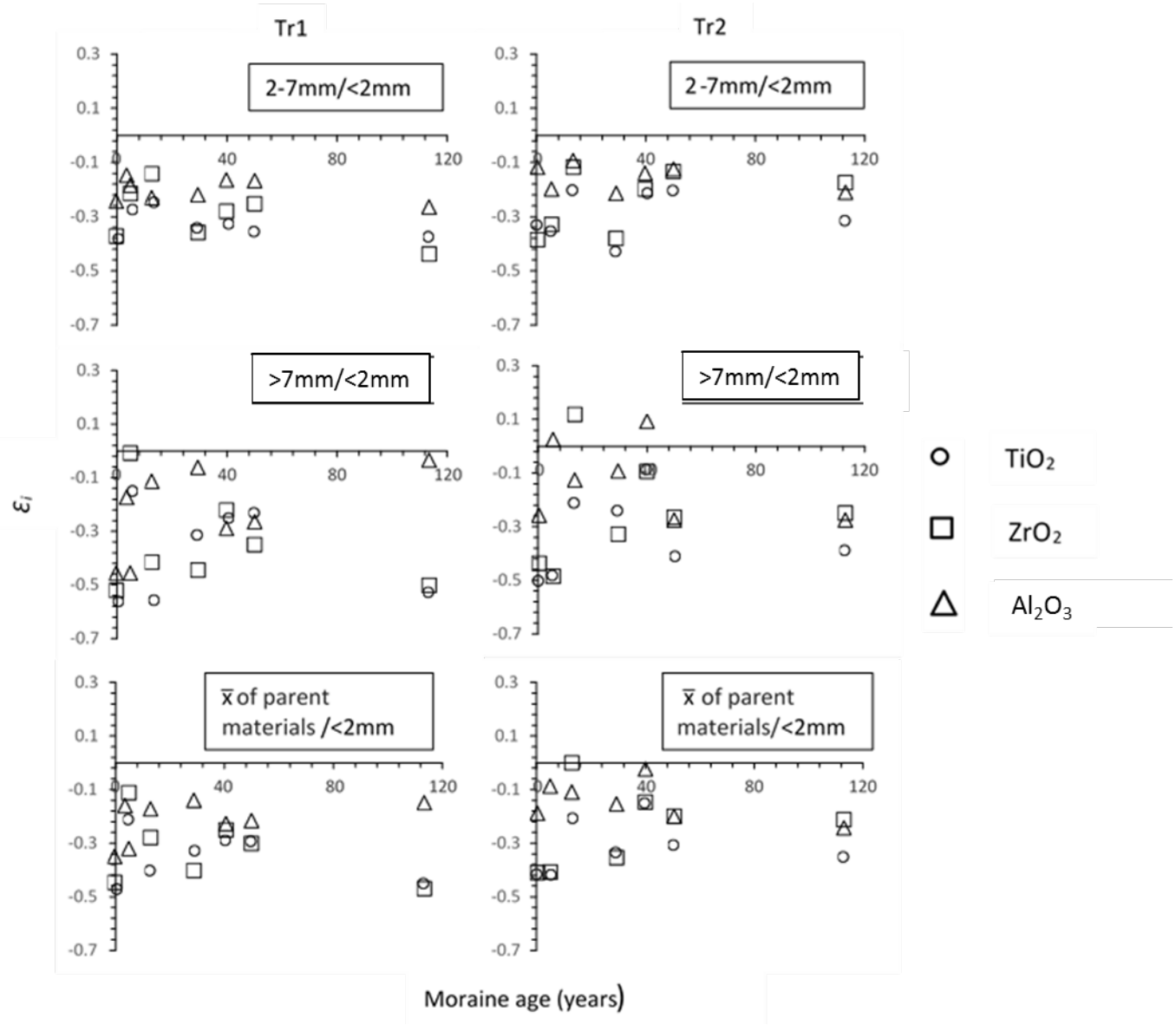

Figure. B.5. Immobile elemental oxides changes plotted vs. moraine age in the subglacial (Tr1) and supraglacial (Tr2) debris for the two parent material fractions 2-7mm and 7mm – 2cm relative to the soil fraction <2mm. Triangles represent Al_2O_3, squares = ZrO_2 and circles = TiO_2. Zero = equals no change in the soil fraction relative to the parent matterial, Equ 2.

Table. B.19. XRD quantification for the modal distribution of minerals in the 2013 <7mm samples. Mineral phases fitting assumed 100 % sum, while the precision of each fitting is reflexed in their goodness of fit (GOF) and weighted profile Rietfeld factor R_wp.

Sample no.	Age	Quartz	Chlorite	Dolomite	Muscovite	Calcite	Albite	GOF	R_wp
#	(years)	%	%	%	%	%	%		
TR1									
Subglacial 0-15 cm									
S13.1.10.1.a	0	58	8	-	6	-	22	3	14
S13.1.10.2.a	0	51	6	4	11	4	21	3	13
S13.1.10.3.a	0	55	8	-	8	-	23	3	13
S13.1.11.1.a	2	58	8	-	10	-	19	4	16
S13.1.11.2.a	2	57	7	-	10	-	20	3	14
S13.1.11.3.a	2	57	7	-	8	-	22	3	15
S13.1.20.1.a	3	48	8	-	11	-	26	3	12
S13.1.20.2.a	3	56	8	-	8	-	23	3	14
S13.1.20.3.a	3	55	8	-	6	-	26	3	13
S13.1.30.1.a	5	51	7	-	15	-	21	3	15
S13.1.30.2.a	5	51	8	-	9	5	23	3	13
S13.1.30.3.a	5	51	8	-	11	-	23	2	11
S13.1.31.1.a	13	54	9	-	6	-	25	3	14
S13.1.31.2.a	13	54	6	-	11	-	23	3	13
S13.1.31.3.a	13	56	7	-	8	-	23	3	12
S13.1.32.1.a	21	52	9	-	8	-	25	2	12
S13.1.32.2.a	21	53	8	-	10	-	23	3	15
S13.1.32.3.a	21	52	8	-	6	-	27	2	12
S13.1.40.1.a	29	57	6	4	6	-	23	2	14
S13.1.40.2.a	29	52	8	-	7	-	26	2	13

S13.1.40.3.a	29	54	7	-	5	-	27	2	13
S13.1.41.1.a	40	52	9	-	7	-	26	2	12
S13.1.41.2.a	40	53	7	-	7	-	24	2	12
S13.1.41.3.a	40	61	8	-	7	-	21	2	13
S13.1.50.1.a	50	52	8	5	6	-	25	2	12
S13.1.50.2.a	50	54	9	-	7	-	23	2	11
S13.1.50.3.a	50	51	6	-	11	-	26	2	13
S13.1.60.1.a	113	59	8	4	9	-	16	3	14
S13.1.60.2.a	113	55	9	5	7	-	21	2	11
S13.1.60.3.a	113	54	10	4	8	-	20	2	11
TR1									
Subglacial									
15-30 cm									
S13.1.10.1.b	0	57	3	6	9	4	20	2	14
S13.1.10.2.b	0	57	4	-	9	-	22	3	14
S13.1.10.3.b	0	54	4	4	10	-	22	2	11
S13.1.11.1.b	2	55	8	-	9	-	22	2	11
S13.1.11.2.b	2	53	9	-	7	-	25	3	12
S13.1.11.3.b	2	60	6	-	9	-	20	4	15
S13.1.20.1.b	3	55	7	-	9	-	22	3	13
S13.1.20.2.b	3	49	8	-	13	-	23	3	13
S13.1.20.3.b	3	53	8	-	11	-	20	3	15
S13.1.30.1.b	5	58	9	-	4	-	20	3	16
S13.1.30.2.b	5	64	6	-	6	-	18	2	11
S13.1.30.3.b	5	58	7	-	6	-	20	2	11
S13.1.31.1.b	13	55	8	-	12	-	20	3	15
S13.1.31.2.b	13	56	6	-	10	-	21	3	15
S13.1.31.3.b	13	58	7	-	9	-	20	3	12

S13.1.32.1.b	21	50	11	-	7	-	24	2	12
S13.1.32.2.b	21	51	9	-	12	-	23	2	12
S13.1.32.3.b	21	56	6	5	7	-	22	3	14
S13.1.40.1.b	29	52	11	-	4	-	25	2	13
S13.1.40.2.b	29	54	7	5	8	-	21	2	13
S13.1.40.3.b	29	61	8	-	4	-	19	3	15
S13.1.41.1.b	40	55	9	4	7	-	22	2	12
S13.1.41.2.b	40	54	8	7	6	-	20	2	12
S13.1.41.3.b	40	49	9	5	9	-	23	3	13
S13.1.50.1.b	50	53	8	-	8	-	24	2	12
S13.1.50.2.b	50	61	6	-	7	-	18	2	12
S13.1.50.3.b	50	57	7	-	6	-	23	2	12
S13.1.60.1.b	113	58	7	4	8	-	20	2	13
S13.1.60.2.b	113	53	9	7	7	-	21	2	13
S13.1.60.3.b	113	60	6	4	5	-	21	2	12
TR2									
Supraglacial									
0-15 cm									
S13.2.10.1.a	0	51	9	-	9	-	25	2	12
S13.2.10.2.a	0	56	8	-	4	-	27	2	13
S13.2.10.3.a	0	57	8	-	6	-	22	2	11
S13.2.11.1.a	2	55	8	-	6	-	24	2	11
S13.2.11.2.a	2	54	8	-	6	-	25	2	13
S13.2.11.3.a	2	49	9	-	9	-	26	2	14
S13.2.20.1.a	3	58	8	-	7	-	22	2	14
S13.2.20.2.a	3	56	9	-	6	-	23	2	11
S13.2.20.3.a	3	56	11	-	6	-	21	2	12
S13.2.30.1.a.	5	50	11	-	8	-	25	2	12

S13.2.30.2.a.	5	57	11	-	7	-	20	2	13
S13.2.30.3.a.	5	61	9	-	7	-	18	2	11
S13.2.31.1.a	13	59	8	-	6	-	20	2	11
S13.2.31.2.a	13	62	6	-	5	-	20	3	17
S13.2.31.3.a	13	63	5	-	5	-	20	2	14
S13.2.32.1.a	21	54	9	4	5	-	25	2	11
S13.2.32.2.a	21	61	8	4	4	-	20	2	14
S13.2.32.3.a	21	54	11	-	8	-	21	2	11
S13.2.32.1.a	25	57	9	-	4	-	23	2	14
S13.2.33.2.a	25	54	8	7	6	-	21	2	14
S13.2.33.3.a	25	54	11	5	8	-	19	2	11
S13.2.40.1.a	29	55	8	-	9	-	22	2	14
S13.2.40.2.a	29	59	8	-	8	-	21	3	16
S13.2.40.3.a	29	56	10	-	7	-	22	2	13
S13.2.41.1.a	40	62	6	-	6	-	19	2	12
S13.2.41.2.a	40	51	8	-	8	-	26	2	14
S13.2.41.3.a	40	55	6	4	8	-	23	2	13
S13.2.50.1.a	50	53	11	4	8	-	22	2	13
S13.2.50.2.a	50	60	8	-	6	-	21	2	12
S13.2.50.3.a	50	50	10	-	9	-	25	2	12
S13.2.51.1.a	73	54	9	-	5	4	24	2	12
S13.2.51.2.a	73	58	7	-	6	-	25	2	14
S13.2.51.3.a	73	56	6	5	5	-	24	2	14
S13.2.60.1.a	113	58	7	4	8	-	20	2	12
S13.2.60.2.a	113	56	8	-	9	-	21	2	12
S13.2.60.3.a	113	54	7	5	7	-	23	2	14
S13.2.10.1.b	0	55	10	-	15	-	16	2	11
S13.2.10.2.b	0	55	7	-	13	-	19	2	12

S13.2.10.3.b	0	65	5	-	7	-	17	3	18
TR2									
Supraglacial									
15-30 cm									
S13.2.11.1.b	2	55	8	-	6	-	24	2	13
S13.2.11.2.b	2	56	9	-	7	-	23	3	14
S13.2.11.3.b	2	49	9	-	9	-	26	2	11
S13.2.20.1.b	3	57	12	-	7	-	20	2	13
S13.2.20.2.b	3	50	11	-	8	-	25	2	12
S13.2.20.3.b	3	56	9	-	7	-	21	2	14
S13.2.30.1.b	5	56	8	-	5	-	26	2	14
S13.2.30.2.b	5	50	10	-	9	-	25	2	12
S13.2.30.3.b	5	52	11	-	8	-	22	2	12
S13.2.31.1.b	13	56	8	-	8	-	22	2	12
S13.2.31.2.b	13	56	7	-	9	-	22	2	14
S13.2.31.3.b	13	55	8	-	9	-	23	2	11
S13.2.32.1.b	21	56	8	-	8	-	24	2	14
S13.2.32.2.b	21	52	9	-	9	-	25	2	13
S13.2.32.3.b	21	49	9	-	9	-	26	2	11
S13.2.33.1.b	25	58	7	-	4	-	24	2	11
S13.2.33.2.b	25	59	8	-	9	-	19	2	14
S13.2.33.3.b	25	60	7	5	5	-	20	2	14
S13.2.40.1.b	29	58	8	4	7	-	21	3	17
S13.2.40.2.b	29	57	7	-	5	-	25	2	11
S13.2.40.3.b	29	54	6	-	8	-	26	2	11
S13.2.41.1.b	40	60	6	-	7	-	21	2	12
S13.2.41.2.b	40	58	6	-	7	-	24	2	13
S13.2.41.3.b	40	55	9	-	7	-	23	3	14

S13.2.60.1.b	50	55	7	5	8	4	20	2	11
S13.2.60.2.b	50	43	12	6	11	4	22	3	15
S13.2.60.3.b	50	49	7	7	8	-	25	2	13
S13.2.50.1.b	73	58	9	-	5	-	24	2	14
S13.2.50.2.b	73	62	4	-	4	-	24	2	12
S13.2.50.3.b	73	60	5	-	6	-	23	2	16
S13.2.51.1.b	113	54	7	6	8	-	22	2	12
S13.2.51.2.b	113	52	6	6	7	-	24	3	15
S13.2.51.3.b	113	53	9	-	7	-	24	2	11
S13.3.10.1.a	0	51	10	5	5	-	24	2	12
S13.3.10.2.a	0	49	10	7	8	5	19	2	12
S13.3.10.3.a	0	51	11	7	6	-	22	2	13
TR3									
Supraglacial									
0-15 cm									
S13.3.11.1.a	2	56	10	-	5	-	22	2	11
S13.3.11.2.a	2	55	9	4	3	4	24	2	13
S13.3.11.3.a	2	38	11	4	12	4	28	2	13
S13.3.20.1.a	3	52	9	4	4	4	25	2	12
S13.3.20.2.a	3	51	8	5	4	-	28	3	15
S13.3.20.3.a	3	60	7	5	4	-	20	3	16
S13.3.30.1.a	5	48	13	4	8	-	24	2	13
S13.3.30.2.a	5	52	10	5	5	-	24	2	11
S13.3.30.3.a	5	53	9	6	6	-	22	2	12
S13.3.31.1.a	13	56	10	5	7	-	19	2	11
S13.3.31.2.a	13	56	10	5	5	-	20	2	12
S13.3.31.3.a	13	49	11	6	2	5	25	2	12
S13.3.32.1.a	21	62	6	4	6	-	20	2	14

S13.3.32.2.a	21	49	8	7	6	-	28	2	15
S13.3.32.3.a	21	56	9	-	4	-	25	2	13
S13.3.40.1.a	29	58	8	-	9	-	19	2	14
S13.3.40.2.a	29	59	7	5	5	-	20	2	14
S13.3.40.3.a	29	57	8	4	7	-	21	3	17
S13.3.41.1.a	40	62	8	4	4	-	20	2	13
S13.3.41.2.a	40	59	10	4	6	-	18	2	11
S13.3.41.3.a	40	60	9	4	5	-	19	2	14
S13.3.50.1.a	50	56	8	7	5	-	21	2	12
S13.3.50.2.a	50	60	9	5	4	-	20	2	11
S13.3.50.3.a	50	60	9	6	4	-	17	2	11
S13.3.60.1.a	113	55	8	6	4	-	25	2	13
S13.3.60.2.a	113	56	10	5	7	-	20	2	13
S13.3.60.3.a	113	56	7	7	6	4	17	2	12
S13.3.10.1.b	0	54	8	7	6	-	22	2	13
S13.3.10.2.b	0	56	8	-	10	-	21	2	13
S13.3.10.3.b	0	55	9	6	6	-	19	2	12
TR3									
Supraglacial									
15-30 cm									
S13.3.11.1.b	2	50	8	-	5	-	29	2	12
S13.3.11.2.b	2	55	11	4	5	-	21	2	12
S13.3.11.3.b	2	49	10	4	7	-	25	2	13
S13.3.20.1.b	3	55	8	6	5	-	21	3	18
S13.3.20.2.b	3	51	12	7	4	-	21	2	12
S13.3.20.3.b	3	53	10	7	5	-	21	2	11
S13.3.30.1.b	5	48	10	7	4	-	27	2	13
S13.3.30.2.b	5	54	7	8	5	6	18	3	17

S13.3.30.3.b	5	51	9	8	7	-	20	2	11
S13.3.31.1.b	13	48	7	9	7	-	23	2	11
S13.3.31.2.b	13	56	7	7	6	-	21	2	13
S13.3.31.3.b	13	53	6	9	5	-	23	2	11
S13.3.32.1.b	21	47	9	6	7	5	24	2	12
S13.3.32.2.b	21	60	8	5	5	-	18	2	11
S13.3.32.3.b	21	62	6	5	4	-	19	2	14
S13.3.40.1.b	29	59	5	-	9	-	21	2	14
S13.3.40.2.b	29	58	10	6	5	-	18	2	14
S13.3.40.3.b	29	56	9	6	7	-	18	2	16
S13.3.41.1.b	40	57	7	5	8	-	21	2	13
S13.3.41.2.b	40	57	8	8	4	-	18	2	14
S13.3.41.3.b	40	58	9	5	7	-	18	2	12
S13.3.50.1.b	50	58	9	5	9	-	17	2	14
S13.3.50.2.b	50	55	8	6	9	-	19	2	12
S13.3.50.3.b	50	55	8	8	5	-	20	2	13
S13.3.60.1.b	113	62	7	7	3	-	17	2	12
S13.3.60.2.b	113	60	8	5	6	-	19	3	16
S13.3.60.3.b	113	51	9	7	7	-	21	2	13
Replicate									
S13.1.20.1.b	3	55	7	-	9	-	22	3	13
(b)		55	8	-	10	-	21	2	13
(c)		60	9	-	8	-	19	3	18
(d)		58	8	-	7	-	19	2	12
(e)		60	10	-	5	-	19	2	12
Mean $\bar{x}$		58	8	-	8	-	20	2	13
Sd 1 σ		3	1	-	2	-	1	1	2

S13.1.50.1.a	50	52	8	5	6	-	25	2	12
(b)		53	10	7	4	-	21	2	11
(c)		59	7	6	4	-	20	2	14
(d)		53	7	6	7	-	21	2	12
(e)		59	10	6	5	-	18	2	13
Mean $\bar{x}$		55	8	6	5	-	21	2	13
Sd 1 σ		3	2	1	1	-	3	0	1
S13.2.60.1.b	113	57	7	-	8	4	20	2	11
(b)		56	10	4	5	-	21	2	13
(c)		62	7	5	4	-	19	2	11
(d)		53	7	6	7	-	21	3	17
(e)		60	10	-	5	-	19	2	11
Mean $\bar{x}$		58	8	5	6	-	20	2	13
Sd 1 σ		4	2	1	2	-	1	0	3
S13.3.11.2.a	2	55	9	4	3	4	24	2	13
(b)		53	6	8	5	-	25	2	14
(c)		61	7	5	7	-	18	2	11
(d)		52	11	5	8	-	20	3	15
(e)		58	7	6	4	-	22	3	16
Mean $\bar{x}$		56	8	6	5	-	22	2	14
Sd 1 σ		4	2	2	2	-	3	1	2
S13.3.30.3.b	5	58	7	-	6	-	20	2	11
(b)	5	54	11	5	10	-	16	2	12
(c)	5	58	10	-	6	4	20	2	13
(d)	5	53	6	5	8	4	22	3	12
(e)	5	58	7	4	6	-	21	2	12
Mean $\bar{x}$		56	8	5	7	4	20	2	12
Sd 1 σ		2	2	1	1		2	0	1

Table. B.20. Clay mineral separates

Sample no.	sample no.	Age	Quartz	Albite	Kaolinite	Muscovite - 2M1	Chlorite
S13.1.10.3.b	1	0	16	6	20	30	27
S13.1.20.2.a	2	3	15	6	16	36	26
S13.1.41.3.b	3	40	10	-	16	46	25
S13.3.40.1.b.	4	29	13	8	16	44	18
S13.2.60.1.a.	5	100	13	6	17	41	23
S13.1.60.3.a	6	100	10	6	17	46	21
	Replicates						
	5a	n/a	13	6	17	41	23
	b	n/a	12	6	17	42	23
	c	n/a	13	6	17	44	20
	Mean	n/a	13	6	17	42	22
	1σSD	n/a	1	0	0	2	2

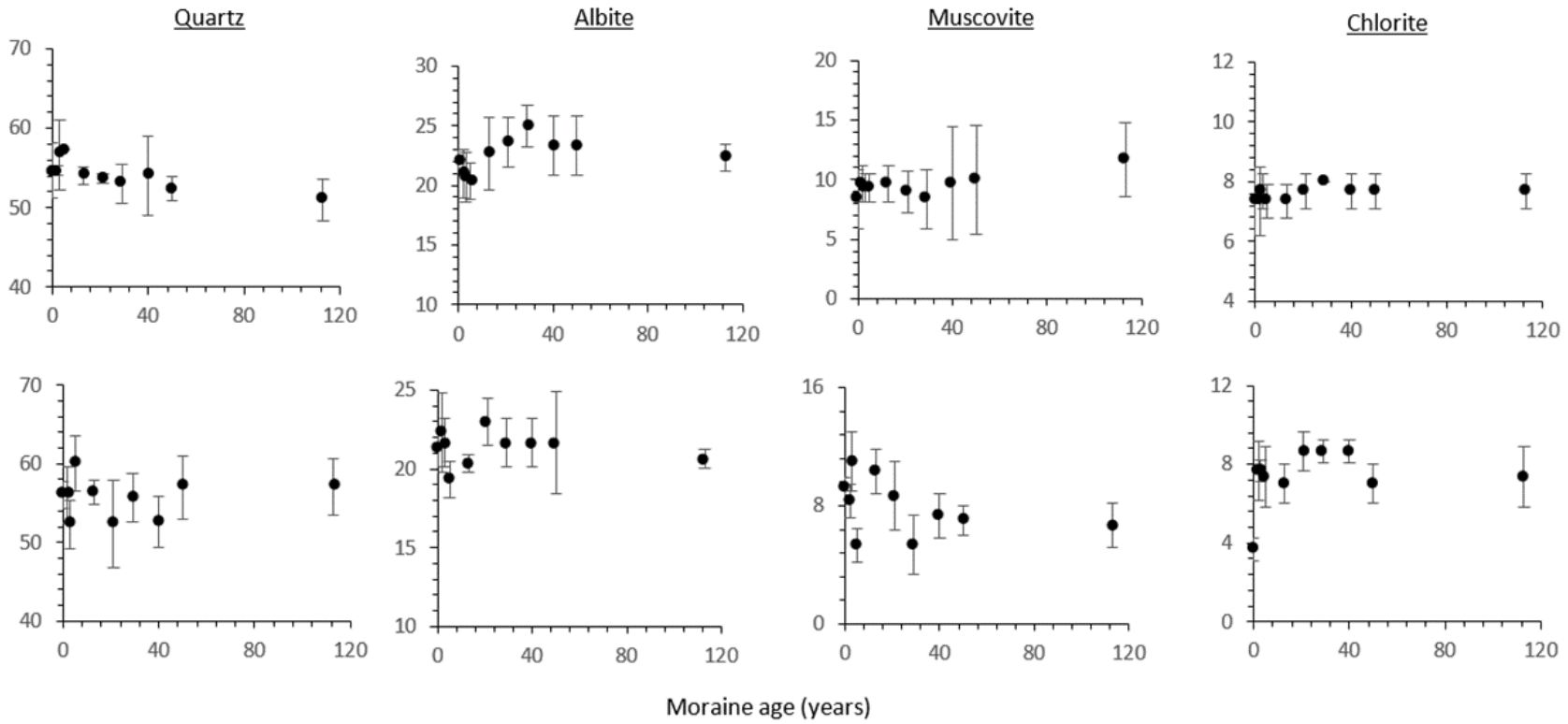

Figure. B.6. Mineralogical composition data for each of the major mineral constituents in bulk samples (<7mm) collected in 2013 from Tr1. Top plots are depth (a) and bottom depth (b).

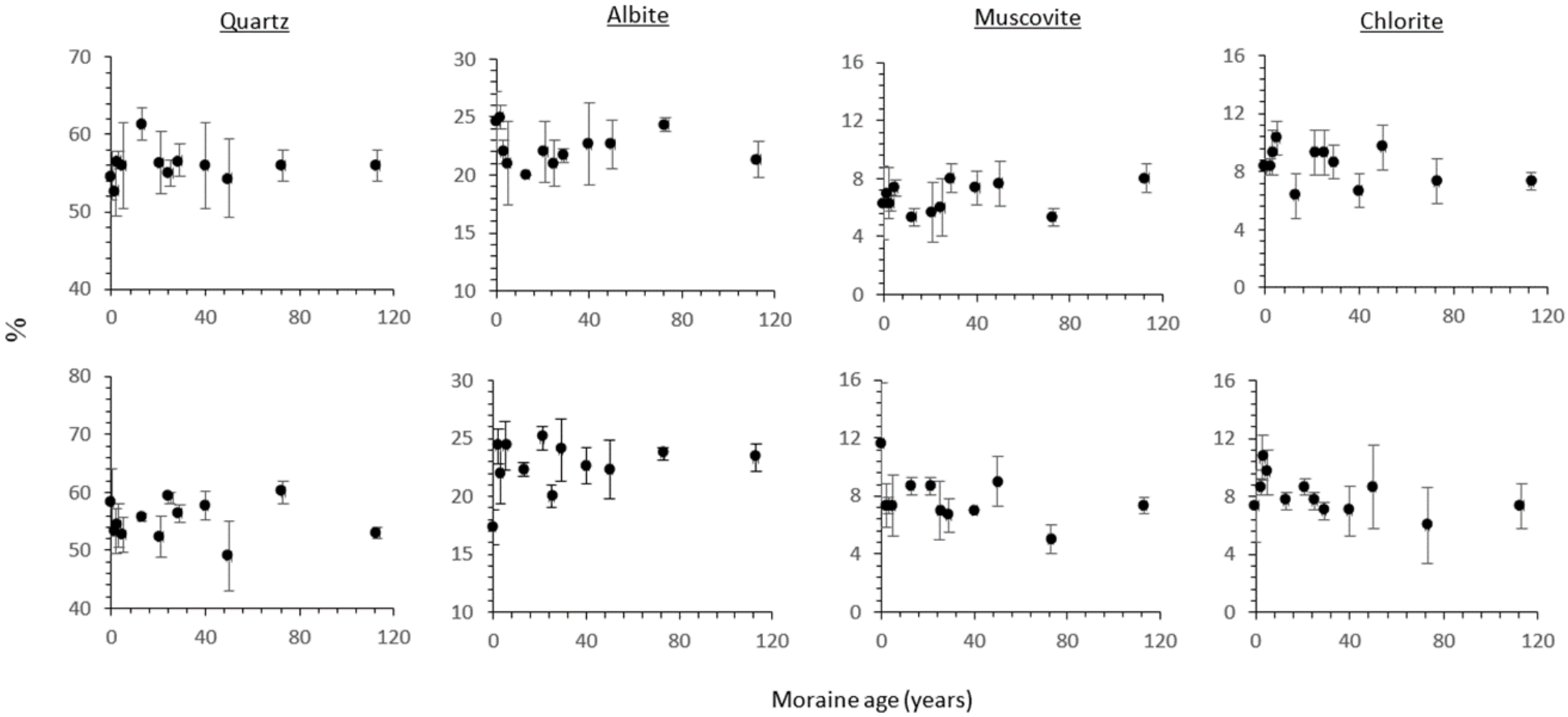

Figure. B.7. Mineralogical composition data for each of the major mineral constituents in bulk samples (<7mm) collected in 2013 from Tr2. Top plots are depth (a) and bottom depth (b).

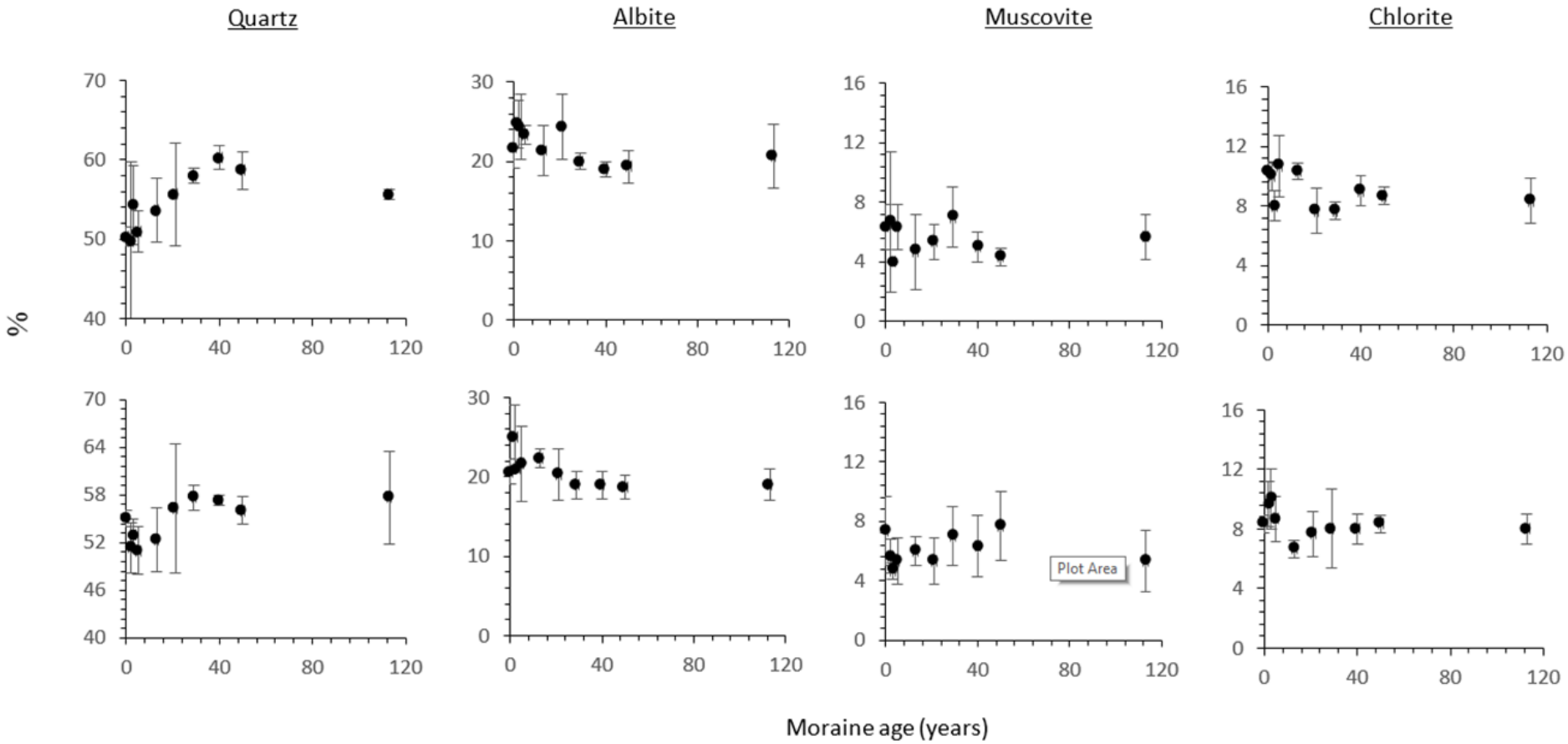

Figure. B.8. Mineralogical composition data for each of the major mineral constituents in bulk samples (<7mm) collected in 2013 from Tr3. Top plots are depth (a) and bottom depth (b).

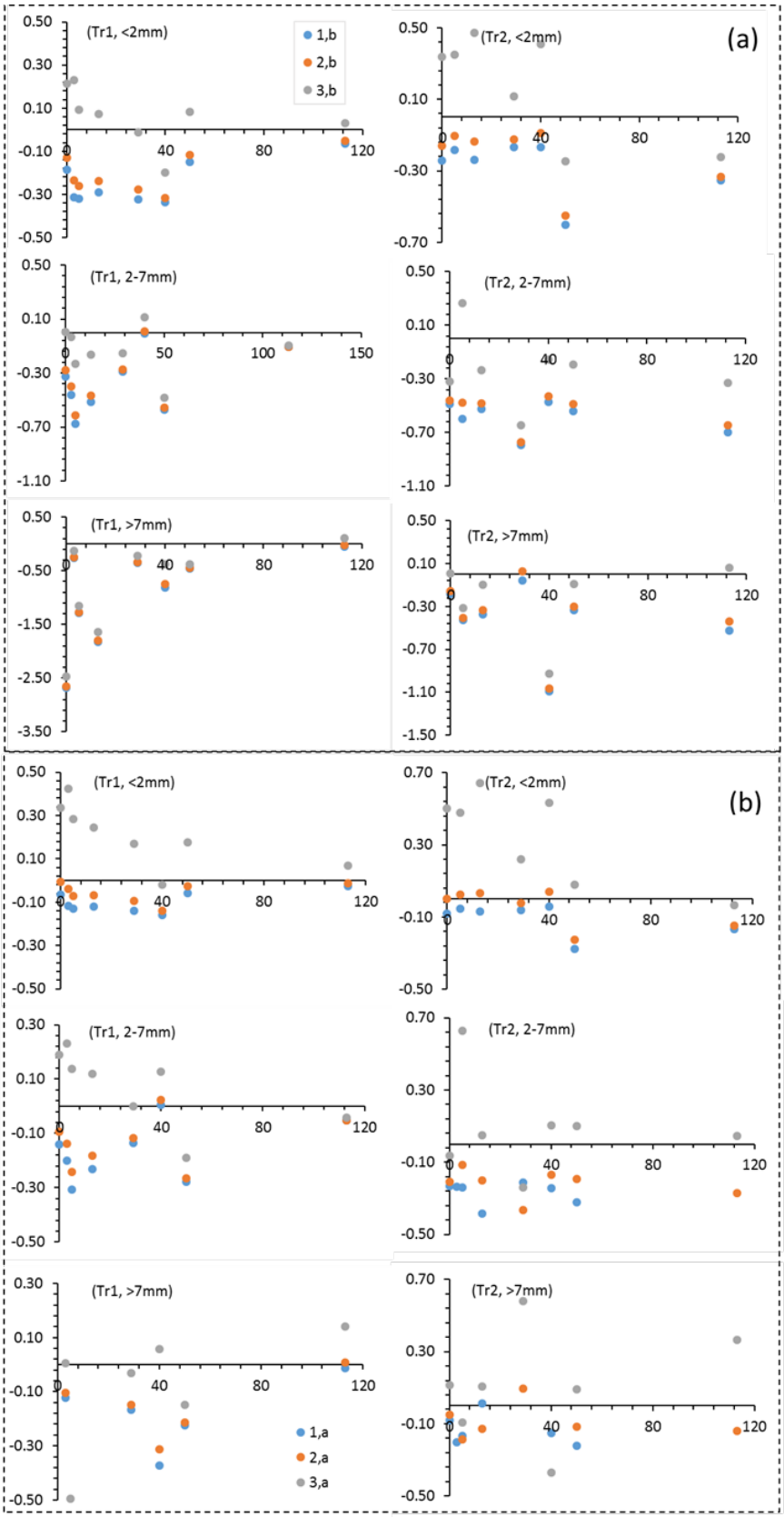

Figure. B.9.$TS_{sulfide}$ (pyrite) oxidation and carbonate dissolution theoretical reactions 1b,2b,3b Table. 4.4. compared to the measured concentrations of TSsulfide and TICcarbonate and their reaction stoichiometry. Values closest to zero denote the measured concentrations of $TS_{sulfide}$ and $TIC_{crustal}$ and their reaction stoichiometry that are closest to their theoretical stoichiometry (highlighted in grey).

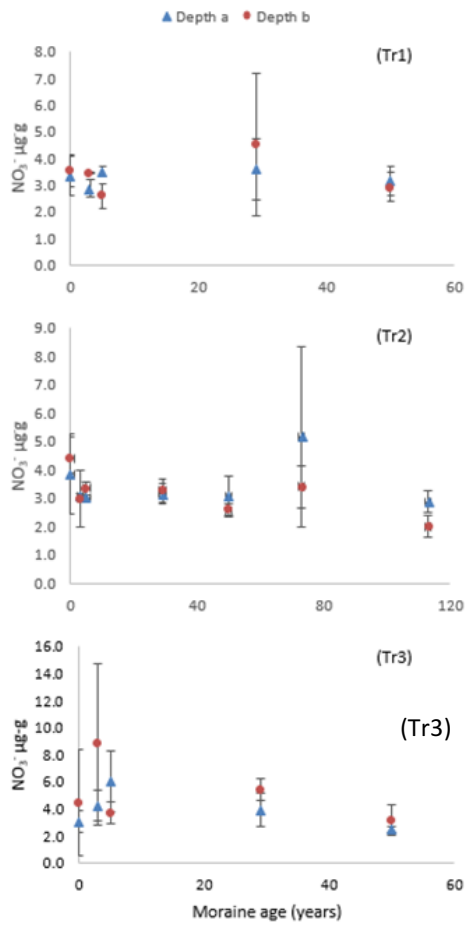

Figure. B.10. Nitrate concentations as a function of moraine age for each transect Tr1, Tr2 and Tr3. Symbols denote the $\bar{x}$ of *n*=3 sample pHs taken at each moraine age along a 10-meter travers and bars repersent 1σ sd. Note: this data was measured by Thomas Turpin-Jelfs from the University of Bristol. Tr1 and Tr3 were only analysed for nitrate up to the 60-year-old moraine. For method used see below.

Method for Nitrate extraction: carried out by Thomas Turpin-Jelfs from the University of Bristol.
Concentrations of exchangeable ammonium (NH_4^-N) and nitrate (NO_3^-N) in soil were extracted with 2M KCl (1:50 m/v soil:extractant) and determined colourimetrically using a flow injection analyser (Lachat QuikChem 8500 Series 2 FIA system, Loveland, CO, USA) where the precision error for NH_4^-N and NO_3^-N was ±3.7% and ±0.9%, respectively according to mid-range standards (calibration range: 0-0.5 mg L-1). Thus, for each sample, 0.2 g of fresh soil was added to 10 mL of 2M KCl, shaken for 30 minutes at 160 rpm, centrifuged for 5 minutes at 4,500 rpm and filtered to 0.45 µm using Whatman WCN plain cellulose nitrate filtrate papers. Extracts were then analysed for NH_4^-N using the Berthelot reaction (Willis et al., 1993) and NO_3^-N using the cadmium reduction method (Willis and Gentry, 1987). The detection limits for NH_4^-N and NO_3^-N were 0.041 µg N g−1 and 0.006 µg N g−1 for dry sediment, respectively. In addition, concentrations of total organic N (TON) were determined for all samples by subtracting the sum of their individual NH_4^-N and NO_3^-N concentrations from their respective concentrations of total N, which were obtained via the dry combustion method using a Eurovector EA3000 Elemental Analyser. All results were reported on a dry weight basis by calculation using the dry matter content data.

Appendix C.

Table. C.1. Total organic carbon and δ13Corganic concentration and their 1*σ from n=3 replicate measurements, from Midtre Lovénbreen, Storglaciären and Rabot's forefields.

Forefield	Sample No.	Moraine age	TOC	$\delta^{13}C_{org}$	Standard deviation	Standard deviation	Total Inorganic Carbon
#	#	(years)	%	‰	%	‰	(wt%)
ML	S13.1.10.1.a	0	0.07	-19.96	0.00	0.18	0.36
	S13.1.10.2.a	0	0.07	-19.28	0.00	0.97	0.22
	S13.1.10.3.a	0	0.07	-18.71	0.00	0.44	0.28
	S13.1.11.1.a	2	0.07	-19.21	0.00	0.18	0.21
	S13.1.11.2.a	2	0.10	-20.68	0.01	0.51	0.26
	S13.1.11.3.a	2	0.08	-20.30	0.01	0.08	0.18
	S13.1.20.1.a	3	0.07	-19.17	0.00	0.01	0.20
	S13.1.20.2.a	3	0.07	-18.98	0.00	0.06	0.26
	S13.1.20.3.a	3	0.08	-19.21	0.00	0.23	0.25
	S13.1.30.1.a	5	0.08	-20.82	0.01	0.12	0.18
	S13.1.30.2.a	5	0.08	-19.59	0.00	0.08	0.23
	S13.1.30.3.a	5	0.08	-20.07	0.00	0.53	0.20
	S13.1.31.3.a	13	0.09	-20.02	0.00	0.03	0.17
	S13.1.31.3.a	13	0.08	-20.05	0.00	0.08	0.21
	S13.1.31.3.a	13	0.09	-20.62	0.00	0.18	0.18
	S13.1.32.3.a	21	0.10	-21.39	0.01	0.18	0.13
	S13.1.32.3.a	21	0.11	-21.62	0.00	0.01	0.13
	S13.1.32.3.a	21	0.13	-22.01	0.01	0.41	0.20
	S13.1.40.1.a	29	0.12	-22.75	0.02	0.71	0.12
	S13.1.40.2.a	29	0.09	-21.53	0.00	0.04	0.29
	S13.1.40.3.a	29	0.15	-22.89	0.00	0.20	0.15
	S13.1.41.3.a	40	0.07	-19.55	0.00	0.11	0.25
	S13.1.41.3.a	40	0.18	-24.16	0.06	0.06	0.21
	S13.1.41.3.a	40	0.08	-19.84	0.00	0.10	0.25
	S13.1.50.1.a	50	0.22	-24.10	0.01	0.10	0.13
	S13.1.50.2.a	50	0.17	-23.16	0.01	0.49	0.09
	S13.1.50.3.a	50	0.15	-23.76	0.01	0.15	0.08
	S13.1.60.1.a	113	0.28	-24.56	0.01	0.14	0.12
	S13.1.60.2.a	113	0.20	-23.74	0.02	0.31	0.14
	S13.1.60.3.a	113	0.30	-24.65	0.02	0.15	0.14
	S13.1.10.1.b	0	0.09	-20.24	0.00	0.18	-
	S13.1.10.2.b	0	0.10	-20.67	0.00	0.09	-
	S13.1.10.3.b	0	0.07	-19.49	0.01	0.06	-
	S13.1.11.1.b	2	0.08	-20.25	0.00	0.01	-
	S13.1.11.2.b	2	0.08	-20.34	0.00	0.44	-
	S13.1.11.3.b	2	0.09	-20.61	0.00	0.07	-
	S13.1.20.1.b	3	0.10	-21.41	0.00	0.17	-
	S13.1.20.2.b	3	0.09	-21.44	0.01	0.22	-
	S13.1.20.3.b	3	-	-	-	-	-
	S13.1.30.1.b	5	0.11	-20.58	0.04	0.58	-
	S13.1.30.2.b	5	0.08	-19.38	0.00	0.14	-
	S13.1.30.3.b	5	0.08	-18.95	0.01	0.40	-

S13.1.31.3.b	13	0.11	-21.07	0.00	0.16	-
S13.1.31.3.b	13	0.12	-21.65	0.01	0.26	-
S13.1.31.3.b	13	0.07	-20.25	0.00	0.26	-
S13.1.32.3.b	21	0.10	-21.32	0.00	0.43	-
S13.1.32.3.b	21	0.10	-21.55	0.01	0.03	-
S13.1.32.3.b	21	0.12	-21.22	0.00	0.16	-
S13.1.40.1.b	29	0.08	-20.62	0.01	0.25	-
S13.1.40.2.b	29	0.09	-20.21	0.00	0.14	-
S13.1.40.3.b	29	0.17	-23.26	0.03	0.24	-
S13.1.41.3.b	40	0.19	-22.80	0.01	0.10	-
S13.1.41.3.b	40	0.18	-22.97	0.02	0.27	-
S13.1.41.3.b	40	0.12	-22.02	0.01	0.65	-
S13.1.50.1.b	50	0.12	-22.21	0.01	0.33	-
S13.1.50.2.b	50	0.10	-21.02	0.00	0.04	-
S13.1.50.3.b	50	0.17	-23.08	0.02	0.32	-
S13.1.60.1.b	113	0.16	-23.54	0.03	0.22	-
S13.1.60.2.b	113	0.20	-23.98	0.04	0.82	-
S13.1.60.3.b	113	0.10	-20.76	0.00	0.04	-
S13.2.10.1.a	0	0.15	-23.19	0.01	0.40	-
S13.2.10.2.a	0	0.17	-23.88	0.02	0.23	-
S13.2.10.3.a	0	0.12	-21.51	0.01	0.19	-
S13.2.11.1.a	2	0.14	-23.34	0.01	0.05	-
S13.2.11.2.a	2	0.33	-25.47	0.00	0.03	-
S13.2.11.3.a	2	0.15	-23.42	0.02	0.30	-
S13.2.20.1.a	3	2.53	-26.37	0.17	0.37	-
S13.2.20.2.a	3	3.93	-26.08	0.26	0.07	-
S13.2.20.3.a	3	2.35	-26.03	0.37	0.06	-
S13.2.30.1.a.	5	0.07	-19.64	0.01	0.76	-
S13.2.30.2.a.	5	0.09	-19.17	0.01	0.24	-
S13.2.30.3.a.	5	0.09	-20.79	0.00	0.56	-
S13.2.31.1.a	13	0.08	-20.95	0.00	0.02	-
S13.2.31.2.a	13	0.08	-19.76	0.00	0.06	-
S13.2.31.3.a	13	0.12	-20.91	0.00	0.17	-
S13.2.32.1.a	21	0.08	-20.21	0.01	0.27	-
S13.2.32.1.a	21	0.09	-20.60	0.00	0.19	-
S13.2.32.3.a	21	0.08	-20.42	0.00	0.09	-
S13.2.32.1.a	25	0.09	-21.08	0.00	0.01	-
S13.2.33.1.a	25	0.09	-20.97	0.00	0.16	-
S13.2.33.3.a	25	0.06	-18.85	0.00	0.04	-
S13.2.40.1.a	29	0.10	-22.86	0.01	0.04	-
S13.2.40.2.a	29	0.12	-22.40	0.02	0.47	-
S13.2.40.3.a	29	0.12	-22.85	0.01	0.44	-
S13.2.41.1.a	40	0.15	-23.55	0.03	0.55	-
S13.2.41.2.a	40	0.11	-21.42	0.02	0.32	-
S13.2.41.3.a	40	0.08	-20.73	0.00	0.17	-
S13.2.50.1.a	50	0.08	-22.02	0.00	0.01	-
S13.2.50.2.a	50	0.10	-21.72	0.01	0.27	-
S13.2.50.3.a	50	0.26	-23.75	0.02	0.37	-
S13.2.51.1.a	73	0.15	-23.00	0.01	0.08	-
S13.2.51.2.a	73	0.14	-22.51	0.02	0.13	-

S13.2.51.3.a	73	0.18	-24.47	0.01	0.08	-
S13.2.60.1.a	113	0.12	-23.53	0.02	1.03	-
S13.2.60.2.a	113	0.11	-21.68	0.00	0.19	-
S13.2.60.3.a	113	0.12	-21.78	0.02	0.11	-
S13.2.70.1.a	~2000	0.16	-23.46	0.03	1.18	-
S13.2.70.2.a	~2000	0.18	-22.90	0.01	0.24	-
S13.2.70.3.a	~2000	0.07	-19.69	0.01	0.22	-
S13.2.10.1.b	0	0.07	-19.13	0.00	0.25	-
S13.2.10.2.b	0	0.07	-19.62	0.01	0.14	-
S13.2.10.3.b	0	0.09	-21.43	-	-	-
S13.2.11.1.b	2	0.08	-20.85	0.01	0.39	-
S13.2.11.2.b	2	0.08	-20.82	0.00	0.10	-
S13.2.11.3.b	2	0.08	-20.58	0.00	0.07	-
S13.2.20.1.b	3	0.08	-20.49	0.01	0.31	-
S13.2.20.2.b	3	0.10	-21.43	0.01	0.40	-
S13.2.20.3.b	3	0.07	-20.10	0.00	0.27	-
S13.2.30.1.b	5	0.07	-19.28	0.00	0.10	-
S13.2.30.2.b	5	0.07	-19.56	0.00	0.01	-
S13.2.30.3.b	5	0.07	-20.40	0.00	0.08	-
S13.2.31.1.b	13	0.07	-21.32	0.01	0.02	-
S13.2.31.2.b	13	0.06	-19.98	0.00	0.12	-
S13.2.31.3.b	13	0.15	-23.01	0.02	0.49	-
S13.2.32.1.b	21	0.20	-23.40	0.02	0.19	-
S13.2.32.2.b	21	0.07	-20.40	0.00	0.38	-
S13.2.32.3.b	21	0.08	-20.24	0.00	0.17	-
S13.2.33.1.b	25	0.07	-19.16	0.00	0.22	-
S13.2.33.2.b	25	0.26	-24.75	0.04	0.54	-
S13.2.33.3.b	25	0.09	-22.10	0.01	1.17	-
S13.2.40.1.b	29	0.12	-21.70	0.01	0.07	-
S13.2.40.2.b	29	0.11	-21.77	0.00	0.14	-
S13.2.40.3.b	29	0.12	-21.86	0.01	0.12	-
S13.2.41.1.b	40	0.17	-23.57	0.01	0.52	-
S13.2.41.2.b	40	0.18	-23.14	0.04	0.62	-
S13.2.41.1.b	40	0.25	-23.83	0.02	0.94	-
S13.2.60.1.b	50	0.26	-24.28	0.01	0.23	-
S13.2.60.2.b	50	0.13	-22.29	0.00	0.28	-
S13.2.60.3.b	50	0.05	-20.44	0.00	0.09	-
S13.2.50.1.b	73	0.06	-20.82	0.00	0.15	-
S13.2.50.2.b	73	0.07	-19.88	0.00	0.18	-
S13.2.50.3.b	73	0.08	-20.13	0.01	0.02	-
S13.2.51.1.b	113	0.10	-20.03	0.01	0.80	-
S13.2.51.2.b	113	0.08	-19.92	0.00	0.14	-
S13.2.51.3.b	113	0.07	-19.11	0.00	0.09	-
S13.1.10.1.a	0	0.07	-20.24	0.01	1.63	-
S13.1.10.2.a	0	0.10	-21.70	0.01	0.77	-
S13.1.10.3.a	0	0.09	-20.17	0.00	0.28	-
S13.1.11.1.a	2	0.08	-20.33	0.00	0.18	-
S13.1.11.2.a	2	0.05	-20.49	0.00	0.35	-
S13.1.11.3.a	2	0.07	-20.68	0.01	0.94	-
S13.1.20.1.a	3	0.08	-21.71	0.00	0.13	-

S13.1.20.2.a	3	0.11	-21.40	0.01	0.31	-
S13.1.20.3.a	3	0.08	-19.26	0.00	0.16	-
S13.1.30.1.a	5	0.14	-22.65	0.00	0.11	-
S13.1.30.2.a	5	0.15	-21.38	0.02	1.41	-
S13.1.30.3.a	5	0.09	-20.24	0.00	0.20	-
S13.1.31.3.a	13	0.12	-21.48	0.02	0.50	-
S13.1.31.3.a	13	0.13	-22.77	0.00	0.13	-
S13.1.31.3.a	13	0.08	-21.06	0.00	0.54	-
S13.1.32.3.a	21	0.12	-21.75	0.00	0.02	-
S13.1.32.3.a	21	0.16	-23.73	0.02	0.95	-
S13.1.32.3.a	21	0.09	-20.40	0.00	0.10	-
S13.1.40.1.a	29	0.10	-21.44	0.01	1.26	-
S13.1.40.2.a	29	0.10	-22.69	0.01	0.37	-
S13.1.40.3.a	29	0.10	-20.78	0.00	0.33	-
S13.1.41.3.a	40	0.20	-23.71	0.00	0.76	-
S13.1.41.3.a	40	0.20	-22.66	0.01	0.71	-
S13.1.41.3.a	40	0.24	-23.11	0.01	0.10	-
S13.1.50.1.a	50	0.14	-23.52	0.01	0.80	-
S13.1.50.2.a	50	0.24	-24.08	0.07	1.14	-
S13.1.50.3.a	50	0.07	-21.50	0.00	0.08	-
S13.1.60.1.a	113	0.05	-19.47	0.00	0.02	-
S13.1.60.2.a	113	0.09	-22.76	0.04	2.85	-
S13.1.60.3.a	113	0.06	-21.80	0.02	2.19	-
S13.1.10.1.b	0	0.08	-20.31	0.00	0.14	-
S13.1.10.2.b	0	0.12	-20.78	0.01	0.05	-
S13.1.10.3.b	0	0.08	-18.49	0.01	0.29	-
S13.1.11.1.b	2	0.22	-23.34	0.03	0.18	-
S13.1.11.2.b	2	0.08	-20.53	0.00	0.40	-
S13.1.11.3.b	2	0.08	-19.50	0.01	0.15	-
S13.1.20.1.b	3	0.07	-18.89	0.00	0.35	-
S13.1.20.2.b	3	0.08	-20.30	0.00	0.22	-
S13.1.20.3.b	3	0.15	-20.82	0.01	0.17	-
S13.1.30.1.b	5	0.09	-21.22	0.00	0.21	-
S13.1.30.2.b	5	0.06	-19.22	0.00	0.22	-
S13.1.30.3.b	5	0.09	-20.60	0.00	0.11	-
S13.1.31.3.b	13	0.07	-20.05	0.00	0.07	-
S13.1.31.3.b	13	0.08	-20.20	0.00	0.01	-
S13.1.31.3.b	13	0.07	-19.55	0.00	0.16	-
S13.1.32.3.b	21	0.07	-19.45	0.00	0.21	-
S13.1.32.3.b	21	0.12	-22.53	0.01	0.44	-
S13.1.32.3.b	21	0.09	-20.94	0.00	0.39	-
S13.1.40.1.b	29	0.11	-22.04	0.00	0.15	-
S13.1.40.2.b	29	0.08	-19.69	0.00	0.49	-
S13.1.40.3.b	29	0.12	-21.59	0.01	0.00	-
S13.1.41.3.b	40	0.08	-21.41	0.01	0.65	-
S13.1.41.3.b	40	0.08	-21.05	0.01	0.04	-
S13.1.41.3.b	40	0.07	-19.06	0.00	0.19	-
S13.1.50.1.b	50	0.19	-23.53	0.00	0.08	-
S13.1.50.2.b	50	0.11	-21.53	0.00	0.32	-
S13.1.50.3.b	50	0.10	-21.81	0.00	0.19	-

	S13.1.60.1.b	113	0.08	-21.78	0.01	1.26	-
	S13.1.60.2.b	113	0.17	-22.93	0.02	0.40	-
	S13.1.60.3.b	113	0.21	-23.16	0.05	0.91	-
ST	ST 2a	24	0.04	-23.60	0.00	0.32	0.82
	ST 2b	24	0.04	-24.37	0.00	0.60	0.71
	ST 2c	24	0.05	-24.72	0.00	0.16	0.79
	ST 3a	27	0.20	-25.15	0.01	0.31	3.05
	ST 3b	27	0.20	-24.45	0.01	0.20	3.32
	ST 3c	27	0.39	-24.77	0.01	0.23	3.61
	ST 4a	34	0.04	-24.06	0.00	0.16	0.63
	ST 4b	34	0.04	-23.70	0.00	0.44	0.84
	ST 4c	34	0.09	-25.64	0.03	1.14	2.32
	ST 5a	55	0.08	-24.87	0.02	0.25	1.16
	ST 5b	55	0.03	-24.67	0.01	0.81	0.49
	ST 5c	55	0.03	-24.44	0.01	1.09	0.81
	ST 6a	80	0.20	-25.42	0.05	0.28	3.65
	ST 6b	80	0.27	-26.29	0.01	0.29	5.26
	ST 6c	80	0.57	-26.63	0.04	0.13	6.37
	ST 7a	31	0.06	-23.84	0.00	0.34	1.37
	ST 7b	31	0.05	-23.69	0.00	0.45	1.38
	ST 7c	31	0.03	-23.55	0.00	0.24	0.63
	ST 8a	45	0.05	-23.83	0.00	0.12	1.26
	ST 8b	45	0.03	-24.66	0.00	0.37	0.63
	ST 8c	45	0.03	-23.35	0.01	0.28	0.54
	ST 9a	80	0.06	-24.70	0.01	0.57	1.07
	ST 9b	80	0.05	-24.83	0.01	1.12	1.58
	ST 9c	80	0.02	-23.44	0.00	0.90	0.53
	ST 10a	N/A	0.01	-24.39	0.00	1.41	0.25
	ST 10b	N/A	0.01	-23.91	0.00	0.47	0.22
	ST 10c	N/A	0.01	-23.69	0.00	1.13	0.30
	ST 11a	N/A	0.34	-25.16	0.01	0.09	7.84
	ST 11b	N/A	0.23	-24.72	0.01	0.07	5.30
	ST 11c	N/A	0.36	-26.07	0.01	0.16	10.72
	ST 12	N/A	1.26	-24.05	0.03	0.11	77.88
	ST 15a	0	0.02	-22.90	0.00	0.91	0.89
	ST 15b	0	0.01	-24.15	0.00	0.00	0.34
	ST 15c	0	0.02	-23.21	0.00	1.04	0.27
	ST 16a	15	0.02	-23.44	0.00	0.07	0.36
	ST 16b	15	0.01	-23.19	0.00	0.08	0.28
	ST 16c	15	0.01	-22.96	0.00	0.91	0.38
	ST 17a	20	0.01	-22.19	0.00	0.42	0.40
	ST 17b	20	0.02	-23.01	0.00	0.01	0.32
	ST 17c	20	0.02	-23.63	0.00	1.85	0.32
RB	RB 1a	0	0.03	-22.66	0.00	0.17	0.52
	RB 1b	0	0.03	-23.64	0.01	1.43	0.56
	RB 1c	0	0.07	-23.13	0.00	0.16	1.65
	RB 2a	16	0.02	-21.36	0.00	0.88	0.43
	RB 2b	16	0.01	-22.39	0.00	2.79	0.32
	RB 2c	16	0.02	-19.96	0.00	0.14	0.43
	RB 3a	34	0.02	-20.27	0.00	0.38	0.51

RB 3b	34	0.02	-23.08	0.01	2.08	0.62
RB 3c	34	0.02	-21.45	0.00	0.36	0.58
RB 4a	62	0.03	-21.90	0.00	1.51	0.77
RB 4b	62	0.08	-24.08	0.02	1.59	1.14
RB 4c	62	0.11	-23.92	0.02	0.32	1.31
RB 5a	104	0.08	-24.63	0.02	0.96	1.25
RB 5b	104	0.14	-25.26	0.01	0.03	2.08
RB 5c	104	0.05	-24.20	0.02	1.28	1.22
RB 6	104	1.06	-22.77	0.24	0.90	48.80
RB 0	N/A	1.00	-24.34	0.15	0.90	61.79

Note: Samples ST 10 (a,b,c) and ST 11 (a,b,c) were taken from proglacial ephemeral streams, in addition to ST 12 that was taken from cyroconite on the glacier surface of Storglaciären. These were obtained as they could be a potential input to the forefield. RB 6 was obtained prior to helicopter pick-up and due to time constraints only one sample could be taken. Sample RB 0 was taken from cyroconite on the surface of Rabot's glacier and could be a potential input into its forefield.

Table. C.2. Source rocks from Midtre Lovénbreen forefield and their TOC, TIC and TC concentration

Source rock label #	TOC (wt%)	TIC (wt%)	TC (wt%)
Dolomite (1)	0.00	10.54	10.54
Dolomite (2)	0.00	10.09	10.09
Dolomite (3)	0.00	10.69	10.69
Conglomerate	0.06	0.01	0.07
Sandstone	0.10	2.83	2.93
Psammite (1)	0.00	2.93	2.93
Psammite (2)	0.03	0.04	0.07
Psammite (3)	0.00	0.41	0.41
Mica schist (1)	0.00	0.00	0.00
Mica schist (2)	0.00	0.10	0.10
Phylite	0.00	0.12	0.12
Sum	0.19	37.77	37.96
Mean	0.02	3.43	3.45
SD 1σ	0.03	4.63	4.62

Table. C.3. Sensitivity analysis for the max, min, linear decrease and literature values for bulk density used in SOC stock calculations (Equ.A.10).

Forefield	Bulk density (g/cm^3)	SOC stock (slope) $kg^{-}m^2 a^{-1}$	(y) intercept	*r* value	P value
Midtre Lovénbreen	1.8	0.003	0.0751	0.90	<0.001
	0.8	0.0014	0.0325	0.90	<0.001
	Linear decrease (step 1/n)	0.0012	0.00734	0.82	<0.001
	*1.4	0.0024	0.0569	0.90	<0.001
Storglaciären	1.8	0.0008	0.02	0.52	<0.05
	0.8	0.0004	0.0089	0.52	<0.05
	Linear decrease (step 1/n)	0.0003	0.0217	0.46	<0.05
	**1.1	0.0006	0.0155	0.52	<0.05
Rabot's	1.8	0.0009	0.02	0.65	<0.05
	0.8	0.0004	0.008	0.65	<0.05
	Linear decrease (step 1/n)	0.0003	0.0232	0.44	>0.05
	**1.1	0.0007	0.0156	0.65	<0.05

Note: *1.4 is the average bulk density from He and Tang, 2008 and **1.1 Fuchs et al., 2015 for 100 years of deglaciation; grey highlighted cells are the values deemed the most representative of the bulk density of soils sampled in these forefields based on their similar forefield lithology.

Table. C.4. The analytical precision and limit of detection (LD) for the operationally defined iron fractions, measured using atomic absorbance spectroscopy (AAS).

	Ferrihydrite		*Fe oxides		Magnetite		**Fe sheet-silicates	
	blanks	5ppm	blanks	5ppm	blanks	5ppm	blanks	5ppm
1	0.00	4.99	0.02	4.88	0.00	5.00	-0.02	4.89
2	-0.01	4.97	-0.03	4.85	0.00	4.97	-0.02	5.00
3	-0.01	4.96	-0.02	5.03	-0.02	5.09	-0.02	4.99
4	-0.01	5.00	0.00	5.05	-0.02	4.99	-0.02	4.99
5	0.00	4.99	-0.03	5.00	0.00	4.97	-0.03	5.00
6	0.00	4.99	-0.02	5.00	-0.01	5.01	0.00	5.10
7	0.00	5.00	0.00	4.97	0.01	4.99	0.00	5.04
8	0.00	4.94	0.01	5.08	-0.01	5.07	-0.02	5.06
Mean	0.00	4.98	-0.01	4.98	-0.01	5.01	-0.02	5.01
STD	0.00	0.02	0.02	0.08	0.01	0.05	0.01	0.06
95% confidence int.	0.00	0.02	0.01	0.07	0.01	0.04	0.01	0.05
LD	0.01	0.07	0.05	0.24	0.03	0.14	0.03	0.19

Note: *Fe oxides = 'reducible' Fe oxides (goethite, hematite and akaganeite and carbonates e.g. siderite and ankerite);
**Fe silicate =; silicates = sheet-silicate minerals (e.g. nontronite, chlorite, glauconite, biotite).

Table. C.5. Operationally defined iron fractions sample analytical replicates, measured using AAS.

Sample No.	Ferrihydrite (wt%)	*Fe oxides (wt%)	Magnetite (wt%)	**Fe sheet-silicates (wt%)	Σ extraction pools (wt%)
S13.1.60.2.b	0.05	0.22	0.24	1.45	1.97
S13.1.60.2.b	0.05	0.22	0.25	1.27	1.80
S13.1.60.2.b	0.08	0.18	0.28	1.40	1.94
S13.1.60.2.b	0.07	0.20	0.23	1.27	1.77
S13.1.60.2.b	0.07	0.19	0.27	1.22	1.75
Mean	0.06	0.20	0.26	1.38	1.90
STD	0.02	0.02	0.02	0.09	0.09
95% confid.	0.02	0.03	0.03	0.12	0.11

Sample No.	Ferrihydrite (wt%)	*Fe oxides (wt%)	Magnetite (wt%)	**Fe sheet-silicates (wt%)	Σ extraction pools (wt%)
S13.3.60.3.a	0.053	0.24	0.33	0.95	1.58
S13.3.60.3.a	0.049	0.20	0.28	0.77	1.30
S13.3.60.3.a	0.053	0.25	0.28	1.00	1.58
S13.3.60.3.a	0.054	0.25	0.29	0.84	1.43
S13.3.60.3.a	0.052	0.23	0.31	0.97	1.57
Mean	0.052	0.23	0.29	0.91	1.49
STD	0.002	0.02	0.03	0.12	0.16
95% confid.	0.003	0.03	0.04	0.15	0.20

Sample No.	Ferrihydrite (wt%)	*Fe oxides (wt%)	Magnetite (wt%)	**Fe sheet-silicates (wt%)	Σ extraction pools (wt%)
S13.1.10.3.a	0.073	0.14	0.322	0.92	1.46
S13.1.10.3.a	0.067	0.13	0.324	1.06	1.58
S13.1.10.3.a	0.076	0.14	0.326	0.96	1.51
S13.1.10.3.a	0.071	0.13	0.339	1.02	1.56
S13.1.10.3.a	0.067	0.12	0.285	0.90	1.37
Mean	0.072	0.14	0.324	0.98	1.52
STD	0.005	0.01	0.002	0.07	0.06
95% confid.	0.006	0.01	0.003	0.09	0.08

Note: *Fe oxides = 'reducible' Fe oxides (goethite, hematite and akaganeite and carbonates e.g. siderite and ankerite) **Fe sheet-silicate minerals (e.g. nontronite, chlorite, glauconite, biotite).

Table. C.6. Operationally defined iron fractions, internal standard used in each of the **extraction runs.**

Sample No. #	Ferrihydrite (wt%)	*Fe oxides (wt%)	Magnetite (wt%)	**Fe sheet-silicates (wt%)	Σ extraction pools (wt%)
S13.3.60.1.a	0.076	0.16	0.22	1.23	1.69
S13.3.60.1.a	0.076	0.15	0.22	1.20	1.65
S13.3.60.1.a	0.081	0.18	0.28	0.75	1.29
S13.3.60.1.a	0.071	0.14	0.25	1.08	1.53
S13.3.60.1.a	0.072	0.16	0.26	0.94	1.44
S13.3.60.1.a	0.071	0.15	0.23	0.85	1.30
S13.3.60.1.a	0.070	0.16	0.26	1.07	1.56
Mean	0.074	0.16	0.25	1.02	1.49
STD	0.004	0.01	0.02	0.18	0.16
95% confid.	0.004	0.01	0.02	0.16	0.14

Note: *Fe oxides = 'reducible' Fe oxides (goethite, hematite and akaganeite and carbonates e.g. siderite and ankerite);
**Fe silicate =; silicates = sheet-silicate minerals (e.g. nontronite, chlorite, glauconite, biotite).

Table. C.7. Operationally defined iron fractions for Midtre Lovénbreen (ML), Storglaciären (ST) and Rabot's (RB).

Forefield *transect no* depth (cm)	Sample No. #	Moraine age (years)	Ferrihydrite (wt%)	*Fe oxides (wt%)	Magnetite (wt%)	**Fe sheet-silicate (wt%)	Σ extraction pools (wt%)	Total Fe_2O_3 (wt%)	Total Fe (wt%)	Unreactive Fe (wt%)
ML.*Tr1*. 0-15	S13.1.10.1.a	0	0.043	0.12	0.29	0.86	1.30	3.05	2.13	0.83
	S13.1.10.2.a	0	0.060	0.14	0.32	0.82	1.34	3.37	2.36	1.02
	S13.1.10.3.a	0	0.073	0.14	0.32	0.92	1.46	3.46	2.42	0.96
	S13.1.11.1.a	2	0.067	0.27	0.25	1.45	2.03	3.75	2.62	0.59
	S13.1.11.2.a	2	0.052	0.26	0.26	1.33	1.91	3.72	2.60	0.69
	S13.1.11.3.a	2	0.075	0.26	0.25	1.36	1.94	3.84	2.69	0.75
	S13.1.20.1.a	3	0.081	0.27	0.23	1.40	1.98	3.96	2.77	0.79
	S13.1.20.2.a	3	0.070	0.33	0.23	1.22	1.85	3.63	2.54	0.69
	S13.1.20.3.a	3	0.075	0.34	0.24	1.38	2.04	3.85	2.69	0.66
	S13.1.30.1.a	5	0.053	0.14	0.30	1.21	1.71	3.56	2.49	0.78
	S13.1.30.2.a	5	0.060	0.14	0.33	0.95	1.48	3.54	2.47	1.00
	S13.1.30.3.a	5	0.061	0.18	0.32	1.20	1.76	3.56	2.49	0.73
	S13.1.31.3.a	13	0.070	0.15	0.29	1.05	1.56	3.51	2.46	0.90
	S13.1.31.3.a	13	0.079	0.15	0.35	0.99	1.57	3.72	2.60	1.03
	S13.1.31.3.a	13	0.075	0.15	0.32	1.10	1.65	3.45	2.41	0.77
	S13.1.32.3.a	21	0.060	0.36	0.19	1.29	1.89	3.43	2.40	0.51
	S13.1.32.3.a	21	0.070	0.39	0.20	1.30	1.96	3.62	2.53	0.58
	S13.1.32.3.a	21	0.073	0.36	0.21	1.38	2.03	3.79	2.65	0.62
	S13.1.40.1.a	29	0.066	0.20	0.22	1.11	1.59	3.52	2.46	0.87
	S13.1.40.2.a	29	0.059	0.22	0.23	1.44	1.95	3.50	2.45	0.50
	S13.1.40.3.a	29	0.064	0.24	0.26	1.43	1.99	3.98	2.78	0.80
	S13.1.41.3.a	40	0.076	0.17	0.29	0.95	1.48	3.38	2.37	0.88
	S13.1.41.3.a	40	0.071	0.17	0.27	1.02	1.53	3.46	2.42	0.90
	S13.1.41.3.a	40	0.067	0.21	0.31	0.99	1.57	3.42	2.39	0.82
	S13.1.50.1.a	50	0.072	0.20	0.33	1.06	1.67	3.57	2.50	0.83
	S13.1.50.2.a	50	0.082	0.19	0.31	1.07	1.65	3.62	2.53	0.88
	S13.1.50.3.a	50	0.086	0.17	0.53	1.07	1.85	3.26	2.28	0.43
	S13.1.60.1.a	113	0.066	0.23	0.35	1.17	1.81	3.79	2.65	0.84
	S13.1.60.2.a	113	0.075	0.17	0.31	1.13	1.68	3.78	2.64	0.96
	S13.1.60.3.a	113	0.074	0.24	0.33	1.08	1.73	3.68	2.57	0.85
ML.*Tr1*. 15-30	S13.1.10.1.b	0	0.055	0.21	0.25	1.39	1.91	3.45	2.41	0.51
	S13.1.10.2.b	0	-	-	-	-	-	3.58	2.50	-
	S13.1.10.3.b	0	-	-	-	-	-	3.86	2.70	-

	S13.1.11.1.b	2	0.077	0.26	0.26	1.48	2.08	3.96	2.77	0.69
	S13.1.11.2.b	2	0.080	0.25	0.25	1.38	1.97	3.64	2.55	0.58
	S13.1.11.3.b	2	0.076	0.27	0.26	1.41	2.01	3.39	2.37	0.36
	S13.1.20.1.b	3	0.073	0.32	0.23	1.48	2.10	3.69	2.58	0.48
	S13.1.20.2.b	3	0.073	0.35	0.24	1.42	2.08	4.02	2.81	0.73
	S13.1.20.3.b	3	0.067	0.39	0.23	1.44	2.12	3.64	2.55	0.42
	S13.1.30.1.b	5	0.057	0.14	0.33	1.20	1.73	3.69	2.58	0.85
	S13.1.30.2.b	5	0.053	0.12	0.28	1.05	1.50	3.70	2.59	1.09
	S13.1.30.3.b	5	0.067	0.16	0.40	1.33	1.96	3.81	2.66	0.71
	S13.1.31.3.b	13	0.069	0.27	0.21	1.22	1.78	3.17	2.22	0.44
	S13.1.31.3.b	13	0.037	0.29	0.30	1.15	1.78	3.29	2.30	0.52
	S13.1.31.3.b	13	0.060	0.30	0.19	0.81	1.36	3.42	2.39	1.03
	S13.1.32.3.b	21	0.071	0.47	0.26	1.24	2.03	3.96	2.77	0.73
	S13.1.32.3.b	21	0.064	0.22	0.24	1.58	2.10	3.88	2.71	0.62
	S13.1.32.3.b	21	0.047	0.18	0.20	1.38	1.81	-	-	-
	S13.1.40.1.b	29	0.064	0.25	0.28	1.58	2.18	4.12	2.88	0.70
	S13.1.40.2.b	29	0.069	0.24	0.29	1.62	2.22	3.67	2.57	0.34
	S13.1.40.3.b	29	0.063	0.34	0.22	1.15	1.77	3.57	2.50	0.72
	S13.1.41.3.b	40	0.082	0.39	0.25	1.67	2.39	3.66	2.56	0.17
	S13.1.41.3.b	40	0.061	0.29	0.20	1.46	2.02	3.74	2.61	0.59
	S13.1.41.3.b	40	0.048	0.25	0.15	1.06	1.50	3.86	2.70	1.20
	S13.1.50.1.b	50	0.097	0.43	0.36	1.83	2.72	3.77	2.64	-0.09
	S13.1.50.2.b	50	0.070	0.28	0.22	1.15	1.72	3.80	2.66	0.94
	S13.1.50.3.b	50	0.072	0.39	0.28	1.55	2.29	3.89	2.72	0.43
	S13.1.60.1.b	113	0.084	0.48	0.29	1.64	2.50	3.86	2.70	0.21
	S13.1.60.2.b	113	0.081	0.38	0.28	1.40	2.15	3.93	2.75	0.60
	S13.1.60.3.b	113	0.067	0.24	0.29	1.39	1.99	4.11	2.87	0.89
ML.*Tr2*. 0-15	S13.2.10.1.a	0	0.087	0.22	0.40	1.76	2.47	3.63	2.54	0.07
	S13.2.10.2.a	0	0.083	0.19	0.44	1.48	2.20	3.55	2.49	0.29
	S13.2.10.3.a	0	0.062	0.16	0.33	1.37	1.92	3.15	2.20	0.28
	S13.2.11.1.a	2	0.042	0.12	0.27	0.98	1.42	3.51	2.46	1.04
	S13.2.11.2.a	2	0.060	0.24	0.30	0.77	1.37	3.53	2.47	1.10
	S13.2.11.3.a	2	0.047	0.13	0.34	1.11	1.63	3.84	2.69	1.05
	S13.2.20.1.a	3	0.053	0.18	0.28	1.46	1.98	3.61	2.53	0.55
	S13.2.20.2.a	3	0.051	0.15	0.30	1.55	2.06	3.63	2.54	0.48
	S13.2.20.3.a	3	0.063	0.19	0.34	1.47	2.06	-	-	-
	S13.2.30.1.a.	5	0.079	0.22	0.37	1.12	1.79	3.64	2.55	0.75
	S13.2.30.2.a.	5	0.058	0.18	0.38	0.97	1.58	3.89	2.72	1.14

	S13.2.30.3.a.	5	0.041	0.28	0.21	1.04	1.57	3.52	2.46	0.89
	S13.2.31.1.a	13	0.067	0.34	0.22	1.30	1.93	3.86	2.70	0.77
	S13.2.31.2.a	13	0.051	0.27	0.14	0.91	1.37	3.98	2.78	1.41
	S13.2.31.3.a	13	0.081	0.36	0.19	1.10	1.73	3.52	2.46	0.73
	S13.2.32.1.a	21	0.063	0.17	0.37	1.20	1.80	3.79	2.65	0.85
	S13.2.32.1.a	21	0.055	0.14	0.36	0.97	1.53	3.07	2.15	0.62
	S13.2.32.3.a	21	0.061	0.18	0.38	1.24	1.73	3.42	2.39	1.20
	S13.2.32.1.a	25	0.055	0.16	0.37	1.08	1.66	-	-	-
	S13.2.33.1.a	25	0.063	0.24	0.35	1.27	1.91	2.89	2.02	0.11
	S13.2.33.3.a	25	0.068	0.22	0.37	1.09	1.74	-	-	-
	S13.2.40.1.a	29	0.067	0.40	0.18	1.04	1.68	-	-	-
	S13.2.40.2.a	29	0.062	0.31	0.23	1.00	1.61	4.20	2.94	1.33
	S13.2.40.3.a	29	0.088	0.43	0.19	1.43	2.14	3.74	2.62	0.48
	S13.2.41.1.a	40	0.063	0.29	0.23	0.86	1.45	3.49	2.44	1.00
	S13.2.41.2.a	40	0.137	0.23	0.37	1.48	2.22	3.70	2.59	0.37
	S13.2.41.3.a	40	0.097	0.18	0.28	0.80	1.35	-	-	-
	S13.2.50.1.a	50	0.068	0.24	0.34	1.00	1.64	3.34	2.34	0.69
	S13.2.50.2.a	50	0.072	0.31	0.33	0.86	1.57	3.63	2.54	0.97
	S13.2.50.3.a	50	0.093	0.25	0.38	0.97	1.69	3.54	2.48	0.78
	S13.2.51.1.a	73	0.051	0.16	0.11	0.87	1.19	3.17	2.22	1.03
	S13.2.51.2.a	73	0.067	0.21	0.12	1.01	1.40	3.10	2.17	0.77
	S13.2.51.3.a	73	0.053	0.16	0.11	0.87	1.20	2.78	1.94	0.75
	S13.2.60.1.a	113	0.065	0.11	0.21	1.10	1.48	2.90	2.03	0.55
	S13.2.60.2.a	113	0.077	0.13	0.18	0.85	1.24	2.77	1.94	0.70
	S13.2.60.3.a	113	0.058	0.13	0.19	0.83	1.20	-	-	-
	S13.2.70.1.a	~2000	0.218	0.22	0.18	0.84	1.45	3.01	2.10	0.65
	S13.2.70.2.a	~2000	0.262	0.22	0.20	0.84	1.52	2.23	1.56	0.04
	S13.2.70.3.a	~2000	0.180	0.22	0.19	0.81	1.40	2.40	1.68	0.28
ML.*Tr2*. 15-30	S13.2.10.1.b	0	0.053	0.19	0.18	1.06	1.47	3.67	2.57	1.09
	S13.2.10.2.b	0	0.059	0.19	0.17	0.94	1.37	3.88	2.71	1.35
	S13.2.10.3.b	0	0.125	0.25	0.22	1.25	1.85	4.15	2.90	1.05
	S13.2.11.1.b	2	0.073	0.33	0.24	1.04	1.68	4.02	2.81	1.13
	S13.2.11.2.b	2	0.049	0.37	0.24	1.14	1.80	3.08	2.15	0.35
	S13.2.11.3.b	2	0.059	0.26	0.26	1.39	1.97	3.58	2.50	0.53
	S13.2.20.1.b	3	0.050	0.28	0.25	1.35	1.92	3.54	2.47	0.55
	S13.2.20.2.b	3	0.052	0.22	0.25	1.49	2.01	3.72	2.60	0.59
	S13.2.20.3.b	3	0.050	0.24	0.22	1.26	1.76	3.78	2.65	0.89
	S13.2.30.1.b	5	0.044	0.37	0.32	1.16	1.89	3.72	2.60	0.71

	S13.2.30.2.b	5	0.061	0.84	0.29	1.33	2.53	3.78	2.64	0.12
	S13.2.30.3.b	5	0.068	0.39	0.78	1.61	2.85	3.69	2.58	-0.27
	S13.2.31.1.b	13	0.084	0.37	0.27	1.38	2.10	3.58	2.50	0.40
	S13.2.31.2.b	13	0.082	0.27	0.29	1.22	1.86	3.70	2.59	0.73
	S13.2.31.3.b	13	0.049	0.13	0.30	0.83	1.31	3.74	2.62	1.31
	S13.2.32.1.b	21	0.042	0.12	0.28	-	-	3.79	2.65	-
	S13.2.32.2.b	21	0.068	0.15	0.41	-	-	3.41	2.39	-
	S13.2.32.3.b	21	0.056	0.17	0.34	1.11	1.68	4.36	3.05	1.37
	S13.2.33.1.b	25	0.055	0.16	0.34	0.98	1.54	3.54	2.48	0.93
	S13.2.33.2.b	25	0.065	0.15	0.35	1.03	1.60	3.78	2.64	1.05
	S13.2.33.3.b	25	0.049	0.19	0.40	0.88	1.51	3.35	2.34	0.83
	S13.2.40.1.b	29	0.063	0.26	0.31	1.51	2.14	3.87	2.71	0.56
	S13.2.40.2.b	29	0.094	0.38	0.51	1.60	2.57	3.47	2.43	-0.14
	S13.2.40.3.b	29	0.052	0.20	0.35	0.98	1.58	3.56	2.49	0.91
	S13.2.41.1.b	40	0.069	0.24	0.32	1.32	1.95	3.82	2.67	0.73
	S13.2.41.2.b	40	0.091	0.24	0.36	1.22	1.91	3.61	2.53	0.62
	S13.2.41.1.b	40	0.066	0.20	0.33	0.90	1.50	3.59	2.51	1.01
	S13.2.60.1.b	50	0.072	0.43	0.28	1.04	1.82	2.91	2.03	0.21
	S13.2.60.2.b	50	0.075	0.00	0.37	1.08	1.52	2.69	1.88	0.36
	S13.2.60.3.b	50	0.070	0.43	0.28	1.42	2.20	2.91	2.03	-0.17
	S13.2.50.1.b	73	0.052	0.19	0.24	0.94	1.42	4.21	2.94	1.52
	S13.2.50.2.b	73	0.059	0.25	0.28	0.89	1.48	-	-	-
	S13.2.50.3.b	73	0.058	0.23	0.27	0.88	1.47	4.38	3.07	1.63
	S13.2.51.1.b	113	0.060	0.16	0.21	0.82	1.24	3.57	2.50	1.26
	S13.2.51.2.b	113	0.061	0.45	0.16	0.90	1.57	3.20	2.24	0.67
	S13.2.51.3.b	113	0.056	0.15	0.17	0.63	1.01	2.66	1.86	0.85
ML.*Tr3*. 0-15	S13.3.10.1.a	0	0.059	0.21	0.39	0.66	1.32	3.84	2.69	1.37
	S13.3.10.2.a	0	0.049	0.14	0.30	0.89	1.38	3.85	2.69	1.31
	S13.3.10.3.a	0	0.092	0.15	0.23	1.23	1.70	3.59	2.51	0.81
	S13.3.11.1.a	2	0.046	0.14	0.33	1.04	1.56	3.58	2.50	0.94
	S13.3.11.2.a	2	0.044	0.14	0.30	1.14	1.62	4.05	2.83	1.21
	S13.3.11.3.a	2	0.061	0.21	0.38	1.23	1.88	4.40	3.08	1.20
	S13.3.20.1.a	3	0.078	0.34	0.25	1.20	1.87	4.04	2.83	0.95
	S13.3.20.2.a	3	0.070	0.32	0.24	1.35	1.98	-	-	-
	S13.3.20.3.a	3	0.052	0.29	0.21	1.29	1.84	3.74	2.62	0.78
	S13.3.30.1.a	5	0.072	0.24	0.17	1.11	1.60	2.87	2.01	0.41
	S13.3.30.2.a	5	0.077	0.35	0.22	1.32	1.96	3.73	2.61	0.65
	S13.3.30.3.a	5	0.059	0.31	0.18	0.99	1.53	3.69	2.58	1.05

	S13.3.31.3.a	13	0.085	0.20	0.44	1.26	1.97	3.45	2.41	0.44
	S13.3.31.3.a	13	0.064	0.15	0.32	1.14	1.67	5.11	3.57	1.90
	S13.3.31.3.a	13	0.068	0.16	0.36	1.21	1.80	3.66	2.56	0.77
	S13.3.32.3.a	21	0.069	0.17	0.24	0.96	1.43	2.88	2.01	0.58
	S13.3.32.3.a	21	0.081	0.22	0.41	1.21	1.92	3.48	2.43	0.51
	S13.3.32.3.a	21	0.057	0.20	0.46	0.86	1.58	3.34	2.34	0.76
	S13.3.40.1.a	29	0.127	0.25	0.20	1.72	2.29	3.55	2.48	0.19
	S13.3.40.2.a	29	0.097	0.22	0.18	1.32	1.81	3.28	2.30	0.48
	S13.3.40.3.a	29	0.075	0.49	0.21	1.25	2.03	3.16	2.21	0.18
	S13.3.41.3.a	40	0.060	0.15	0.27	1.12	1.60	4.36	3.05	1.45
	S13.3.41.3.a	40	0.058	0.18	0.32	1.20	1.76	3.67	2.57	0.81
	S13.3.41.3.a	40	0.066	0.15	0.21	0.96	1.38	3.66	2.56	1.18
	S13.3.50.1.a	50	0.078	0.24	0.34	0.81	1.46	3.77	2.64	1.17
	S13.3.50.2.a	50	0.094	0.28	0.32	1.20	1.89	3.68	2.58	0.69
	S13.3.50.3.a	50	0.079	0.25	0.39	1.17	1.89	3.62	2.53	0.64
	S13.3.60.1.a	113	0.076	0.16	0.21	0.97	1.42	3.24	2.27	0.85
	S13.3.60.2.a	113	0.071	0.25	0.36	0.83	1.51	3.68	2.57	1.07
	S13.3.60.3.a	113	0.053	0.25	0.28	1.00	1.58	3.24	2.27	0.68
	S13.3.10.1.b	0	0.062	0.39	0.23	1.07	1.76	-	-	-
	S13.3.10.2.b	0	0.038	0.27	0.25	1.40	1.96	3.80	2.65	0.70
ML.*Tr3*. 15-30	S13.3.10.3.b	0	0.053	0.30	0.20	1.11	1.67	4.61	3.22	1.56
	S13.3.11.1.b	2	0.055	0.46	0.18	1.20	1.88	3.75	2.62	0.74
	S13.3.11.2.b	2	0.059	0.43	0.26	1.28	2.02	3.69	2.58	0.56
	S13.3.11.3.b	2	0.051	0.36	0.24	1.45	2.10	3.87	2.71	0.60
	S13.3.20.1.b	3	0.048	0.26	0.23	1.47	2.00	3.77	2.64	0.64
	S13.3.20.2.b	3	0.117	0.51	0.32	1.41	2.36	3.79	2.65	0.29
	S13.3.20.3.b	3	0.122	0.76	0.19	1.48	2.55	3.66	2.56	0.01
	S13.3.30.1.b	5	0.077	0.42	0.25	1.28	2.02	4.14	2.90	0.88
	S13.3.30.2.b	5	0.061	0.17	0.14	1.25	1.61	3.77	2.64	1.03
	S13.3.30.3.b	5	0.071	0.39	0.21	1.35	2.02	3.63	2.54	0.52
	S13.3.31.3.b	13	0.061	0.37	0.25	1.24	1.92	3.99	2.79	0.87
	S13.3.31.3.b	13	0.064	0.42	0.26	1.29	2.03	-	-	-
	S13.3.31.3.b	13	0.047	0.28	0.24	1.35	1.92	-	-	-
	S13.3.32.3.b	21	0.060	0.29	0.24	1.36	1.95	3.90	2.73	0.78
	S13.3.32.3.b	21	0.061	0.49	0.21	1.27	2.02	3.22	2.25	0.23
	S13.3.32.3.b	21	0.065	0.31	0.30	1.18	1.85	3.51	2.46	0.61
	S13.3.40.1.b	29	0.052	0.38	0.15	1.21	1.79	3.56	2.49	0.70
	S13.3.40.2.b	29	0.077	0.32	0.27	0.85	1.52	3.41	2.38	0.87

	S13.3.40.3.b	29	0.065	0.45	0.20	0.71	1.42	3.60	2.52	1.10
	S13.3.41.3.b	40	0.064	0.41	0.22	0.84	1.53	3.54	2.48	0.94
	S13.3.41.3.b	40	0.049	0.31	0.13	1.08	1.57	3.59	2.51	0.94
	S13.3.41.3.b	40	0.078	0.22	0.20	1.05	1.55	3.59	2.51	0.96
	S13.3.50.1.b	50	0.055	0.38	0.17	0.87	1.47	3.44	2.41	0.94
	S13.3.50.2.b	50	0.066	0.41	0.21	0.80	1.48	3.52	2.46	0.98
	S13.3.50.3.b	50	0.084	0.56	0.19	1.01	1.84	3.74	2.62	0.77
	S13.3.60.1.b	113	0.069	0.44	0.20	0.84	1.55	3.73	2.61	1.06
	S13.3.60.2.b	113	0.063	0.23	0.13	0.69	1.12	3.74	2.61	1.49
	S13.3.60.3.b	113	0.071	0.51	0.17	0.83	1.57	3.92	2.74	1.17
ST 0-15cm	ST2a	24	0.093	0.18	0.09	0.37	0.73	12.36	8.65	7.91
	ST2b	24	0.063	0.16	0.07	0.27	0.56	12.54	8.77	8.21
	ST2c	24	0.109	0.17	0.12	0.38	0.78	12.37	8.65	7.87
	ST3a	27	0.075	0.11	0.09	0.29	0.57	12.74	8.91	8.34
	ST3b	27	0.078	0.10	0.10	0.24	0.51	11.18	7.82	7.30
	ST3c	27	0.071	0.16	0.11	0.22	0.56	11.49	8.04	7.47
	ST4a	34	0.068	0.16	0.12	0.32	0.67	12.63	8.83	8.17
	ST4b	34	0.077	0.17	0.11	0.38	0.74	12.70	8.88	8.14
	ST4c	34	0.095	0.15	0.13	0.25	0.63	12.73	8.90	8.27
	ST5a	55	0.084	0.22	0.12	0.03	0.45	11.66	8.16	7.71
	ST5b	55	0.061	0.16	0.10	0.25	0.57	12.29	8.60	8.03
	ST5c	55	0.082	0.20	0.12	0.23	0.64	12.14	8.49	7.85
	ST6a	80	0.097	0.16	0.11	0.23	0.60	11.77	8.23	7.63
	ST6b	80	0.105	0.18	0.11	0.23	0.63	11.91	8.33	7.70
	ST6c	80	0.081	0.21	0.15	0.31	0.75	11.20	7.83	7.08
	ST7a	31	0.071	0.20	0.14	0.25	0.66	12.50	8.74	8.09
	ST7b	31	0.069	0.18	0.13	0.29	0.66	11.42	7.99	7.32
	ST7c	31	0.088	0.17	0.12	0.26	0.64	12.27	8.58	7.94
	ST8a	45	0.060	0.17	0.12	0.33	0.68	12.29	8.60	7.92
	ST8b	45	0.077	0.20	0.13	0.31	0.72	12.25	8.57	7.84
	ST8c	45	0.078	0.20	0.14	0.30	0.71	12.68	8.87	8.15
	ST9a	80	0.076	0.18	0.13	0.19	0.59	12.05	8.43	7.84
	ST9b	80	0.072	0.18	0.11	0.29	0.66	12.63	8.83	8.18
	ST9c	80	0.076	0.18	0.13	0.25	0.63	12.21	8.54	7.91
	ST10a	N/A	0.070	0.20	0.14	0.32	0.73	11.80	8.25	7.52
	ST10b	N/A	0.029	0.00	0.00	0.50	0.53	13.47	9.42	8.89
	ST10c	N/A	0.072	0.21	0.10	0.30	0.68	12.49	8.74	8.05
	ST11a	N/A	0.127	0.14	0.08	0.25	0.60	12.28	8.59	7.99

	ST11b	N/A	0.034	0.16	0.04	0.27	0.50	12.47	8.72	8.22
	ST11c	N/A	0.117	0.12	0.08	0.30	0.62	12.67	8.86	8.24
	ST15a	0	0.119	0.14	0.08	0.21	0.54	12.41	8.68	8.14
	ST15b	0	0.111	0.16	0.08	0.18	0.53	12.53	8.76	8.23
	ST15c	0	0.046	0.16	0.11	0.25	0.56	12.22	8.55	7.98
	ST16a	15	0.042	0.17	0.10	0.22	0.53	12.53	8.76	7.69
	ST16b	15	0.044	0.15	0.10	0.19	0.49	12.40	8.67	8.18
	ST16c	15	0.032	0.14	0.10	0.29	0.57	13.02	9.11	8.54
	ST17a	20	0.050	0.17	0.11	0.28	0.61	11.82	8.27	7.66
	ST17b	20	0.051	0.17	0.10	0.26	0.58	12.64	8.84	8.26
	ST17c	20	0.054	0.19	0.10	0.21	0.56	12.62	8.83	8.27
RB 0-15cm	RB 1a	0	0.060	0.16	0.07	0.27	0.56	12.58	8.80	8.24
	RB 1b	0	0.069	0.17	0.08	0.27	0.59	12.56	8.79	8.19
	RB 1c	0	0.108	0.19	0.11	0.22	0.63	11.48	8.03	7.40
	RB 2a	16	0.056	0.21	0.12	0.27	0.66	11.48	8.03	7.37
	RB 2b	16	0.049	0.21	0.11	0.32	0.69	12.25	8.57	7.88
	RB 2c	16	0.045	0.23	0.12	0.21	0.60	11.51	8.05	7.45
	RB 3a	34	0.082	0.18	0.09	0.29	0.65	12.31	8.61	7.96
	RB 3b	34	0.072	0.19	0.09	0.23	0.59	12.57	8.79	8.20
	RB 3c	34	0.079	0.20	0.11	0.25	0.64	12.55	8.78	8.14
	RB 4a	62	0.063	0.20	0.11	0.24	0.60	11.99	8.39	7.79
	RB 4b	62	0.074	0.22	0.12	0.28	0.68	12.24	8.56	7.88
	RB 4c	62	0.081	0.22	0.13	0.31	0.74	11.66	8.16	7.41
	RB 5a	104	0.080	0.27	0.13	0.27	0.75	11.87	8.30	7.55
	RB 5b	104	0.078	0.23	0.10	0.23	0.64	11.64	8.14	7.50
	RB 5c	104	0.093	0.17	0.13	0.23	0.62	11.79	8.25	7.63
	RB 6	104	0.372	0.56	0.11	0.27	1.31	9.66	6.76	5.45
	RB 0	N/A	0.214	0.59	0.22	0.50	1.53	8.60	6.02	4.48

Note: Iron fractions ferrihydrite, Fe oxides, magnetite and Fe sheet-silicates were measured using atomic absorbance spectroscopy (AAS). Total Fe_2O_3 was measured on XRF and Total Fe was calculated using Fe3+ oxide ratio. *Fe oxides = 'reducible' Fe oxides (goethite, hematite and akaganeite and carbonates e.g. siderite and ankerite); **Fe silicate =; silicates = sheet-silicate minerals (e.g. nontronite, chlorite, glauconite, biotite).

Table. C.8. XRF data for major elements for samples taken in Storglaciären (ST) and Rabot's (RB). Note: for XRF precision data see Appendix B. Table B.10 & 11 and XRF for Midtre Lovénbreen, see Table B.12.

Forefield location	Sample no.	SiO_2	TiO_2	Al_2O_3	Fe_2O_3	MnO	MgO	CaO	Na_2O	K_2O	P_2O_5	LOI	Sum
#	#	(wt %)	(wt %)	(wt %)	(wt %)	(wt %)	(wt %)	(wt %)	(wt %)	(wt %)	(wt %)	(wt %)	(wt %)
ST	ST2a	49.88	1.70	14.18	12.36	0.19	6.63	9.79	2.65	0.52	0.16	1.29	99.35
	ST2b	49.98	1.76	14.12	12.54	0.19	6.67	9.86	2.46	0.51	0.16	1.36	99.62
	ST2c	49.67	1.65	14.17	12.37	0.18	6.77	9.79	2.62	0.51	0.17	1.56	99.46
	ST3a	48.84	2.04	13.99	12.74	0.19	6.68	9.85	2.30	0.46	0.17	2.21	99.47
	ST3b	50.39	1.65	14.32	11.18	0.18	6.71	9.93	2.28	0.47	0.17	2.25	99.53
	ST3c	49.63	1.52	14.25	11.49	0.17	6.37	9.70	2.59	0.47	0.17	2.53	98.89
	ST4a	50.30	1.66	14.08	12.63	0.19	6.89	9.91	2.03	0.49	0.15	1.30	99.64
	ST4b	49.88	1.84	14.07	12.70	0.20	6.77	9.90	2.24	0.46	0.16	1.40	99.62
	ST4c	49.56	1.73	14.04	12.73	0.20	6.87	9.96	1.97	0.45	0.15	2.02	99.68
	ST5a	50.53	1.73	14.44	11.66	0.19	6.74	10.03	1.99	0.47	0.17	1.68	99.62
	ST5b	50.26	1.70	14.31	12.29	0.19	6.71	9.94	2.19	0.46	0.17	1.39	99.61
	ST5c	49.86	1.66	14.29	12.14	0.18	6.65	9.85	2.51	0.49	0.17	1.51	99.31
	ST6a	49.87	1.69	14.28	11.77	0.18	6.40	9.63	2.44	0.45	0.16	2.52	99.39
	ST6b	49.20	1.65	14.07	11.91	0.18	6.52	9.68	2.52	0.46	0.16	3.10	99.45
	ST6c	49.71	1.48	14.27	11.20	0.17	6.20	9.45	2.76	0.47	0.17	3.56	99.44
	ST7a	49.91	1.71	14.09	12.50	0.19	6.83	9.95	2.09	0.46	0.16	1.58	99.48
	ST7b	50.27	1.71	14.20	11.42	0.19	6.99	10.12	2.29	0.48	0.15	1.65	99.47
	ST7c	50.15	1.77	14.30	12.27	0.19	6.71	9.82	2.21	0.47	0.17	1.40	99.45
	ST8a	48.99	1.74	13.98	12.29	0.19	6.70	9.83	3.29	0.53	0.18	1.61	99.32
	ST8b	50.05	1.71	14.27	12.25	0.18	6.69	9.92	2.24	0.48	0.17	1.48	99.45
	ST8c	49.85	1.72	14.10	12.68	0.19	6.96	10.02	2.08	0.47	0.17	1.38	99.61
	ST9a	49.77	1.61	14.26	12.05	0.18	6.63	9.89	2.79	0.50	0.16	1.54	99.38
	ST9b	49.39	1.83	14.03	12.63	0.19	6.83	9.98	2.46	0.47	0.16	1.75	99.72
	ST9c	49.81	1.68	14.26	12.21	0.18	6.64	9.88	2.65	0.49	0.17	1.34	99.32
	ST10a	50.54	1.54	14.48	11.80	0.18	6.86	10.38	2.28	0.41	0.15	1.06	99.68
	ST10b	47.39	1.67	14.18	13.47	0.21	7.52	11.26	1.91	0.40	0.11	1.24	99.36
	ST10c	49.27	2.08	14.18	12.49	0.20	6.88	10.54	2.16	0.38	0.15	1.28	99.61
	ST11a	46.95	2.02	13.77	12.28	0.19	6.66	9.89	2.80	0.46	0.18	4.27	99.47
	ST11b	46.72	2.05	13.65	12.47	0.19	6.70	9.86	3.55	0.50	0.17	3.21	99.07
	ST11c	46.65	2.03	13.70	12.67	0.19	6.62	9.80	2.11	0.42	0.16	5.13	99.49
	ST12 cryo	36.91	1.21	10.57	7.82	0.12	4.28	5.44	2.88	0.71	0.14	29.03	99.10

	ST15a	49.72	1.58	14.19	12.41	0.19	7.03	10.16	2.23	0.48	0.16	1.26	99.41
	ST15b	49.16	1.58	13.89	12.53	0.19	7.09	10.20	2.82	0.50	0.15	1.13	99.23
	ST15c	50.39	1.65	14.30	12.22	0.18	6.76	10.05	2.08	0.48	0.17	1.23	99.51
	ST16a	49.96	1.82	14.19	12.53	0.19	6.88	10.09	2.15	0.45	0.16	1.18	99.60
	ST16b	50.25	1.76	14.26	12.40	0.19	6.79	10.03	2.03	0.43	0.17	1.14	99.45
	ST16c	49.51	1.69	14.07	13.02	0.20	7.24	10.37	1.82	0.45	0.14	1.13	99.64
	ST17a	50.39	1.75	14.30	11.82	0.19	7.12	10.27	2.01	0.44	0.15	1.23	99.67
	ST17b	49.61	1.77	14.23	12.64	0.19	6.93	10.15	2.23	0.45	0.16	1.27	99.63
	ST17c	49.77	1.77	14.33	12.62	0.19	6.93	10.14	1.99	0.43	0.16	1.27	99.60
	RB1a	49.73	1.74	14.29	12.58	0.21	7.12	9.77	2.14	0.46	0.15	1.29	99.48
RB	RB1b	50.02	1.66	14.22	12.56	0.20	7.15	9.77	2.11	0.45	0.15	1.28	99.58
	RB1c	50.67	1.60	14.73	11.48	0.17	6.64	9.55	2.30	0.47	0.18	1.77	99.56
	RB2a	51.20	1.59	14.54	11.48	0.17	6.79	9.54	2.28	0.53	0.17	1.31	99.60
	RB2b	50.66	1.74	14.19	12.25	0.20	6.98	9.54	2.15	0.51	0.15	1.18	99.55
	RB2c	51.94	1.55	14.79	11.51	0.17	6.81	9.54	2.46	0.58	0.17	1.35	99.87
	RB3a	49.52	1.66	13.92	12.31	0.19	7.16	9.71	2.07	0.45	0.16	1.21	98.36
	RB3b	50.13	1.60	13.88	12.57	0.20	7.37	9.75	2.05	0.48	0.15	1.30	99.47
	RB3c	49.98	1.68	14.22	12.55	0.20	7.13	9.75	2.10	0.45	0.16	1.31	99.53
	RB4a	50.85	1.65	14.41	11.99	0.19	6.80	9.48	2.21	0.51	0.14	1.38	99.61
	RB4b	50.09	1.59	14.17	12.24	0.19	7.11	9.76	2.16	0.48	0.15	1.56	99.50
	RB4c	50.66	1.60	14.51	11.66	0.17	6.79	9.50	2.25	0.52	0.16	1.74	99.57
	RB5a	50.84	1.56	14.32	11.87	0.18	6.86	9.65	2.21	0.46	0.14	1.50	99.60
	RB5b	50.92	1.54	14.33	11.64	0.18	6.73	9.58	2.23	0.45	0.14	1.86	99.59
	RB5c	50.98	1.56	14.41	11.79	0.18	6.79	9.64	2.25	0.46	0.14	1.36	99.56
	RB6	41.94	1.31	12.11	9.66	0.13	5.74	6.68	1.79	0.47	0.17	19.48	99.48
	RB0cryo	40.20	1.33	11.67	8.60	0.11	4.89	6.01	1.79	0.66	0.15	24.10	99.51

Table. C.9. Basic field measurements, soil colour, soil strength, pH, conductivity and soil moisture for Midtre Lovénbreen (ML), Svalbard, Storglaciären (ST) and Rabot's glacier (RB) forefields.

Forefield locale	Sample number	Sample age (years)	Soil colour Munsell HVC data	Soil strength ±= *1σ of n=3* ($kg^{-}cm^{2}$)	pH	Con (µS)	Soil moisture (%)
ML	S13.1.10.1. a	0	N/A	N/A	8.5	N/A	100
	S13.1.10.2. a	0	N/A	N/A	8.1	N/A	100
	S13.1.10.3. a	0	N/A	N/A	8.4	N/A	100
	S13.1.12.1. a	2	N/A	N/A	8	N/A	60
	S13.1.12.2. a	2	N/A	N/A	8	N/A	55
	S13.1.12.3. a	2	N/A	N/A	8.1	N/A	60
	S13.1.20.1. a	3	N/A	N/A	8.2	N/A	<LD
	S13.1.20.2. a	3	N/A	N/A	8.1	N/A	<LD
	S13.1.20.3. a	3	N/A	N/A	8	N/A	<LD
	S13.1.30.1. a	5	N/A	N/A	7.9	N/A	10
	S13.1.30.2. a	5	N/A	N/A	7.7	N/A	35
	S13.1.30.3. a	5	N/A	N/A	7.5	N/A	30
	S13.1.13.1. a	13	N/A	N/A	7.9	N/A	<LD
	S13.1.13.2. a	13	N/A	N/A	7.4	N/A	<LD
	S13.1.13.3. a	13	N/A	N/A	7.5	N/A	<LD
	S13.1.31.1. a	21	N/A	N/A	7.9	N/A	<LD
	S13.1.31.2. a	21	N/A	N/A	8	N/A	<LD
	S13.1.31.3. a	21	N/A	N/A	7.4	N/A	<LD
	S13.1.40.1. a	29	N/A	N/A	7.5	N/A	10
	S13.1.40.2. a	29	N/A	N/A	7.5	N/A	10
	S13.1.40.3. a	29	N/A	N/A	7.5	N/A	15
	S13.1.32.1. a	40	N/A	N/A	7.7	N/A	LD
	S13.1.32.2. a	40	N/A	N/A	7.3	N/A	<LD
	S13.1.32.3. a	40	N/A	N/A	7.6	N/A	<LD
	S13.1.50.1. a	50	N/A	N/A	7	N/A	10
	S13.1.50.2. a	50	N/A	N/A	7.2	N/A	10
	S13.1.50.3. a	50	N/A	N/A	7.3	N/A	10

	S13.1.60.1. a	113	N/A	N/A	7	N/A	<LD
	S13.1.60.2. a	113	N/A	N/A	7	N/A	<LD
	S13.1.60.3. a	113	N/A	N/A	7.1	N/A	<LD
ST	9a	0	Dark olive/grey (5gy 4/1)	0.7 ± 0.1	6.5	3.86	14
	9b	0	Dark olive/grey (5gy 4/1)	0.9 ± 0.4	6.5	3.71	12
	9c	0	Dark olive/grey (5gy 4/1)	0.9 ± 0.1	6.5	3.13	18
	10a	15	Dark greenish/grey (5g 2/1)	<LD	6.5	3.12	16
	10b	15	Dark greenish/grey (5g 2/1)	<LD	6.7	4.82	26
	10c	15	Dark greenish/grey (5g 2/1)	<LD	6.5	3.49	21
	11a	20	Olive black (10y 3/1)	0.5 ± 0.1	7.9	7.76	45
	11b	20	Olive black (10y 3/1)	0.9 ± 0.2	7.6	5.89	14
	11c	20	Olive black (10y 3/1)	0.8 ± 0.4	7.4	4.95	24
	2a	24	Dark olive/grey (5gy 3/1)	0.3 ± 0.1	5.6	8.7	14
	2b	24	Dark olive/grey (5gy 3/1)	0.8 ± 0.8	5.9	3.6	7
	2c	24	Dark olive/grey (5gy 3/1)	1.1 ± 0.5	6.4	3.4	8
	3a	27	Dark olive/grey (2.5gy 3/1)	1.3 ± 0.9	6.9	6.4	24
	3b	27	Dark olive/grey (2.5gy 3/1)	1.9 ± 0.2	6.0	3.69	10
	3c	27	Dark olive/grey (5gy 5/1)	1.1 ± 0.5	6.2	3.44	11
	7a	31	Dark olive/grey (5gy 4/1)	1 ± 0.2	6.3	2.63	31
	7b	31	Dark olive/grey (5gy 4/1)	1.5 ± 0.3	6.4	2.69	35
	7c	31	Dark olive/grey (5gy 4/1)	1.1 ± 0.7	6.5	3.13	12
	4a	34	Dark olive/grey (5gy 5/1)	0.2 ± 0.2	6.3	3.33	5
	4b	34	Dark olive/grey (2.5gy 4/1)	0.5 ± 0.3	6.4	3.25	10
	4c	34	Dark olive/grey (2.5gy 4/1)	0.7 ± 0.5	6.3	3.46	4
	8a	45	Dark olive/grey (5gy 4/1)	0.8 ± 0.2	6.4	3.72	10
	8b	45	Dark olive/grey (5gy 4/1)	0.9 ± 0.2	6.4	3.58	13
	8c	45	Dark olive/grey (5gy 4/1)	0.4 ± 0.2	6.4	3.23	14
	5a	80	Dark greenish/grey (7.5gy 3/1)	0.1 ± 0.1	6.3	5.17	14
	5b	80	Dark greenish/grey (7.5gy 3/1)	0.9 ± 0.1	6.4	5.08	17
	5c	80	Dark olive/grey (5gy 4/1)	1 ± 0.2	6.5	4.03	15
	6a	80	Dark olive/grey (5gy 4/1)	1.3 ± 0.2	6.3	4.12	27
	6b	80	Dark olive/grey (5gy 4/1)	1.8 ± 0.3	6.5	2.73	27
	6c	80	Dark olive/grey (5gy 4/1)	1.3 ± 0.1	6.5	2.52	33

RB	1a	0	Greenish black 7.5gy 2/1	0.1 ± 0.1	6.5	1.94	11
	1b	0	Greenish black 7.5gy 2/1	0.4 ± 0.2	6.6	1.97	15
	1c	0	Greenish black 7.5gy 2/1	0.1 ± 0.2	7.2	1.81	38
	2a	16	Dark olive/grey (2.5gy 4/1)	0.5 ± 0.1	7.3	6.61	18
	2b	16	Dark olive/grey (2.5gy 4/1)	0.2 ± 0.2	7.4	4.01	20
	2c	16	Dark olive/grey (5gy 5/1)	0.3 ± 0.1	7.6	4.21	22
	3a	34	Greenish black 7.5gy 2/1	0.1 ± 0.2	7.2	1.67	10
	3b	34	Greenish black 7.5gy 2/1	0.4 ± 0.2	6.7	1.8	9
	3c	34	Greenish black 7.5gy 2/1	0.1 ± 0.1	6.7	1.84	7
	4a	62	Dark olive/grey (2.5gy 3/1)	1 ± 0.2	6.8	2.35	9
	4b	62	Olive grey 10y 4/2	0.9 ± 0.1	6.5	3.03	7
	4c	62	Olive black 7.5y 3/2	1 ± 0.1	6.8	3.28	14
	5a	104	Olive black 7.5y 3/3	1.4 ± 0.3	6.7	2.03	9
	5b	104	Olive black 7.5y 3/4	1.2 ± 0.6	6.6	1.94	<LD
	5c	104	Olive black 7.5y 3/4	1.7 ± 0.1	5.9	2.35	<LD
	6	104	Brownish black 2.5y 2/1	N/A	5.7	2.36	<LD

Note: Soil colour and soil strength were not measured at ML. A Munsell soil chart was used for Soil colour HVC = visual description of soil colour. Soil moisture accuracy was

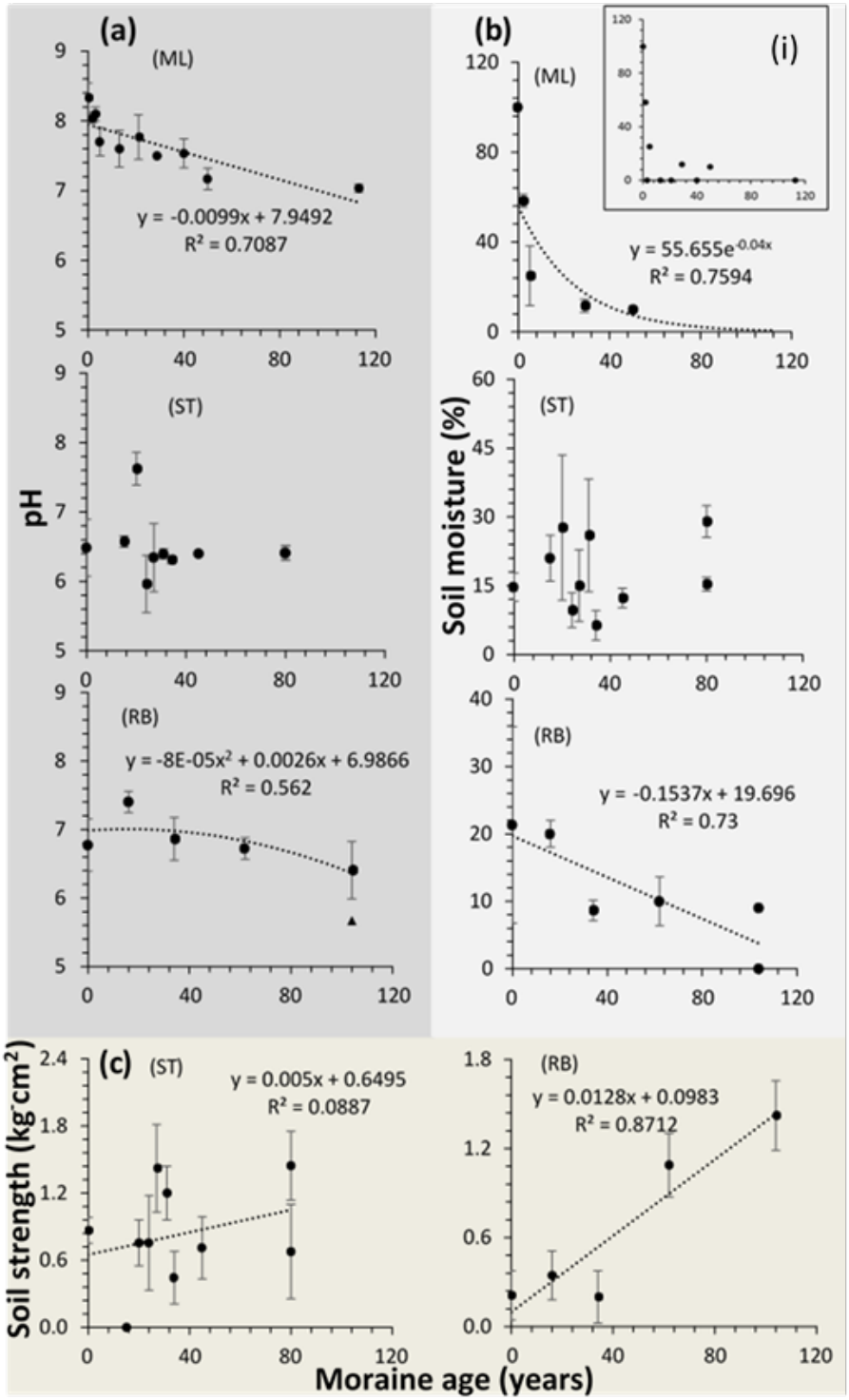

Figure. C.1. Plots (a) are the average pH and plots (b) average soil moisture and (c) average soil strength (penetrometer) measurements, all as a function of moraine age from Midtre Lovénbreen (ML), Svalbard, Storglaciären (ST) and Rabot's glacier (RB) in Sweden forefields. Soil strength measurements were only taken in the Swedish forefields. Uncertainty bars represent 1σ of triplicate samples from the same aged site. (i) is an inset of plot (b, ML) including sites with soil moisture values below the limit of detection

Table. C.10. Pearson's *r* correlation coefficients for all forefields

Variables (dep *vs.* indep.)	Forefield	*r* (R^2) value	Critical *r* value	Sig. level (p value)	*n*
Total organic carbon *vs.* moraine age	Midtre Lovénbreen	0.97 (0.95)	0.597	0.01	30
	Storglaciären	0.64 (0.42)	0.381	0.05	27
		0.44 (0.21)	0.349	0.05	33
	Rabot's	0.81 (0.66)	0.497	0.05	16
$\delta^{13}C_{org}$ vs. moraine age	Midtre Lovénbreen	-0.81 (0.75)	0.597	0.01	30
	Storglaciären	-0.67 (0.46)	0.445	0.01	27
		-0.68 (0.46)	0.409	0.01	33
	Rabot's	-0.7 (0.5)	0.497	0.05	16
$\delta^{13}C_{org}$ vs. 1/Total organic carbon	Midtre Lovénbreen	0.97 (0.94)	0.554	0.01	30
	Storglaciären	0.77 (0.59)	0.519	0.01	33
	Rabot's	0.83 (0.69)	0.708	0.01	16

Note: Dependent and independent variable abbreviated to *dep* and *indep.*, respectively. Grey and red text represents the line of best fit data from Fig.b.

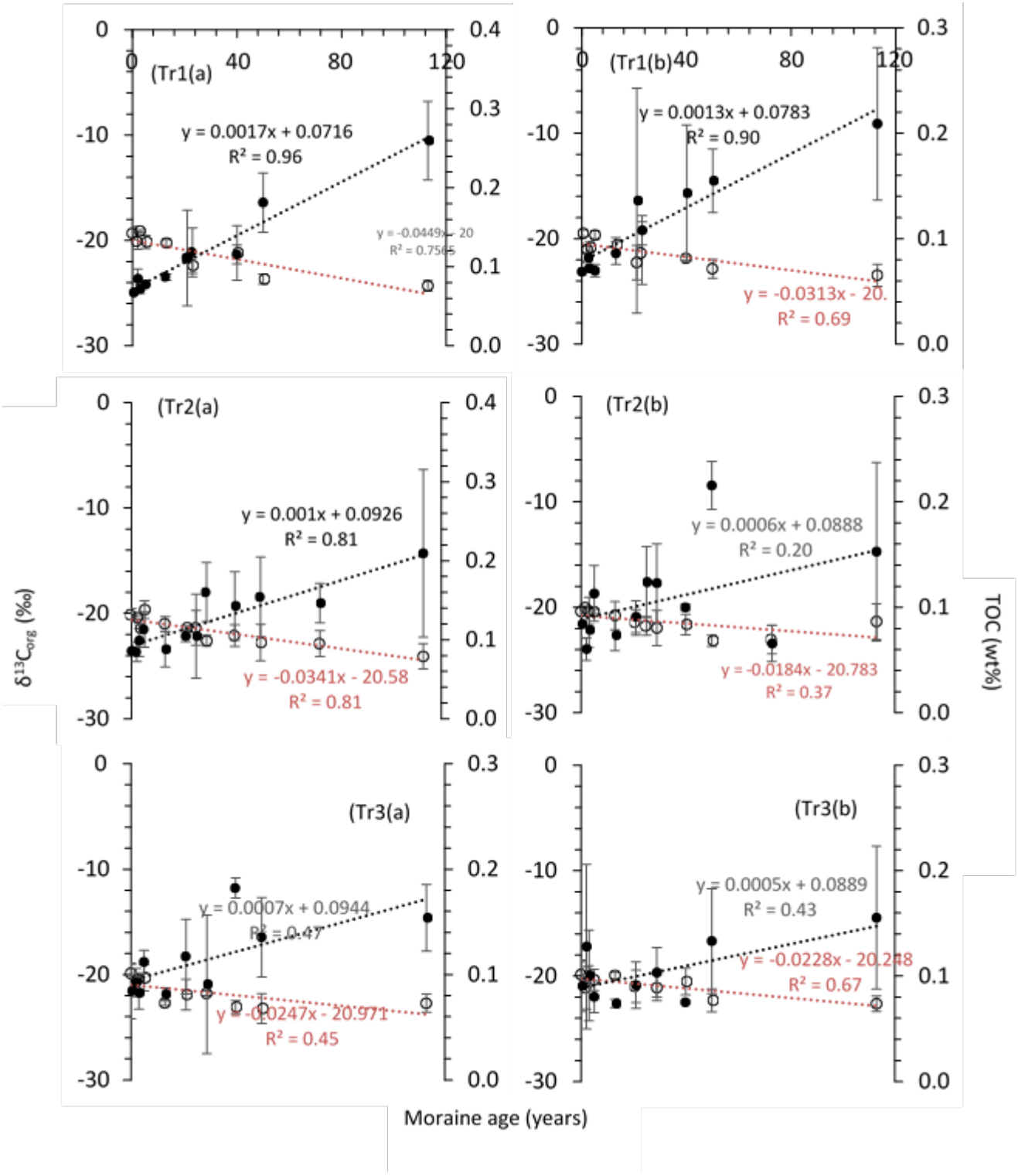

Figure. C.2. Average isotopic $\delta^{13}C_{org}$ (‰) PDB and TOC plotted as a function of moraine age from Midtre Lovénbreen (ML) the transects (Tr1, Tr2, Tr3) at both the surface (a) and subsurface (b), Svalbard, Storglaciären (ST) and Rabot's glacier (RB), Sweden, forefields. Black circles represent TOC and white circles $\delta^{13}C_{org}$. Uncertainty bars represent 1σ of triplicate samples from the same aged site.

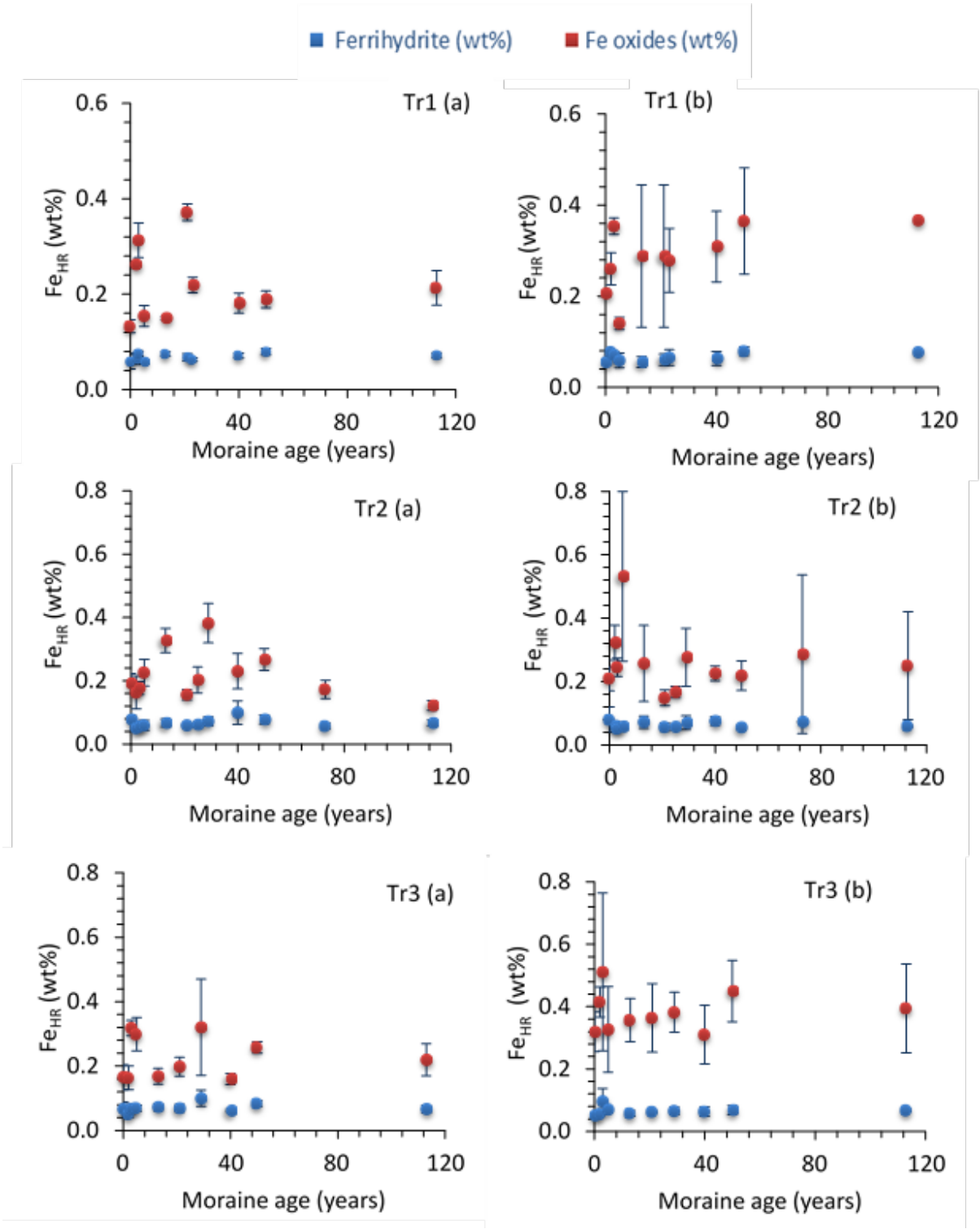

Figure. C. 3. High reactive iron phases (Fe_{HR}) ferrihydrite and Fe oxides as a function of moraine age for Tr1, Tr2 and Tr3 at depths a and b in Midtre Lovénbreen (ML). Uncertainty bars represent 1σ of triplicate samples from the same aged site.

One way ANOVA methodology (testing >2 independent variables): test results for operationally defined iron fractions from Midtre Lovénbreen, Storglaciären and Rabot's forefield
Prior to test using this test the following assumptions were addressed.

1) Your dependent variable should be measured at the interval or ratio level (i.e., they are continuous).
2) An independent variable should consist of two or more categorical, independent groups.
3) Data should have independence of observations, which means that there is no relationship between the observations in each group or between the groups themselves.
4) A dependent variable should be approximately normally distributed for each category of the independent variable.
5) There needs to be homogeneity of variances.

To compare the means (Table. 9) of Ferrihydrite (a) and Fe oxide (b) in Fig, 3 from each forefield, firstly 1) the data was tested for normality, then 2) a Levene's test for homogeneity of variances and finally 3) Welch's ANOVA test to compare their means.

Table. C.11. Ferrihydrite (a) and Fe oxide (b) comparison of means for each forefield

Iron fraction	Forefield	N	Mean	Std.	Std. Error	95% Confidence Interval for Mean Lower Bound	95% Confidence Interval for Mean Upper Bound	Min	Max
(a) Ferrihydrite	ML	30	.0680	.01031	.00188	.0642	.0718	.04	.09
	S	40	.0712	.02911	.00460	.0619	.0806	.00	.13
	RB	17	.0976	.07934	.01924	.0569	.1384	.04	.37
	Total	87	.0753	.04142	.00444	.0665	.0841	.00	.37
(b)Fe oxides	ML	30	.2187	.07596	.01387	.1903	.2470	.12	.39
	ST	40	.1565	.05211	.00824	.1398	.1732	.00	.22
	RB	17	.2471	.12643	.03066	.1821	.3121	.16	.59
	Total	87	.1956	.08701	.00933	.1771	.2142	.00	.59

Table. C.12. Levene's test of homogeneity of variances and Welch's ANOVA test for comparing the means of Ferrihydrite and Fe oxides in ML, S and RB to calculate their statistical significance.

Iron fraction	Stat. test	df	Sig.
(a) Ferrihydrite	Levene's Statistic	2	0.000
	Welch's ANOVA	2	0.279
(b)Fe oxides	Levene's Statistic	2	0.011
	Welch's ANOVA	2	0.000

Note: If the p value (sig.) from Levene's Statistic is less than the significance level 0.05 the data has unequal variance and a Welch ANOVA test was used instead of an oneway-ANOVA test. If the p value (sig.) from Welch's ANOVA is > 0.05 there is no significant difference between the means of each of the forefields.

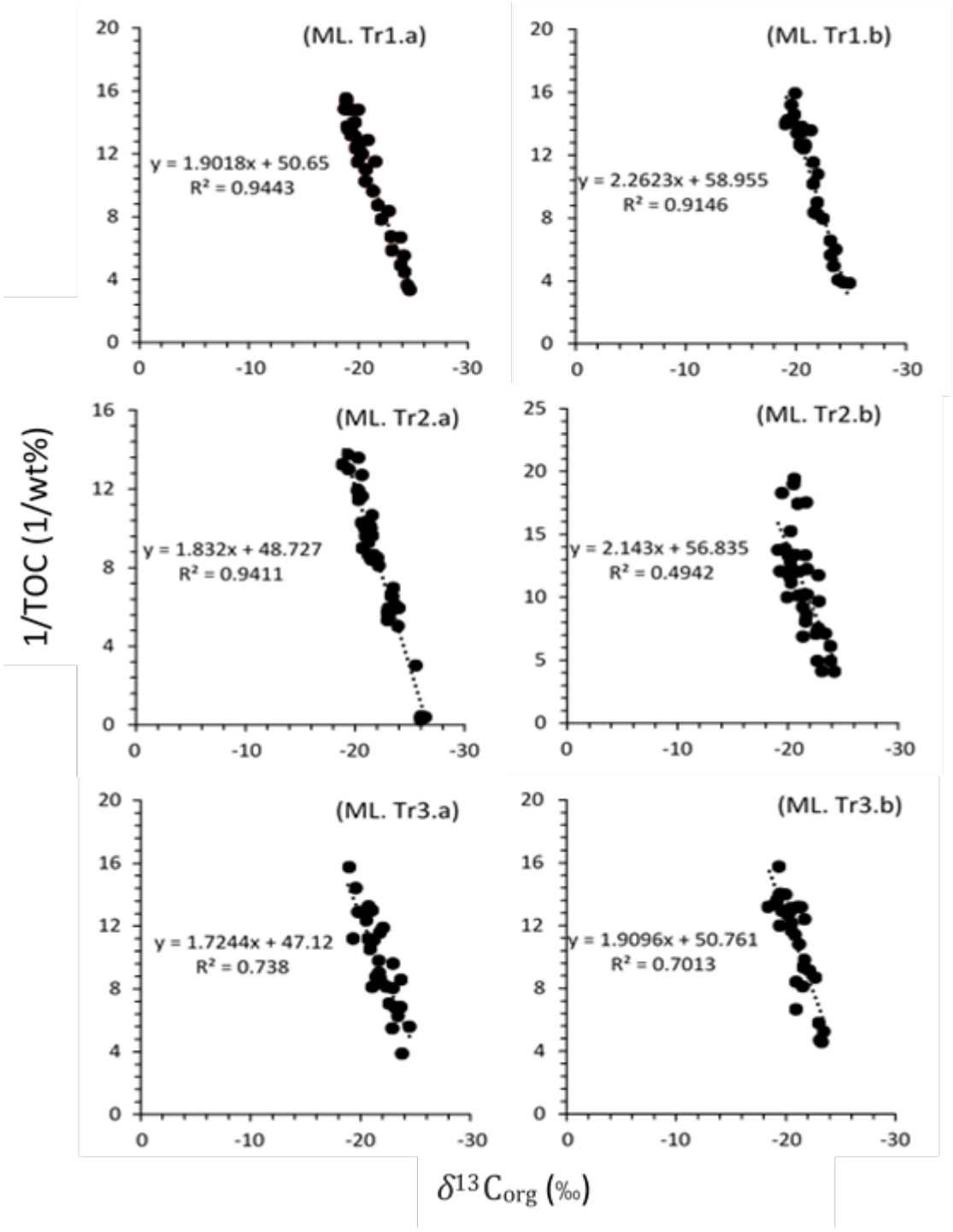

Figure. C.3. Isotopic $\delta^{13}C_{org}$ (‰) PDB *vs.* 1/TOC from Midtre Lovénbreen (ML) at both the surface (a) and subsurface (b) from the transects (Tr1, Tr2, Tr3), Svalbard

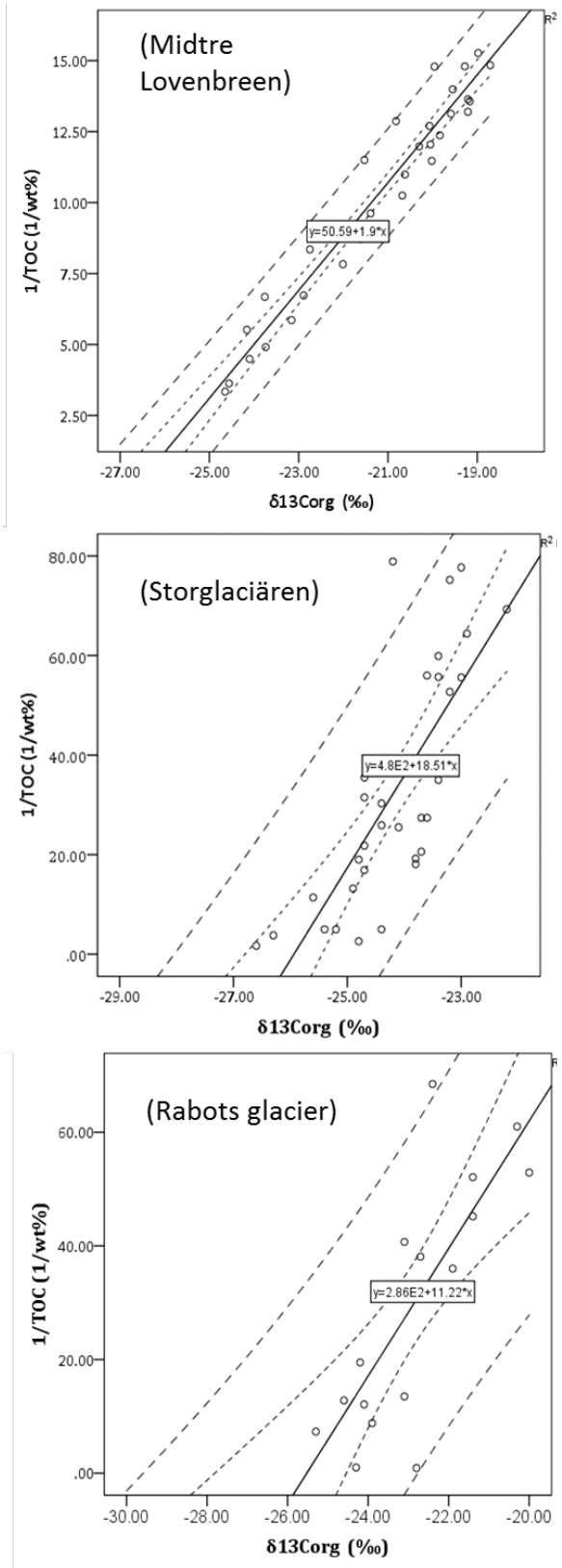

- The difference between a prediction interval and a confidence interval is the standard error.
- The standard error for a confidence interval on the mean considers the uncertainty due to sampling. The line you computed from your sample will be different from the line that would have been computed if you had the entire population, the standard error takes this uncertainty into account.

- The standard error for a prediction interval on an individual observation considers the uncertainty due to sampling like above, but also considers the variability of the individuals around the predicted mean. The se for the prediction interval will be wider than for the confidence interval and hence the prediction interval will be wider than the confidence interval.

Figure. C.4. Plots of isotopic linear mixing models for Midtre Lovénbreen, Storglaciären and Rabot's. The solid line delineates the line of linear regression, the small dashed line 95% confidence interval for the mean and the large dashed line 95% prediction intervals for individual sample

Table. C.13. Carbon budget for Midtre Lovénbreen

Soil age (years)	Autotrophic biomass µg/g	Autotrophic biomass (1σ SD)	Heterotrophic biomass µg/g	Heterotrophic biomass (1σ SD)	OCkerogen, corr µg/g	OCmicrobe µg/g	OCmicrobe (1σ SD)	OCveg µg/g	OCveg (1σ SD)	TOC µg/g	TOC (1σ SD)
0	0.17	0.04	0.06	0.03	790.00	0.23	0.04	0.00	120.00	790.00	120.00
3	0.29	0.16	0.06	0.03	632.00	0.35	0.16	6.23	54.39	716.58	54.39
5	0.56	0.14	0.08	0.07	505.60	0.64	0.14	11.85	12.81	775.25	12.81
29	1.07	0.49	0.24	0.14	404.48	1.32	0.49	551.03	308.56	1184.34	308.56
50	1.50	0.60	0.20	0.18	360.00	1.69	0.60	1179.66	376.23	1811.35	376.23
113	2.58	0.93	2.00	0.89	360.00	4.58	0.93	1960.75	499.16	2595.33	499.16

Note: OC_{plant} = TOC-Total microbial biomass Eq. b.4. The standard deviation of OC has been calculated using error propagation, Eq. XX. All microbial biomasses are measured from the same sample set (an aliquot) as this study at Bristol University using florescence, see Bradley et al., 2016 for obtained values and methodology.

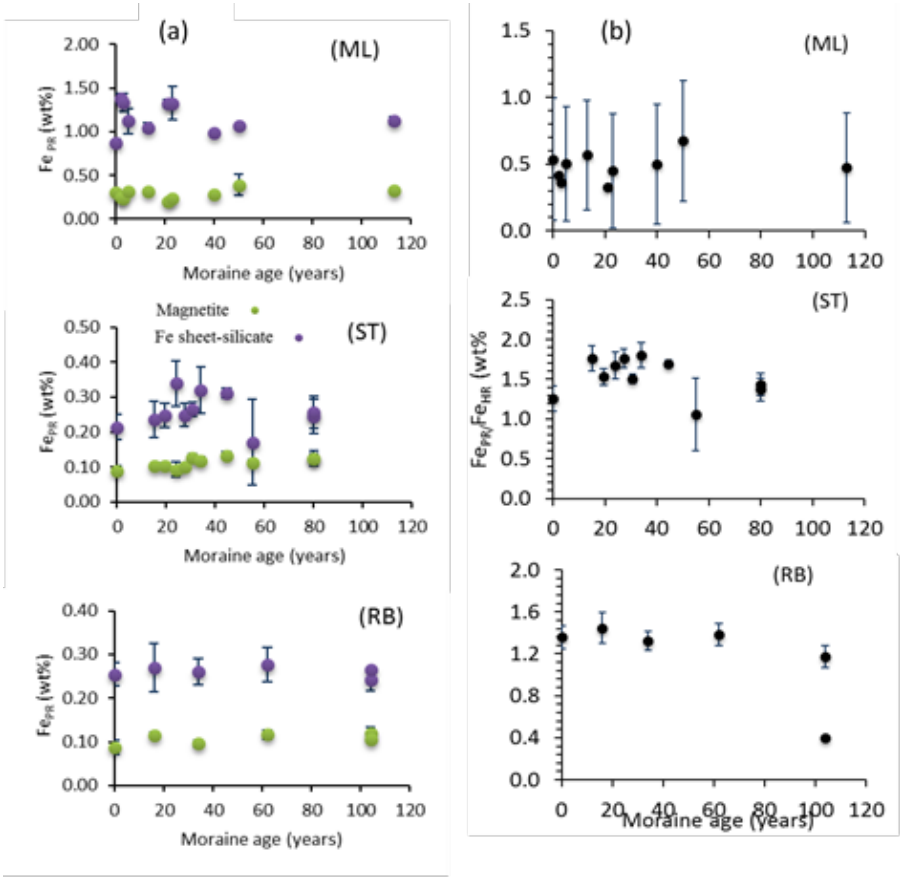

Figure. C.5. (a) Poorly reactive iron phases (Fe_{PR}) Magnetite and Fe Sheet-Silicates as a function of moraine age and (b) Fe_{PR}/Fe_{HR} also as a function of moraine age for Midtre Lovénbreen (ML), Svalbard and Storglaciären (ST) and Rabot's glacier (RB), Sweden. Uncertainty bars represent 1σ of triplicate samples from the same aged site

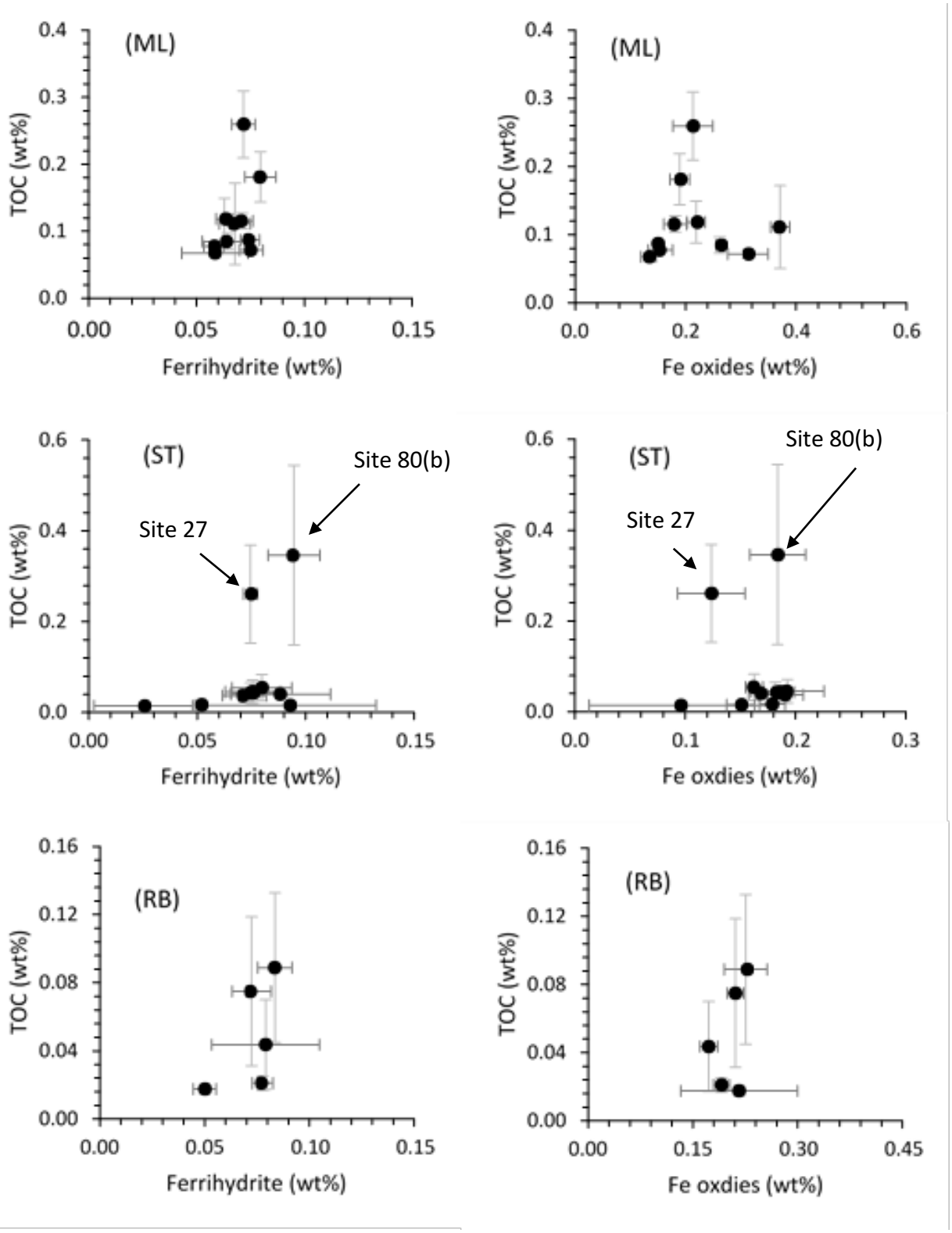

Figure. C.6. TOC as a function of Ferrihydrite and Fe oxides for ML, RB and ST including Fioutliers in ST at the ages 27 and 80(b)-years-old.

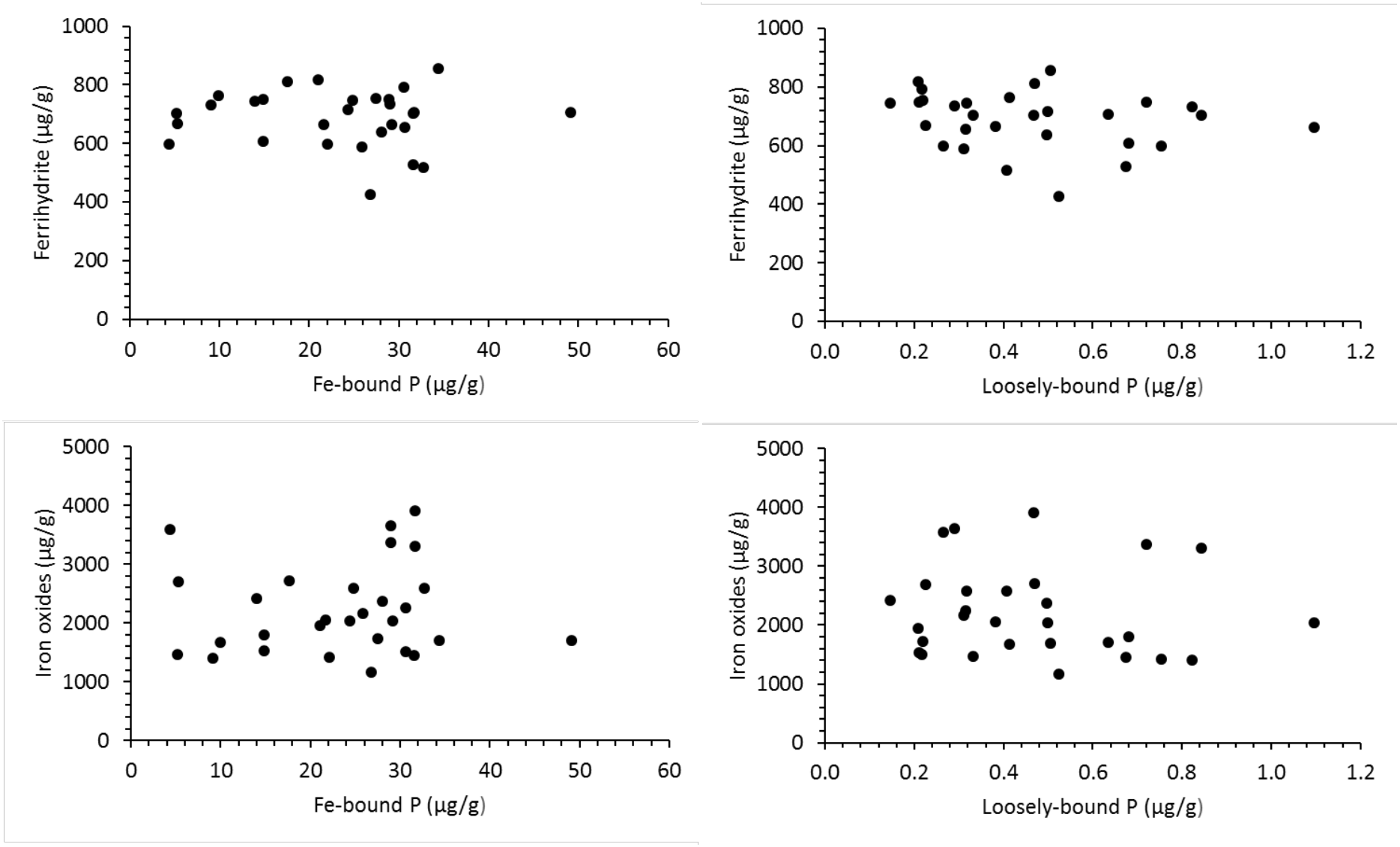

Figure. C.7. High reactive iron phases ferrihydrite and iron oxides as a function of Fe-bound P and Loosely-bound P from ML forefield.

Table. C.14. Internal standard used to derive of the operationally defined phosphorous species precision for transects 1 (Tr1) in Midtre Lovénbreen.

Sample label	Loosely-bound P (µg/g)	Fe-bound P (µg/g)	Authigenic, Biogenic and CaCO3 bound (µg/g)	Detrital P (µg/g)	Organic P (µg/g)
55a	0.7	30.7	6.5	36.1	6.4
55b	0.6	34.3	9.0	35.3	6.1
55c	0.6	32.7	6.0	35.5	5.9
55d	0.8	32.8	5.6	35.4	5.8
55e	0.6	39.1	5.1	33.8	5.5
Mean	0.6	33.9	6.4	35.2	5.9
SD	0.1	3.2	1.5	0.8	0.3
95% con.	0.1	3.00	1.43	0.8	0.3

Table. C.15. Operationally defined phosphorous species for transects 1 (Tr1) in Midtre Lovénbreen from the bulk soil at a depth of 0-15cm.

Sample no.	Sample label	Moraine age (yeas)	Loosely-bound P (µg/g)	Fe-bound P (µg/g)	Authigenic, Biogenic and CaCO3 bound P **apatite** (µg/g)	Detrital P (ug/g) (µg/g)	Organic P (µg/g)	Unreactive P (g/kg)	TP (g/kg)
1	S13.1.10.1.a	0	0.5	26.8	7.5	28.8	0.4	0.39	0.4
2	S13.1.10.2.a	0	0.8	22.1	6.9	30.7	0.1	0.41	0.42
3	S13.1.10.3.a	0	0.8	9.1	4.1	31.5	0.4	0.42	0.42
4	S13.1.11.1.a	2	0.2	5.3	3.0	30.5	0.5	0.50	0.5
5	S13.1.11.2.a	2	0.4	32.7	10.7	36.3	0.4	0.45	0.46
6	S13.1.11.3.a	2	0.3	24.8	9.4	33.2	1.9	0.44	0.45
7	S13.1.20.1.a	3	0.5	17.6	6.3	30.8	2.6	0.42	0.43
8	S13.1.20.2.a	3	0.8	31.6	7.6	29.5	2.7	0.43	0.44
9	S13.1.20.3.a	3	0.7	28.9	7.9	32.1	1.1	0.46	0.47
10	S13.1.30.1.a	5	0.7	31.6	8.0	30.2	3.3	0.45	0.46
11	S13.1.30.2.a	5	-	-	-		-	-	-
12	S13.1.30.3.a	5	0.7	14.8	8.8	34.1	2.1	0.43	0.44
13	S13.1.31.3.a	13	0.3	5.2	4.2	34.0	2.3	0.50	0.5
14	S13.1.31.3.a	13	0.2	30.6	7.1	32.2	1.9	0.47	0.48
15	S13.1.31.3.a	13	0.2	14.9	3.2	32.0	2.8	0.48	0.49
16	S13.1.32.3.a	21	0.3	4.4	3.1	32.1	3.8	0.47	0.47
17	S13.1.32.3.a	21	0.5	31.7	2.7	34.3	2.4	0.47	0.48
18	S13.1.32.3.a	21	0.3	29.0	1.9	33.6	3.4	0.48	0.49
19	S13.1.40.1.a	29	1.1	29.2	7.6	28.6	3.6	0.44	0.45
20	S13.1.40.2.a	29	0.3	25.9	8.7	34.7	4.6	0.54	0.55
21	S13.1.40.3.a	29	0.5	28.0	7.4	37.9	4.4	0.53	0.54
22	S13.1.41.3.a	40	0.4	9.9	8.2	35.7	3.1	0.43	0.43

23	S13.1.41.3.a	40	0.6	49.1	1.4	29.3	2.8	0.44	0.45
24	S13.1.41.3.a	40	0.4	21.7	8.2	31.6	3.4	0.45	0.46
25	S13.1.50.1.a	50	0.5	24.4	10.1	33.5	4.5	0.49	0.5
26	S13.1.50.2.a	50	0.2	21.0	7.9	36.2	5.1	0.52	0.53
27	S13.1.50.3.a	50	0.5	34.4	2.7	35.8	7.2	0.50	0.51
28	S13.1.60.1.a	113	0.3	30.6	11.2	35.6	4.7	0.58	0.59
	S13.1.60.2.a	113	0.2	27.5	2.5	35.5	6.2	0.54	0.55
30	S13.1.60.3.a	113	0.1	14.0	6.8	36.2	1.8	0.55	0.56

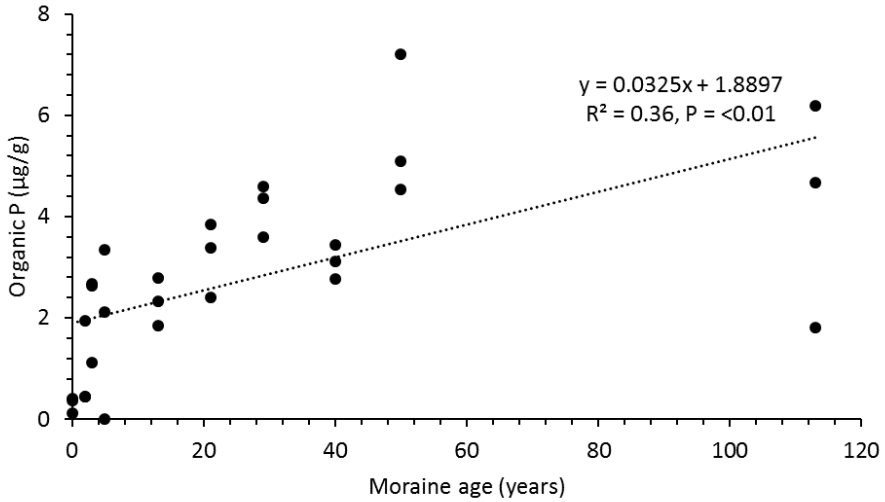

Figure. C.8. Organic P as a function of moraine age from ML forefield. Black dashed line is a linear best fit. See, Table B. 12 & 13 for data.

Table. C.16. Mass of each grain size fractions at each moraine age from Midtre Lovénbreen

Forefield #	Moraine age (years)	<2mm (g)	2-7mm (g)	>7mm (g)	SUM (g)	Sum of 2-7 and >7mm (g)
ML	0	114	49	37	200	86
	0	71	67	62	200	129
	0	67	76	57	200	133
	3	94	55	51	200	106
	3	76	82	42	200	124
	3	118	54	28	200	82
	5	114	32	54	200	86
	5	88	51	61	200	112
	5	98	38	64	200	102
	13	77	89	34	200	123
	13	87	54	59	200	113
	13	123	62	15	200	77
	29	86	84	30	200	114
	29	109	64	27	200	91
	29	70	104	26	200	130
	40	110	74	16	200	90
	40	99	50	51	200	101
	40	115	56	29	200	85
	50	91	61	48	200	109
	50	110	53	37	200	90
	50	112	65	23	200	88
	113	123	62	15	200	77
	113	103	82	15	200	97
	113	134	48	18	200	66

Table. C.17. Mass of each grain size fraction at each moraine age from Storglaciären and Rabot's

Forefield #	Moraine age (years)	<2mm (g)	>2mm (g)	SUM (g)
ST	0	114	86	200
	0	71	129	200
	0	80	120	200
	15	99	101	200
	15	91	109	200
	15	73	127	200
	20	135	65	200
	20	82	118	200
	20	72	128	200
	24	69	131	200
	24	59	141	200
	24	123	77	200
	27	126	74	200
	27	118	82	200
	27	124	76	200
	31	79	121	200
	31	121	79	200
	31	111	89	200

	34	141	59	200
	34	67	133	200
	34	51	149	200
	45	89	111	200
	45	78	122	200
	45	95	105	200
	55	172	28	200
	55	143	57	200
	55	121	79	200
	80	95	105	200
	80	125	75	200
	80	111	89	200
	80	112	88	200
	80	122	78	200
	80	115	85	200
RB	0	68	132	200
	0	52	148	200
	0	97	103	200
	16	83	117	200
	16	76	124	200
	16	78	122	200
	34	81	119	200
	34	120	80	200
	34	58	142	200
	62	117	83	200
	62	97	103	200
	62	66	134	200
	104	85	115	200
	104	101	99	200
	104	87	113	200
	104	170	30	200